Rates and processes of active folding in the central Zagros - Iran

Behnam Oveisi

École Doctorale – Terre Univers Environment
OBSERVATOIRE DES SCIENCES DE
L'UNIVERS DE GRENOBLE
Laboratoire de Geodynamique des Chaînes Alpines (LGCA)

THESE

Présentée pour obtenir le grade de

DOCTEUR EN SCIENCES DE L'UNIVERSITÈ
JOSEPH FOURIER – GRENOBLE I

Spécialité Sciences de la Terre de l'Univers et de l'Environment

Rates and processes of active folding in the central Zagros - IRAN

Vitesses et processus des plissements récents dans le Zagros central - IRAN

Par

Behnam OVEISI

Soutenue publiquement le 10 Mai 2007 devant le jury composé de :

M. Olivier Bellier	**Rapporteur**
M. Olivier Lacombe	**Rapporteur**
M. Peter Van der Beek	**Directeur de thèse**
M. Jérôme Lavé	**Co-Directeur de thèse**
M. Denis Hatzfeld	**Examinateur**
M. Manuchehr Quraishi	**Examinateur**

ACKNOWLEDGMENTS

Many individuals and organizations deserve recognition and abundant thanks for their support and aid with this project from the very beginning.

Financial support was provided by the the French Embassy in Iran, and the INSU program Dyeti. Logistical support for the fieldwork was provided by the Geological Survey of Iran (GSI).

In particular, special thanks are due to the project directors, Peter Van der Beek and Jeromé Lave for recognizing the importance of this interdisciplinary project, and supporting it. Without their help the most important parts of the program would never have been completed.

Their help in the sampling/mapping program during the several field works in the Zagros was also critical in getting the project underway. Special thanks is extended to both for their help and participation, but also for their excitement, enthusiasm and patience.

Danis Hatzfeld and Manouchehr Ghoraishi deserves additional thanks for his enthusiasm, support, and information concerning the seismicity and the neotectonics of the central Zagros.

The CEREGE lab facilities was critical in helping for ^{36}Cl and ^{10}Be cosmogenic data which was important for providing absolute dating control in the project. Appreciation and thanks is also due to Julien Carcaillet (LGCA) and Régis Braucher (Cerege) for taking time to talk with me. They generously offered me use of their lab facilities, and was critical in helping me to learn and to approach to new technology of ^{10}Be cosmogenic dating method.

Without the help of Riad Hassani (Laboratoire de Géophysique Interne et de Tectonophysique - Université de Savoie) the program of numerical modeling would never have been completed. Special thanks is extended to him for his help and participation, but also for his excitement, enthusiasm and patience.

The library of the Masion du la Geoscience was extremely helpful in obtaining most of my critical book and article requests.

Special thanks are due to my thesis committee members O. Bellier, O. Lacombe, P. Van der Beek, J. Lavé, D. Hatzfeld and M. Quraishi for their enthusiasm and patience.

A. Saidi (GSI-NGDIR) deserves special thanks for his enthusiasm, support, and his role in getting the project underway. Amir Bolorchi (GSI) deserves special thanks for his role in setting up the field project with our team, and for providing abundant financial and logistical support throughout the project.

It is also necessary to acknowledge the detailed proofreading and correcting that Jeromé Lave and Peter Van der Beek did on earlier copies of this manuscript. Their suggestions and comments have helped to clarify and tremendously improve the final work. All errors, inconsistencies, or omissions that remain are my own.

Finally, to Marzieh and Ava and all friends who have endured the ompromises associated with writing and completing this manuscript, I offer you the final version of my thesis, and my profound thanks and appreciation for all your support and understanding.

LGCA, Mars 2007, Behnam

CONTENTS

INTRODUCTION GENERALE

INTRODUCTION GÉNÉRALE

Les topographies continentales représentent le produit de processus internes tectoniques et de processus externes érosifs. De ce point de vue, le relief terrestre constitue une source importante d'informations sur les processus tectoniques sous-jacents. L'accès aisé à des données topographiques de qualité ou à des méthodes géodésiques rapides à mettre en œuvre, de même que le développement de nouvelles méthodes de datation absolue des objets géomorphologiques, permettent désormais d'étudier des structures et des processus tectoniques dans la lithosphère sur des échelles de temps recouvrant plusieurs cycles sismiques. La déformation dans la croûte peut en effet être inégalement distribuée dans l'espace et dans le temps, et son étude requiert le recours à diverses méthodes et disciplines des géosciences.

Dans le cas de la jeune chaîne du Zagros, d'un côté une résolution temporelle supérieure au million d'années est difficilement accessible par les méthodes géologiques et structurales classiques pour décrire l'évolution des différentes structures plicatives, et ce même si les strates de croissance identifiées en sismique réflexion peuvent localement fournir une résolution temporelle accrue. A l'autre bout du spectre, les méthodes géodésiques renseignent sur la déformation récente sur une échelle de quelques années à quelques dizaines d'années, c'est-à-dire à des échelles de temps pour lesquelles la déformation enregistrée relève plus du signal transitoire durant la phase intersismique du cycle sismique que de la déformation permanente. La déformation semble très différente du point de vue de ces deux perspectives, et les méthodes morphotectoniques, mises en œuvre dans le cadre de ce travail de thèse, tentent de faire le pont entre ces deux approches temporellement opposées, et de combler la gamme des échelles de temps allant de mille à un million d'années pour contraindre le mode de fonctionnement des plis et failles qui déforment le Zagros. De même, pour comprendre la distribution spatiale et temporelle des séismes, ce qui est fondamental pour évaluer le risque séismique de cette région, l'étude de la déformation à ces échelles de temps est déterminante.

Bien que les caractéristiques générales de la géologie et la structure de la chaîne du Zagros soient maintenant bien comprises, des données détaillées sur la distribution de la déformation active et du comportement sismotectonique de cet orogène sont encore relativement mal contraintes. Ce travail de thèse vise donc avant tout à fournir une vue quantitative de la distribution de la déformation récente dans le Zagros central à des échelles de temps intermédiaires (de l'ordre de 10^4-10^6 ans) au moyen de marqueurs géomorphologiques datés. Pour ceci, une combinaison de méthodes néotectoniques, comme le relevé de profils

topographiques de marqueurs géomorphologiques déformés, l'étude de leur relation avec les structures géologiques, et la datation de ces marqueurs a été mise en œuvre.

Même si les méthodes morphotectoniques mises en œuvre ne permettent pas de résoudre l'ensemble de la problématique posée, il est important de conserver en toile de fond un certain nombre de questions qui ont guidé le travail de cette thèse :

- quelles sont les variations spatiales et temporelles du taux de déformation au travers le Zagros ?
- quels sont les facteurs contrôlant la géométrie actuelle des montagnes du Zagros ?
- quel est le rôle des conditions aux limites, de la profondeur et de la nature du décollement sous le prisme sédimentaire, des failles crustales dans le socle cristallin, sur la déformation du prisme du Zagros ? Et plus spécifiquement, quel est le mécanisme de déformation dominant actuellement : une tectonique de couverture ou bien du raccourcissement à l'échelle crustale ?
- quel est le modèle de la propagation de la déformation au travers du Zagros ?
- y a-t-il une séquence de propagation normale de la déformation vers l'avant pays ou bien une réactivation significative en hors-séquence au sein du prisme orogénique ?
- Comment s'articulent déformations plicatives et fonctionnement des décrochements au sein du prisme ?

La structure du manuscrit présenté dans la suite illustre en quelque sorte notre cheminement au travers de ces questions.

Dans le chapitre I, le contexte géologique et sismotectonique général du Zagros est présenté. Suit dans le chapitre II, un survol des méthodes morphotectoniques et des méthodes de datation mises en œuvre au cours de la thèse.

Les chapitres III et IV s'attachent à des structures plicatives particulières au front et au cœur du Zagros, en mettant l'accent sur le lien entre modèles de plissement et déformation observée en surface. Le chapitre III a pour objet l'étude détaillée de la déformation plicative d'un anticlinal côtier, le pli de Mand, dont la déformation peut être suivie à l'aide de terrasses marines basculées et d'âges distincts. Cet exemple spectaculaire nous renseigne sur le mode de fonctionnement d'un pli de détachement et sur la quantité de raccourcissement enregistrée sur cette structure frontale du Zagros central. Le chapitre IV met l'accent sur des structures synclinales dans les parties plus internes du Zagros central. Des surfaces pleistocènes y ont en effet enregistré une déformation verticale très particulière, à savoir la réactivation de cœurs de

synclinaux au dessus de niveaux ductiles dans la pile sédimentaire. Une modélisation numérique simplifiée du problème est présentée en accompagnement des objets géologiques.
Dans le chapitre V, l'ensemble des données précédentes est reprise rapidement et complétées par l'étude de la déformation de terrasses fluviales et du profil en long de deux grandes rivières traversant le Zagros (les rivières Dalaki et Mand) dans le but de fournir un profil de la déformation verticale et du raccourcissement au travers du Zagros, et d'obtenir une compréhension plus claire de la variation spatiale du taux de déformation, et de l'activité des différents plis et plus particulièrement des plis frontaux. Le résultat est comparé à la déformation intersismique obtenue à partir des données GPS, afin de mieux appréhender le rapport entre ces déformations enregistrées à des échelles de temps distinctes dans le Zagros central. Par ailleurs, la longueur d'onde de la déformation enregistrée par ces marqueurs, ainsi que la mise en correspondance ou non des zones soulevées avec la localisation supposée des failles de socle, permettent de documenter la nature superficielle ou profonde de la tectonique dans le Zagros central, c'est-à-dire de discriminer entre plis de couverture et l'expression superficielle de failles de socle.

Le chapitre VI propose une synthèse générale des observations morpho-tectoniques et des modèles sismo-tectoniques ou structuraux proposés au gré des chapitres III à V.

Cette thèse a été effectuée au Laboratoire de Géodynamique des Chaînes Alpines (LGCA) à l'Université Joseph Fourier (Grenoble-I) dans le cadre d'une collaboration avec la Commission Géologique de l'Iran (GSI). Le travail de thèse a de plus bénéficié de collaborations fructueuses avec le CEREGE, Université Paul Cézanne (Aix-en-Provence), et le Laboratoire de Géophysique Interne et de Tectonophysique - Université de Savoie (Chambéry).

GENERAL INTRODUCTION

The Earth's surface constitutes an important source of information regarding tectonic processes operating within the Earth. Topography represents the net product of tectonic and surface processes. A primary challenge in this field is to unravel the complexities and intricacies of the highly coupled system of tectonic and surface processes. In order to do this, digital topographic data is now readily availabale and new geodetic and imagining have been developed. Such data present new opportunities to study structures and tectonic processes within the lithosphere. Willett et al. (2003) noted, however, that our ability to infer tectonic information from surface observations is hampered by a lack of quantification of the causal links between tectonic activity and topography. In fact, tectonic activity creates the surface relief but surface processes simultaneously destroy relief by redistributing mass. These processes are coupled insofar as there is a deformational response to surface change and the resultant gravitational forces. Interactions between tectonic and surficial processes are complex and involve coupling with feedback through diverse mechanisms (Fig. 1). For instance, fluvial incision rates increase in

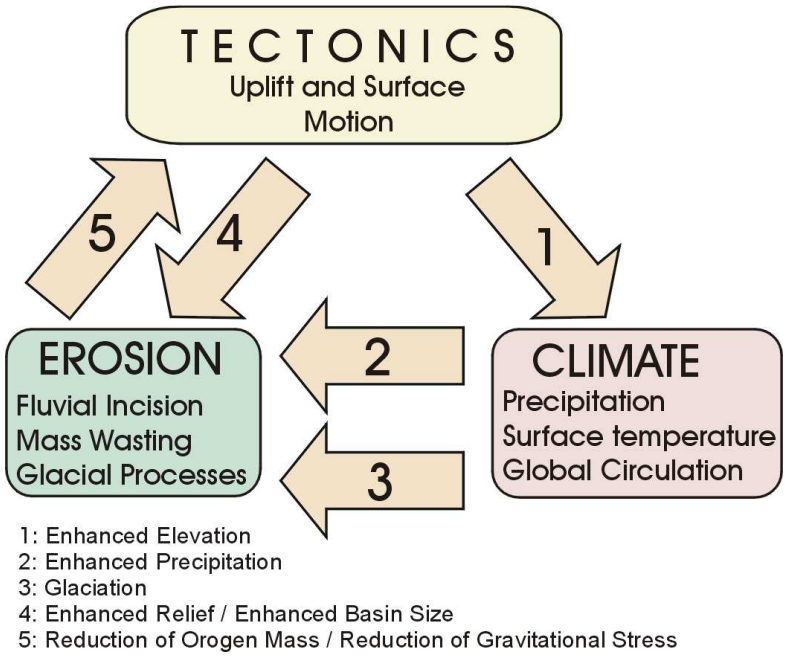

Figure 1. Feedback loops within the dynamic system defined by tectonics, climate and erosional surface processes. There are two feedback loops; a direct path (1) whereby tectonics increases erosion rates by increasing elevation, relief and drainage basin areas and an indirect loop (2), whereby increased elevation induces increased erosion rates through changes in climate. Climate change is in the form of enhanced precipitation or lower temperatures, which lead to glaciation. In each case, there is feedback in the tectonic response to surface mass redistribution. More complex processes and pathways are likely to exist (Modified from Willett e t al. 2003).

response to a tectonically-driven increase in channel slope, but may also increase or decrease in response to changes in drainage area as water divides are moved or created by tectonic activity. Crustal deformation is unevenly distributedin space and time and thus its study has become partitioned into disciplines with tools of markedly different precision and researchers with markedly different perspectives (Fig. 2).

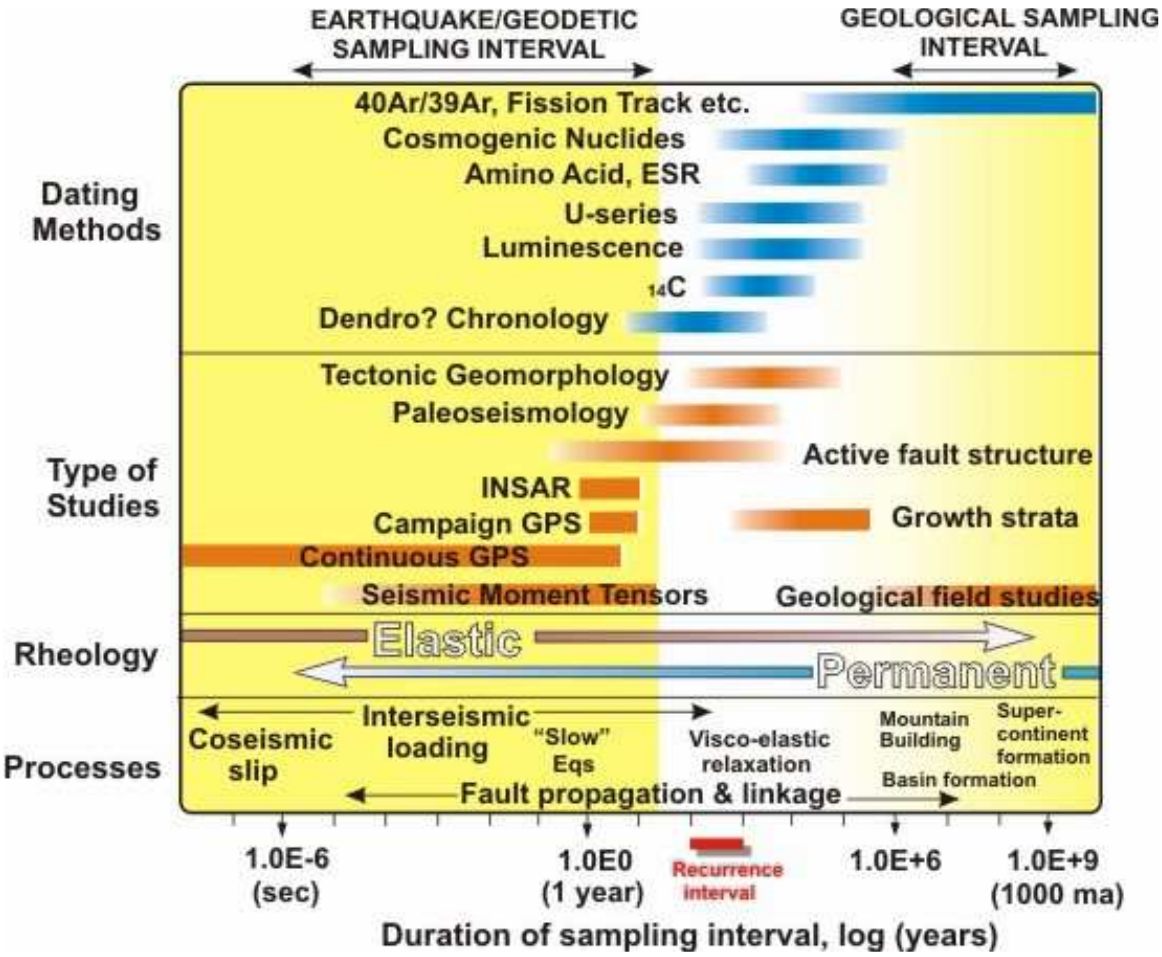

Figure 2. Earth scientists study deformation across more than 15 orders of magnitude of temporal sampling windows. Processes, rheologies, types of studies, and methods used vary enormously across this range. The white band, corresponding to times from decades to a million years, is the least understood part of the range and thus the missing link in relating earthquakes to orogenesis ;
[New Departures in Structural Geology and Tectonics, National Science Foundation (GEO/EAR) http://pangea.stanford.edu/~dpollard/NSF/main.html].

Field relations through the young Zagros Mountain belt seldom allow age constraints tighter than 1 Myr to be placed on individual structures, although growth strata imaged by seismic reflection locally permit increased temporal resolution. Deformation at these time scales is definitely permanent. On the other hand, the transient elastic strain measured at 10 years and less is an insignificant fraction of the total finite strain recorded in the belt. Deformation appears very different from these two perspectives. The temporal and conceptual gap between them is one of the most fertile areas for future research (Goodwin, et al., 2003).

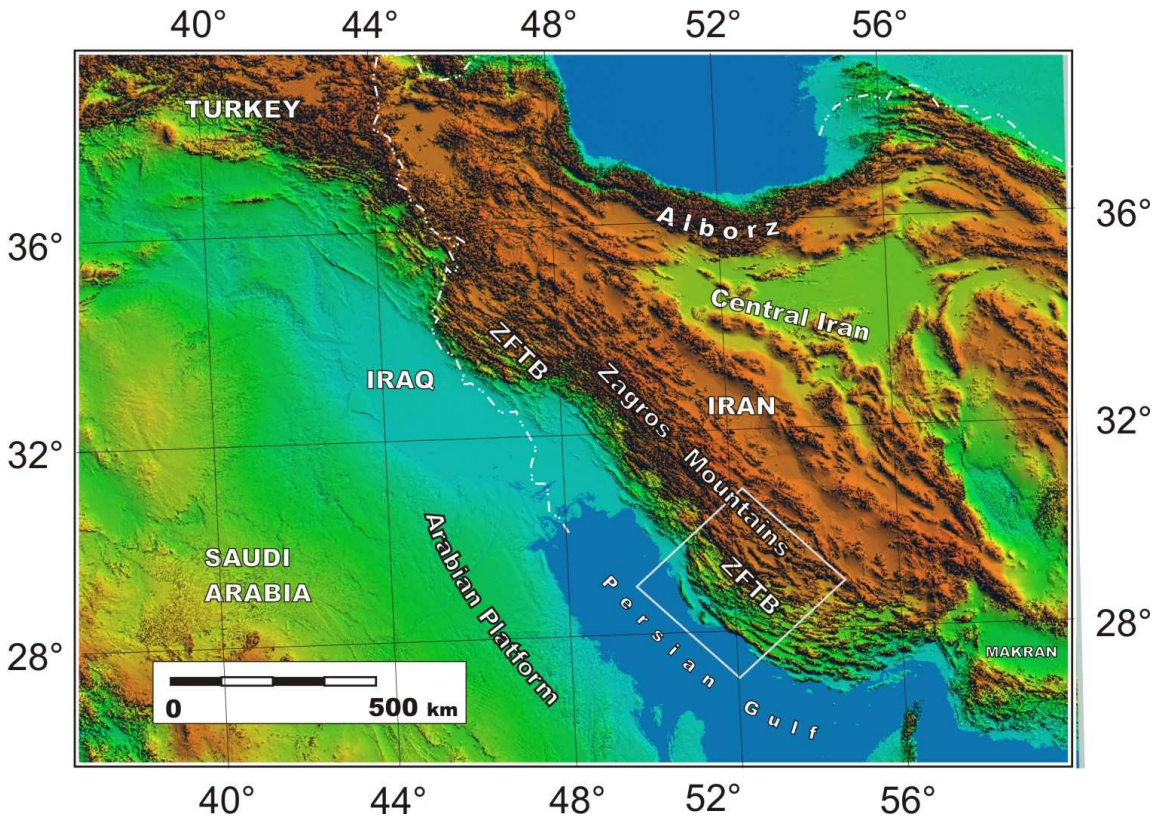

Figure 3. Physical position of the Zagros Mountains of Iran. White box show area of thesis. ZFTB: Zagros Fold-Thrust Belt.

Although the general features of the geology and the structure of the Zagros belt are now well understood, detailed data on the distribution of active deformation and seismotectonic behaviour across the belt are still poorly constrained :

- What are the spatial and temporal variations in deformation rate ?
- Which factors control the present-day surface geometry through the Zagros Mountains ?
- What are the role of boundary conditions, the depth and nature of the decollement and basement faultig in ongoing surface deformation ?

- What is the style of Zagros wedge propagation ?
- Is there any complex forward wedge propagation due to significant out-of-sequence reactivation through the tectonically active areas ?
- What is the role of thin- and/or thick-skinned systems in wedge propagation ?

GOAL OF THESIS

This thesis aims to provide a quantitative view of the distribution of recent crustal deformation through the central Zagros by means of dateable geomorphic markers at intermediate time scales i.e. on the order of 10^4-10^5 yr. In order to this, a combination of the neotectonic data (e.g. topographic profiles of deformed geomorphic markers) and fault attitudes have been used to constrain a neotectonic reconstruction for the present day active deformation. Neotectonic markers (e.g. terraces) and river long profiles (long profile) are generated using bedrock measurements and available fold theories and results are compared with field measurements to constrain the styles and rates of deformation. The particular goals of the thesis are :

- As many fold-and-thrust belt, the time range from 10^2 to 10^6 years is the missing link in the Zagros. Without studies at these time scales, we are unlikely to understand the spatial and temporal distribution of earthquakes, for example, which is fundamental for evaluating seismic hazard (Goodwin, et al., 2003). Throughout the central Zagros, the ongoing deformation is difficult to address due to unclear geometry and kinematics of both the bedrock and neotectonic features. Moreover, a persisting question in the Zagros is: how does deformation at the time scale of decades and less, which includes elastic strain as well as permanent deformation accomplished by seismic and aseismic fault movement, integrate over hundreds of thousands to millions of years to form major tectonic structures? The main goal of this thesis is to obtain a clearer understanding of the spatial variation in deformation rate, which can be due to thick- and/or thin-skinned tectonics through the central Zagros. To do this, tectonic geomorphology techniques have been used. The neotectonic markers and river profiles help us to image the localized or distributed pattern of deformation that results from oblique shortening across the central Zagros. The result is compared with interseismic deformation from GPS sata to understand the relationship between short-tem and intermediate time scale rate and patterns of deformation within the central Zagros. This thesis adds an intermediate temporal perspective to the surveyed vertical active deformation and quantified rates of uplifting and shortening using cosmogenic exposure age dating methods.

- Furthermore, this thesis tests conceptual models of surface deformation that have been generated through field research, using numerical modelling. This study attempts to integrate an approach of experimental determination of rheological and geometric key parameters associated with the observed active superficial deformation ; in order to do this, mechanical models of deformation in the upper few kilometers of the crust have been developed and compared with characterized structures to provide a better understanding of their relationship to factors of topography and tectonic geomorphology.

This thesis has carried out at the Laboratoire de Géodynamique des Chaînes Alpines (LGCA) of the University of Joseph Fourier – Grenoble-I within the framework of a collaboration with the Geological Survey of Iran (GSI). Other institutions involved in this work were the Cerege Aix-en-Provence, Cergy Pontoise and Laboratoire de Géophysique Interne et de Tectonophysique - Université de Savoie

CHAPTER I

TECTONIC AND GEODYNAMIC SETTING OF THE ZAGROS MOUNTAINS

CHAPITRE I

CONTEXTE TECTONIQUE ET GEODYNAMIQUE DU ZAGROS

Résumé en français

La chaîne du Zagros forme une partie de la vaste ceinture orogénique alpino-himalayenne. Elle se situe entre le Plateau central iranien au nord-est, le Taurus en Turquie au nord-ouest, la faille d'Oman au sud-est et le Golfe Persique au sud-ouest (Falcon 1967 ; Fig. I-1). La chaîne du Zagros, longue d'environ 2000 km pour une largeur de 200-300 km, résulte de la convergence entre les plaques arabe et iranienne et de la fermeture de la Néo-Téthys au Crétacé supérieur (Sengor & Kidd 1979; Berberian & King 1981; Stoneley 1981; Snyder & Barazangi 1986; Beydoun et al. 1992; Berberian 1995; Talbot & Alavi 1996). La chaîne représente en fait la frontière sud d'une plus large zone de collision entre l'Arabie et l'Eurasie qui absorbe une convergence à un taux de 20-30 mm a^{-1} et s'étend jusqu'à la mer Caspienne (Jackson et al., 1995). Le Zagros est une région très actives sismiquement et des données de déformation actuelle par GPS (Vernant et al., 2004) montrent que cette chaîne absorbe une partie importante de la convergence globale entre les plaques Arabie et Eurasie. Le Zagros est bordé au sud-ouest par un bassin d'avant-pays, constitué du Bassin Mésopotamien et du Golfe Persique, qui s'étend sur plus de 200 km à l'avant du front de la chaîne. A son extrémité méridionale, la largeur de la chaîne atteint 350 km.

Le socle cristallin du Zagros est recouvert par 10 à 14 km de sédiments d'age Précambrien à Quaternaire ; cette série contient de multiples couches incompétentes et plusieurs niveaux évaporitiques qui semblent contrôler fortement la déformation, notamment dans la partie sud-est du Zagros. Le niveau de décollement le plus important est constitué par les évaporites néo-protérozoïques d'Hormuz à la base de la série. Les séries sédimentaires du Zagros enregistrent une histoire tectonique qui peut être divisée en trois grands épisodes tectoniques distincts : (1) une phase de plateforme stable pendant le Paléozoïque inférieur, (2) extension et ouverture de la Téthys au Permo-Trias, et (3) une phase de convergence Cénozoïque.

La chaîne du Zagros s'est développée dans sa partie externe comme un prisme de chevauchements imbriqués, et surtout comme une succession de plis qui déforment la couverture de sédiments phanérozoïques. La déformation s'est propagée vers le sud-ouest au cours du temps (Alavi, 1991; 1994). La partie externe du Zagros est caractérisée par des plis symétriques associés à des chevauchements, avec sédimentation syn-tectonique dans les synclinaux (Koyi, 1988 ; Bahroudi & Koyi, 2003). Peu de données existent actuellement sur la distribution de la déformation à travers la chaîne. Blanc et al. (2003) ont estimé un raccourcissement de 46 km le long d'une coupe de 170 km de long à travers le nord-est du Zagros.

La chaîne est caractérisée par une surface topographique plongeant à ~1° vers l'avant-pays (Oberlander, 1965). Le décollement basal semble quasi-horizontal sur les coupes géologiques publiées mais la pénétration des profils sismiques de cette région est insuffisante pour confirmer cette géométrie. En outre, la géométrie du décollement basal est probablement perturbée par l'activation possible de failles de socle. Dans tous les cas, néanmoins, l'angle d'ouverture du prisme du Zagros semble être inférieur ou égal à 1° (Talbot & Alavi, 1996), indiquant un prisme orogénique à très faible friction basale, même si le fonctionnement du prisme reste controversé (Ford, 2004 ; Mouthereau et al ., 2006).

Afin de poser le problème de la déformation actuelle et récente de la chaîne dans son cadre géodynamique, ce chapitre propose une discussion succincte de l'évolution tectonique du Zagros pendant les phases pré- et post-collision, de sa structure actuelle et des failles (actives ou non) les plus importantes. Les données sismologiques et géodésiques (GPS) portant sur la déformation actuelle de la chaîne sont passées en revue. Finalement, nous discutons des modèles de déformation du Zagros publiés ces dernières années et notamment du rôle du socle et des niveaux de décollement sur cette déformation.

1. INTRODUCTION AND PLATE TECTONIC CONTEXT

The Zagros mountains extend for 2000 km between the central Iran plateau in the north, the Taurus in Turkey to the NW (Scott 1981), the Oman Fault in the SE and the Persian Gulf foreland to the SW (e.g. Falcon 1967) (Fig. I-1). The Zagros marks the present southern front of the broad Arabia-Eurasia collision zone, and the region's seismicity shows that it absorbs an important part of the overall convergence. The 200-300 km wide Zagros fold and thrust belt is part of the Alpine-Himalayan belt and results from the closure of the Neo-Tethys ocean and convergence between the Arabian and Iranian plates. The Neo-Tethys sutured during the late Cretaceous (Sengor & Kidd 1979; Berberian & King 1981; Stoneley 1981; Snyder & Barazangi 1986; Beydoun et al. 1992; Berberian 1995; Talbot & Alavi 1996) and

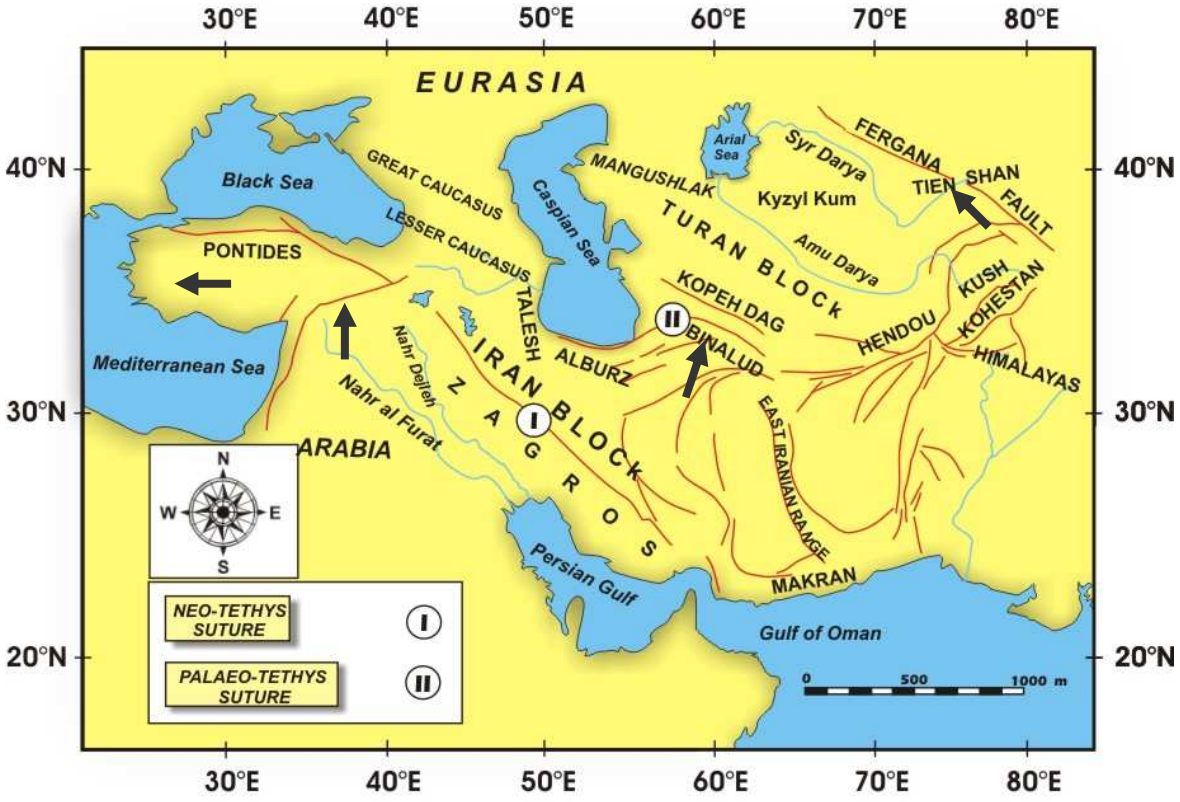

Figure I-1. Map of the Central Asia showing the Iranian block and its surrounding territories. Thick arrows in black show movement relative to the Eurasia plate (modified from Lyberis and Manby, 1999).

the fold and thrust belt is currently being shortened at a rate of ~8 mm a^{-1} (Vernant *et. al.*, 2004). The external part of the Zagros fold belt records ongoing syntectonic sedimentation above symmetrical folds and associated thrusts (Koyi, 1988; Bahroudi & Koyi, 2003).

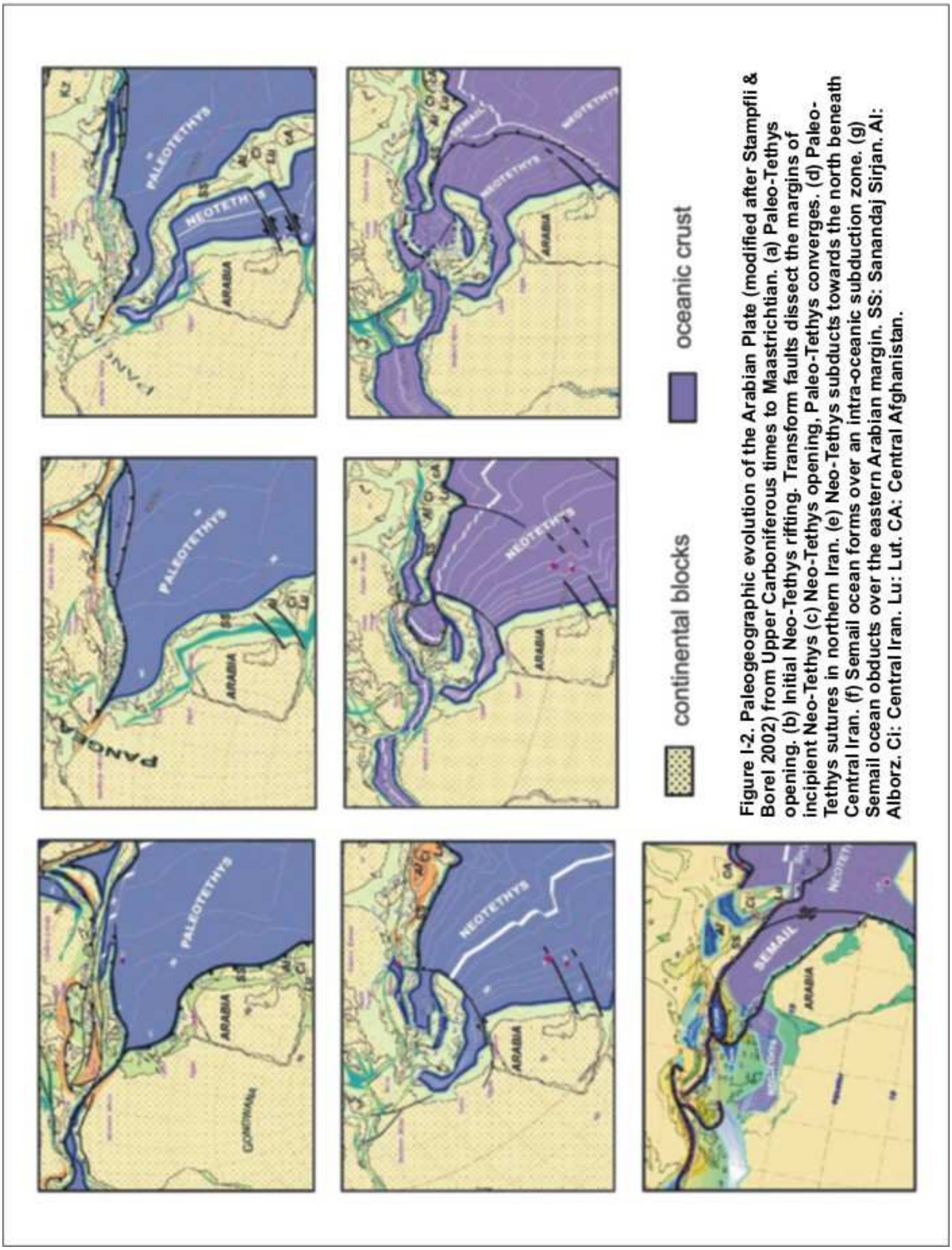

Figure I-2. Paleogeographic evolution of the Arabian Plate (modified after Stampfli & Borel 2002) from Upper Carboniferous times to Maastrichtian. (a) Paleo-Tethys opening. (b) Initial Neo-Tethys rifting. Transform faults dissect the margins of incipient Neo-Tethys (c) Neo-Tethys opening, Paleo-Tethys converges. (d) Paleo-Tethys sutures in northern Iran. (e) Neo-Tethys subducts towards the north beneath Central Iran. (f) Semail ocean forms over an intra-oceanic subduction zone. (g) Semail ocean obducts over the eastern Arabian margin. SS: Sanandaj Sirjan. Al: Alborz. Ci: Central Iran. Lu: Lut. CA: Central Afghanistan.

Crystalline basement within the Zagros is overlain by 10–14 km of Precambrian to Recent sediments. The sequence contains multiple incompetent layers and several evaporitic levels, the most important of which is the Neo-Proterozoic Hormuz Salt, which directly overlies the basement and controls deformational style in the SE Zagros. The incompetent layers and evaporitic levels have caused a complex deformation history.

The Zagros belt has structurally evolved as a prism of stacked thrust sheets, composed of uppermost Neoproterozoic and Phanerozoic sedimentary strata, in the external part of the southwest-migrating Zagros orogenic wedge (Alavi, 1991;1994). Very little detailed data are available on the distribution of deformation across the fold belt. Blanc et al. (2003) propose 46 km of shortening across a 170 km wide cross section through the Simple Folded Zone in the NE Zagros. The foredeep (Mesopotamian foredeep–Persian Gulf) continues for over 200 km to the SW of the thrust front. At the southern end of the Zagros the width of the fold belt reaches 350 km. The fold belt has a topographic surface dipping at 1° toward the foreland (Oberlander, 1965). The décollement in Cambrian evaporites appears to be close to horizontal on cross sections but images provided by seismic lines do not penetrate deep enough to confirm this. The basal decollement is complicated by the possible activity of basement faults. Overal the taper angle of the Zagros wedge appears to be less than or equal to 1° (Talbot & Alavi, 1996).

The tectonic history of the Zagros belt can be divided into three distinct tectonic episodes: (1) a stable platform phase during early Paleozoic, (2) Permo-Triassic extension, and (3) a Cenozoic contractional phase.

2. GEODYNAMIC EVOLUTION OF THE ZAGROS

2.1. Prior to continental collision

The Paleo-Tethys (Fig. I-3), which separated Laurasia from Gondwana, has existed since late Palaeozoic times. During the earliest Triassic, the Neo-Tethys Ocean opened between the Afro-Arabian and Iranian blocks ; the Paleo-Tethys began to close at the same time. The Neo-Tethys Ocean started to open along what is now called the “Crush Zone” or “Imbricated Zone” in the northern, internal part of the Zagros. At the beginning of the Mesozoic, due to the development of the Neo-Tethys and the displacement of the Iranian block towards the NE, the Paleo-Tethys Ocean closed and continental collision between the Iranian block and the Eurasian plate took place. The zone of collision stretches out towards

NE of the Caucasus and Talesh mountaines in NW Iran and up to the Kopet-Dagh (Sengor, 1979). Throughout the middle Cretaceous the Afro-Arabian and Eurasian plates converged and the Neo-Tethys Ocean began to close. During the Late Cretaceous, the NE margin of the Arabian plate started to be subducted under Central Iran. The closure of the Neo-Tethys was marked by several tectonic events on the Zagros platform. The first was the Early Coniacian - Late Santonian (89.3±1.0 – 83.5±0.7) obduction of ophiolites onto the continental crust (Ricou, 1971; Falcon, 1974; Berberian and King, 1981; Berberian, 1995), that changed the architecture of the sedimentary basin. The second event was pronounced reactivation of deep-seated, pre-existing north-south faults following older Panafrican basement trends (Koop and Stoneley, 1982).

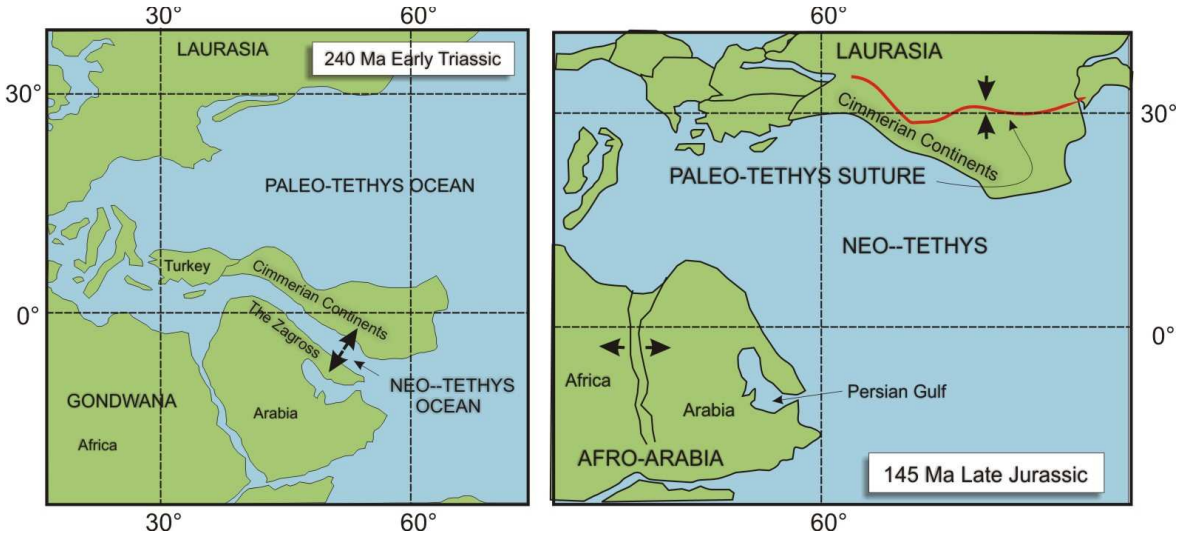

Figure I-3. The construction of the Iranian platform and the situation of Paleo- and Neo-Tethys : (A) Lower Triassic, (b) Upper Jurassic, (Trowell, 1995).

2.2. Post collisional tectonics

Throughout the upper Oligocene and lower Miocene, the Red Sea opened and subduction of the Arabian plate under central Iran intensified. The separation of the Arabian Plate from Africa along the Red Sea, which is widening at ~1.2 cm per year in a NNE direction, has propelled the Arabian Plate towards Iran. Continent-continent collision between Arabia and Central Iran plates began during middle Miocene time (Alavi, 1994; Berberian, 1995; Hempton, 1987). Zagros folding began during lower Miocene times, with thin-skinned décollement and southwestward propagation of the foreland depocenter (Fig. I-3).

Compression in the Zagros margin continued during the middle Miocene and tectonic units were formed. The Neogene Zagros orogeny partitioned the evolving foreland basin into sub-basins with different sedimentary and tectonic signatures (Bahroudi and Koyi, 2003).

During late Miocene and Pliocene times, regression of the sea and the creation of mountainous relief by folding and thrusting resulted in a continental environment. Large quantities of clastic material and red beds were developed in synclines (Berberian and King, 1981). Hempton (1987) mentioned in some extrusion occurred at the north of the suture zone

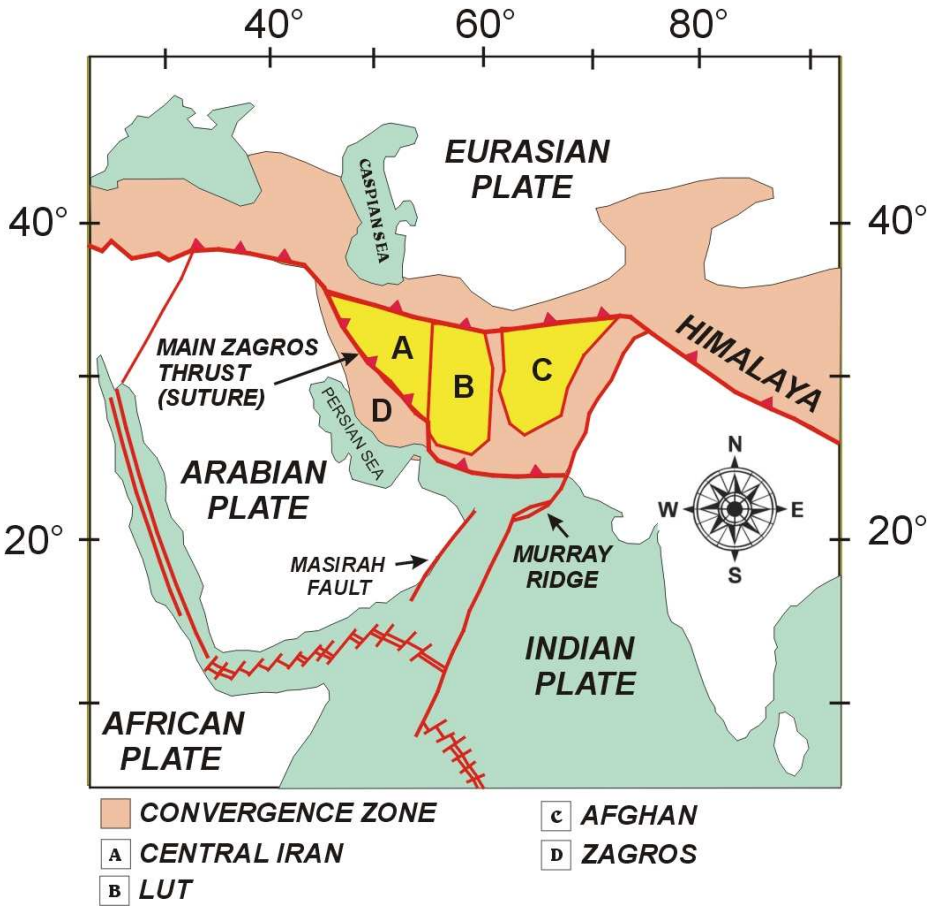

Figure I-4. Plate tectonic setting map. The border between the Arabian plate and central Iran unit is a zone of suture, marked by ophiolites. The Main Zagros Thrus (MZT) marks this border.

due to the movement of Arabia toward the North. He suggests that such extrusion at the begining of Pliocene allowed the Arabian plate to move northward faster than Africa. Convergence is partly taken up in the Alborz Mts in the North, as well as by strike slip faults in general located on the border of the different continental blocks (Fig. I-4).

3. STRUCTURE OF THE ZAGROS FOLD-THRUST BELT

3.1. Morphotectonic units of the Zagros Mountains

Various schemes exist for the subdivisions of the Zagros (Stöcklin 1968; Falcon, 1974; Alavi, 1994; Berberian 1995). The Zagros belt can be divided by major faults and/or abrupt changes in geomorphology into five morphotectonic units from northeast to southwest (Fig. I-5), which step down as five prominent topographic levels to the southwest with different characteristics in terms of thrusting, folding, uplift, erosion and sedimentation (Berberian, 1995). Each unit has its own characteristics and deformation style, which will be discussed in the following sections (Fig. I-6):

1) The High Zagros Thrust Belt (HZTB) or Imbricated Zone

2) The Simply Folded Belt (SFB)

3) The Zagros Foredeep (ZF)

4) The Mesopotamian lowland - Zagros Coastal Plain (ZCP), and
5) The Persian Gulf

The boundaries of the units are defined on the basis of (1) surface topography and morphotectonic features, (2) style of deformation, (3) subsurface geologic data, and (4) the regional seismicity.
Salt tectonics (disharmonic folding, flow and diapirism) is an important phenomenon in the Zagros. The styles of structural deformation change in the Zagros from salt-related detachment folding, to salt swells and pillows associated with fault-propogation folding, and fault-bend folding, as the thickness of the paleo-Hormuz salt basin diminishes (McQuarrie, 2004).

Although the amplitude and wavelength of the folds within the Zagros, permit basement shortening, basement deformation is not required by the geometry of the structures or by earthquake focal mechanisms. The geometry of deformation within the Zagros fold thrust belt suggests that many of the folds are cored by faults in the lower Paleozoic strata. The inferred dips and locations of these faults are compatible with the magnitude, depth, and nodal plane orientation of earthquakes throughout the fold–thrust belt (Talebian and Jackson 2004). Quaternary folding becomes younger from northeast to southwest, demonstrating that

the deformation front is migrating from the suture towards the foredeep (Berberian 1995, Hessami et al. 2002).

An important change in the fault configuration occurs along strike of the belt. In the NW, overall convergence is oblique to the trend of the belt and the surface anticlines, and is achieved by a spatial separation or partitioning of the orthogonal strike-slip and shortening components on separate parallel fault system (e.g. Authemayou, et. al. 2003). In contrast, in the SE, the overal convergence is orthogonal to the regional strike and achieved purely by thrusting (Talebian and Jackson 2004). In the central Zagros, between these two structural regimes, deformation involves parallel strike-slip faults that rotate about vertical axes, allowing extension along the strike of the belt.

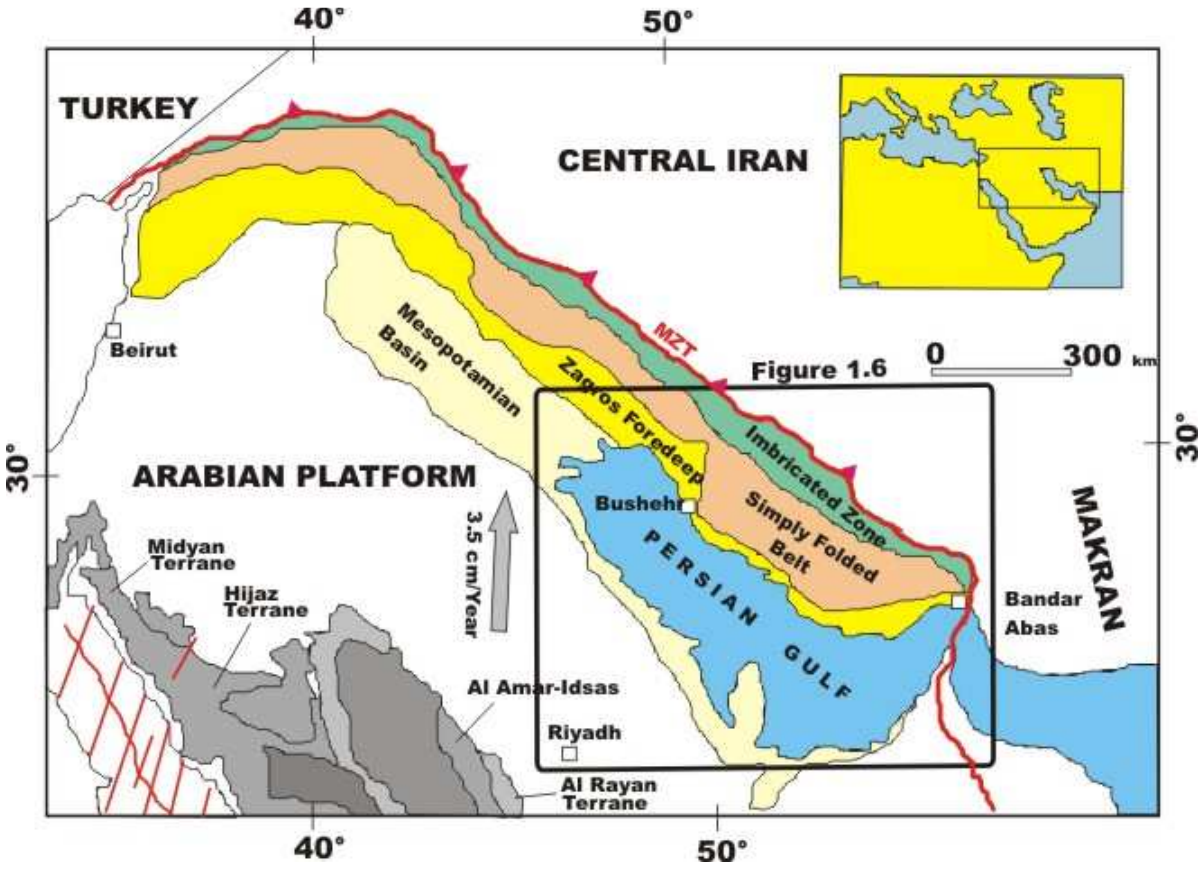

Figure I-5. Main structural units in the Zagros fold-thrust belt (Modified after Beydoun, 1991; Berberian, 1995; Alsharhan and Nairn, 1997; Husseini, 2000).

3.1.1 The Zagros Imbricate Zone

The Zagros Imbricate Zone or the High Zagros is a narrow thrust belt up to 80 km wide, with a NW-SE trend between the Main Zagros Thrust (MZT) or the Zagros suture to the northeast and the High Zagros fault (HZF) to the southwest (Fig. I-5 and I-6). The High Zagros is characterised by the highest topography of the belt, with summits over 4000 m above sea level. The belt is strongly dissected by numerous reverse faults and is upthrusted to the southwest along different segments of the High Zagros fault (Berberian, 1995). The High Zagros is characterized by strongly deformed overthrust anticlines, mainly composed of autochonous Jurassic-Cretaceous series with Paleozoic cores along some reverse faults. The belt was affected by Late Cretaceous obduction and Pliocene continent-continent collision

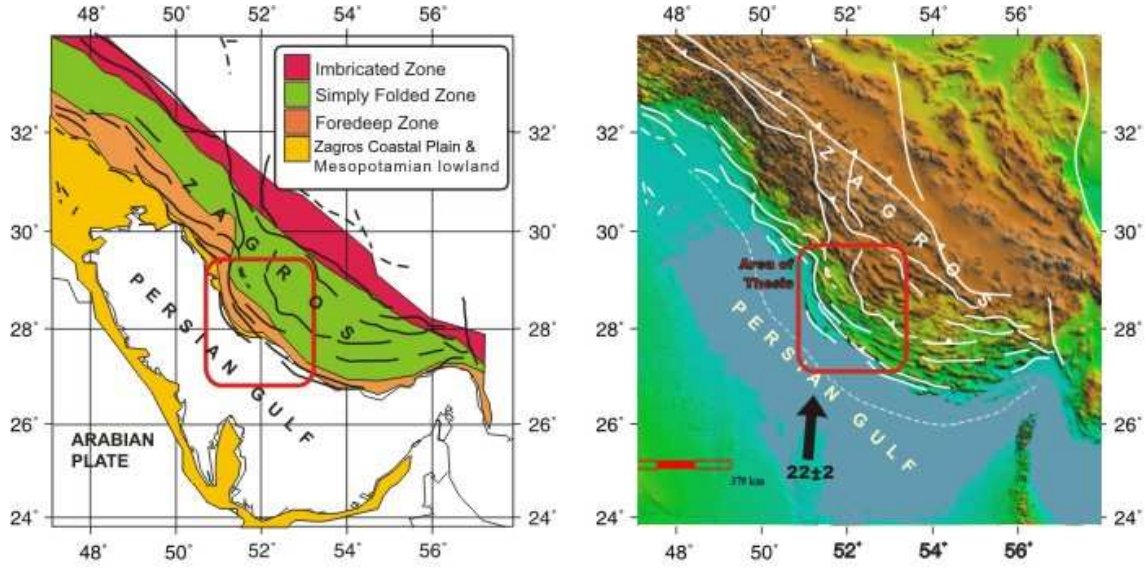

Figure I-6. Main structural units and location of main thrust fults in the Zagros fold-thrust belt. Red box show the area of thesis.

(Stocklin, 1968; Falcon, 1969, 1974; Huber, 1977; Berberian, 1976, 1977, 1981, 1983; Berberian and King, 1981; F. Berberian et al., 1982). To the SW, the High Zagros Thrust Belt contains highly imbricated slices of the Arabian margin and fragments of Cretaceous ophiolites (Alavi 1994; Berberian 1995).

3.1.2 The Zagros Simply Folded Belt

The Simply Folded Belt (SFB) of the Zagros (Fig. I-6) is limited to the northeast by the High Zagros fault (HZF) and to the southwest by the Mountain Front fault (MFF). It has

an average width of about 250 km to the southeast (Fig. I-6), 120 km to the northwest, and a length of 1375 km in Iran. The Simple Fold Belt contains characteristic elongated hogback or box-shaped anticlines, penetrated by salt plugs from the Hormuz Salt and forming mountainous terrain where calcareous ranges of the Eocene-Oligocene Asmari Limestone and Mesozoic formations dominate the topography. Within this belt, aspect ratios of the folds (length:height) are variable, and have been used to suggest that both forced fold (high aspect ratio > 10) and buckle folds (low aspect ratio < 10) are present (Sattarzadeh et al., 2000). The sedimentary column of the belt (Fig. I-17) is estimated to be up to 12 km thick (James and Wynd, 1965; Falcon, 1974; Huber, 1977; Alavi, 2003). The belt was folded during Miocene-Pliocene continent-continent collision. Incompetent units are present as first- and second-order detachment levels. The Hormuz Salt and the Miocene Gachsaran Evaporites have facilitated décollement in the lower and the upper parts of the Phanerozoic sedimentary cover (Stocklin, 1968; Falcon, 1961, 1969, 1974; Huber, 1977; M. Berberian, 1983). Paleozoic strata are very rarely exposed, but salt from the upper Proterozoic Hormuz Series crops out in diapirs in the east of the Zagros (Gansser 1992; Talbot & Alavi 1996). The Hormuz Salt does not appear in the SFB west of the Kazerun Fault, but crops out in the Zagros Imbricate Zone or the High Zagros to the NW.

3.1.3 The Zagros Foredeep

The Zagros Foredeep is bounded to the northeast by the MFF and to the southwest by the Zagros Foredeep fault (ZFF), which marks the northeastern edge of the Coastal Plain of the Persian Gulf. The formation of the Zagros Foredeep was associated with motion along the MFF and uplift of the Simply Folded Belt (SFB) (Fig. I-6). The Zagros Foredeep, which consists of elongate, symmetrical folds, is characterized by badlands of the Miocene Fars Group sediments (Gachsaran, Mishan and Aghajari formations), sheared off from the subsurface Eocene-Oligocene Asmari Limestone base along décollement thrusts in the Gachsaran Evaporites. There is a thick sequence of the Lower Miocene to Pleistocene synorogenic molasse cover (Aghajari-Bakhtiari formations) in the belt. The growth of the Zagros Foredeep structures was coeval with deposition of the Upper Pliocene-Pleistocene Bakhtiari conglomerate. The anticlines associated with the Zagros Foredeep are actively growing, and the evidence from continuous unconformities in the Pliocene freshwater sediments and folded recent gravels shows they have been active since the beginning of the Pliocene (Lees and Falcon, 1952; Falcon, 1961).

3.1.4 The Zagros Coastal Plain and Mesopotamian lowland

The Zagros Coastal Plain (Figs. I-6) is a narrow feature bounded to the north by the Zagros Foredeep fault (ZFF) and to the south by the Persian Gulf, which is the southern edge of the Zagros orogen. The Coastal Plain slopes very gently to the south at a rate of 0.2%. The morphotectonic unit of Mesopotamian lowland lies south and southwest of the Zagros Coastal Plain and is partly covered by the Persian Gulf.

3.1.5 The Persian Gulf

This morphotectonic unit with an area of about 226,000 km^2, 800 km long and from 115 to 185 km wide is a shallow epicontinental sea. The Gulf results from foreland flexure and covers the Arabian shelf platform with shallow water depths (~35 m average depth and ~110 m maximum depth). Some small islands in the Persian Gulf are Hormuz salt plugs, partly fringed by the Neogene clastic and marine deposits and by recent coral reefs. The larger islands near the Iranian coast are gentle anticlines (Seibold and Vollbrecht, 1969; Kassler, 1973; Ross et al., 1986). The Persian Gulf does not seem to deform as much as the Zagros Mountains, which is consistent with the lack of seismicity. Lambeck and Chappell (2001) noted that the sedimentary record of the Gulf indicates that deposition was controlled by the tectonics and sea level changes during Quaternary glaciations. AMS ^{14}C ages indicate that the axial zone of the Persian Gulf experienced rapid flooding leading to the deposition of Holocene marls due to a combination of tectonic subsidence and a major glacial melt water pulse 9500–8500 years ago when sea level rose from ~50 to ~28 m (Lambeck and Chappell ; 2001). It suggests that the region of Gulf-Mesopotamian lowland has undergone regional subsidence disrupted by local uplifts. The rate of this subsidence, in contrast to the northeast side of the Persian Gulf, is much less. It was low enough that sedimentation has been able to keep up (Uchupi *et. al*., 1999).

3.2. Major Fault Structures

3.2.1 The Main Zagros Thrust (MZT) or the Zagros Suture

The original Arabia-Eurasia (Zagros) suture is also known as the Main Zagros Thrust (MZT). The MZT indicates a fundamental change in paleogeography, structure, sedimentary

history, morphology and seismicity (Berberian, 1995) (Fig. I-7). It marks the suture between the two colliding plates of the central Iranian active continental margin (to the northeast) and the Afro-Arabian passive continental margin (the Zagros fold-thrust belt to the southwest). It has a NW-SE strike from western Iran to the area north of Bandar Abbas, where it changes to a N-S trend (Minab Fault) and marks the boundary between the Zagros belt (to the west) and the Makran accretionary wedge and the active subduction zone (to the east).

3.2.2 The Main Recent Fault (MRF)

Part of the MZT in the NW Zagros known as the Main Recent Fault (MRF), (Tchalenko and Braud, 1974), a major seismically active right-lateral strike-slip fault with a NW-SE trend that more or less follows the trace of the MZT (Fig. I-7). Geodetic measurement in the Fars arc/Central Zagros indicate that the MZT in the SE is inactive there (Tatar et al. 2002). Based on earthquake focal mechanisms analysis (Talebian and Jackson, 2004), propose that oblique shortening is partitioned into right-lateral strike-slip on the MRF. This proposition is, however, not consistent with mechanical modelling of oblique convergence in the Zagros (Vernant and Chéry, 2006). Strike-slip movement from the MRF appears to be transmitted to the NS-trending right-lateral Kazerun and Karebass faults (Autemayou *et al*. 2006). Gidon et al. (1974) suggested right-lateral displacement of 10-60 km of a geological marker bed in the northwestern Zagros by the segments of the MRF. If slip began around Pliocene times (5 Ma) this displacement yields an average slip rate of 2-12 mm/yr (Berberian, 1995). The MRF is morphologically and structurally distinct along its entire length, and the component of right-lateral strike-slip motion between Arabia and central Iran takes place preferentially along different segments of the MRF in western Iran (Jackson, 1992). Earthquake mechanisms and seismic potential of the MRF are quite different from those of the earthquakes of the Zagros fold-thrust belt. Notably earthquakes of larger magnitudes than those within the Zagros Fold-Thrust belt have taken place along the MRF. Talebian and Jackson (2002) demonstrated that a right-lateral strike-slip offset of ~50 km on the Main Recent Fault is compatible with a restoration of the drainage, geological markers and the length of the pull-appart basins. They present evidence that show the offset may be as much as ~70 km. The configuration of active faulting and earthquake slip vectors today shows that this offset is geometrically linked to a shortening of ~50 km across the NW Zagros and to a total N-S convergence of ~70 km, which is a substantial fraction of the 85-140 km total Arabia-Eurasia convergence over the last 3-5 Myr (Talebian and Jackson, 2002).

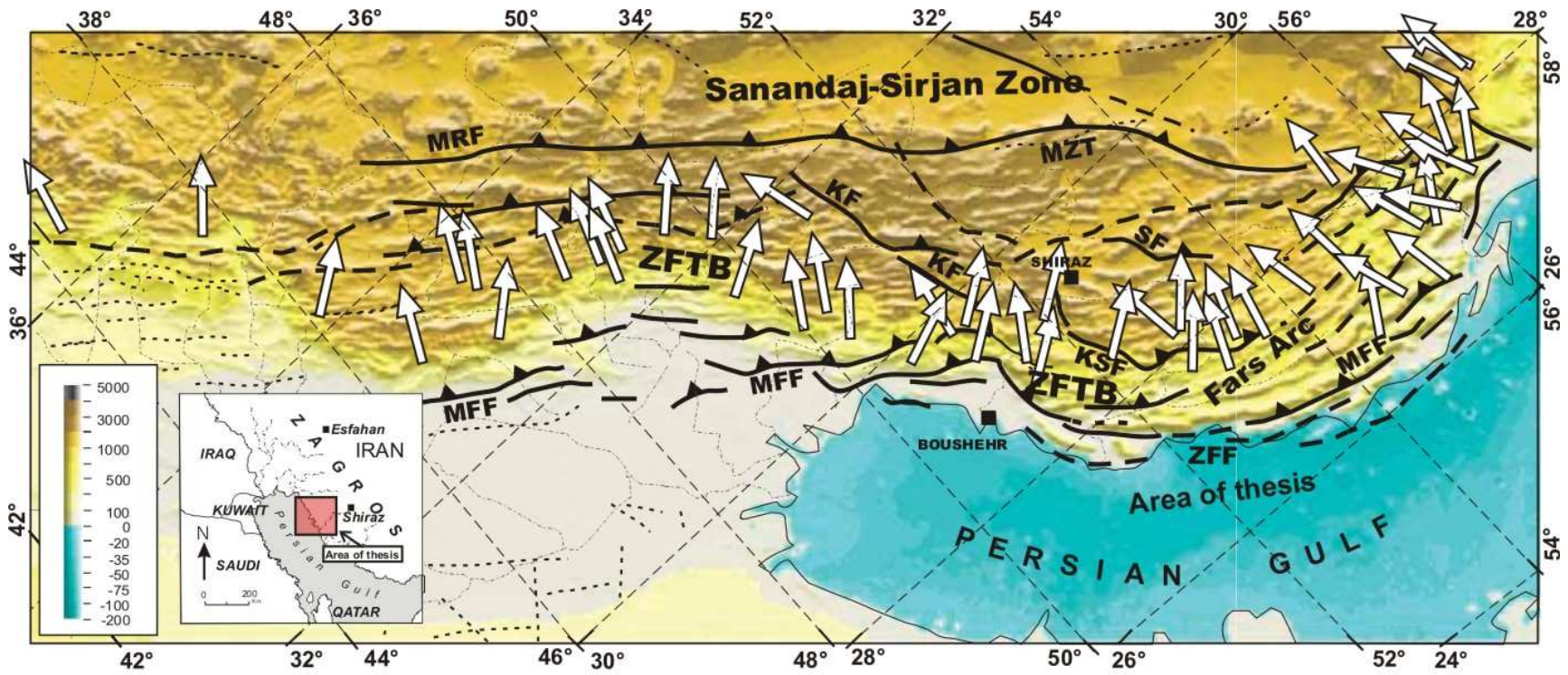

Fig. I-7. Map of master faults in the Zagros. MRF : Main Recent Fault. MZT : Main Zagros Thrust. KF : Kzerun Fault. KSF : Karebas Fault. FS : Sarvestan Fault. MFF : Mountain Front Fault. ZFF : Zagros Foredeep Fault. White arrows are the slip vectores from thrust or reverse faults (modified from Talebian and Jackson, 2004).

3.2.3 The High Zagros fault (HZF)

The HZF (the southern boundary of the thrust zone of Berberian and Tchalenko, 1976) separates the thrust belt of the High Zagros or Zagros Imbricate Zone (to the northeast) from the Simply Folded belt (to the southwest) (Fig. I-7). The High Zagros is up-thrusted to the southwest along discontinuous segments of the HZF (Berberian and Qorashi, 1986). Geological evidence, based on the present position of the Paleozoic rocks (Huber, 1977) demonstrates vertical displacement along the HZF to be more than 6 km. The Hormuz Salt is intruded along different segments of the HZF, locally reaching the surface. This indicates that the HZF is a deep-seated fault, cutting the Lower Cambrian Hormuz Salt horizon, and its activity extends through the Phanerozoic sedimentary cover (Berberian, 1981). Wedging of the post-Asmari deposits (Miocene Gachsaran evaporites together with the Lower Miocene to Pleistocene Aghajari-Bakhtiari synorogenic molasse) towards the High Zagros (James and Wynd, 1965; Falcon, 1974; Huber, 1977), suggests uplift of the High Zagros along the HZF since the Early Miocene, contemporaneous with subsidence of the Zagros Foredeep and deformation and outward migration of the Zagros basin. In the Khurgu area, north of Bandar Abbas in the southeastern Zagros, the HZF reaches the Mountain Front fault (MFF), and to the northwest of this intersection, it diverts from the MFF and becomes parallel to the Zagros suture (MZRF).

3.2.4 The Mountain Front fault (MFF)

The MFF [approximately the mountain front flexure of Falcon (1961) and the Mountain Front of Berberian and Tchalenko (1976)], marke a clear major topographic step and is a segmented major blind thrust fault with a clear structural, topographic, geomorphic and seismotectonic expression (Figs. I-7 and I-9). This fault zone subdivides the Simply Folded Belt and has exerted a major control on sedimentation of the Zagros foreland basin since early Tertiary times [e.g. Sepehr and Cosgrove, 2004; Sherkati and Letouzey, 2004]. Pronounced subsidence of the Zagros Foredeep and the Dezful Embayment, as indicated by thickening of the post-Asmari deposits (Neogene Gachsaran Evaporites and the Aghajari-Bakhtiari synorogenic molasse), provides evidence of relative motion along the MFF and the Dezful Embayment fault since Early Miocene times. Geological evidence, based on the present position of the top of the Asmari Formation from stratigraphic, seismic and borehole data (Falcon, 1974; Huber, 1977; Berberian, 1986, 1989), demonstrates that vertical

displacement along this thrust is more than 6 km. The southwestern edge of the Zagros Simply Folded Belt is being uplifted mainly along the underlying MFF and the frontal asymmetric surface folds associated with it. Evidence for active surface uplift is provided by terraces related to the incised river system. The MFF is composed of discontinuous, complex thrust segments of 15-115 km length, with a total length of more than 1350 km in Iran (Fig. I-7). The fault segments at depth, together with their contiguous asymmetric folds at the surface, are separated by gaps and steps in the observed topographic and morphotectonic features. They form two broad arcs in Fars (the southeastern Zagros) and Lorestan (the northwestern Zagros), and are arranged in left- and right-stepping en échelon pattern at the eastern and the western sides of these two arcs respectively (Fig. I-7). The MFF is a major topographic front. It is marked at the surface by the 500 m contour east of the Kazerun-Borazjan transverse fault in Fars province and west of the Kabir Kuh in Lorestan province to the north-west (Fig. I-7). It follows the 1000 m contour south of the Bakhtiari culmination (north of the Dezful Embayment) between the Kazerun-Borazjan active fault to the east and the Kabir Kuh anticline in the west (Berberian, 1995).

3.2.5 The Zagros Foredeep fault (ZFF)

The ZFF separates the Zagros Foredeep (to the north and northeast) from the Zagros Coastal Plain (in the south and southwest). It forms the northeastern edge of the alluvially covered Coastal Plain of the Persian Gulf and is principally a reverse-slip system (Berberian, 1995). The ZFF is discontinuous and runs roughly parallel to the MFF at an altitude of less than a hundred metres above sea level. Berberian (1995) proposed that this fault have been displaced for about 150 km right-laterally by the Kazerun-Borazjan strike-slip fault; however, there are not geomorphic markers to show an active component of strike slip movement. As with the MFF, displacement was accompanied by an increasing surface expression of the ZFF in the area west of the Kazerun-Borazjan fault. In this area, the ZFF constitutes the southwestern limit of the Dezful Embayment and is expressed at the surface by segments of thrust faults cutting the southwestern inverted limbs of anticlines. Earthquakes associated with reactivation of this blind fault are indicated in Fig. I-9.

3.2.6 The Kazerun-Borazjan fault (KF)

The Kazerun fault is seismically active at the present day, with sesimicity indicating right lateral movement in the Precambrian basement (Berberian, 1995). It trends N-S fault cross the ZFB causing bending, dragging and offsetting of the fold axes in a right-lateral sense. The fault consists of two right-stepping segments : the Kazerun fault to the north and Borazjan fault (considered as a tear segment of the MFF in this thesis) in the south, with a gap in between (Berberian, 1981). Berberian (1995) suggested that a cumulative right-lateral displacement of 140 and 150 km of the Zagros Mountain Front (MFF) and the Zagros Foredeep faults (ZFF) can be measured, respectively, along the Kazerun-Borazjan fault. He proposed an average slip rate of 14.5 mm/yr, if slip began after deposition of the Lower Miocene Gachsaran Formation (around 10 Ma). The fault is clearly visible on the aeromagnetic map of the region as a sharp magnetic lineament. Movement along the Kazerun Fault can be traced back to the Cambrian, when it controlled the distribution of the Hormuz salt (e.g., Talbot and Alavi, 1996). The region to the east of the Kazerun Fault (the Fars region) contains more than 100 Hormuz salt diapirs emerging at the surface. However, this salt formation, which is probably between 1 and 2 km thick, does not exist to the west of the fault zone in the Dezful Embayment, as indicated conclusion is supported by the fact that no Hormuz salt diapirs are found to the west of the Kazerun Fault, even on seismic profiles, and no Hormuz salt has been encountered in any of the hundreds of wells which have been drilled in this region. Berberian and Tchalenko (1976) proposed that the KF that is located along a line marking the projected continuation of the Qatar Peninsula into Iran. Authemayou et al. (2005) suggest that the KF, as a system of active right-lateral strike-slip faults, has propagated southwestward from the MRF toward the main Arabian indenter due to anticlockwise rotation of Arabia. They propose an important role for the KF and assosiated faults in transmitting and distributing of partitioned strike-slip motion of oblique plate covergence.

3.2.7 The Karebas (KBF) strike-slip fault

The Karebas fault, with a total length of 160 km is situated about 65 km east of the Kazerun fault and 35 km west of the city of Shiraz. It is a nearly N-S-trending right-lateral strike-slip fault, which like the Kazerun fault, has dragged and displaced anticlinal axes for at least 10 km (M. Berberian and Tchalenko, 1976a). The Karebas Plain is a small pull-apart

depression (90-km^2) formed along the Karebass fault. Five large Hormuz salt domes have intruded along the fault. The southern segment of the Karebass fault turns toward the east to form the Surmeh thrust fault, chracterised by the only exposed lower Paleozoic anticlinal core in the Simple Fold Belt. No large earthquake has yet been directly associated with motion along the Karebass transverse fault.

3.3. Seismicity in the Zagros

The Zagros is one of the most important seismic regions between the Anatolian region and eastern Asia (Fig. I-8). Over 50 percent of teleseismically recorded earthquakes in Iran have occurred within the Zagros. Earthquakes occur throughout the 200-300 km width of the belt with an abrupt limit in the northeast (Fig. I-9), roughly coincident with the Main Zagros Fault. Early seismic studies of the Zagros Mountains in southwestern Iran found evidence of seismicity at upper mantle depths (depper than 50 km in the Internatioal Seimological Centre (ISC) or US Geological Survey (USGS) catalogues), indicating the occurrence of brittle deformation in the upper mantle. These have been used to postulate subduction of the

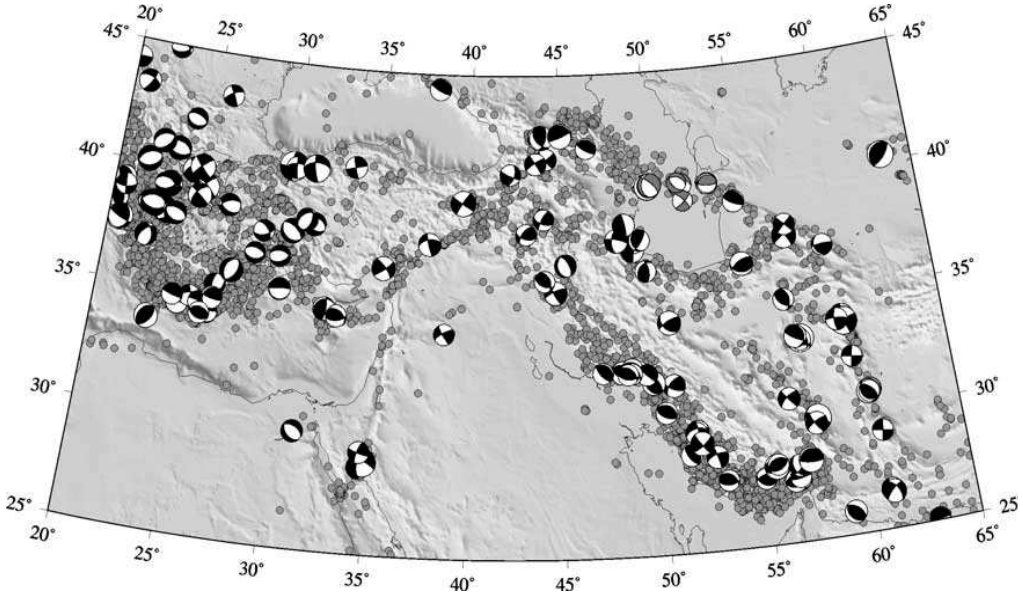

Figure I-8. Best-double-couple CMT solution (Iran and Anatolian region) from the Harvard catalogue for earthquakes with depth ≤30 km, Mw ≥ 5.5 and double-couple component ≥70%, in the interval 1977–2001. Focal mechanisms in gray in the Caspian Sea are for earthquakes deeper than 30 km and are taken from Jackson et al. [2002]. Epicenters are from the catalogue of Engdahl et al. [1998]. Earthquakes deeper than 30 km associated with the subduction zones in the Makran and Hellenic Trench have been omitted. From Allen *et. al.* (2004).

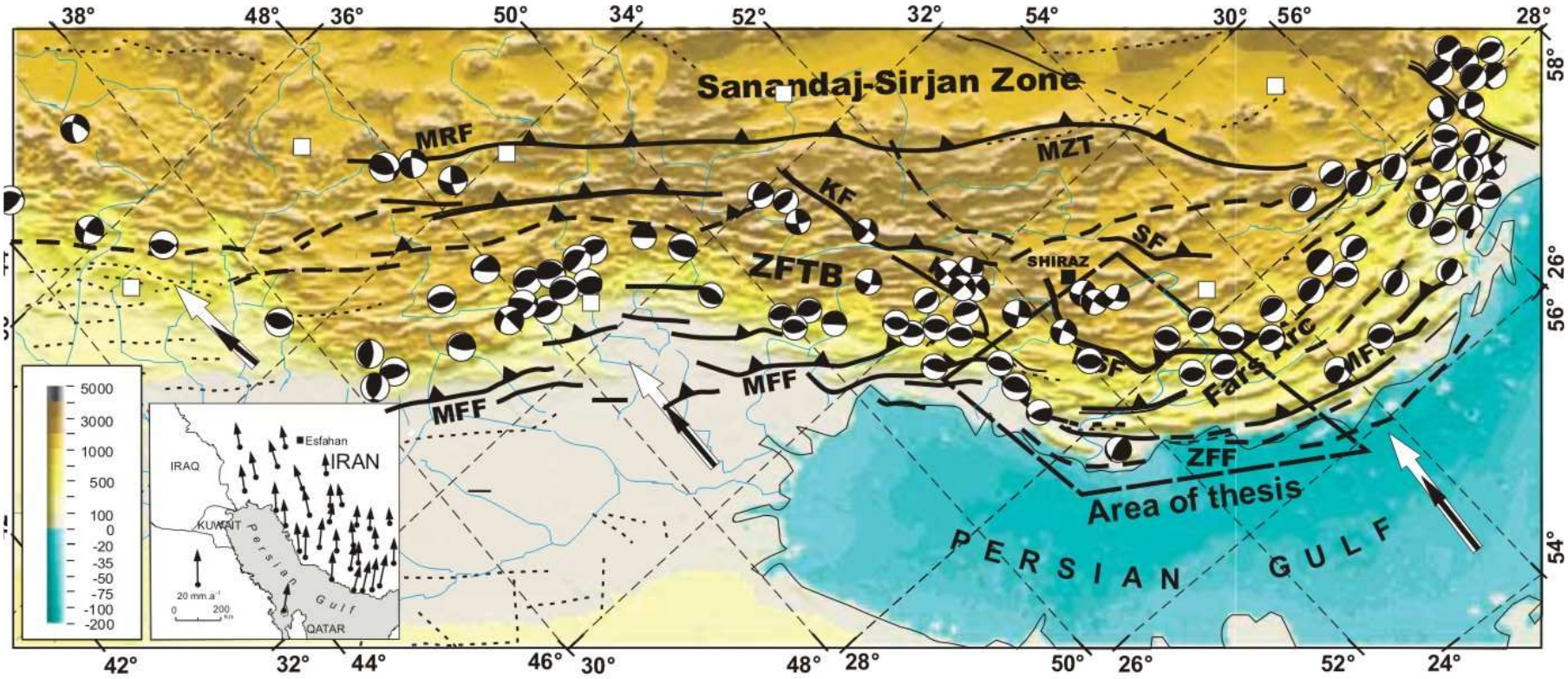

Fig. I-9. Map of fault plane solutions in the Zagros (modified from Talebian and Jackson 2004). Arrows are the directions and rates of the overall Arabia-Eurasia motion from De Mets et al. (1994, big arrow) and Sella et al. (small arrow). (Source of physical map : GEBCO data). The withe arrow shows NUVEL-1A plate motion relative to Eurasia. Inset in left panel show present-day shortening rates and direction ina Eurasia-fixed reference frame for the period 1998-2001.

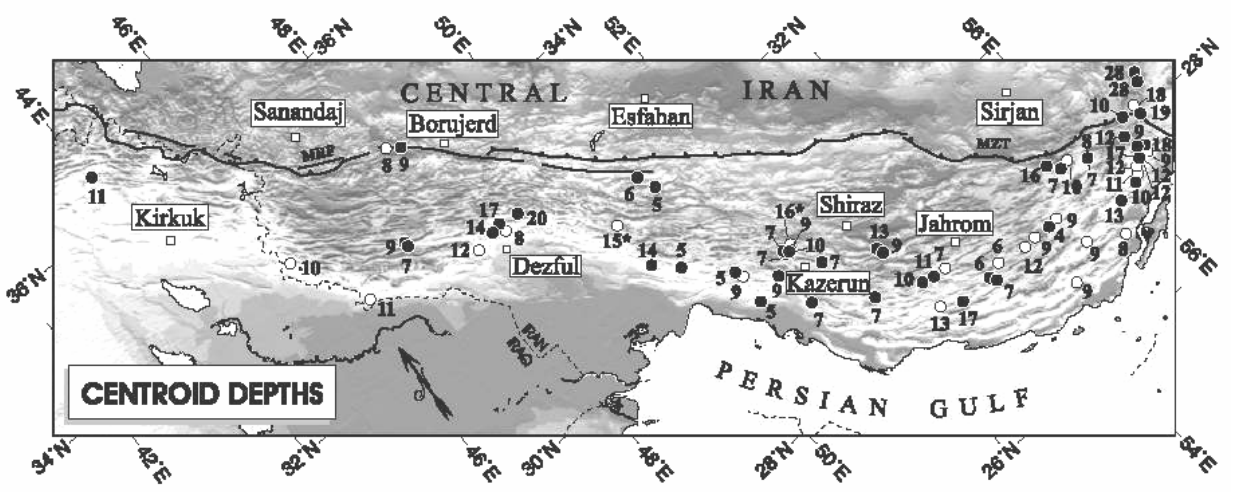

Figure I-10. Earthquake centroid depths determined from waveform modeling (Talebian and Jackson, 2004). Numbers are depths in km. Black circles are those determined from long-period P and SH waves. Open circles are those determined from P waves alone.

continental Arabian shield beneath the Zagros (Nowroozi 1971; Haynes & McQuillan 1974; Bird et al. 1975; e.g. Moores & Twiss 1995). Recent recalculations of source depths of earthquakes at teleseismic distances, however, have found no evidence of seismicity within the upper mantle beneath the Zagros Mountains. Neither local seismograph networks, nor the modelling of teleseismic body waves from the larger earthquakes have found any focal depths deeper than 15-20 km (e.g. Jackson & Fitch 1981; Ni & Barazangi, 1986; Baker *et al*. 1993; Maggi *et al.*, 2000a). Maggi et al. (2000a) investigated three large earthquakes and showed that they were all shallow (10-15 km). They proposed that there was no evidence for any earthquakes deeper than about 20 km in the Zagros; a recent study (Talebian & Jackson, 2004) confirms this view. Thus there is no evidence, at least in the form of sub-crustal earthquakes, for continuing subduction of Arabia beneath Iran. Most teleseismic determinations of focal mechanisms in the Zagros show reverse faulting with strikes parallel to those of the local fold axes. Talebian and Jackson (2004) show that seismicity appears to be confined to the upper half of the crust through the Zagros, which is a result also found by microearthquake surveys (e.g. Tatar et al., 2004). The centroid depths (Figs. I-10 and I-11), are compatible with the majority of earthquakes occurring in the basement beneath the sedimentary cover.

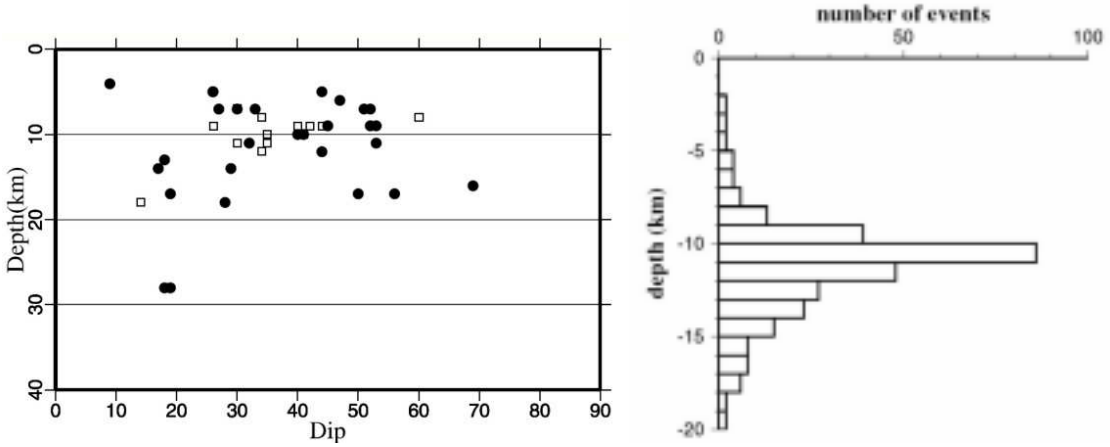

Figure I-11. (Left) a plot of the dips of north dipping nodal planes for reverse and thrust earthquakes against their centroid depths (after Talebian and Jackson, 2004). Black circles are events constrained by P and SH modeling. Open squares are those constrained by P waveforms alone. The aim of this plot was to see whether the deeper events had shallower dips, as might be expected if the steeper nodal planes were fault splaying off deeper, detachment. (Right) histogram of the depth of the relocated events showing that most seismicity is located between 8 and 14 km, and therefore likely beneath the sedimentary cover (Tatar et al., 2004). Note different depth scales between the two plots.

3.4. Geodetic (GPS) measurements

The shortening that results due to collision between Arabia and Eurasia is distributed on the whole region from Persian Gulf to the Caspian Sea. Two main types of mechanisms are considered to absorb this shortening: 1) intra-continental shortening which manifests itself in the form of chain of mountains and 2) big indentations. Due to ongoing process of Tertiary collision (e.g. Tatar at al., 2004; Allen et al., 2004; Regard et al, 2004; Vernant et al., 2004), between the Arabia and Iranian, both types of shortening are active. Such ongoing process accounts for the folding, thrusting and large-scale strike-slip faulting associated with crustal shortening in the Zagros. The GPS measurements of 1999–2001 in Iran (Vernant et. al., 2004) and northern Oman provide new velocity data to quantify the present-day plate motions in the Middle East. Their results show that GPS velocities along the northeastern boundary of the Arabian Plate relative to Eurasia are systematically smaller than the NUVEL-1A estimations (about 10 mm/year less). Sites on the Central Iranian Block move in a coherent fashion, as predicted by Jackson & McKenzie (1984), with internal deformation smaller than 2 mm/year.

Geodetic measurements (Tatar et al., 2002) indicate that the total present–day shortening across the central Zagros mountain belt is about 10 mm/yr, in a NNE-SSW

direction. Shortening across the Zagros therefore accomodates about 50% of the total 21 mm/yr convergence between Arabia and Eurasia as deduced from the IGS stations. Nilforoshan et al (2003) proposed ~2.5 cm/year NS shortening from Arabia to Eurasia. The subduction velocity beneath the Makran is ~1.8 cm/year and decreases toward the west. Nilforoshan *et al.* (2003) show that the transition from subduction (Makran) to collision (Zagros) is very sharp. In the eastern part of Iran, most of the shortening is accommodated in the Makran, while in the western part shortening is more distributed from South (Zagros: ~0.8 cm/year) to North (Alborz: ~0.8 cm/year). GPS measurements and analyses of the 1998, 1999 and 2001 campaigns (Hessami et. al., 2006) indicate that the current rate of shortening across the SE Zagros is 9 ± 3 mm/year, whereas in the NW Zagros it is 5 ± 3 mm/year. The GPS velocities also indicate that shortening is not distributed homogeneously along or across the belt. In the NW Zagros (west of the Kazerun Fault) shortening is accommodated mainly along

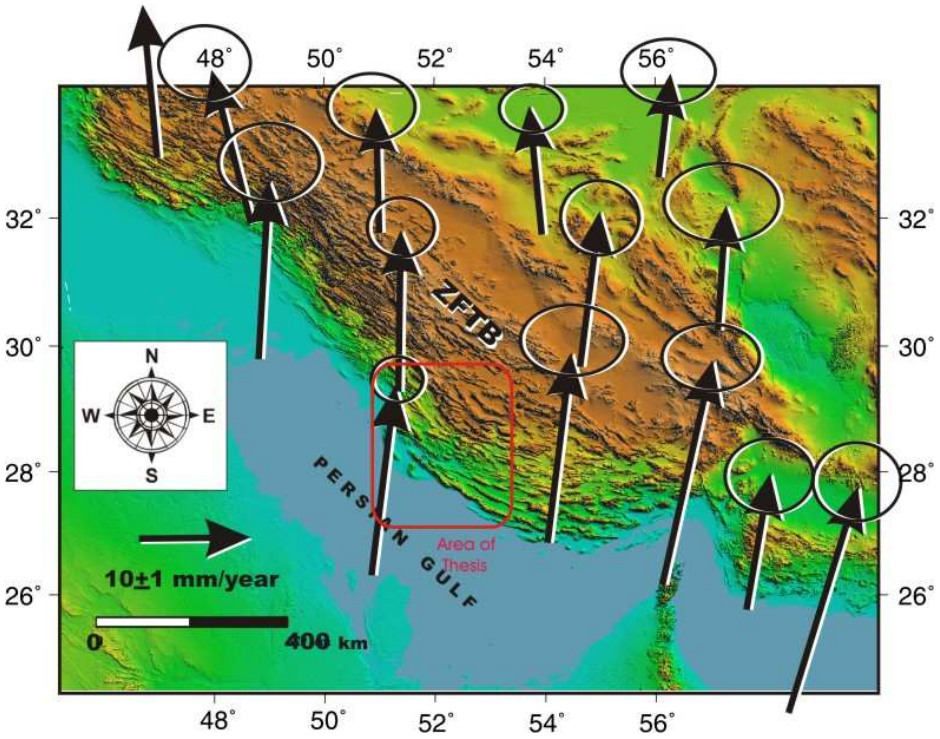

Figure I-12. horizontal GPS velocities (in Eurasia-fixed reference frame) for the Zagros Fold-Thrust Belt (modified after Vernant et al., 2004). To avoid clutter some sites have been removed.

the Mountain Front Fault, where most of the major earthquakes occur, and along the Zagros Front. The geodetic data suggest that the Main Zagros Reverse Fault, which is the main structural boundary between Arabia and Central Iran at the west of the Kazerun Fault, is currently inactive. But east of the Kazerun Fault, however, most rapid shortening seems to

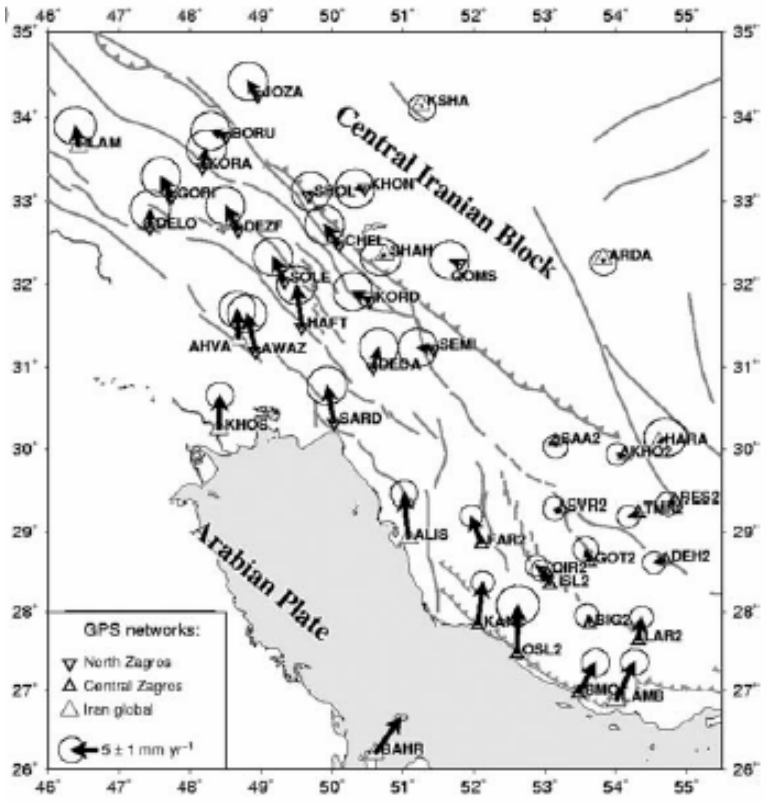

Figure I-13. (a) North Zagros and Central Zagros velocity fields with respect to the Central Iranian block. The error ellipses indicate formal errors within a 95 per cent confidence interval. The different networks (North Zagros, Central Zagros and Iran Global) are marked with different symbols. A different velocity field is present on both sides of the Kazerun fault system. From Walpersdorf *et. al.* (2006).

occur along a zone of active thrusting within the SE Zagros and along the old suture zone (Main Zagros Reverse Fault), both areas where seismicity is concentrated. Along the Zagros, the Karebass and Sabzpushan strike slip fault zones appear to contribute to the total active deformation that affects the central Zagros. The along-strike extension of the Zagros belt across the Kazerun and Karebass faults implies that the deformation in this mountain belt is not accommodated by simple across-strike shortening and thickening.

Based upon GPS measurements, Walpersdorf *et. al.* (2006) have estimated 6±2 mm/year present-day displacement rates (maximum value inferred across the whole Kazerun strike-slip fault system) and 2 mm/year (restricted to the Kazerun fault *sensu stricto*). They mention that the northern region of the Zagros is not deforming relatively to the Central Iranian block is spread over a larger zone, and the shortening is more concentrated along the coast of the Persian Gulf (Fig. I-13).

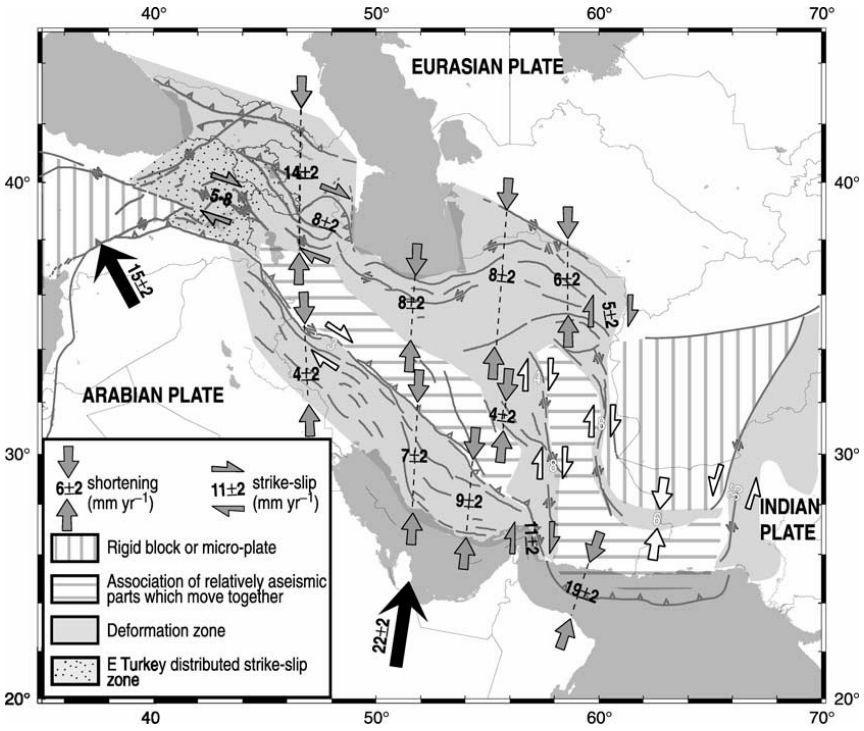

Figure I-14. Schematic illustration of the main GPS results (Vernant et. al., 2004). Hatching shows areas of coherent motion, grey zones are actively deforming areas (see legend). Heavy arrows in black indicate the present-day motion of the Arabian plate relative to Eurasia. Grey arrows are deformation rates directly measured with GPS. Rates in eastern Turkey are deduced from McClusky et al. (2000). White arrows are deduced rates from GPS, geological evidence and seismology. All the rates are given in mm yr-1. From Vernant *et al*. (2004).

3.5. Crustal and lithospheric structure

The crustal and lithospheric geometry of the Zagros Mountains, which have been constrained by geophysical studies, suggest that the Zagros Mountains are underlain by a crustal root with maximum depths to Moho of ~45–50 km. This geometry was confirmed by gravity data (Dehghani & Makris 1984, Snyder & Barazangi 1986), seismological information (Hatzfeld et al. 2003) and mantle tomography (Paysanos & Walter 2002). The Moho depth map of Iran (Dehghani and Makris, 1984 ; Fig. I-15), shows a 50-55 km thick crust along the HZ (the northeastern margin of the belt). This gradually thins out towards the southwest, to about 35 km thick crust along the Zagros foredeep at the northern shorelines of the Persian Gulf. P-wave amplitude ratios (Al-Amri & Gharib 2000) and gravity modelling (Snyder & Barazangi 1986) suggest 40 km depth to Moho underneath the Persian gulf. The Bouguer gravity map of Iran (Dehghani and Makris, 1984), shows anomalies of -220 to -230 mgal along the MZT which increase to -50 to -60 mgal along the Persian Gulf

coast. According to Berberian (1981), a thicker crust along the High Zagros could be due to the fact that this marginal belt has undergone two major collisional orogenies during the Late Cretaceous and the Late Miocene-Pleistocene times. Molinaro et al. (2004) proposed a lithospheric model based on a combined interpretation of gravity, geoid and topography data. This model predicts a Moho depth of 52 km beneath the Zagros, similar (although toward the high end) to those proposed by previous authors. Their model suggests a thinned lithospheric mantle below the crustal root, which they attribute to recent slab break-off. They suggested

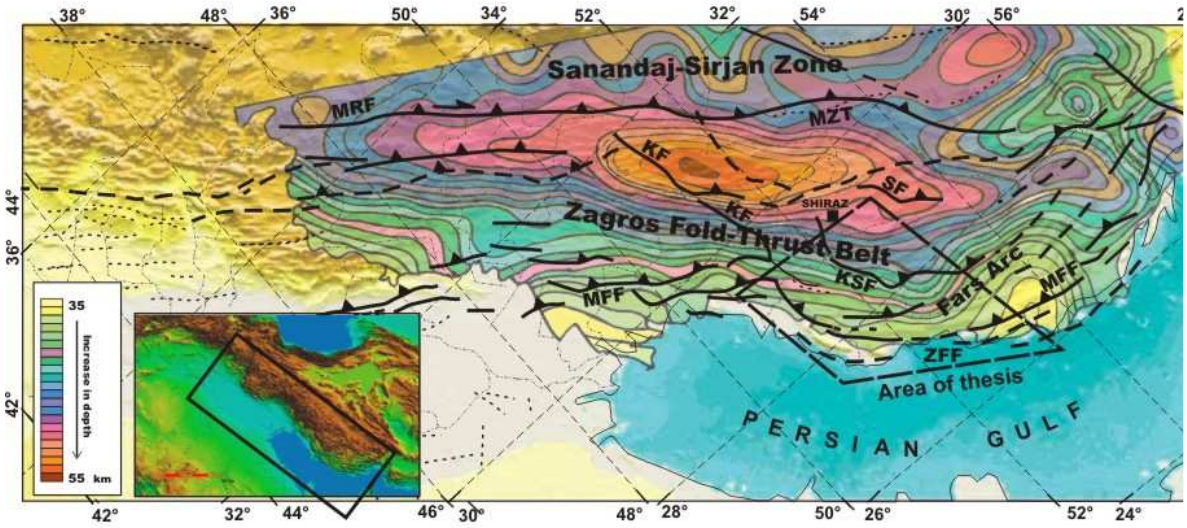

Figure I-15. Gravimetric Moho depth map (modified after Dehghani and Makris, 1983). Isolines in km ; contour interval 1-km.

that thermal uplift and surface erosion generated by this event likely modified the orogenic wedge taper in Zagros and triggered the involvement of deeper levels of the crust in the deformation. The sudden and widespread occurrence of Plio-Pleistocene Bakhtyari conglomerates could be the sedimentary marker of this major change in tectonic regime.

Bijwaard and Spakman (2000) and Bijwaard et al. (1998) show a pronounced negative velocity anomaly through the lithospheric structure beneath Central Iran and extending below the Zagros using global tomographic models (Fig. I-16). They suggest a relatively warm and thin lithospheric structure in this region.

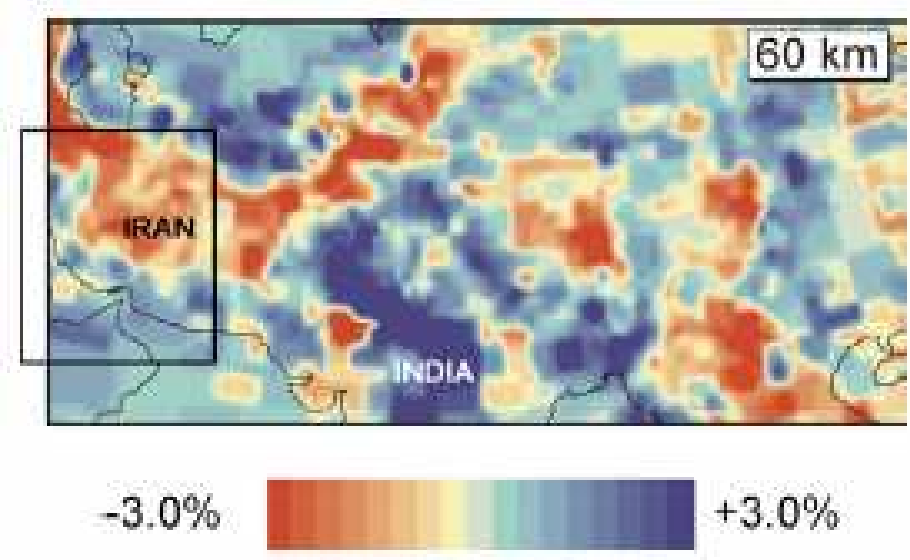

Figure I-16. Tomography layer section of the Indian and Iranian regions at 60 km depth, modified after Bijwaard & Spakman (2000).

3.6. Structure of the Zagros belt

3.6.1 Introduction

The Zagros orogen is known for the spectacular fold structures that affect its thick sedimentary cover [e.g., Farhoudi, 1978; Letouzey *et al.*, 1995] with widely distributed resistant limestone anticlines displaying the large-scale "whale backs" that characterize the morphology of the region. The large-scale morphology of the Zagros fold–thrust belt (characterised by a topographic step at the MFF), appears to be a function of pre-existing basement structures. If so, basement deformation within the Zagros has important implications for both the timing and style of deformation through the fold–thrust belt. It is well known that several tectonic movements involving the basement affected the Zagros platform before the Neogene (Stocklin, 1968; Berberian and King, 1981; Koop and Stoneley, 1982; Sherkati and Letouzey, 2004). Basement faulting during Permian-Triassic Neo-Tethys rifting has played an important role in salt dome initiation and distributing of deformation through the ZSFB and HZ. Many of the major faults in the Zagros have been attributed to reactivation of those basement faults (Jackson 1980). The basement in most of the Zagros has been considered as a continuation of the Pan-African rocks exposed in the Arabian Shield and is segmented into blocks by the same faults (Bahroudi and Talbot, 2003). In general,

basement deformation in fold–thrust belts typically falls into two categories (Yonkee and Mitra, 1993) :

1- Thick-imbricate thrust sheets with relatively steeply dipping faults (30–60°) that accommodate small (1–5 km) offsets; and

2- Thin-imbricate thrust sheets that are transported several tens of km along regional décollements, the basal décollement typically being the brittle–ductile transition zone.

3.6.2 Stratigraphy and major decoupling surfaces

The Zagros fold and thrust belt consists of a thick sequence of sediments with widely varying competence. The base of the Zagros sedimentary sequence, particularly in the Fars region, is promed by the thick (1–2 km) Cambrian Hormuz salt, which acted as the major detachment during the Late Tertiary deformation. Other detachment horizons, such as the Triassic Dashtak Formation (evaporite), the Cretaceous Kazhdumi Formation (shale) and the lower Miocene Gachsaran Formation (evaporite), occur in the sedimentary pile (Fig. I-17). The existence of these décollement horizons allows decoupling of the deformation between the basement and cover and between different units within the cover sequence and plays an important role in controlling the pattern and distribution of deformation [e. g. Sepehr and Cosgrove, 2004]. Within the sedimentary succession of the area studied in this thesis, both the Eocambrian Hormuz evaporites and the Miocene Gachsaran salt layers influence the structural style (Fig. I-17 & 18).

Earthquake focal mechanisms through the belt show that the basement is currently uplifted stepwise toward the north over the major ramps, but the restoration of the transects shown in Figure I-9 indicates that with wathever form of basement deformation, a very mobile medium (Hormuz Salt) is required to maintain a constant structural high over the width of the fold–thrust belt by dampening out the amplitude of the basement folds (McQuarrie, 2004). In contrast, Neogene gypsum and marls of the Gachsaran Formation play an important role by decoupling thin-skinned deformation within Neogene-Quaternary sediments from lower portions of the rock cover (e. g. this work). So there is a discrepancy between basement and cover shortening, due to presence of such basal décollement in the Lower Paleozoic series.

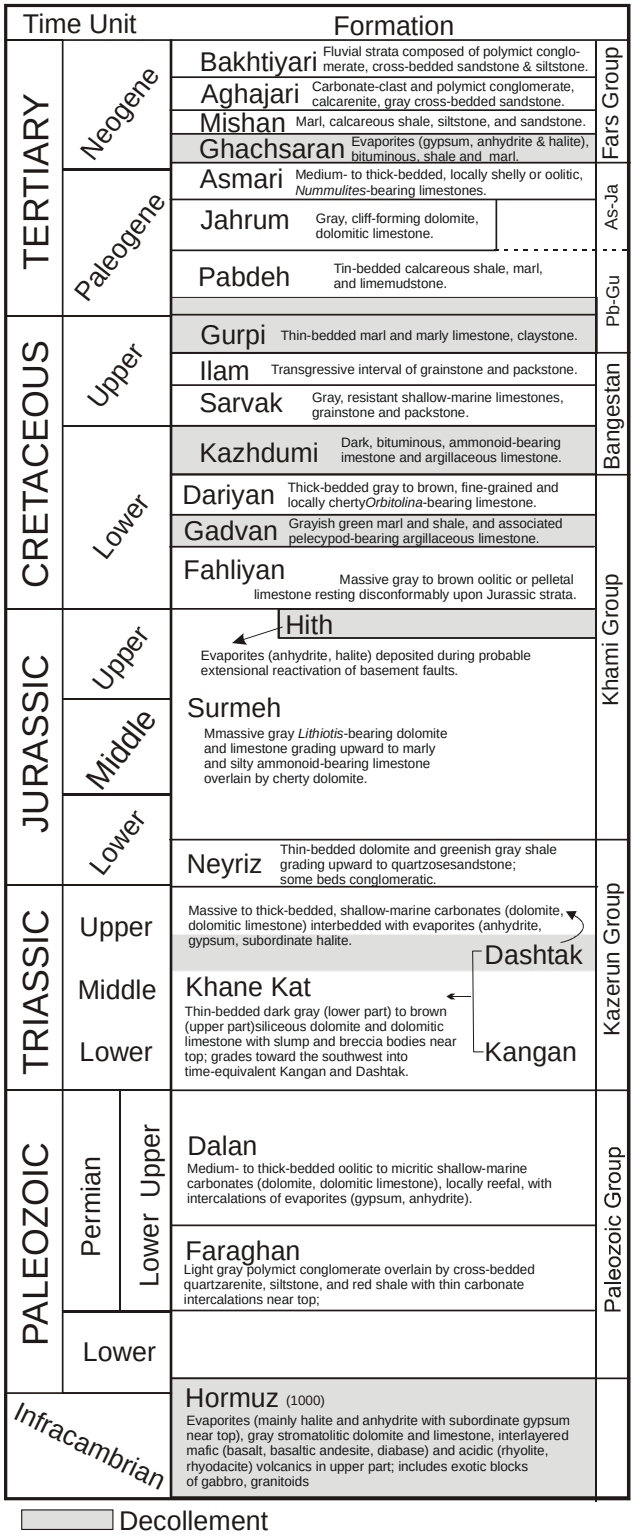

Figure I-17. Regional stratigraphic column of the cover rocks showing major decoupling horizons.

Hormuz Salt (Lower detachment level)

The Hormuz series was deposited in the Persian Gulf and Zagros areas in latest Proterozoic-Lower Paleozoic times. Throughout the Zagros belt this unit cropps out only as allochthonous salt plugs. Within the Persian Gulf, circular structures are thought to be draped over deep pillows of Hormuz salt (Edgell, 1996). Deposition of the Hormuz salt was followed by a long period of remarkable tectonic quiescence from the Palaeozoic until the middle Cretaceous. A Late Proterozoic to Early Cambrian age was attributed to this series (Kent, 1958), and this age has been confirmed for the equivalent Ara Formation in Oman (Konert *et al*., 2001; Jeroen *et al*., 2003). The Hormuz evaporites mainly consist of halite and anhydrite with subordinate gypsum near the top. The Upper part of the unit comprises gray dolomite and limestone, and red fluvial siliciclastics (polymict conglomerate, sandstone, siltstone, shale) with interlayered mafic (basalt, basaltic andesite, diabase) and acidic (rhyolite, rhyodacite) volcanics. U-Pb zircon dating provides an age of ~547 Ma for exotic blocks of gabbro and granitoids within the unit (Ramezani and Tucker, 2003). Other exotic blocks are metamorphic rocks (slate, phyllite and schist) presumably derived from the underlying

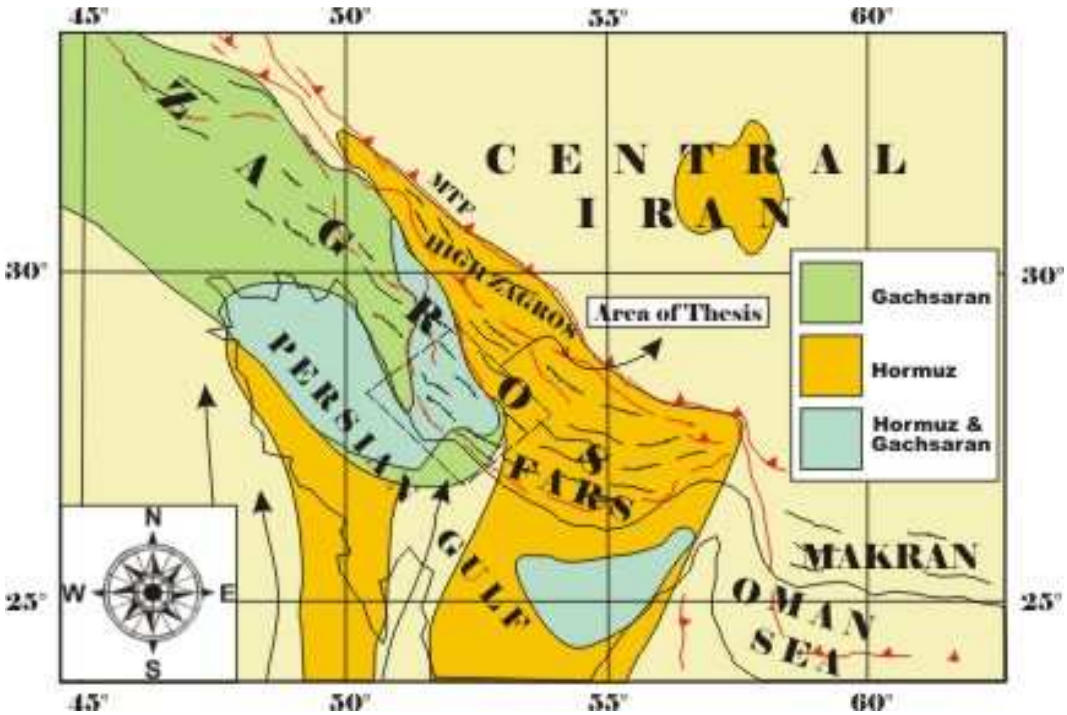

Figure I-18. The distribution of the Eocambrian Hormuz evaporites and the Miocene Gachsaran salt layers though the ZFTB. Both these units influence the distribution of deformation and structural style (modified after Sherkati and Letouzey, 2004).

basement. Some volcanic rocks present as inclusions in the salt plug of Hormuz Island were radiometrically dated and attributed to the Permian-Triassic boundary (Eliassi *et al*., 1977).

The old seismic data in the Zagros Simply folded belt does not usually clearly image the Hormuz salt series, or the deep décollement level (Letouzey & Sherkati, 2004). Low basal friction above the salt could explain the observed free development of fore-thrusts and back-thrusts without any preferred vergence (Letouzey *et al*., 1995). It would suggest that the symmetry of numerous detachment anticlines in the Zagros results due to the action of the Hormuz salt as a basal décollement level. The Hormuz salt is believed to fill the core of each anticline. However, recent studies of the Zagros fold belt show the effect of intermediate décollement levels in folding (Letouzey *et al*., 2002; Sherkati and Letouzey, 2004). The effect of the Hormuz salt is to reduce the frictional resistance at the base of the cover sequence to the east of the Kazerun Fault compared to the west, resulting in a relatively low taper angle of the fold belt in the Fars region and a relatively high taper angle to the west of the fault [Talbot and Alavi, 1994; Bahrudi and Koyi, 2003; McQuarrie, 2004], where the salt layer is absent or much thinner.

Gachsaran Formation (Upper detachment level)

The Miocene Gachsaran formation generally covers the anticlines and is composed of marls, anhydrite, thin limestone and locally large quantities of salt. Disharmonic features in this level are well imaged by seismic data. This formation has been identified as a level of décollement and disharmony by previous workers (ColmanSadd, 1978; O'Brien, 1950). Based on some seismic evidence, Sherkati et al. (2004) suggest that it is likely that large thrust faults climb from the basal décollement in the Lower Palaeozoic to Triassic evaporites, up to the Miocene Gachsaran Formation.

3.6.3 Structural models of the Zagros belt

Some general sections of the Zagros fold belt have been proposed in recent papers [Berberian, 1995; Blanc *et al.*, 2003; McQuarrie, 2004; Sherkati and Letouzey, 2004]; however, aspects such as the kinematics of individual folds, the sequence of fold and thrust development, the relationship between fold and fault deformation and the evolution from symmetric detachment folds to asymmetric fault-related folds remain to be investigated. At the base of the sedimentary cover, Lower Cambrian [Berberian, 1995] incompetent Hormuz

series directly overlie the crystalline basement as a basal detachment level and play an important role in guiding the deformation. This lower detachment level (~1000 m salt) beneath the thick sedimentary layers (~10 km), completly decouples shortening within the cover rocks from shortening within the basement. The stratigraphic succession of rock series with highly variable mechanical properties strongly controls deformation in the ZSFB [e.g., Sherkati and Letouzey, 2004]. Bahroudi and Talbot (2003), proposed a model for the structural configuration of the basement of the Zagros Basin. They used geophysical and isopach maps of the Zagros Basin to demonstrate the comprehensive reactivation of the main basement structures. The model confirms that the basement of the Arabian Plate has exhibited heterogeneous tectonic activity since the opening of Tethys in Permian times. Since then it has been divided into two mega-blocks an active East Arabian-Zagros Block, and a passive block. The East Arabian-Zagros Block is characterised by a sedimentary and tectonic history complicated by repeated reactivation of old basement structures. Bahroudi and Talbot (2003) attribute the arcuate shape of the Zagros belt east of the Kazerun fault to the reactivation of basement blocks beneath a cover decoupled in a patchwork pattern by the ductile décollement of Hormuz salt. Geologic studies have shown that some broad, equal-amplitude fold trains through the Zagros occur over basement platforms with little to no topography (Laubscher, 1986). Wallace and Hanks (1990) proposed that basement duplexing within the Zagros commonly imparts a structural topography (structural highs over basement highs) to the overlying detachment folds. The topographic steps accompanied by the progressive northeastward thinning of the Mio-Pliocene units filling the synclines require that the depth of the base of the sedimentary sequence decrease to the northeast. Talbot and Alavi (1996), proposed normal faults and associated transfer zones for basement that pre-date the Paleozoic and younger platform sediments of the region, which perhaps formed through an early, extensional Proto–Tethyan event. The geometry of the proposed rift would mimic the geometry of the present day fold–thrust belt. Total shortening since ~5 Ma in the ZSFB is estimated to range between 50 and 80 km [Blanc *et al*, 2003; McQuarrie, 2004]. Hessami *et al*.(2001) based on the recognition of local syn-folding unconformities have proposed that folding started at the end of the Eocene and migrated progressively in-sequence southwards.

Most teleseismic determinations of focal mechanisms in the Zagros show reverse faulting with strike parallel to those of the local fold axes. Jackson (1980), observed that dips of nodal planes are typically in the range 30-60°, similar to that observed for active normal faults worldwide, and suggested that today's reverse faulting earthquakes occur on reactivated normal faults derived from the Paleozoic-Mesozoic extension of the Arabian margin. In the

case of the Zagros, this reactivation mechanism remains speculation, although it has now been demonstrated elsewhere (e.g. Badley *et al.* 1989).

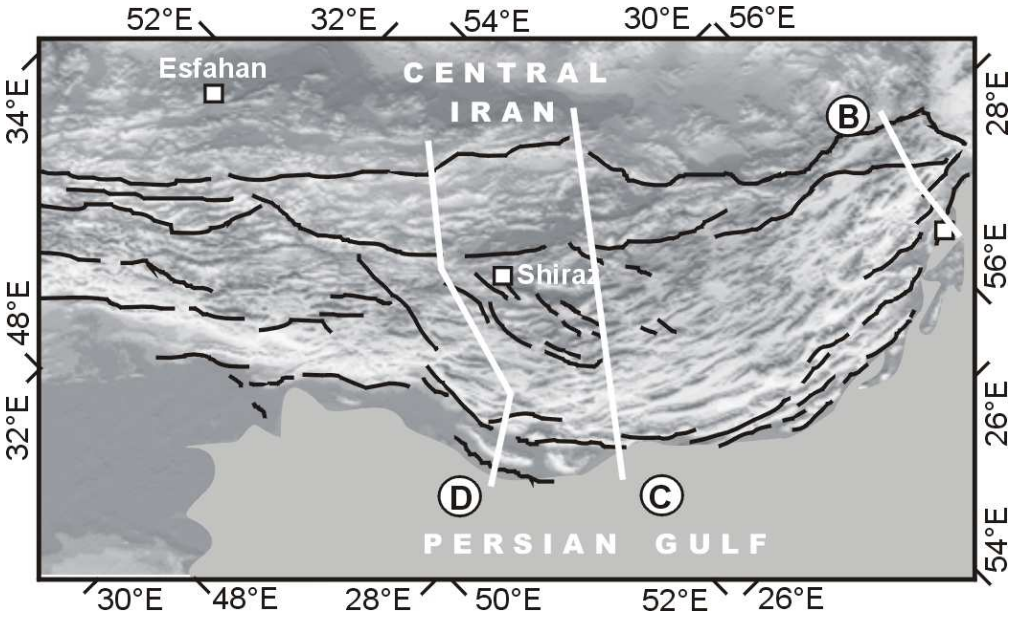

Figure I-19. The paths of the structural cross-sections; B: Molinaro *et. al.* (2003); C: MaQuarrie (2004) ; D: Sherkati and Letouzey (2004).

Hatzfeld *et al*. (2003) used arrival times of local events recorded on a dense seismological network to infer the upper-crust velocity structure for the central Zagros. They proposed 11 km thick sedimentary layer and a 8 km thick upper crystalline crust. These estimates, although obtained with a small amount of data, are the first quantitative seismological estimates in the central Zagros. Hatzfeld *et al*. (2003) suggest that the total thickness (~35 km) of the crystalline crust therefore looks similar to the thickness of the stretched margin of the Arabian Platform. Therefore the shortening of the Zagros basement may be small and has only started recently, whereas the shortening recorded by the folded sediments is due to the long-term scraping of the sediments above the basement.

The micro seismicity within the Central Zagros, which was surveyed by Tatar *et. al*. (2004), is spread over the width of the Zagros and is not confined to a single blind-fault. Tatar *et. al*. (2004) proposed that micro earthquakes are located at depths of 8-15 km, in the upper crystalline crust beneath the thick sedimentary layer and not along a flat décollement possibly related to the Hormuz salt sequence. Based on the results of their micro earthquakes survey, both NE and SW alignments have been proposed. They suggested that the deformation in Zagros is accommodated by several NW-SE trending basement reverse faults connected by

NNW-SSE to NS striking right-lateral strike slip fault. Tatar *et. al*. (2004) suggest that microseismicity represents the response of a prefractured crust to the shortening rather than the motion on large faults.

In general, recent studies [e.g. Blanc et. al. (2003), Sherkati et. al., (2004), Molinaro et al. (2004), Mouthereau et al. (2006) and this work] would suggested that both thin- and thick-skinned system of deformation are permissible through the Zagros. In thick-skinned model, it supposed that a number of basement thrusts controlling a south-west plunge of the top of the basement of 1-2°, i.e. slightly more than the topography. Because the base of the crust plunges gently (1-2°) to the north-east [Paul *et al.*, 2006], a space problem occurs between the top of the basement and the base of the sedimentary cover. In the recent cross-sections (e. g. Fig. I-20A & B), the void between folded strata and the crystalline basement has been filled both by basement imbrications (i.e., thick-skinned deformation) and local thickening of Hormuz evaporites in the core of anticlines. McQuarrie (2004) has proposed to fill such voids with locally more than 5 km of deformed Hormuz salt (Fig. I-20C). She suggest that the broad arcs of the Zagros, commonly cited as classic examples of a fold–thrust belt with salt controlled morphology, would have more to do with the extensional basin geometry regardless of the actual distribution of salt within that basin. MacQuarrie (2003) suggest that basement deformation through the Zagros is not required by the geometry of the structures or by earthquake focal mechanisms, however the amplitude and wavelength of the folds within the Zagros, especially the frontal folds that produce the MFF, permit basement shortening. The inferred dips and locations of fault surfaces that core many of the folds are compatible with the magnitude, depth, and nodal plane orientation of earthquakes throughout the fold–thrust belt (MacQuarri, 2003). However, Mouthereau et al. (2006) have shown that such thicknesses of weak salt can not mechanically sustain the load of the overlying units over geological timescales; the salt would be rapidly squeezed out.

Molinaro *et al.* (2005) propose two main stages of deformation within the southeastern ZFTB. In the first stage the deformation was thin-skinned in style. A series of large symmetrical detachment folds have been folded across the SFB due to detaching of sedimentary cover along the basal Hormuz evaporites. They suggest that due to the propagation of forelimb thrusts, migration of salt toward the cores of folds and ongoing shortening resulted. Meanwhile, the lower Miocene Mishan marls play an important role to dissipate displacement propagation and thrust movements. They attribute that oversteepening of the limbs of the anticlines as resulting from gravity collapse structures within the Guri

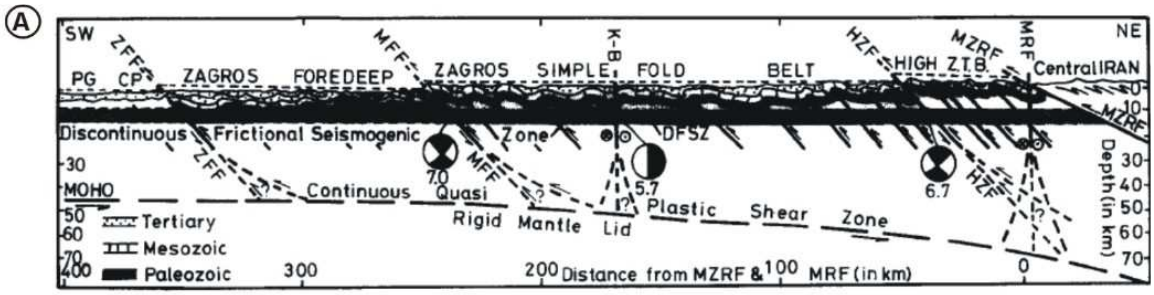

Figure 20A. Major morphotectonic units along a simplified transverse cross section of the Zagros active fold-thrust mountain belt (after Berberian 1994).

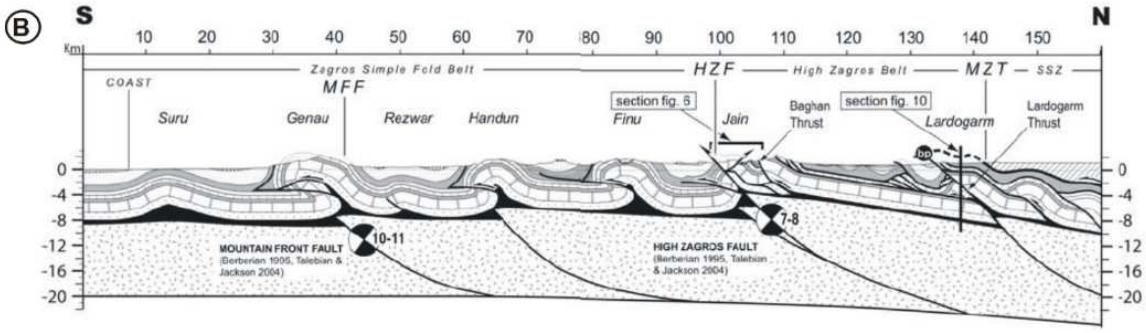

Figure 20B. Regional balanced and restored cross section through the southeastern Zagros Fold-Thrust Belt (after Molinaro *et. al.* 2005).

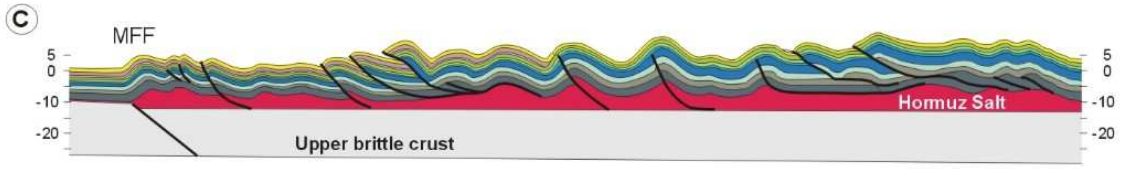

Figure 20C. Regional balanced cross section through the Zagros Fold-Thrust Belt (modified from McQuarrie 2004).

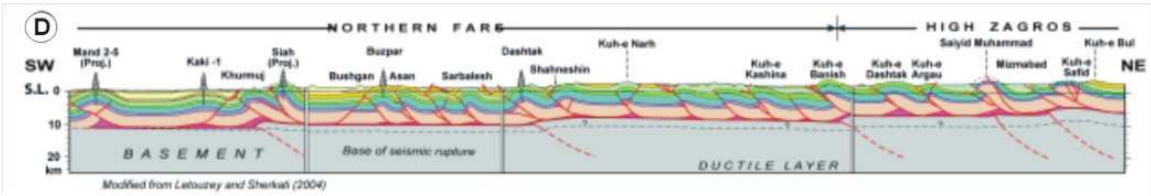

Figure 20D. Structural transect and regional balanced cross section through the cental Zagros Fold-and-Thrust Belt (for location refer to Fig. I-19) (modified Sherkati and Letouzey, 2004).

limestone beds. Molinaro *et al.* (2005) suggest that thick-skinned of deformation has been overprinted to thin-skinned across the first main stage of deformation. Strong seismicity record within the Zagros underline such ongoing thick-skinned of deformation. They note that out-of-sequence thrusts, which cut through sedimentray succession and cover structures, are linked to deep-seated basement faults. In order to demonstrate the post-effect of thick-skinned deformation, they refer to the intersection at oblique angles between preexisting folds and these new thrusts led to the development of structures with characteristic map patterns. They suggest that due to readjustment of the mountain belt as a whole, the basement-involved deformation also may have shifted toward the foreland. Based upon this, of results that the late stage involvement of the basement in foreland Zagros could be viewed as a step toward the reestablishment of the critical taper throughout the entire mountain belt (in the sense of Davis et al., 1983). Based upon this, they suggest that the major reorganization of the Arabia-Eurasia collision reported by several authors at about 3–5 Ma (Westaway, 1994; Allen et al., 2004; Regard et al., 2004), could be related to this change in the mechanism of deformation in the Zagros. Mouthereau *et al*. (2006) suggest that a possible mechanism that controlls growth of the topography in the Fars is the shortening and thickening of the Precambrian basement. They note that the deformation in the cover seems to have little effect on the growth of the topography even though it may strongly control the deformation styles observed at the surface. They have concluded that basement-involved thickening and shortening is mechanically required to produce the shape of the Zagros Folded Belt since at least 10 Ma. Moreover, the involvement of the basement provides mechanical and kinematic constraints that should be accounted for cross-sections balancing and further assessing the evolution of Zagros at crustal or lithospheric scales.

CHAPTER II

METHODOLOGY

CHAPITRE II

MÉTHODOLOGIE

Résumé en français

Les formes du relief sont régies par l'érosion et par les mouvements de la lithosphère terrestre. A ce dernier titre, elles contiennent des informations précieuses sur la déformation et la tectonique active. La morpho-tectonique consiste donc à mettre à profit ces formes du relief qui résultent de l'interaction entre les processus tectoniques et érosifs, pour en déduire la tectonique sous-jacente.

L'une des méthodes les plus communément employées en morpho-tectonique utilise des éléments du paysage, connu comme des *marqueurs passifs de la déformation*, pour quantifier la déformation. Un marqueur passif est un élément du paysage, comme par exemple une terrasse marine ou fluviale, qui n'a pas subi d'évolution notoire de sa surface et qui a enregistré de manière passive depuis sa formation une déformation tectonique. Ces marqueurs peuvent être déformées par des mouvements tectoniques associés à des failles ou des plis actifs ; en comparant leurs formes actuelle et initiale la quantité de déformation peut alors être quantifiée. En conséquence, l'identification et la cartographie (en 3 dimensions) de ces marqueurs déplacés ou déformés constituent un élément essentiel de beaucoup d'études en morpho-tectonique, et qui permettent de remonter éventuellement à la quantité de soulèvement subie par ces marqueurs géomorphologiques. Des modèles de déformation plicative sont alors utilisés pour traduire les quantités de soulèvement en termes de raccourcissement au travers de la structure active. Pour quantifier les *taux* de déformation, il est indispensable de pouvoir dater les marqueurs. Des techniques de datation relative basées par exemple sur la forme du marqueur (cette forme étant affectée de façon prévisible par l'érosion), son degré d'altération, ou sa position stratigraphique, sont classiquement utilisées pour définir des corrélations entre différents marqueurs. Des techniques de datation d'exposition de surfaces par isotopes cosmogéniques, ainsi que des datations par ^{14}C de restes organiques contenu dans les marqueurs, fournissent quant à eux des ages absolus.

En résumé, pour être utilisable pour l'analyse de la déformation active, un marqueur géomorphologique doit se conformer à deux critères essentiels : (1) la géométrie initiale doit être connue et reconstructible ; (2) l'âge du marqueur doit être connu ou doit pouvoir être déterminé par l'une des méthodes de datation dont l'on dispose. Un troisième critère est souvent utile pour reconstruire la déformation au travers d'une zone étendue comme un pli (par opposition à une faille) : la conservation de nombreux fragments de ce marqueur au

travers de la structure déformée est cruciale pour reconstruire l'enveloppe de cette déformation.

Dans ce travail de thèse, nous avons cartographié des terrasses fluviales pléistocènes le long de deux rivières (les rivières Dalaki et Mand) traversant la chaîne plissée du Zagros, ainsi que des terrasses marines le long du front de la chaîne en bordure du Golfe Persique. Ces marqueurs fournissent de précieuses informations sur le style structural, la géométrie des structures en profondeur, et les taux de déformation moyennés dans le temps (sur une échelle de temps variant de 10^4 à 10^6 ans) à travers la chaîne. Cette information peut servir ensuite à la comparaison des mesures géologiques (à long terme) et géodésiques (instantanées) de taux de déformation, à la quantification du partitionnement régional de la déformation, et à l'étude de l'évolution temporelle de structures individuelles à travers la chaîne.

Dans ce chapitre, nous fournissons un résumé décrivant les marqueurs géomorphologiques les plus courants ainsi que les méthodes de datation absolue employées. Les mécanismes de formation et d'abandon des terrasses fluviales et marines sont décrits, ainsi que l'information qui peut être tirée de l'étude des profils en long actuels de rivières. Ensuite, les bases théoriques des méthodes de datation par ^{14}C et par isotopes cosmogéniques sont passées en revue.

1. TECTONIC GEOMORPHOLOGY

1.1. Introduction

One of the fundamental ways to learn about recent deformation and active tectonics is through the landforms that are created and altered by motion of the Earth's crust. Tectonic geomorphology is the study of landforms that result from tectonism and the interaction between tectonic and geomorphic processes. The unrelenting competition between tectonic processes that build topography and erosion that tend to tear it down represents the core of tectonic geomorphology (Burbank & Anderson, 2001). In addition, if we can identify an old surface and measure how much it has changed, then that information can tell us about the rates and patterns of tectonic processes.

The distribution, timing and nature of faulting and seismicity can be discerned by dating and paleoseismic studies on various timescales. The instrumental recordings that are available for very short times, and paleoseismicity based on the interpretation of small-scale geomorphic or stratigraphic features, enable us to determine the past behaviour of seismogenic structures and, hence, better evaluate the risk to society resulting from future earthquakes.

Through the method of tectonic geomorphology, landscape features such as marine or fluvial terraces can be used to track deformation. Prior to deformation, the surfaces of these landscape elements known as *geomorphic markers*, represented planar or linear forms. The initial geometry of markers can be predictably tracked across the landscape. Faulting or folding can subsequently deform such markers and documenting departures from their unperturbed shape can serve to define the magnitude of deformation. Consequently, the recognition and measurement of such displaced or deformed markers are critical to many tectonic geomorphology studies. Mapping the deformation of fluvial and marine terraces is an important tool to constrain the rates and patterns of deformation and rock uplift associated with active faulting and folding processes.

In order to define *rates* of deformation, it is necessary to define both the timing and amount of deformation. Relative dating techniques based on landform shape, degree of rock weathering, and stratigraphic position, have been used to draw broad correlations between the timing of marker formation. Recently developed cosmogenic exposure age dating techniques and ^{14}C isotopic dating methods provide absolute dating of markers. Escarpments and mountain fronts are two types of landforms that have long survival times. Such long-term

records often obscure short-term variations in uplift, because the precision of the record is inversely proportional to its length. The uplift history of a landform can be measured differently using each type of record. This difference is sometimes expressed by different average uplift rates, which are calculated by dividing the total (cumulative) uplift by the period of record.

2. GEOMORPHIC MARKERS

2.1. Introduction

In order to measure the amount of deformation due to tectonic processes, we need to have an identifiable displaced feature. For instance, river terraces that formerly extended across a faulted or folded region in an unbroken pattern provide a datum for vertical deformation. The initial or pre-deformational geometry of the geomorphic marker (offset feature) has to be reconstructed accurately to calculate the displacement reliably. This thesis is concerned with identifiable geomorphic surfaces such as marine and fluvial terraces, which help us to provide a reference frame to determine differential or absolute deformation. In order to be useful for the analysis of active crustal deformation these markers should conform to three criteria: 1) the initial, undeformed geometry can be reconstructed; 2) the age is known or can be measured; and 3) a high preservation potential with respect to the relevant time scale. Often, only some of these criteria may have been met for a displaced marker. As geomorphic markers record surface deformation, their most critical attribute is initial geometry. Geomorphic markers may be modified due to subsequent erosion or deposition, in which case the initial geometry of a currently offset geomorphic surface may become difficult to define. In such cases, an undeformed modern analogue (comparison method) may help us to predict a probable initial geometry. In recent years, the utility of flvuial and marine terraces has increased as tools for characterizing tectonic activity, due to the availability of more reliable dating methods. The geometry of a dated fluvial terrace above the modern river channel provides the rate of incision or provides the rock uplift rate if we assume a steady channel elevation (with respect to a fixed external reference frame such as sea level). Marine terraces provide a direct record of rock uplift with respect to sea level. At Holocene time scales, climatic conditions have varied relatively little and markers show little modification due to climatic factors. At time scales of 100,000 years or more, complete or multiple glacial-interglacial cycles have occurred (Figure II-1) and due to the large-scale variations in discharge and sediment flux of rivers and in sea level, strong imprints have been left on the

landscape. These climatic cycles are generally at the origin of the formation of geomorphic markers such as marine or fluvial terraces, and the climate record can serve as a guide for inferring their ages.

In this thesis, we use mapped and dated Pleistocene terraces along two rivers crossing the Zagros Simply Folded Belt (the Dalaki and Mand rivers), and marine terraces close to the inferred Zagros Foredeep Fault, noting their relationship with mapped structures. The structural style of deformation, geometry of sub-surface structures and time-averaged deformation rates at multiple space and time scales are important constraints that can be provided by these markers. Moreover, a linkage between geologic and geodetic measures of deformation rates, regional strain partitioning and the interaction and evolution of individual structures can be provided using such information.

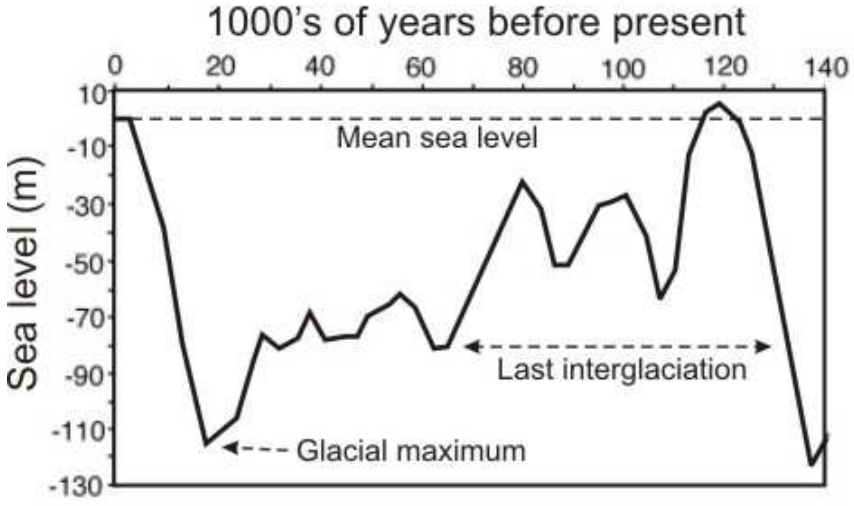

Figure II-1: Variation in global sea level based primarily on dated terraces on the Huon Peninsula, New Guinea (Chappell, 1974; Burbank and Anderson, 2001)

2.2. Marine terraces

Marine terraces are created by the interaction of the ocean with the adjacent coastline. Marine terraces can be divided into two classes: *constructional terraces* associated with coral reefs, and *destructional* or *erosional terraces*. Terraces ultimately result from the wide variation in sea level with time. A combination of global eustatic variations and the history of local tectonic movement of the coastline with respect to the geoid result in a unique local sea level variation through time. At Pleistocene time scales, changes in the volumes of the

continental ice sheets have controlled global or eustatic sea level changes. Only 18 kyr ago, sea level was ~120 m below its present level (Fairbanks, 1989) (Fig. II-1). The constant attack of the shoreline by waves creates erosional marine platforms. Along many tectonically rising coasts, direct evidence for multiple decreases in relative sea level can be detected from flights of marine terraces. In order to calculate vertical deformation rates, we should have knowledge of the global eustatic history and we need to be able to correlate between individual terraces and former sea level positions.

2.3. Fluvial Terraces

Many river systems retain a fluvial strath-terrace record of discontinuous downcutting into bedrock through the Quaternary. These are recognised in the field as flat elevated surface features within or adjacent to the active floodplain, which consist of remnants of former floodplains or planar surfaces of fluvial erosion. These features are left stranded above the floodplain during periods of active incision or downcutting by the stream. They are most prominently preserved when the rate of downcutting exceeds the rate of lateral migration and erosion of the stream channel across its floodplain. Straths are cut when the channel floor is

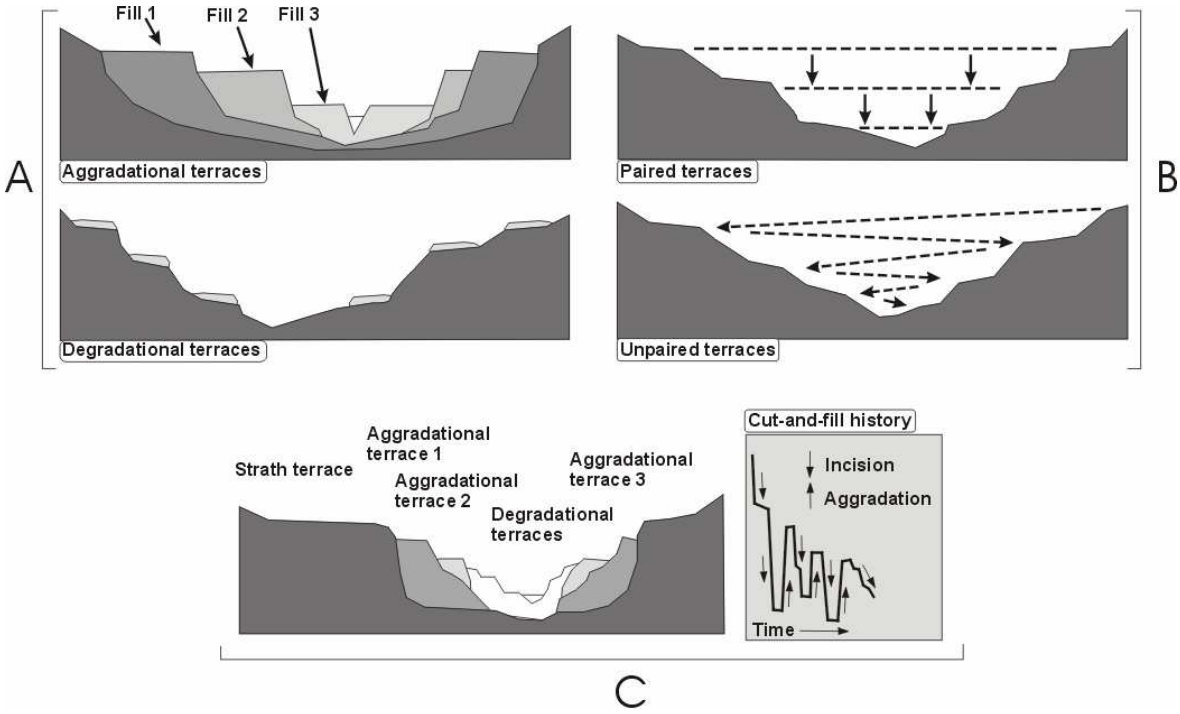

Figure II-2 : Schematic configurations of river terraces (from Burbank and Anderson, 2001). A. Cross-sectional sketches of aggradational and degradational fluvial terraces. B. Paired and unpaired river terraces. C. Cross-section showing complex sequence of aggradational and degradational surfaces. Multiple cut-and-fill events are outlined in the right-hand box.

protected from erosion by sediment and are abandoned—and terraces formed—when incision can resume following sediment-cover thinning. Therefore, terrace formation has been attributed to changes in sediment supply and/or water discharge produced by late Quaternary climatic fluctuations. Their importance lies in their use to interpret climatic events in the headwaters and to determine long-term incision rates.

Alluvial channels are very sensitive to active tectonics (Burnett and Schumm, 1983; Ouchi, 1985), and adjust to vertical deformation or base level change by channel modifications, specifically by incising, aggrading, or altering sinuosity. Aggradation buries evidence of a stream's prior history. On the other hand, subsequent incision can create a new fill terrace and possibly lower cut terraces carved into the fill if incision is episodic (Fig. II-2) (Burbank & Anderson, 2001). A fill terrace is remnant of a former floodplain that formed by aggradation of fluvial sediment and that is preserved adjacent to the stream after a subsequent period of incision/downcutting. Streambank aggradation or degradation is often a response to stream channel instability. The use of fill terraces, as distinct from strath terraces, for calculating incision rates is complicated by the cyclic alluviation and incision they record.

3. RIVER LONG PROFILE

A river's bed and its floodplain can be used to represent the longitudinal profile of the currently active stream. Longitudinal river profiles ("long profiles") are plots of river length against elevation; the long profile generally decreases in gradient downstream as a function of increasing discharge of the river (Bagnold, 1977) and tangentially approaches sea level in a coastal river (Bloom, 1991). Terraces preserved along valley walls above the active valley bottom record a history of past long profiles. Long profiles can reflect characteristics of a drainage basin including variations in bedrock lithology, variations in resistance due to weathering or fracturing/faulting, and/or show a snapshot of one stage of a river's response to a change in base level. The cross-sectional shape of a river valley also reflects rates of incision and bedrock resistance. Rapid incision and resistant bedrock favour the formation of steep, narrow valleys, while slow incision and erodable rock types favour wide valleys. To a first order, the long profile shape can be explained by variations in stream power (the rate of potential energy expenditure of the river, a function of discharge and local slope), uplift/incision rate and bedrock resistance to lithology (e.g., Whipple and Tucker, 1999). In studying coastal rivers, Pazzaglia et al. (1998) found that when incision rates are controlled by

tectonic uplift, long profiles exhibit a strongly concave-upward shape due to the river's rapid response to changing base level. Relatively smooth concave-upward profiles can be produced by rivers with high stream power that are able to keep up with or exceed the rapid rates of rock uplift. Tectonically active settings can be characterized by such concave-upward profiles.

However, in tectonically stable regions, stream power tends to be limited. In a single long profile, regions of more resistant bedrock often exhibit steeper gradients or lithological knickpoints. After a change in base level the climate and bedrock characteristics are the dominant factors in controlling long profile shape. In regions of resistant bedrock we expect that profiles in tectonically stable regions tend to exhibit knickpoints. Thus, the longitudinal profile can be used as a record of active tectonics, lithological variation, and incision history across active mountain belts.

4. ABSOLUTE DATING METHODS

It is crucial to be able to date formation ages of terraces, because their surfaces provide an invaluable record of uplift-subsidence and fault activity. In-situ Cosmic Ray Exposure (CRE) dating has established itself as a robust method to date fluvial terraces, but the interpretation of cosmogenic nuclide concentrations is complicated by pre-depositional inheritance and post-depositional disturbance of the terrace deposits through pedogenesis and surface inflation or deflation. Thus, careful field inspection is necessary to assess the suitability of a simple surface exposure model. Other methods used to date fluvial terraces are Optically Stimulated Luminescence (OSL), Thermoluminescence (TL) and Electron Spin Resonance (ESR) dating, which use paramagnetic defects in quartz crystals. These methods are based on the quantification of defects generated in quartz crystals by environmental radiation, which subsequently disappear through optical bleaching by sunlight.They are popular because quartz is the most common constituent of fluvial sediments and has a robust crystal structure.

In this thesis, cosmogenic radionuclide dating of displaced geomorphic features has been used to quantify incision rates and the style of onging deformation at a range of time scales ranging from 10^4 to 10^6 years. Moreover, the rate of tilting of marine terraces at the central Zagros front has been provided using ^{14}C dating of bivalve shells.

4.1. C-14 Dating

Radiocarbon dating, which is the most commonly used technique to date geomorphic features and surfaces, is a radiometric dating method that uses the naturally occurring isotope ^{14}C to determine the age of materials that contain organic in carbon up to about 60,000 years. ^{12}C and ^{13}C are two stable and non-radioactive isotopes of carbon. ^{14}C is created in the atmosphere by cosmic ray interaction. The unstable isotope, ^{14}C, is present in tiny amounts on Earth (98.9% ^{12}C, 1.1% ^{13}C, and 1.17×10^{-10}% ^{14}C), most of it in the form of CO_2. ^{14}C is taken up into organic tissues by. This unstable isotope has a half-life of 5735 years. The amount of carbon-14 thus gradually decreases after death of the organism through radioactive decay: $^{14}C \rightarrow {}^{14}N + {}^{0}\beta$. By emitting a β particle (beta decay), carbon-14 is changed into stable (non-radioactive) ^{14}N.

A major unknown in ^{14}C dating is the initial amount of 14C in the atmosphere at the time of formation of the dated specimen; this amount varies through time because of variations in the intensity of cosmic radiation as well as in the magnetic field intensity of the Earth, which deflects cosmic rays. Constantly updated calibration schemes (the most recent one being by van der Plicht et al., 2004) are used to translate raw ^{14}C ages into calibrated calendar-year ages.

4.2. Cosmogenic Radio Nuclides (CRN)

4.2.1 Introduction

Cosmogenic nuclides are nuclides formed by the interaction of *target* atoms with cosmic radiation. Such nuclides are formed in space, in the atmosphere (e.g. ^{14}C and ^{10}Be), and *in situ* within minerals at or near the earth's surface (e.g. ^{10}Be, ^{26}Al, and ^{21}Ne). The age and rate of change of the land surface can be provided by measurements of the amounts of these cosmogenic nuclides that have accumulated over time.

The Earth is under constant bombardment by cosmic radiation. This radiation consists mostly of high-energy (~1-10^{10} GeV) protons and alpha particles emanating from within our galaxy. *Meteoric* cosmogenic nuclides (e.g. ^{14}C and ^{10}Be) are produced due to intraction between these radiation nuclei in the atmosphere. *Terrestrial* cosmogenic nuclides (TCN) are produced because of interaction between primarily neutrons and muons (as a cascade of

secondary particles), and target nuclei within minerals such as quartz and olivine at the Earth's surface (Figure II-3). The cosmogenic nuclide production is limited to the upper few meters of the Earth's crust due to the strong attenuation of the cosmic-ray flux. Therefore, a quantitative record of near-surface exposure can be provided using the concentration of in-situ produced cosmogenic nuclides in a surface sample. Lal (1988) identified 12 cosmogenic isotopes that are produced in terrestrial materials. The cosmogenic nuclides most widely utilized for geologic applications are the radionuclides ^{10}Be, ^{26}Al, and ^{36}Cl, and the stable nuclides ^{3}He and ^{21}Ne (Table II-1).

^{10}Be is a radionuclide with a half-life of 1.5 Myr, is primarily produced by spallation from O, Mg, Si, and Fe, and is most commonly measured in quartz, olivine and magnetite. ^{36}Cl is a radionuclide with a half-life of 0.3 Myr, is mostly formed by spallation from Ca and K and by neutron capture from ^{35}Cl, and is commonly measured in 'whole rock' samples. ^{26}Al is a radionuclide with a half-life of 0.7 Myr, is primarily produced by spallation from Si, Al, and Fe, and is most commonly measured in quartz and olivine. Production rates have been determined both empirically using natural and artificial targets (e.g. Niedermann et al., 1994; Dunai and Wijbrans, 2000), and theoretically (e.g. Masarik, 2002). Knowledge of production mechanisms and production rates are the basis of cosmogenic isotope analysis. Production rates vary with location and time and must be scaled to account for a number of factors

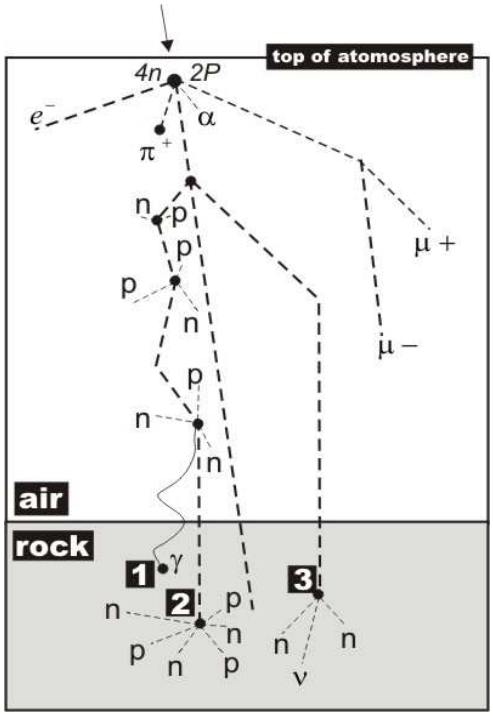

Figure II-3: The major components of a cosmic ray cascade, showing secondary particle production in the atmosphere and rock. Numbers refer to examples of in situ cosmogenic nuclide interactions:

(1) $^{35}Cl(n_{th},g)^{36}Cl$;
(2) $^{16}O(n, 4p3n)^{10}Be$;
(3) $^{28}Si(n,p2n)^{26}Al$.

Vertical scale not linear (from Gosse and Phillips, 2001).

Table 1 Properties of the main terrestrial cosmogenic nuclides used in geomorphologic applications

Isotope	Half-life (yr)	Main target minerals	Measurement	Comments
^{3}He	stable	olivine, pyroxene, hornblende, garnet	mass spectrometry	High production rate, which is relatively well constrained; best results using samples from rocks with ages < 5 Ma.
^{10}Be	1.51×10^{6}	quartz, olivine	AMS	Primary target mineral (quartz) is widespread; long half-life provides possibility of recording long exposure histories; production rate well-constrained only for quartz.
^{14}C	5.73×10^{3}	quartz, calcite	AMS	Target minerals are widespread; short half-life means that recent complex exposure histories can be analysed when paired with a stable cosmogenic nuclide; possibility of contamin- ation by atmospheric ^{14}C.
^{21}Ne	stable	quartz, olivine, garnet; clinopyroxene	mass spectrometry	Target minerals are widespread; potential for recording the longest exposure histories of any cosmogenic isotope as it is stable; however this also means that inheritance from previous exposure is possible.
^{26}Al	7.20×10^{5}	quartz	AMS	Target minerals are widespread but very low concentration (<200 ppm) of total Al in sample required as it is difficult to measure low $^{26}Al/^{27}Al$ ratios by AMS.
^{36}Cl	3.01×10^{5}	K-feldspar, plagioclase, calcite, ^{35}Cl in fluid inclusions in quartz	AMS	Atmospheric production is low so can be used on whole rock (e.g. basalt and limestone); sulphur contamination in samples is typical.

Source: based on Kurz and Brook (1994), Tuniz et al. (1998), Fifield (1999) and Gosse and Phillips (2001). (from Cockburn and Summerfield, 2004)

including depth within a target, altitude (atmospheric shielding) and latitude (primarily the spatial influence of the geomagnetic field; Lal, 1991; Dunai, 2000), topographic shielding and sample surface slope (exposure geometry; Dunne et al., 1999).

The geomorphological applications of in-situ produced cosmogenic isotope analysis are especially related to dating of landforms and have great relevance to problems in Quaternary science. Cosmogenic isotope analysis has become an important tool to address key questions about geomorphic process rates, and it provides the means to answer long-standing questions about landscape evolution (Figure II-4).

4.2.2. Theory of cosmogenic isotope analysis; summary

We consider a geomorphic surface that is fixed in geographic coordinates on the Earth's surface. This surface with defined dip and strike is bombarded by the incident cosmic

radiation. Both stable and radioactive isotopes are created *in-situ* due to this cosmic radiation bombardment; as the cosmic ray particles interact with surface targets they are themselves destroyed; thus the flux in the substrate of the surface decreases exponentially with depth (Figure II-6). Tectonic motion increases or decreases the altitude of the entire geomorphic surface. Moreover, in general, surfaces undergo erosion or ablation, thus decreasing in altitude, or increase in altitude due to sedimentation [double-moving-boundary process, (Cerling & Craig, 1997)]. On the other hand, because the incident cosmic-ray flux is attenuated due to the atmospheric depth, any changes in the altitude of the surface alter the production rate throughout the range of nucleon production in the matrix. Lal (1991), Dunai (2000) and Stone (2000) have developed models for the altitudinal and latitudinal variations

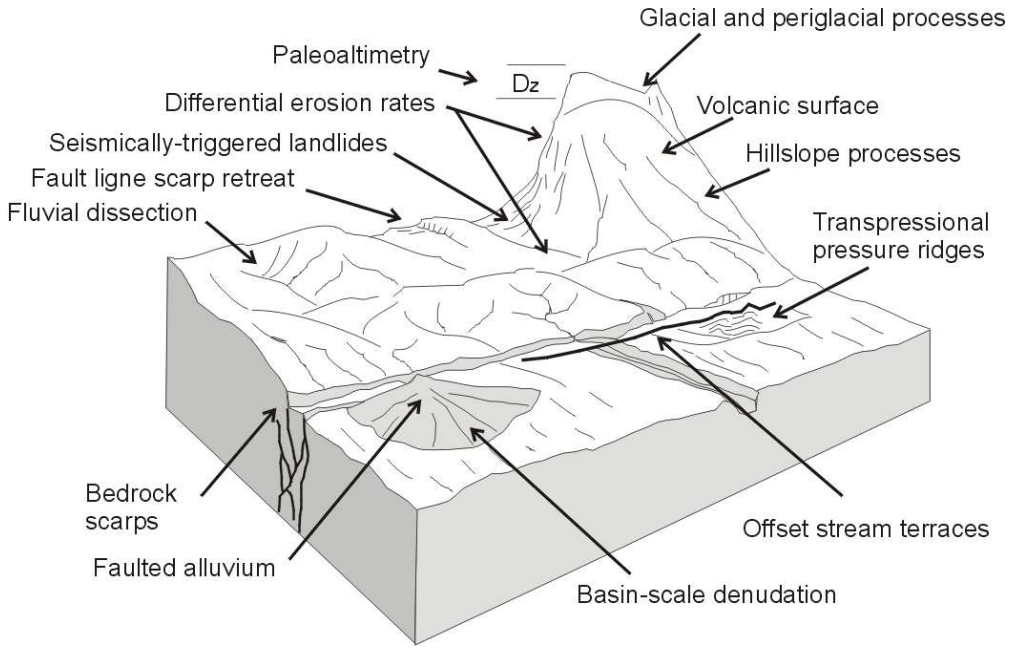

Figure II-4: Some examples of applications of terrestrial in situ cosmogenic nuclides in Earth Sciences (from Gosse and Phillips, 2001).

in production rates using empirical polynomials. Topographic shielding can be calculated using Heidbreder formulations (Heidbreder, 1971).

In this thesis, we will date fluvial terraces using samples collected at the surface or at depths of up to a few meters. We have carefully screened our sampling sites for indications of surface in- or deflation and are confident that all terraces sampled retain pristine surfaces. Therefore, we calculate terraces ages using the cosmogenic age equation for non-eroding surfaces:

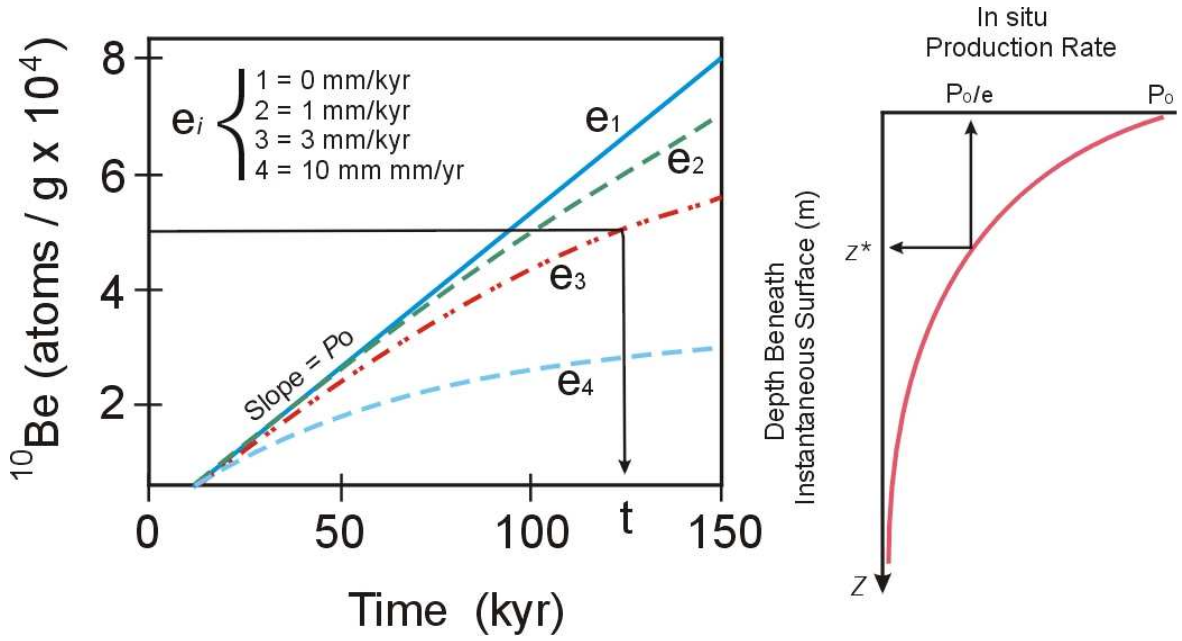

Figure II-6: (left) Cosmogenic ^{10}Be as a function of time and erosion rate. The curves are calculated for various values of the erosion rate. If a measured concentration of ^{10}Be ($P_{10Be(Zo)}$ = 5.5 atoms·g^{-1}·yr^{-1}) is 'Be'= 5.05 x 10^5 atoms/g, then at e = 3 mm/kyr, for example, this corresponds to an exposure age of 127 kyr (assuming no inherited component as described in text); (right) Production rate, P, decays exponentially with depth below the instantaneous surface, z, where the surface production rate, P_o, is scaled by altitude and geomagnetic latitude. The rate of decay beneath the surface is scaled by the attenuation length, z*, which is roughly 50-60 cm for most lithologies. Modified from (Cerling & Craig, 1997)].

$$C(x,t) = C_{(0)}e^{\lambda t} + (1-e^{-\lambda t})\frac{P_0}{\lambda}((P_0(1-F_\mu)e^{-\rho x/\Lambda_n}) + (P_0 F_\mu e^{-\rho x/\Lambda\mu}))$$

where $C(x,t)$ is the concentration of ^{10}Be as a function of time *(t)* and depth *(x)*, P_0 is the local production rate (atom g^{-1} yr $^{-1}$), λ is the radioactive decay constant (yr^{-1}), $C_{(0)}$ is the inherited cosmogenic nuclide concentration at the initiation of the surface exposure episode, ρ is rock density (g cm^{-3}), F_n and F_μ are the neutron and muon contributions to the total production rate, respectively (where F_μ = 0.015 F_n at the surface; Braucher, 1998) and Λ_n (~150 g cm^2) and Λ_μ (~1300 g cm^2) are the attenuation lengths of neutrons and muons, respectively (Brown, 1995). There are two unknowns in this equation: the age *t* and the inherited concentration $C_{(0)}$; to solve for age we must therefore suppose an initial concentration $C_{(0)}$ = 0.

CHAPTER III

ACTIVE FOLDING EVIDENCED AT THE CENTRAL ZAGROS FRONT (IRAN)

CHAPTRE III

EVIDENCES DU PLISSEMENT ACTIF AU FRONT DU ZAGROS CENTRAL

Résumé en français

L'architecture du prisme d'accrétion du Zagros a été intensivement étudiée, notamment en raison de ses implications importantes pour l'exploration d'hydrocarbures. Néanmoins des aspects tels que la cinématique actuelle des différents plis ou leur évolution au cours du plissement restent à étudier en détail. Il est généralement considéré dans les modèles classiques de prisme orogénique que la déformation migre vers le bassin d'avant pays, c'est-à-dire dans le cas de la chaîne du Zagros vers le sud à sud-ouest, et que le front de la chaîne représente la partie la plus active de l'orogène en termes d'accommodation du raccourcissement. Dans la province sud-ouest du Fars (Zagros central), l'anticlinal de Mand est la structure la plus frontale, et de ce fait représente potentiellement une structure très active si l'on s'en tient à un schéma classique. Le pli de Mand se présente comme un pli de détachement en bordure du golfe Persique. Cet anticlinal relativement symétrique s'est développé par le plissement de roches sédimentaires relativement compétentes du Phanérozoïque au-dessus d'une couche ductile de 1 km d'épaisseur environ, le sel d'Hormuz, qui représente par ailleurs un niveau de décollement préférentiel sur l'ensemble du Zagros. Afin de documenter la géométrie et la cinématique de ce pli, nous avons construit plusieurs coupes équilibrées sur la base d'une coupe existante contrainte par des données séismiques [Letouzey et Sherkati, 2004]. Pour prolonger en profondeur la coupe du pli de Mand, il existe plusieurs solutions répondant à l'épineux problème de la conservation des aires ou bien des longueurs des couches plissées. La première solution consiste à opter pour un degré croissant de déformation interne des couches, en l'occurrence de l'épaississement, vers la base de la série déformée ; la seconde solution revient à ne considérer de déformation intense que dans la couche ductile basale du sel d'Hormuz et à accommoder le raccourcissement dans les unités médianes au dessus de ce décollement par une flexure de synclinaux bordant l'anticlinal principal (modèle de Mitra [2003]). L'absence de données sismiques sur le flanc sud-ouest du pli de Mand ne permet pas de choisir l'une de ces deux solutions ou même d'éliminer ou non la présence possible d'une faille aveugle à vergence SW sous le pli [Sherkati et al., 2006]. Des données cinématiques sur le fonctionnement actuel du pli, telles que fournies par des marqueurs passifs de la déformation, peuvent néanmoins apporter des contraintes supplémentaires afin de répondre au problème posé. Sur le flanc sud-ouest de l'anticlinal, de nombreuses terrasses marines et fluvio-marines, inclinées de 1.7° à 4.5°, fournissent une telle contrainte additionnelle sur la cinématique du flanc avant du pli de Mand.

A partir de la géométrie actuelle de ces terrasses, et de leur géométrie initiale, supposée proche de l'horizontale pour les terrasses marines, et des rivières drainant actuellement le pli pour les terrasses fluviales, on peut reconstruire l'amplitude du basculement tectonique subi par

ces terrasses. La datation ^{14}C de coquilles de bivalves inclus dans les faciès marins littoraux de ces terrasses permet de surcroît de calculer des taux de basculement de 0.04 à 0.05 °/ka depuis leur formation au cours de hauts niveaux marins relatifs du Pléistocène terminal.

Le basculement observé des terrasses est cohérent avec un modèle de pli de détachement dans lequel le degré croissant de raccourcissement est absorbé par le basculement des flancs du pli de part et d'autre de charnières fixes, plutôt que par la translation verticale du cœur du pli au dessus d'une rampe associée au pli. Par ailleurs, la position relativement interne du point de rotation pure (c'est-à-dire de soulèvement nul) sur le flanc basculé suggère que la déformation observée est davantage compatible avec un anticlinal de détachement en association avec la flexure de synclinaux bordiers. L'application d'un tel modèle de pli aux terrasses basculées sur le flanc SW de Mand conduit à estimer une vitesse de raccourcissement au travers de, et perpendiculairement à, la structure de 3 à 4 mm/an. Bien que cette évaluation souffre de larges incertitudes, dues aux problèmes éventuels de recristallisation des tests de bivalves qui conduisent à sous-estimer l'âge des terrasses, et à l'absence de contraintes fortes sur le modèle plicatif, nous concluons que le raccourcissement à travers l'anticlinal de Mand peut absorber de 20 à 35% des 8 mm/an de la convergence au travers du Zagros entier. Ce résultat est relativement conforme à une déformation de type pli de couverture se propageant normalement vers le bassin d'avant pays et à une activité intense des structures frontales. Il implique également que la couverture sédimentaire du Zagros frontal sous le pli de Mand est découplée entièrement du substratum de la croûte moyenne, le plus probablement au niveau du sel d'Hormuz, et ce contrairement aux modèles récents [Molinaro et al., 2005 ; Mouthereau et al., 2006] qui suggèrent que la déformation récente de la couverture sédimentaire reflète essentiellement le fonctionnement de failles mi-crustales sous jacentes.

Rates and Processes of active folding evidenced by Pleistocene terraces at the central Zagros front (Iran) *

Behnam Oveisi[1,2], Jérôme Lavé[1], Peter van der Beek[1]

1. Laboratoire de Géodynamique des Chaînes Alpines, Université Joseph Fourier, BP 53, 38041 Grenoble Cedex, France
2. Geological Survey of Iran, Tehran, I.R. Iran

Abstract. The Zagros fold belt results from active collision of the Arabian plate with central Iran, and is characterized by the development of a spectacular >200 km-wide fold-train in its sedimentary cover. Although the architecture of this accretionary prism has been extensively studied, because of its important implications for hydrocarbon exploration, aspects such as the kinematics of individual folds and the sequence of fold development remain to be investigated in detail. It is commonly believed that the ongoing deformation through the Zagros belt has led to the south-westward migration of the front of the fold belt. In the south-western Fars province (central Zagros), the most frontal structure is delineated by the Mand anticline, a well exposed detachment fold on the shore of the Persian Gulf. This near-symmetrical anticline involves relatively competent Phanerozoic sedimentary rocks above a regional décollement in Hormuz salt. In order to document the geometry and kinematics of this fold, we have constructed several balanced cross-sections on the basis of a recently published section constrained by seismic data [Letouzey and Sherkati, 2004]. Several solutions to the length versus area restoration problem common to detachment folds are then proposed: fault-related folding, detachment folding with internal deformation and detachment folding accompanied by the flexure of the flanking synclines below the regional stratigraphic level. On the western limb of the anticline, fluvio-marine terraces, tilted by 1.7 to 4.5°, provide an additional constraint on fold kinematics and suggest that surface deformation is most compatible with a detachment fold, probably associated with synclinal flexure. Applying such a model, as well as new ^{14}C ages for the marine terrace deposits, we calculate tilting rates of 0.04 to 0.05°/kyr, which would be produced by a Late Pleistocene shortening rate (perpendicular to the structure) of 3 to 4 mm/yr. Although this preliminary estimate suffers from relatively large uncertainties, mostly due to the absence of independent dating of the terraces and independent constraints on the folding model, we conclude that shortening across the Mand anticline could absorb 20 to 35% of the 8 mm/yr convergence across the entire Zagros. This result is consistent with a normal forward-propagating deformation sequence in a thin-skinned tectonic regime. It also implies that the sedimentary cover of the frontal Zagros is fully decoupled from the basement, most probably at the level of the Hormuz salt, in contrast to recent models that suggested active deformation of the sedimentary cover to be controlled by thrust faults in the basement.

1. INTRODUCTION

The Zagros fold belt (Figure III-1) results from the collision of the Arabian plate with the central Iran micro-continent. Tectonic convergence is still ongoing in the area and recent deformation of

* This chapter will be published as chapter 14 in "Thrust Belt and Foreland Basin" (editors : O. Lacombe, J. Lavé, F. Roure & J. Vergès), Springer "Frontiers in Earth Sciences" Series, in press.

this intracontinental mountain belt is accompanied by intense seismicity [e.g., Ni and Barazangi, 1986; Berberian, 1995; Talebian and Jackson, 2004]. The Arabian passive margin sequence is commonly believed to be decoupled from its basement at the level of lower Cambrian salt and to be deformed by thin-skinned tectonics. Despite the spectacular deformation of this sedimentary sequence, most of the seismicity occurs within the underlying basement, mainly through high-angle reverse faulting [Jackson and Fitch, 1981; Berberian, 1995]. This rather unique seismotectonic setting has prompted scenarios in which the Zagros convergence is accommodated by distributed basement shortening in conjunction with, but decoupled from, folding of the sedimentary cover [Jackson and Fitch, 1981; Ni and Barazangi, 1986; Berberian, 1995]. The role of the basement faults remains, however, a matter of debate and it has recently been proposed that basement deformation is currently controlling the deformation of the sedimentary cover: a thick-skinned tectonic style would thus have succeeded initial thin-skinned tectonics [Molinaro *et al.*, 2005; Sherkati *et al.*, 2005].

The Zagros orogen is known for the spectacular fold structures that affect its thick sedimentary cover [e.g., Farhoudi, 1978; Letouzey *et al.*, 1995] with widely distributed resistant limestone anticlines displaying the large-scale “whale backs” that characterize the morphology of the region. Many of these anticlines have long been considered as archetypal detachment folds, which formed in response to the ongoing deformation above the basal detachment level of the lower Cambrian Hormuz Salt [e.g., Colman-Sadd, 1978], even if recent studies have proposed alternative structural interpretations [e.g. Sherkati and Letouzey, 2004; Mouthereau et al., 2006]. The geometry and surface structure of such detachment folds are considered to be controlled by the existence of a major low-viscosity basal layer that permits efficient detachment and material migration [e.g. Mitra, 2002]. Various two-dimensional geometric and kinematic models have been proposed to describe detachment folding [e.g., Dahlstrom, 1990; Epard and Groshong, 1995; Poblet and McClay, 1996; Mitra, 2002], which is typically manifested by symmetric or asymmetric folds with cores filled by the basal incompetent unit.

Although the architecture and kinematics of deformation of the sedimentary cover in the Zagros fold belt have important implications for seimic hazard assessment and hydrocarbon exploration, they remain relatively unknown. Some general sections of the Zagros fold belt have been proposed in recent papers [Blanc *et al.*, 2003; McQuarrie, 2004; Sherkati and Letouzey, 2004]; however, aspects such as the kinematics of individual folds, the sequence of fold and thrust

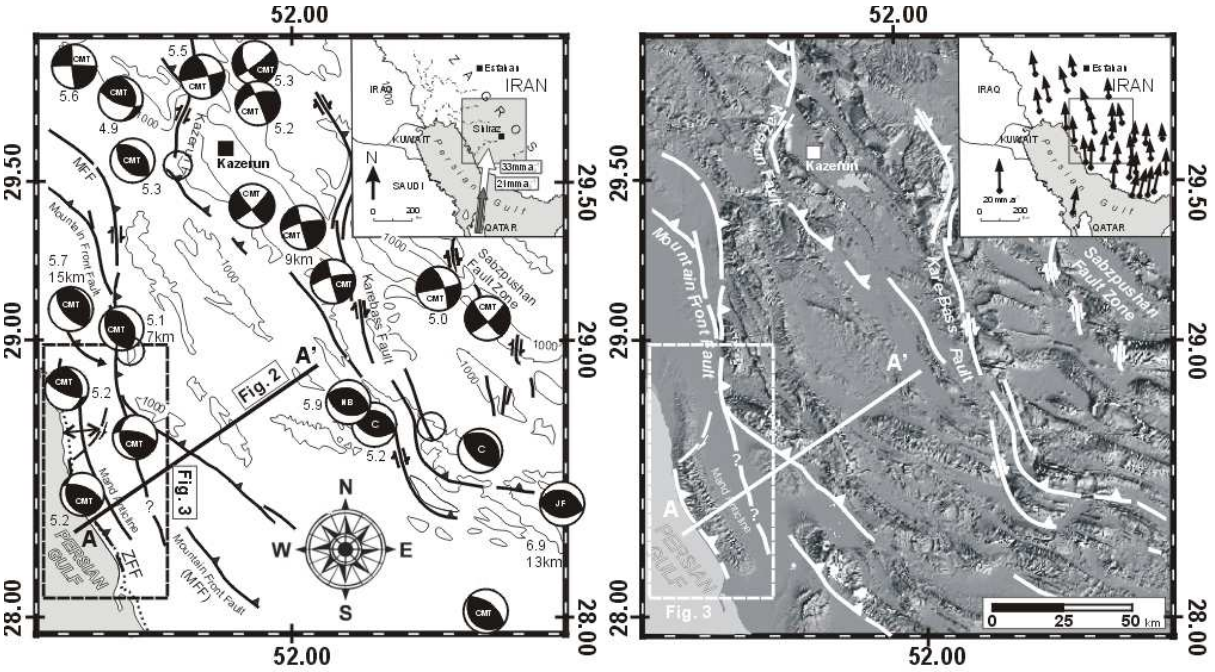

Figure III-1. Seismotectonic (*left panel*) and topographic (*right panel*) map of the Western Fars, central Zagros, showing main surface faults. *Inset in left panel shows* location within Persian Gulf area, as well as Arabia-Eurasia shortening rates from DeMets et al. (1994) and Sella et al. (2002); *inset in right panel shows* GPS velocities (mm/yr) in central Zagros with respect to stable Eurasia (Hessami et al., 2006). Focal mechanism solutions for large earthquakes are from Chandra (1984) (C); Harvard Centroid-moment database (CMT); Jackson and Fitch (1981) (JF); Ni and Barazangi (1986) (NB). Topographic contours with 1000-m interval indicated in left panel. Line shows balanced cross-section of Fig. III-2; box shows location of Fig. III-3.

development, the relationship between fold and fault deformation and the evolution from symmetric detachment folds to asymmetric fault-related folds remain to be investigated.

Here, we focus on a well exposed map-scale detachment fold (the Mand anticline) occurring along the shore of the Persian Gulf at the central Zagros front (Figure III-1). This detachment fold presents near-symmetrically folded Cenozoic strata, formed in the relatively competent rock cover above a regional décollement in Hormuz salt. In order to unravel the recent evolution of this most frontal part of the central Zagros wedge, we first review some aspects of Zagros tectonics and geology that are relevant to our study. We then detail the surface geometry and various possible constructions at depth of the Mand detachment fold, including depth-to-detachment and shortening calculations. In order to evaluate Late Quaternary rates of deformation at the front of the Zagros belt, we surveyed tilted marine and fluvial terraces on the SW frontal limb of the Mand anticline. These warped and tilted geomorphic markers provide new insights on recent fold detachment kinematics and on tectonic uplift, tilting and shortening rates.

2. GEOLOGICAL AND SEISMOLOGICAL SETTING

The Zagros orogen is bordered to the SW by the Persian Gulf, which represents the foredeep basin at its front. To the NE, the Zagros is bordered by the Main Zagros Thrust (MZT), considered by many as the suture of the Neo-Tethys Ocean. Classically, two main structural zones in the Fars arc of the Zagros are distinguished on the basis of distinct topographies and outcropping units: the High Zagros Belt (HZB) to the NE, and the Zagros Simple Fold Belt (ZSFB) to the SW. The High Zagros Fault (HZF) separates these two structural domains. It is generally considered that deformation in the HZB initiated before deformation in the ZSFB, according to a classical forward-propagating sequence scenario [e.g., Hessami *et al*., 2001; Alavi, 2004].

Sedimentation on the Arabian and Zagros platform since the pre-Cambrian has led to deposition of a 5 - 15 km thick sedimentary sequence of passive margin to flexural basin series [Stocklin, 1968; Falcon, 1969; Colman-Sadd, 1978], interrupted by several sedimentary hiatuses [e.g., Alavi, 2004]. During Paleozoic times, clastics and carbonates were deposited, partly in association with the opening of the Neo-Tethys. Subsequently, Upper Triassic to Lower Cretaceous carbonates and minor evaporites were deposited on the stable, shallow shelf of the Arabian platform. The emplacement of ophiolites during Late Cretaceous time along the margins of the Arabian plate indicates an initial episode of convergence at that time, the extent and nature of which remain controversial [e.g., Beydoun 1991]. Campanian flysch and radiolaritic nappes accumulated in a flexural basin formed by loading of the continental crust, whereas the Late Eocene to Early Miocene is marked by the deposition of several limestone formations (e.g., Jahrom and Asmari Formations). Tertiary island-arc-type volcanism in Iran indicates that subduction of oceanic crust continued until Miocene times [e.g., Colman-Sadd 1978], when it was followed by the main phase of continental collision in the Zagros. Finally, a major regional angular unconformity between the Agha Jari/Lahbari Formations and the upper Bakhtyari conglomerates is associated with renewed erosion and tectonic activity of the Zagros fold-and-thrust belt: this event is generally dated as Late Pliocene, but could be largely diachronous from NE to SW, accompanying the propagation of the deformation front [Hessami *et al.*, 2001].

Active deformation of the Zagros orogen results from approximately N-S directed collision between Arabia and Continental Eurasia at a rate of 25-30 mm/yr [DeMets *et al*. 1994; Sella *et al*. 2002]. Seismicity [Berberian, 1995; Talebian and Jackson, 2004] and GPS [Tatar *et al.*, 2002] data suggest that present-day convergence across the Zagros is concentrated in the ZSFB, which

constitutes the foreland fold-and-thrust belt of the system. From a recent GPS survey, Tatar *et al.* [2002] proposed a present-day shortening rate of 8-10 mm/yr for the Zagros, which would accommodate about 40-45% of the total ~21 mm/yr convergence between Arabia and Eurasia [Vernant *et al.*, 2004]. Total shortening since ~5 Ma in the ZSFB is estimated to range between 50 and 80 km [Blanc *et al*, 2003; McQuarrie, 2004]. The stratigraphic succession of rock series with highly variable mechanical properties strongly controls deformation in the ZSFB [e.g., Sherkati and Letouzey, 2004]. At the base of the sedimentary cover, Lower Cambrian [Berberian, 1995] incompetent Hormuz series directly overlie the crystalline basement as a basal detachment level and play an important role in guiding the deformation. Talbot and Alavi [1996] suggested a taper angle of ~1° in the Zagros, resulting from very low basal traction in the Hormuz Salt horizon. Reliable waveform modelling shows that large earthquakes in the Zagros often nucleate in the upper crust at depths of 8 to 15 km in the crystalline basement [Jackson and McKenzie, 1984; Ni and Barazangi, 1986; Maggi *et al*., 2000; Talebian & Jackson, 2004]. A recent study of micro-earthquakes in the central Zagros [Tatar *et al.*, 2004] suggests that much of the seismicity is restricted to the upper part of the basement between ~11 km (base of the sedimentary cover), and ~15 km (base of the seismogenic layer). The absence of seismogenic behaviour in the sedimentary cover could partly explain why, according to seismic moment summations, only 5% of the deformation in the Zagros is seismically expressed [Jackson *et al.*, 1995; Masson et al., 2005].

Along its southern front, the Zagros is bounded from its foredeep basin by the Mountain Front Fault (MFF), but local topographic expressions, both onshore and offshore, attest to active folding south-west of this major tectonic boundary; hence, the existence of a more frontal fault, the Zagros Foredeep fault (ZFF), has been proposed by Berberian [1995] (cf. Figure III-1). The Mand anticline, which will be discussed in detail in the present work, is one of these active structures in front of the MFF. It is singular in several aspects: it represents the westernmost frontal structure of the Fars arc; its general orientation is NNW-SSE to N-S, in contrast with the NW-SE orientation of most folds in the Fars arc; and it is located in the azimuth of the Kazerun Fault, which is one of the major N-S strike slip faults in the Zagros orogen and which corresponds to an inferred boundary between the Fars arc, with Hormuz salt at the base of the sedimentary sequence, and the Dezful embayment where this thick incompetent unit is considered absent or much thinner. The absence of both basal Hormuz salt and of major detachment folds like the Mand anticline further west is probably not coincidental, given the strong control that weak basal layers have on detachment fold development.

2.1. Regional balanced cross section

In order to estimate the finite deformation of the sedimentary cover and constrain the depth to basement, we have constructed a balanced section across the frontal part of the central Zagros (Figure III-2). In the Mand region, Letouzey and Sherkati [2004; see also Sherkati *et al*, 2006] have previously proposed a detailed balanced cross-section based on both surface data and unpublished seismic reflection and well data provided by the National Iranian Oil Company (NIOC). Outcrops and borehole data provided them in particular a good thickness control on Permian to recent sedimentary units. Balanced cross-sections rely on the assumption that no material moves into, or out of, the plane of the section. In the study area, this assumption may not be valid, as there may be a considerable regional component of oblique slip relative to fold orientation (e.g., Figure III-1). In constructing the section of Figure III-2, we have used the cross-section of Letouzey and Sherkati [2004], complementing it to the north-east according to structural data and following the sinuous bed method, which supposes constant bed thickness for the competent layers during shortening [Dahlstrom, 1969]. Although balanced cross-section solutions are non-unique, and the deepest units are poorly imaged by the seimic lines, the surface structures appear to project through a detached fold over the MFF ramp, where the master fault-cored folds converge on a décollement level in the Hormuz Salt. The balanced sections indicate different degrees of fold asymmetry close to the ZFF, where the Mand detachment anticline is distinctly symmetrical, and over the MFF ramp, where a system of master fault-cored folds has developed with a clear foreland-ward vergence, possibly due to thick-skinned deformation (Figure III-2).

In constructing cross sections across the Zagros fold belt, two major problems have to be faced. First, the projection of concentric detachment folds to depth generally produces severe space incompatibilities that require disharmonic folding of the ductile layers above a basal detachment [Mitra, 2003], and lead to different line length versus area restorations.

In the cross-section of Figure III-2, the space problem is generally solved by inferring the presence of thrust faults in the Paleozoic to early Cretaceous competent rocks in the cores of the anticlines, linked to a decreasing ratio of fault offset to layer folding up-sequence. Second,

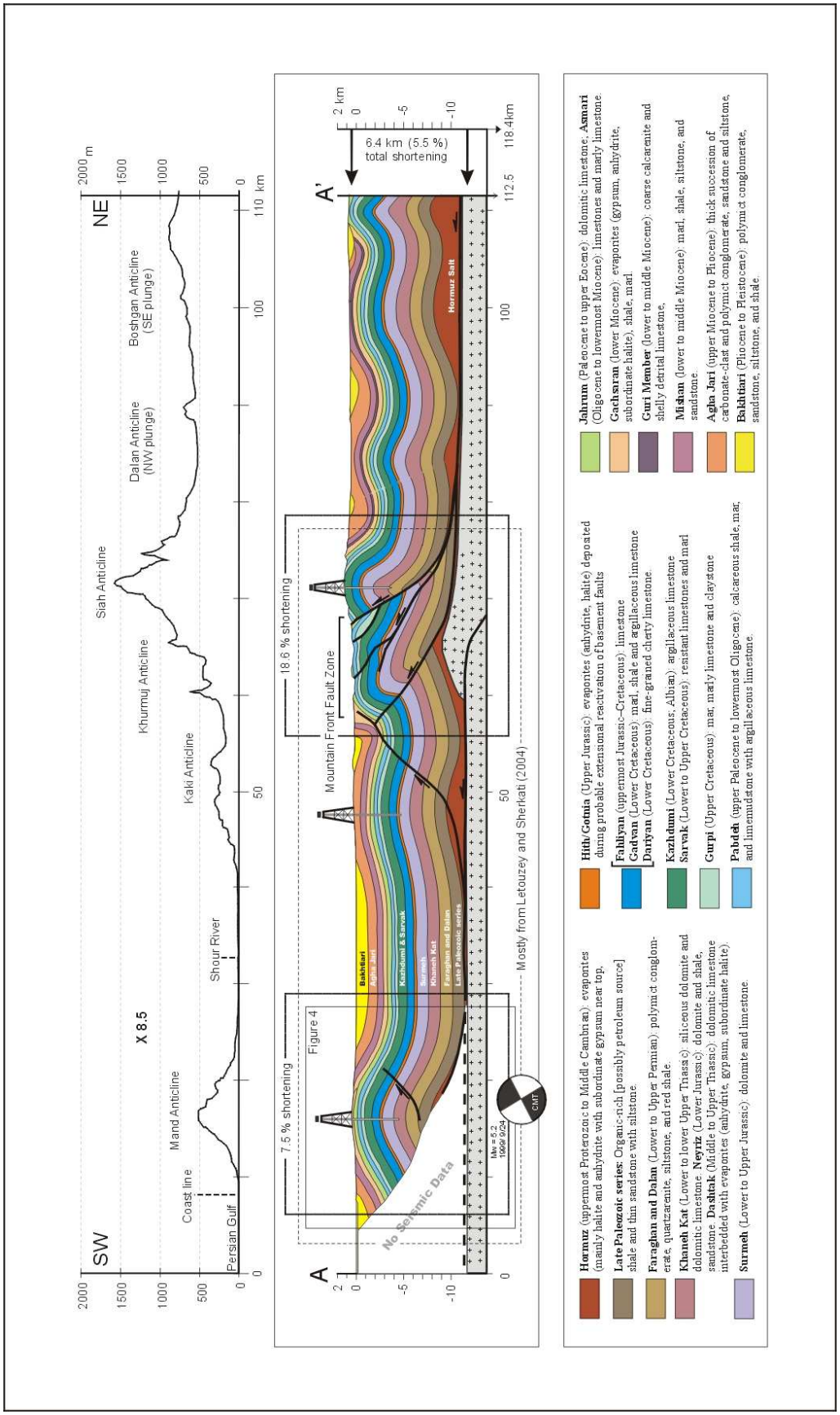
SW
NE
X 8.5
Persian Gulf
Coast line
Mand Anticline
Shour River
Kaki Anticline
Khurmuj Anticline
Siah Anticline
Dalan Anticline (NW plunge)
Boshgan Anticline (SE plunge)
2000 m
1500
1000
500
0
110 km
A
A'
7.5 % shortening
18.6 % shortening
Figure 4
Mountain Front Fault Zone
No Seismic Data
Mostly from Letouzey and SheKati (2004)
6.4 km (5.5 %) total shortening
118.4km
112.5
2 km
-5
-10
Hormuz Salt
Bakhtiari
Agha Jari
Kazhdumi & Sarvak
Gurpi
Pabdeh
Fahliyan and Dariyan
Late Paleozoic series
Khaneh Kat
Surmeh
Hith/Gotnia (Upper Jurassic): evaporites (anhydrite, halite) deposited during probable extensional reactivation of basement faults
Fahliyan (uppermost Jurassic–Cretaceous): limestone
Gadvan (Lower Cretaceous): marl, shale and argillaceous limestone
Dariyan (Lower Cretaceous): fine-grained cherty limestone.
Kazhdumi (Lower Cretaceous, Albian): argillaceous limestone
Sarvak (Lower to Upper Cretaceous): resistant limestones and marl
Gurpi (Upper Cretaceous): mar, marly limestone and claystone
Pabdeh (upper Paleocene to lowermost Oligocene): calcareous shale, mar, and limemudstone with argillaceous limestone.
Johrum (Paleocene to upper Eocene): dolomitic limestone; Asmari (Oligocene to lowermost Miocene): limestones and marly limestone.
Gachsaran (lower Miocene): evaporites (gypsum, anhydrite, subordinate halite), shale, marl
Guri Member (lower to middle Miocene): coarse calcarenite and shelly detrital limestone,
Mishan (lower to middle Miocene) marl, shale, siltstone, and sandstone.
Agha Jari (upper Miocene to Pliocene): thick succession of carbonate-clast and polymict conglomerate, sandstone and siltstone,
Bakhtiari (Pliocene to Pleistocene): polymict conglomerate, sandstone, siltstone, and shale.
Hormuz (uppermost Proterozoic to Middle Cambrian): evaporites (mainly halite and anhydrite with subordinate gypsum near top.
Late Paleozoic series: Organic-rich [possibly petroleum source] shale and thin sandstone with siltstone.
Faraghan and Dalan (Lower to Upper Permian): polymict conglomerate, quartzarenite, siltstone, and red shale.
Khaneh Kat (Lower to lower Upper Triassic): siliceous dolomite and dolomitic limestone. Neyriz (Lower Jurassic): dolomite and shale, sandstone. Dashtak (Middle to Upper Triassic): dolomitic limestone interbedded with evaporites (anhydrite, gypsum, subordinate halite).
Surmeh (Lower to Upper Jurassic): dolomite and limestone.

Figure III-2. Balanced cross section of the frontal Zagros between the Persian Gulf and the hangingwall of the Mountain Front Fault (MFF); modified from Letouzey and Sherkati (2004). Box shows location of detailed cross-sections across Mand anticline shown in Fig. III-4.

topographic steps accompanied by the progressive north-eastward thinning of the Mio-Pliocene units filling the synclines require that the depth of the base of the sedimentary sequence decreases to the north-east. Because the base of the crust plunges gently (1-2°) to the north-east [Paul *et al.*, 2006], a space problem occurs between the top of the basement and the base of the sedimentary cover. McQuarrie [2004] has proposed to fill this void with locally more than 5 km of deformed Hormuz salt, but Mouthereau et al. [2006] have shown that such thicknesses of weak salt cannot mechanically sustain the load of the overlying units over geological timescales; the salt would be rapidly squeezed out. Other authors [e.g Sherkati and Letouzey, 2004; Molinaro et al., 2005; Mouthereau et al., 2006] have invoked thick-skinned tectonics, with a number of basement thrusts controlling a south-west plunge of the top of basement of 1-2°, i.e. slightly more than the topography. In the cross-section of Figure III-2, the south-western part of which was derived from Letouzey and Sherkati [2004], the void between folded strata and the crystalline basement has been filled both by basement imbrications (i.e., thick-skinned deformation) and local thickening of Hormuz evaporites in the core of anticlines. Our balanced cross-section indicates 6.4 km of total horizontal shortening across the most frontal folds that occur along the ZFF and MFF.

3. THE MAND DETACHMENT FOLD

3.1. Structure

The Mand fold is a doubly-plunging detachment anticline with a curvilinear convex-to-the-south hinge, wide crest and quasi-homoclinal fore- and back-limbs. It extends ~100-km along strike (Figure III-3). The topographically expressed width of the fold is laterally constant at ~16 km, but its amplitude shows a gradient, decreasing toward the northwest along the fold axis. Along the anticline, the near-symmetrical dip panels on each side of the fold obscure any structural vergence and no outcropping fore- or back-thrusts (relative to the south-west directed transport of the belt) are associated with the fold. In contrast to the tightly folded anticlines associated with the MFF ramp, the Mand anticline is an open fold (cf. Figure III-2). At the surface, the fold exhibits limbs dominated by gentle bedding dips between 10-27°, and presents a high wavelength/amplitude ratio ($\delta \approx 8.3$ in its central part). According to seismic and well data

[Letouzey and Sherkati, 2004], the flanks of the anticline are buried below 1-2 km of Plio-Pleistocene sediments of the Lahbari and Bakhtiari Formations. The entire width of the anticline may therefore reach 20 to 25 km. The geophysical data and reference cross-section (Figure III-2) provide a tight control on the thickness of sedimentary units involved in the fold, and helped us to derive several sections across the Mand anticline in order to describe its spatial geometry and evolution, as well as to investigate the deformational style (Figure III-4). These balanced cross-sections were constructed orthogonally to the structure, in order to maximize access to structures and bedding exposures. Structural and sedimentological data were mapped in the field and using 1:100,000-scale geologic maps [National Iranian Oil Company, 1976, 1977], Landsat and SPOT satellite images, and a 90m-resolution digital elevation model (SRTM).

3.2. Fold solution and finite shortening

Detachment folds [Jamison, 1987; Mitra, 2003] form in sedimentary units characterized by significant thickness and competency contrasts, in which the basal layer is commonly an incompetent or low viscosity unit such as shale or salt, and is overlain by thick competent units such as carbonates and sandstones. Under subsequent shortening, fold growth is generally considered to occur by two competing mechanisms: limb lengthening by migration of beds through hinges and limb rotation between fixed hinges by internal deformation. Despite numerous structural studies of detachment folds, the kinematic development of these structures, and their related balancing, remains controversial [De Sitter, 1964; Dahlstrom, 1990; Poblet and McClay, 1996; Poblet *et al.*, 1997; Mitra, 2003]. The key questions relate to the relative importance of hinge migration and limb rotation, the amount of internal bed thickening, as well as the nature of deformation of the basal incompetent unit. Fixed hinge models, for example, propose that a detachment fold develops a long wavelength early in its evolution and subsequently evolves primarily by limb rotation and fold tightening [De Sitter, 1964], whereas wavelength is constant in models with mostly hinge migration. In both models, the wavelength/amplitude ratio is considered to be high in the early stages of fold development and to subsequently decrease during fold evolution. These models suffer, however, from an unequal line length versus area restoration and thus require an increase in detachment depth with progressive fold evolution, a solution considered as kinematically and geologically inadmissible [Dahlstrom, 1990]. Several alternative solutions have been proposed to solve the balancing problem. First, most of the shortening could be absorbed by internal deformation in the core of gentle folds, with an increasing degree of internal deformation toward the base in order to solve

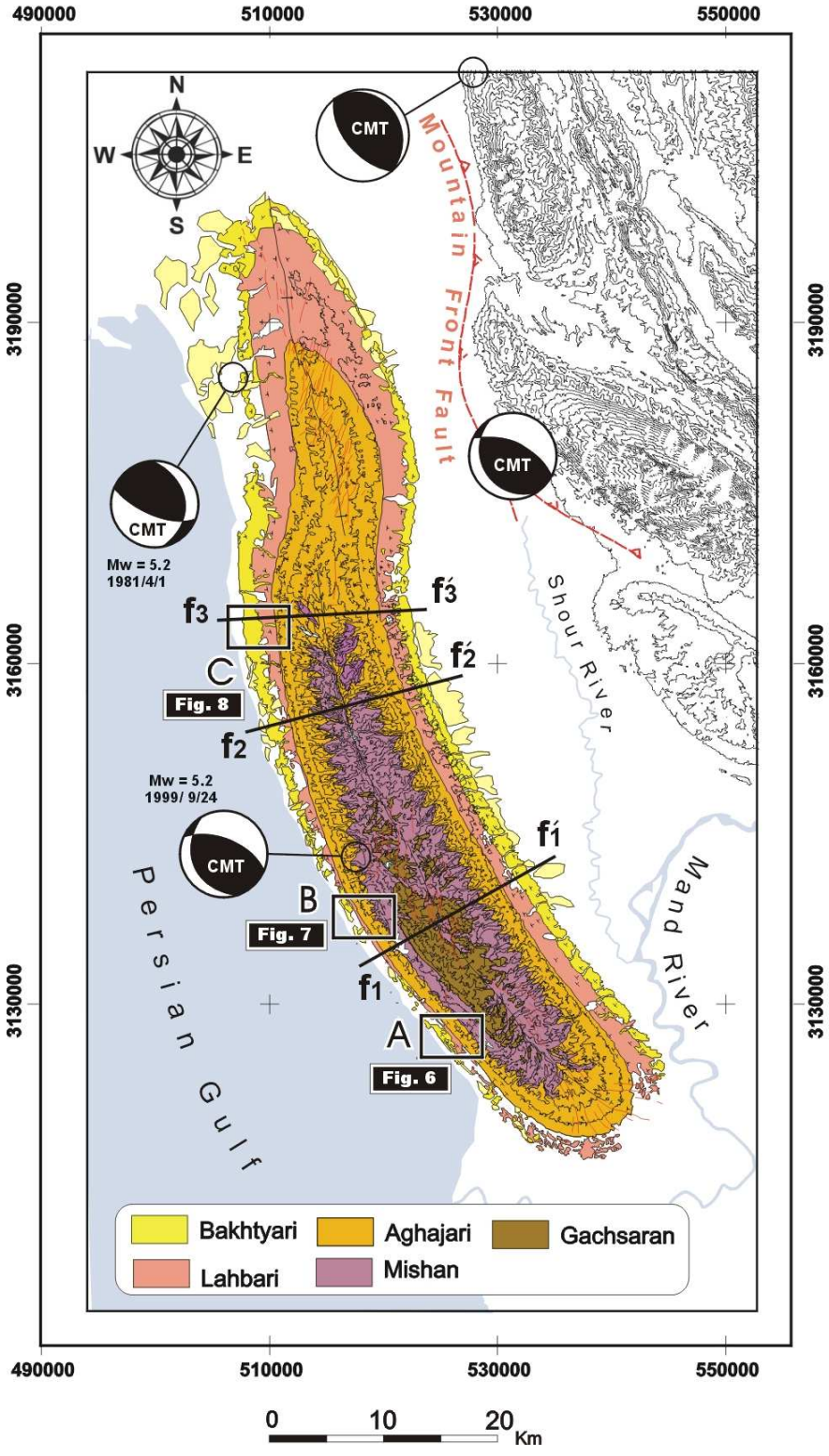

Figure III-3. Geologic map of the Mand anticline with elevation contour lines every 100 m. Focal mechanism solutions for large earthquakes from the Harvard CMT database. Profiles f1-f1', f2-f2' and f3-f3' are shown in Figure 4. Boxes show locations of surveyed terrace sites (Figures III-6-8).

the line lengths versus area restoration at depth [Epard and Groshong, 1995]. Internal strain would be accommodated by secondary faulting in competent units, whereas bed thickening could characterize the incompetent stratigraphic units. On the other hand, Mitra [2002; 2003] has proposed that the balancing problem could be reduced by considering that synclinal flexures flanking detachment anticlines could be deflected below the regional position of the considered stratigraphic level. In this model, affected by variable limb dip and -length, limb rotation is accompanied by hinge migration through the synclinal and/or anticlinal hinges, and at depth by the migration of the basal ductile unit from the base of the syncline toward the anticline core. Synclinal sinking is, however, not commonly recognized, probably because the downward deflection is usually small and occurs over a very broad region [Mitra, 2002; 2003].

In the case of the Mand anticline, the cross-section proposed by Letouzey and Sherkati [2004] (Figure III-2) is unconstrained on its south-western limb due to absence of seismic data, and permits several alternative balanced fold solutions.

Case 1: folding above a SW-vergent fault

Sherkati *et al.* [2006] propose that the Mand detachment fold has evolved towards a fault-bend or fault-propagation fold. The propagation of a forward verging blind fault, with a mean dip of ~30° and associated to a steep (~45°) back-thrust, would have produced a vertical offset of the sedimentary units of several kilometres. Such fault offset would solve the line length versus area problem, but would require more than 2 km offset even for the uppermost sedimentary units close to the surface. There is, however, no topographic indication in the bathymetry of the Persian Gulf for such active faulting. Slip motion on the fault could have been transferred to a more frontal structure, but again the bathymetry does not indicate such a feature.

Case 2: fold detachment with internal deformation

The stratigraphy of the ZSFB contains several incompetent evaporite and shale intervals that may act as décollement levels [e.g., Sherkati and Letouzey, 2004]. The Mand anticline may thicken by internal accommodation strains of such incompetent material (e.g. through homogeneous strain, second order folding, or second order conjugate faulting). Here, we apply the excess area restoration technique [Epard and Groshong, 1993] to evaluate horizontal shortening for different depth levels beneath a reference level. Assuming constant rock density

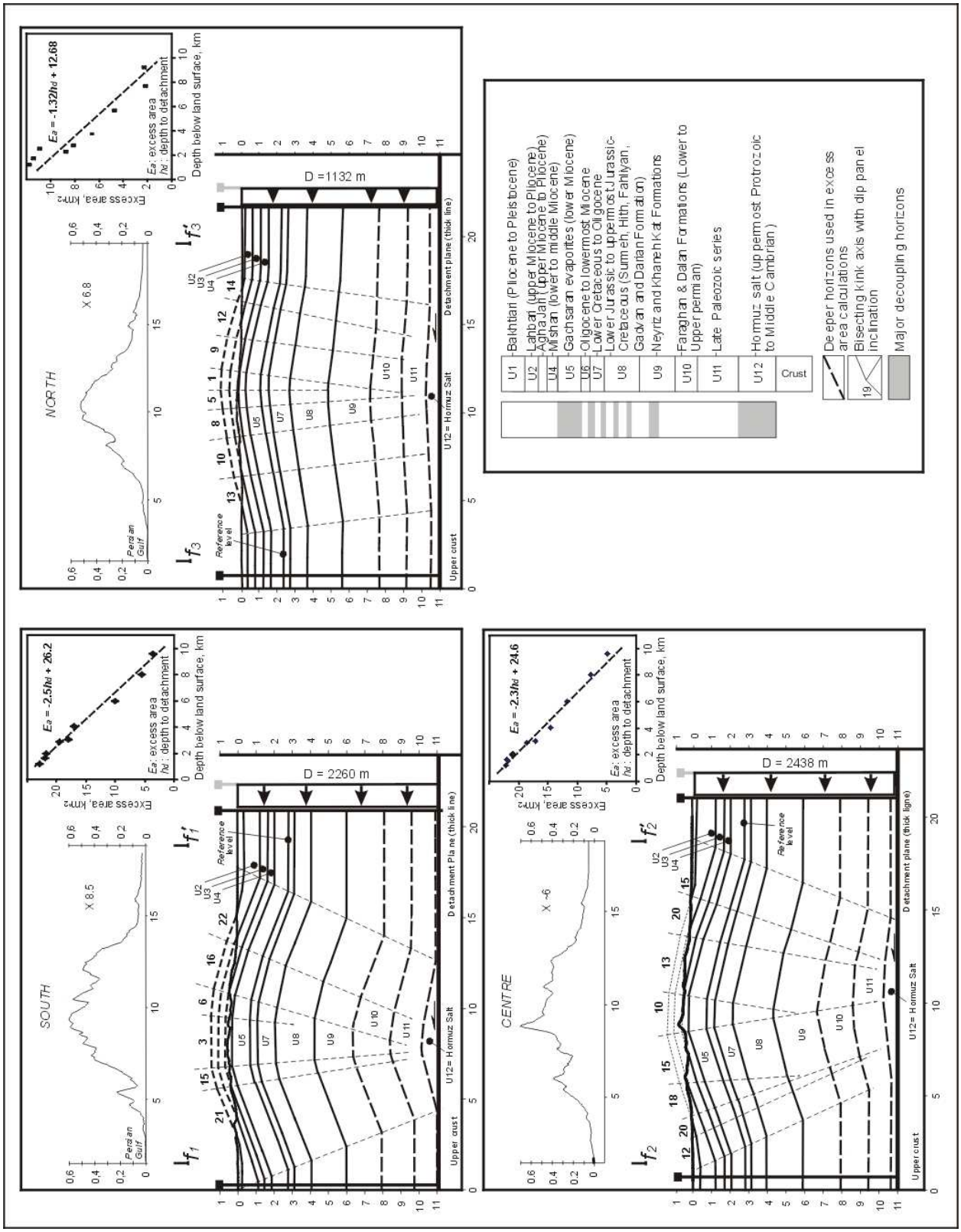
NORTH
SOUTH
CENTRE
Persian Gulf
Reference level
Upper crust
Detachment plane (thick line)
U12= Hormuz Salt
D =1132 m
D = 2260 m
D = 2438 m
Depth below land surface, km
Excess area, km2
Ea: excess area
ht: depth to detachment
Ea = -1.32ht + 12.68
Ea = -2.5ht + 26.2
Ea = -2.3ht + 24.6
X 6.8
X 8.5
X ~6
U1 Bakhtiari (Pliocene to Pleistocene)
U2 Lahbari (upper Miocene to Pliocene)
Agha Jari (Upper Miocene to Pliocene)
U4 Mishan (lower to middle Miocene)
U5 Gachsaran evaporites (lower Miocene)
U6 Oligocene to lowermost Miocene
U7 Lower Cretaceous to Oligocene
U8 Lower Jurassic to uppermost Jurassic-Cretaceous (Surmeh, Hith, Fahliyan, Gadvan and Darian Formation)
U9 Neyriz and Khaneh Kat Formations
U10 Faraghan & Dalan Formations (Lower to Upper permian)
U11 Late Paleozoic series
U12 Hormuz salt (uppermost Protrozoic to Middle Cambrian)
Crust
Deeper horizons used in excess area calculations
Bisecting kink axis with dip panel inclination
Major decoupling horizons

Figure III-4. Fold solutions for the Mand anticline at depth for a detachment fold with bed thickening. The cross-sections are constructed using surface bedding dip, a constant detachment depth and a plot of the relationship between the excess area and depth to the reference horizon (upper right inset diagrams). The compatibility of the restoration is set by adjusting the slope of the excess area versus depth diagram and its intercept with the x-axis that must equal the depth to the detachment. Locations of cross-sections shown in Figure III-3.

during folding, the excess area is equal to the shortening times the depth to the detachment. Therefore, the slope of the statistical best fit line on diagrams of excess-area (E_A) versus depth to detachment (h_d) indicates total horizontal shortening if area is conserved. We adopt a depth of 11 km to the basal detachment level (Hormuz Salt) and evaluate excess area at different stratigraphic levels for three cross-sections across the Mand anticline (Figure III-4). We take the top of the Asmari Fm (U_6 in Fig. III-4) as our reference level, in order to avoid complications due to possible secondary detachments in the overlying incompetent Gahsaran unit. A simple cylindrical fold construction leads to E_A-h_d curves that do not project to $E_A = 0$ at $h_d = 11$ km (i.e., the base of the detachment level). In order to produce a more strongly decreasing gradient in excess area with depth, internal deformation and thickening of the units has to be included. The best-fit line on the resulting E_A-h_d curve for the central part of the Mand anticline ($E_A = -2.31h_d + 24.541$; $r^2 = 0.975$ with the detachment level fixed at 8.7 km beneath the reference level), for instance, is close to the mean total shortening of 2.4 km that can be inferred from the excess area of each unit individually.

Case 3: Detachment fold accompanied by synclinal flexures

The cumulative thickness of the Mishan, Agha Jari and Lahbari Formations reaches 1.4 km according to their outcrop pattern in the Mand anticline (Figures III-3 and 4). If we consider the ages determined by magnetostratigraphy further north-west in Lurestan [Homke *et al.*, 2004], i.e. ~12 Ma for the Gachsaran/Mishan transition, and 3-4 Ma for the Lahbari/Bahktiari transition, a regional sedimentation rate of ~0.17 mm/yr can be computed for this period as a response to regional subsidence, which results from the loading of the Arabian platform by the Zagros wedge. On the basis of seismic line data [Letouzey and Sherkati, 2004], the post-Gachsaran sediment thickness in the syncline north-east of the Mand fold is slightly larger than 3 km. In consequence, sedimentation rates would have been >0.4 mm/yr for the last 4 Myr in the syncline between the Mand and Kaki anticlines. This noticeable change in sedimentation rates, even though poorly constrained in time, may suggest that this syncline has been depressed below the

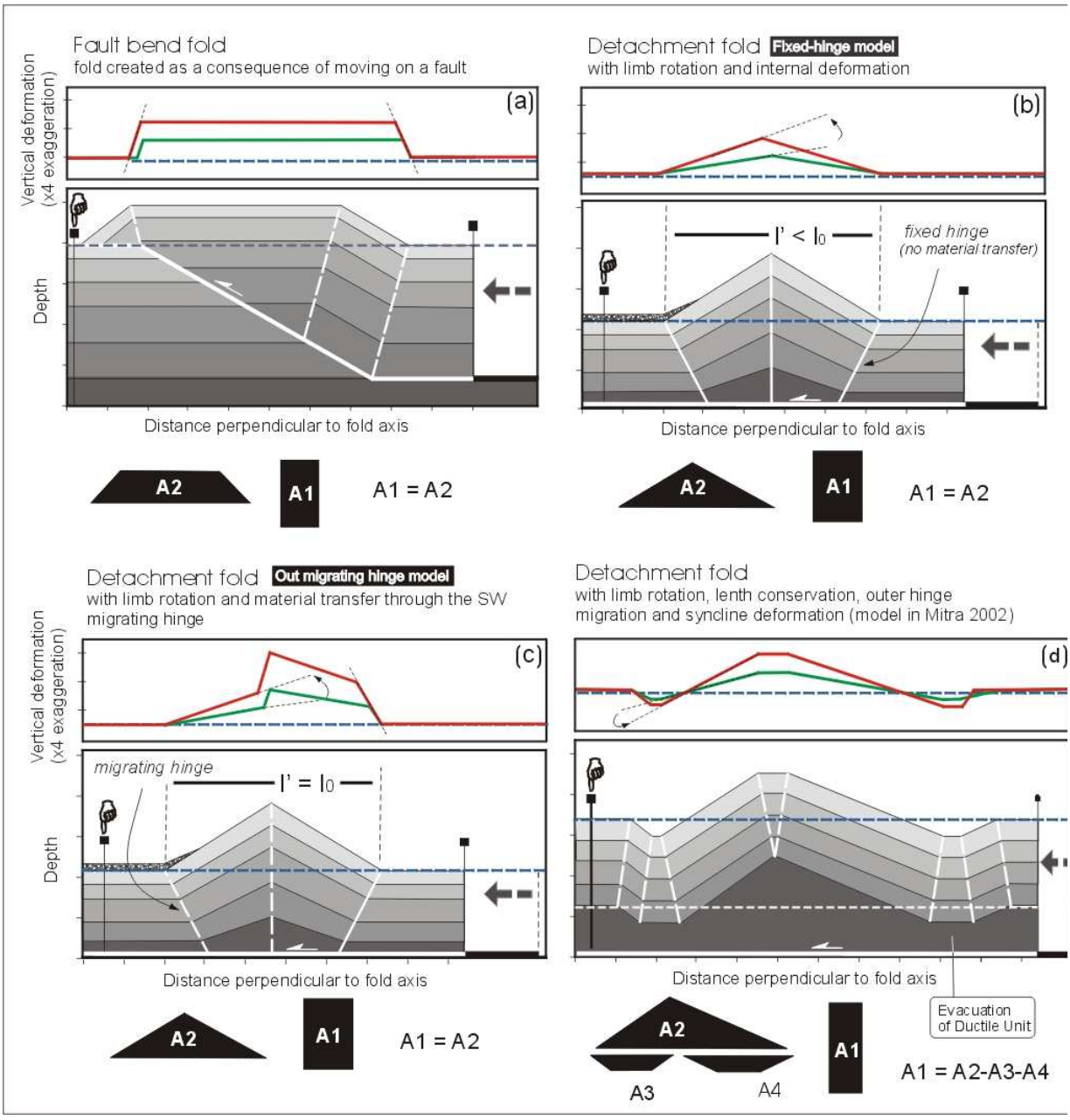

Figure III-5. Different fold models and associated surface deformation (obtained by producing incremental deformation in the different fold models): (a) fault-bend fold, (b) detachment fold with limb rotation and internal deformation, (c) detachment fold with limb rotation and material transfer through the SW axial surface, (d) detachment fold with limb rotation, length conservation, migration of the outer hinges and synclinal flexure. Lower panels show finite deformation after an amount of shortening equal to A1 divided by the depth to detachment; fixed and migrating hinges are presented by solid and dashed white lines respectively. Upper panels show incremental deformation as would be recorded by two marker surfaces with different ages. Method of area balancing for shortening calculations is also indicated for each model.

regional base-level and that this local effect has greatly enhanced the sedimentation rates. Note that, due to the proximity of the coastline, sea-level can be considered as the regional base-level in this area. Such syncline depression would be accompanied at depth by Hormuz salt migration from the syncline base toward Mand and Kaki anticlinal cores. The difficulty to estimate independently and precisely the regional subsidence rate prevents, however, to properly estimate this flexure.

3.3. Fold solution and incremental deformation at the surface

The currently available geological and geophysical data do not permit a clear discrimination of the fold solutions to describe the evolution of the Mand anticline. Additional kinematic information can be gained, however, from surface deformation, in particular if this information can be documented for different time steps. As shown schematically in Figure III-5, different end-member fold models produce distinct incremental deformation patterns, which will be recorded by initially horizontal passive geomorphic marker such as terraces. Fault-bend and fault-propagation folds will lead to uniform uplift above fault segments of constant dip; geomorphic markers will record some tilting where crossing axial surfaces. However, such steeply dipping panels will present a short wavelength and the dip is expected to be similar, i.e. terraces will be parallel, whatever their age (Figure III-5a). In contrast, limb rotation in a detachment fold will produce progressive terrace tilting, long and gently dipping panels and maximum uplift at the anticlinal crest (Figure III-5b). Detachment fold models with hinge migration produce profiles that are composites of the above two cases: progressive tilting of the markers along the limbs, but also steep parallel tilting at the synclinal and anticlinal hinges, with a marked asymmetry of the terrace uplift between the frontal fixed hinge and the backward migrating hinge (Figure III-5c). Finally, adding synclinal flexure to the detachment model will be recorded at the surface by progressive tilting of the marker, but also a transition from uplift to subsidence of the marker somewhere between the anticlinal and synclinal axes (Figure III-5d).

4. RECENT DEFORMATION OF MAND ANTICLINE

4.1. Tilted marine and fluvial terraces

Geomorphic evidence for active tectonics has been reported from several locations within the

Zagros belt along the MFF [Bachmanov *et al.*, 2004] and along the south-eastern coast of the Zagros [Vita-Finzi, 1982]. Around the Mand anticline, numerous discordant Bakhtiari units have been mapped: these units correspond to warped and tilted marine and fluvial terraces. Such terraces are particularly useful features since they can provide information on rates of rock uplift and hence rates of folding.

The terraces in the study area were first recognized on Corona and SPOT images, and then surveyed in detail in the field. They usually correspond to inverted topography: gravels or re-cemented shell-rich marine facies have preserved the underlying unconsolidated marly, silty or sandy Agha Jari/Labhari units from erosion; they consequently appear as isolated remnants at the top of small steep hills within a badland eroded landscape (cf. Figure III-9). We chose terrace treads to be surveyed on the basis of their preservation, in order to ensure continuity of the studied terrace level, such that the correlation of the close disconnected treads does not suffer any ambiguity. The precise locations and elevations of the terraces were measured using kinematic GPS and, where access was too difficult, with a laser distance meter from a GPS-referenced point in order to project all the points in the same geographic projection. The terrace elevations were measured with an accuracy of a few centimetres for the GPS survey and with an accuracy of 0.2–2 m for the distance meter, depending on the ranging distance (between 10 and 250 m). Where possible, we measured the elevation of the top of the terrace gravels or fill material, and also of the unconformity at the base of the terrace or strath level. Along the western limb of Mand anticline, we surveyed three distinct areas (cf. Figure III-3).

Southern site (site A):

In the southern part of the fold, extensive marine terraces have been preserved and display impressive tilted tabular surfaces in the landscape. These marine terraces are constituted by 3-5 m of beach deposits, consisting of a partially to fully cemented sandy matrix with numerous shells (bivalves, oysters, clams…). Two main terrace remnants have been identified at site A, separated by an erosional depression along an ephemeral stream or *wadi* (Figure III-6). Along the shore of the Persian Gulf, they occur 6-9 meters above present-day sea level and are covered by aeolian sand deposits and metre-high dunes. Inland, their remnants are well exposed up to 1 km from the shoreline and at elevations up to 90m above sea level. These marine terraces present remarkably linear profiles sloping at 9 % to the SW (Figure III-9a). Generally, such

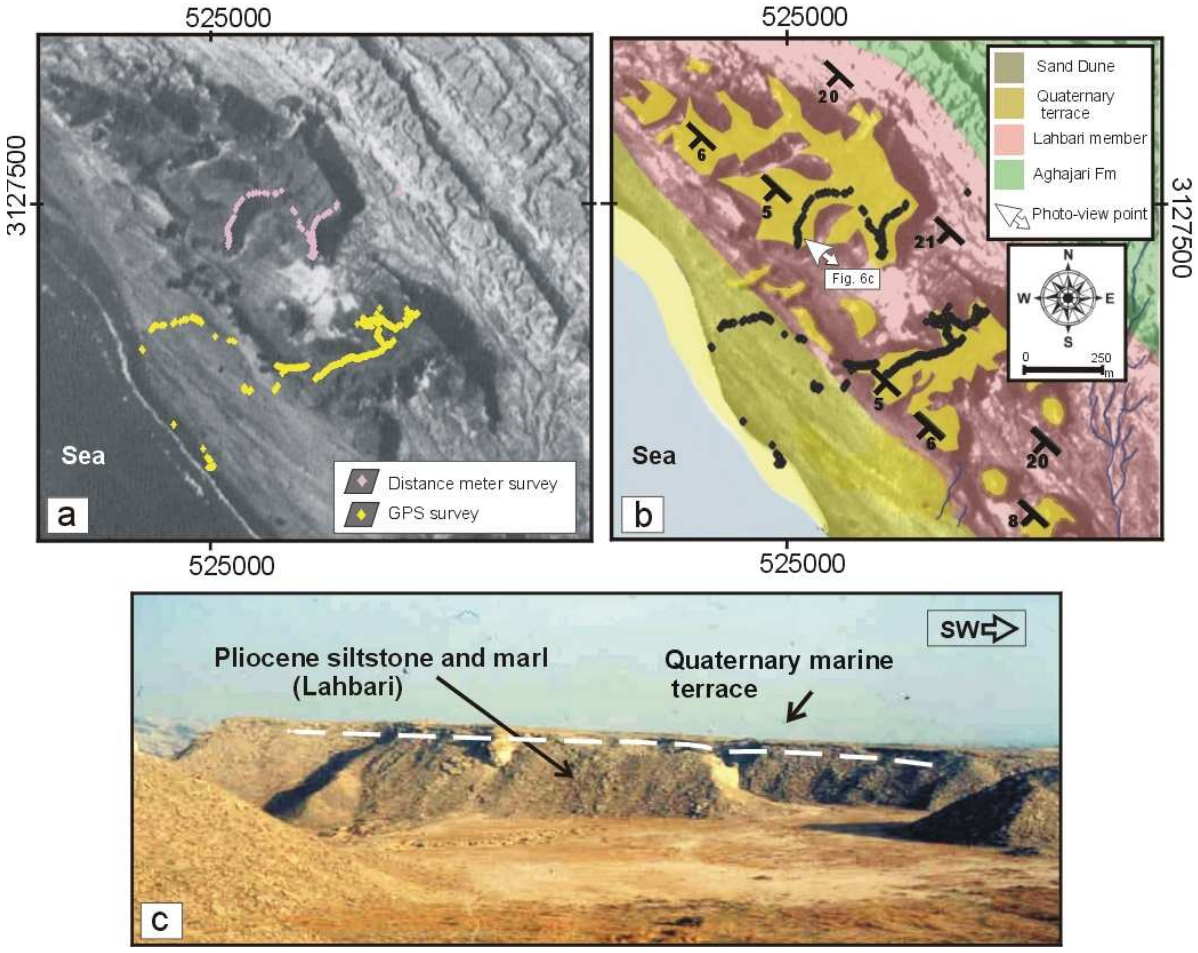

Figure III-6. (a) Corona satellite image and (b) geomorphologic map of the surveyed marine terrace site A in the southern part of Mand anticline (location indicated on Figure III-3). Survey data points for the construction of Figure III-9a are indicated. (c) Field photo of tilted marine terrace, looking SW across the erosional depression created by a *wadi* (photo viewpoint shown in b). The ~4.5° tilt of the terrace, as well as the angular discordance with the underlying Lakhbari Formation, is clearly visible.

marine terraces form in the tidal part of the shoreline, at or a few meters below average sea level, and with an angle of the order of 1 %. Assuming such an initial geometry provides a tilt perpendicular to the fold axis of the order of 8.0±0.4 % (~4.5°) since terrace formation.

The extensive marine terraces of the southern part disappear a few kilometres north of site A, after a progressive north-westward facies variation from cemented shell strata to cemented fossil dunes in the most inland part. Further North, the general elevation of the preserved tabular unconformable surfaces is lower and their slope more subdued. In addition, sedimentary units above the unconformity are mostly of fluvial- or fan-type deposits. Along most of the

Mand anticline, these surfaces are best preserved in a ~500 m wide coastal strip, where they are often partly covered by modern sand dunes. Sporadically, small remnants of these surfaces are preserved and display elongated and small "mesetas" that can be tracked up to 3km landward, at the foot of the rugged relief carved into the Agha Jari sandstone units. These surfaces represent isolated remnants of paleo-fan deposits emplaced onto a pediment zone, which developed south-west of the main fold relief in the non-cohesive and easily erodable silty Lahbari units.

Central site (site B):

In the south-central part of the anticline, an almost continuous tread of fluvial (or fan) terrace remnants were surveyed up to 1.5 km NE from the shoreline (Figure III-7). They form well-preserved flat and inclined surfaces, with straths that lie below 3 to 4 m of gravels. Toward the Persian Gulf coast, the base of the terrace gravels is replaced by a 2m-thick sandy beach facies, including a basal layer rich in marine shells (Figure III-9b). The regional slope of the strath does not change, however, at the transition between fluvial and beach facies. As observed in site A, both the terrace strath and tread are nearly linear in profile, sloping at 4.1% to the WSW (Figure III-9b). We hypothesise that the strath terrace has been carved and the gravels facies of the terrace transported and deposited by a similar *wadi* to the one that currently runs through the site. The latter has a contributing area of 11 km^2 and its gradient reaches 1.2 %. The original geometry of this *wadi* during deposition of the terrace material is difficult to estimate, but the ~3 % difference of slope between the terrace and the modern *wadi* is most probably due to tectonic deformation. Since terrace formation, the planar geometry of the *wadi* has radically changed, however: it was building a narrow fan whereas it is slightly entrenched in its pediment today and locally displays meanders. Such geometric changes, like potential gradient changes, may affect the reconstruction of the initial terrace geometry and the inferred deformation profile [Lavé and Avouac, 2000]. We

suspect that during the fluvial/fan deposition, the *wadi* was braiding and straighter than today. In addition, on the basis of the tilt recorded by the beach facies, which is supposed to be deposited near-horizontally, we suspect that the regional gradient of the fan was closer to the 1.2 % gradient of the present *wadi* than to the 1.6 % gradient of the modern pediment (Figure III-9b).

Assuming such an initial slope provides a tilt perpendicular to the fold axis of the order of $2.9^{+0.2}_{-0.4}$ % (~1.7°) since terrace formation.

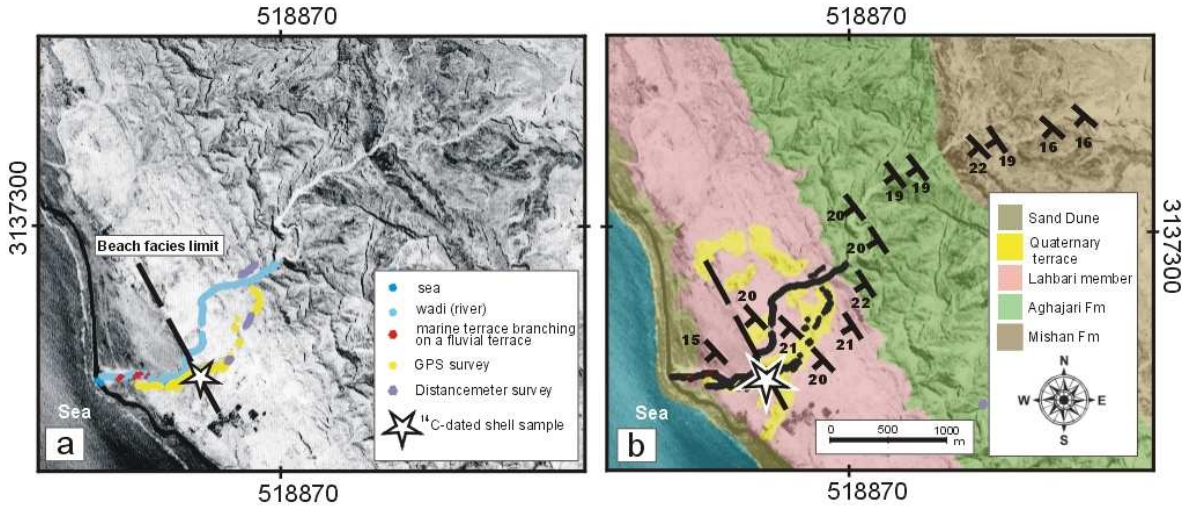

Figure III-7. (a) Corona satellite image and (b) geomorphologic map of surveyed fluvio-marine terraces at site B in the south-central part of Mand anticline (location in Figure III-3). Survey data points for the construction of Figure III-9b are indicated.

Northern site (site C):

In the northern part of the anticline, larger outcropping surfaces of the Lahbari Formation have permitted the development of a larger pediment and locally the preservation of an almost continuous tread of fluvial (or fan) terrace remnants up to 3.5 km from the shoreline (Figure III-8). As in site B, they form well preserved flat and inclined surfaces, with straths lying below 4 to 5 m of gravels. Toward the Persian Gulf, the base of the terrace gravels is replaced by a 4 m-thick sandy beach facies, including several layers rich in marine shells (Figures III-8 and 9c). As in site B, the regional slope of the strath level does not change at the transition between the fluvial and the beach facies. However, the top of the terrace is covered by a 20m-thick series of finer gavels (Figure III-10c). The strath level and the terrace top are close to linear in profile, sloping at 5.1% to the west, whereas the upper surface of the overlying fine gravel deposits close to the shoreline displays a more subdued slope of 1.8%. Considering again that the *wadi*, which has probably carved the strath terrace and transported and deposited the gravels of the terrace, is comparable to the present-day *wadi*, its contributing area is 6 km^2, and its modern gradient reaches 1.1 %. As for site B, and again on the basis of the tilt recorded by the beach facies, we will assume that the initial slope of the fan/terrace deposit was closer to this 1.1% of the present wadi than to the 1.8% gradient of the modern pediment (Figure III-9c). Using this as the initial slope provides a westward tilt of the order of $4^{+0.2}_{-0.4}$% (~2.3°) since terrace formation.

The general pattern displayed by these three sites is remarkably consistent: whatever their nature, the surveyed surfaces record a regional tilt perpendicular to the local fold axis. Except for uncertainties of the order of 5-10 m that result from a small curvature of the modern terrace and wadi profiles close to the Agha Jari relief in site B, these terraces appear to have been affected by large-scale tilting and seem exempt of secondary folding, faulting and other small-scale deformation features. The terraces do, however, record different degrees of tilting that result from differences in either terrace ages or local fold maturity. Because sites A and B are only 15 km apart and are associated with a similar amplitude of the main Mand anticline (cf. Figure III-4), we strongly suspect that terrace A has been affected by a 3 times larger tilting than terrace B because it is older and has thus recorded more deformation. In any case, the set of surveyed terrace levels clearly indicates persistent active folding of the Mand anticline.

In addition, stereographic observations on couples of Corona images indicate that the Bakhtiari and terrace surfaces on the Eastern limb of the anticline are also widely affected by tilting, without evidence for short scale folding or faulting, suggesting that the fold deforms, at least in part, by limb rotation on its eastern flank.

4.2. Terrace dating and rates of tilting

Whole shells as well as shell fragments have been sampled from the beach deposits in the terraces of Sites B and C (see location of samples in Figures III-7 and 8). Three bivalve fragments of apparently non-recrystallized calcite have been dated by Accelerator Mass Spectrometer (AMS) ^{14}C (Table 1). They all provided ^{14}C ages comprised between 28 and 37 kyr B.P., which correspond after a rough calibration [van der Plicht *et al.*, 2004] to ages ranging between 30 and 44 kyr B.P. (Table 1).

Numerous ^{14}C ages in this range have been encountered around the Persian Gulf [Vita-Finzi, 1982; Haghipour and Fontugne, 1993; Uchupi *et al.*, 1999], but several studies [Page *et al.*, 1979; Fontugne *et al.*, 1997] have cast doubt on the validity of such ages because of potential partial recrystallisation of bivalve shells. The main problem concerning these ages is that it is not obvious that the shallow and relatively restricted Persian Gulf was under marine influence during global sealevel lowstands. The global sea level curve [e.g., Lambeck and Chappell, 2001; Thompson and Goldstein, 2006] indicates that sea level was 70-80 m below present

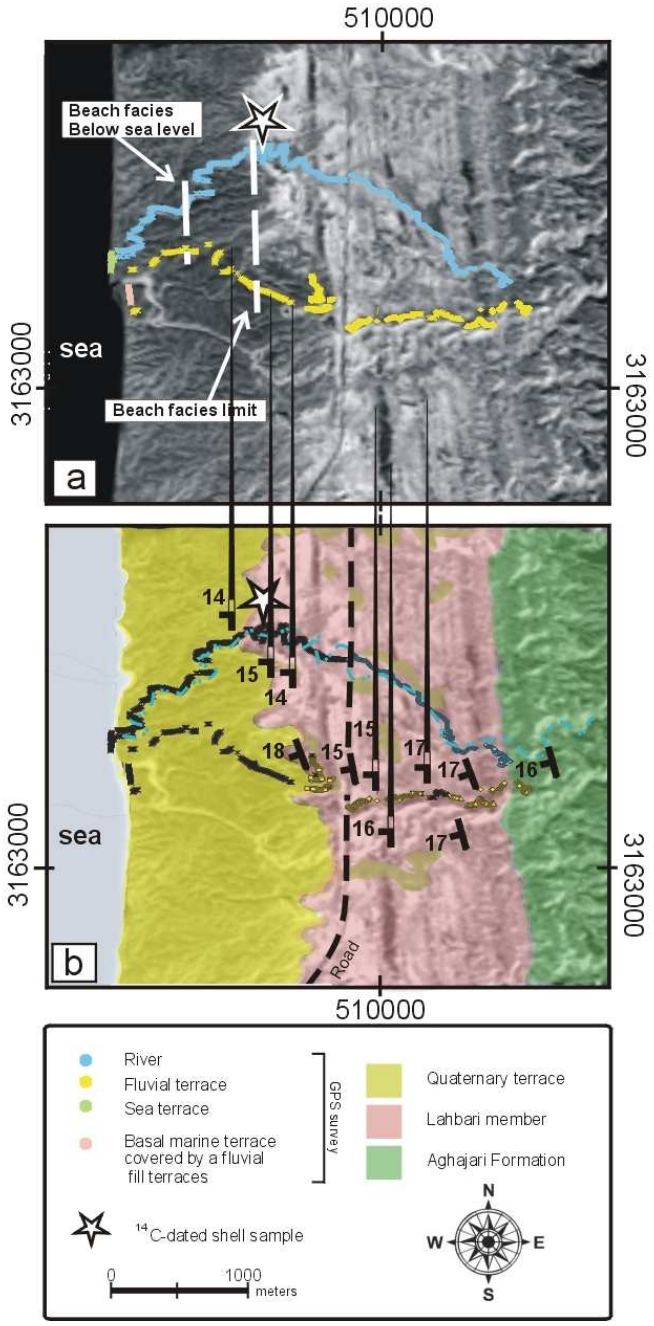

Figure III-8. (a) Corona satellite image and (b) geomorphologic map of surveyed fluvio-marine terraces at site C in the central-north part of Mand anticline (location in Figure III-3). Survey data points for the construction of Figure 9c are indicated.

during this period, with, however, secondary sea-level rises up to -50 to -60 m at 45, 48 and 52 kyr [Chappell, 2002] or at 31.5 and 48 kyr [Thompson and Goldstein, 2006]. A detailed postglacial shoreline reconstruction of the Persian Gulf, based on a glacio-eustatic model [Lambeck, 1996], predicts the central Gulf to be flooded for mean sea levels higher than -60 m. The bathymetry of the Persian Gulf in front of the Mand anticline displays a progressive drop down to a depth of 60 m, but this lowest point is located at ~40 km SW of the Mand anticline coast. However, a sonar survey of recent sediments in the Persian Gulf [Uchupi *et al.*, 1999], indicates that Late Pleistocene/early Holocene (since ~25kyr) sedimentation may amount to more than 10 or 20 m off the Fars coast, in particular along the present study area, where the Gulf receives sediment

Table III-1: AMS ^{14}C ages of bivalves sampled in marine terraces or beach facies:

Sample	*Lab. no.*	*^{14}C Age (yr)*	*Calibrated Age § (kyr BP)*
ZA-2002-16 (*)	Poz-11984	37200 ± 600	~41 [39 - 44]
ZA-2002-7a (*)	Poz-12063	28200 ± 200	~32 [30 - 35]
ZA-2002-7b (#)	001406	34350 ± 270	~39 [36 - 41]

***** *^{14}C dating in the Poznań Radiocarbon Laboratory, Poland.*

 # Laboratoire de Mesures Carbone 14 UMS 2572, CEN Saclay, France.

§Calibration range given by various calibration curves presented in **van der Plicht** *et al.* **[2004],** *after having applied a reservoir correction of ~400 yr.*

input from the two major Fars rivers, the Rud e Mand and Rud e Dalaki (Figure III-1). It is therefore possible that a very shallow sea extended up to the Mand anticline during the short-duration secondary highstands between 31.5 and 48 kyr, and would have left some beach deposits. This period was probably also marked by wetter conditions than today; more efficient rivers could thus have been draining and eroding the anticline, forming large pediments topped by several meters of gravel deposits overlying the Pleistocene Lahbari units.

Marine deposits in site A extend much more prominently than in the other sites. For this reason, we expect them to correspond to a major and long duration high stand associated with a major interglacial period. Marine terraces of Kish island, 300 km SE, correlate for example with high stands of marine isotopes stages (MIS) 5e and 7 [Preusser *et al.*, 2003]. More generally, numerous U/Th ages of corals topping marine terraces around the Makran and Persian Gulf

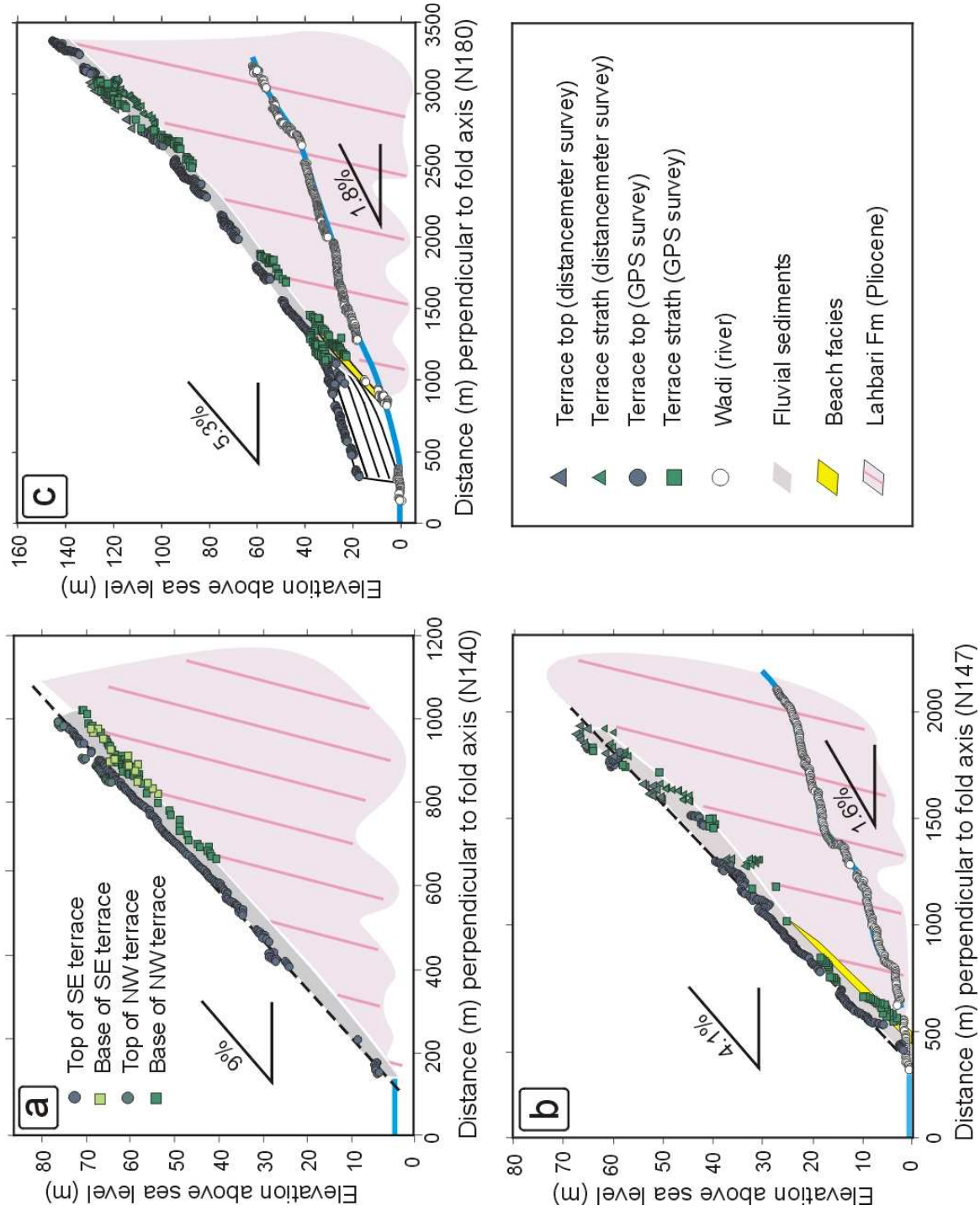

Figure III-9. Topographic profiles of the surveyed tilted terraces at sites A, B and C, along with present-day *wadi* profiles for sites B and C. Slopes of best-fit straight lines through terrace and *wadi* data are indicated.

[Reyss *et al.*, 1998] indicate generally well developed and distributed terraces formed during the penultimate interglacial [MIS 5e; 120-125 kyr, Thompson and Goldstein, 2006]. If marine terrace A would also have formed at this time, the tilting rate in A would reach 0.038 °/kyr, a value comparable to tilting rates ranging between 0.035 and 0.054 °/kyr in site B. Although additional dating of the terraces by an independent method would be welcome, this consistency with the attribution of the marine terraces around site A to the penultimate interglacial at 120 kyr B.P. provides us with some confidence in the ^{14}C shell dating. It should be noted, for example, that associating terrace B to MIS 5e, and terrace A to MIS 7, would provide much less consistent tilting rates of 0.014 °/kyr and 0.022 °/kyr respectively, and would not explain their different sedimentological nature.

4.3. Folding model and shortening rate

The terrace deformation profiles in the three sites provide several first-order observations to unravel the fold kinematics. Firstly, the observed wide-scale tilting precludes uplift above a shallow fault ramp, or would at least require a ramp that progressively flattens upward while transferring slip toward a more frontal structure, which is not observed. Tri-shear models [e.g., Erslev, 1991] could produce progressive tilting of the frontal limb but would be associated with significant bed thickening, in contrast with the constant layer thickness observed on both limbs. On the basis of the fold symmetry, terrace tilting, and increasing tilt with terrace age, it seems that only limb rotation associated to a detachment fold can account for the observed pattern of terrace deformation.

If we consider a simple sinusoidal fold model (Figure III-10), which fits observed surface bedding dips relatively well, the observed bedding of 21°, 16° and 11° along sections f1 (sites A/B), f2, and f3 (site C; cf Figures III-2 and 4), respectively, can be linked to a cosine amplitude of 1.4, 1.1 and 0.9 km, respectively with, importantly, roughly similar wavelengths. Whereas the structural data are not precise enough to detect a possible decrease of the wavelength by fold tightening between sections f3 and f1, these observations do suggest that the Mand detachment fold geometry can be modelled by a simple cosine shape during the different stages of its evolution. In the following, we will therefore assume such a simplified geometry to interpret terrace tilting in terms of shortening across the fold.

The increasing tilt of the terraces with age can be simply related to the evolution of fold amplitude and, with less resolution, to the evolution of fold wavelength. For a high wavelength/

amplitude ratio, the difference of shortening accounting for the different terrace tilting between a model with fixed hinges and constant limb length, and a model with migrating hinges and constant wavelength, was found to be smaller than 3%. Hereafter, we will therefore only present and discuss the results obtained for a fixed-hinge model, i.e. a model where the upper Agha Jari surface is modelled by a cosine curve in the range [-π/2; π/2], with its wavelength decreasing with increasing shortening and an initial and constant length of 12km. Accordingly, in the south-central part of the Mand anticline, a tilting of 4.5° (or 8%) and 1.7° (2.9%) as recorded by the terraces at sites A and B respectively, would have been produced by shortening of the order of 320 m and 125 m respectively (Table 2). For site C, despite a somewhat larger tilt (~2.3°) (or 4%) than in site B, we find a very comparable shortening value of 130 m. This result arises from the decreasing sensitivity of limb rotation to shortening during fold tightening.

As discussed in Section 3.2, one of the main problems with obtaining shortening estimates from detachment folds is related to the incompatibility between line-length versus area restoration. The two previously detailed cases can be examined in terms of present shortening rate:

***Case 1*:** The restoration paradox is solved by bed thickening: the total shortening represents the sum of the shortening absorbed by limb rotation and the shortening absorbed by bed thickening (Figure III-10c). This latter component represents 54 to 65% of the total shortening (Table 2) for limb angles of 21° and 15° respectively (in terms of instantaneous shortening rate, a limb angle of ~30° is required to annihilate the bed thickening component). With such a model, the total shortening rate across the Mand anticline in site C could reach up to 9 mm/yr and be 35 to 50% larger than in sites A and B.

Case 2: the restoration paradox is solved by synclinal flexure below a regional level (Figure III-10d). In this case the additional flexure of the syncline increases the shortening absorbed by limb rotation by only 25%, and provides total shortening rates ranging between 3 and 4 mm/yr for all three sites (Table 2).

Not only do the above two models predict distinct shortening rates, they also display another different feature at the surface: the location of the pivoting point, or point of no uplift during folding. For a similar fold wavelength and amplitude between the anticlinal crest and the

flanking depocentres (whether these are flat or synclinal), the point of no uplift will be closer to the anticlinal axis in the synclinal flexure model (compare Figures III-10 c and d). In the case of the Mand anticline, its topographically expressed width of ~16 km is much shorter than the estimated anticline wavelength of ~24 km. The external parts of the anticline (~4 km on both sides), which have no topographic expression, may therefore be subsiding and affected by a sedimentation at more rapid rates than the local uplift. Long term regional subsidence and sedimentation rates probably range between 0.2 and 0.3 mm/yr, assuming 2-2.5 km of regional sedimentation [Fig. III-10b; Letouzey and Sherkati, 2004] since the end of the Gachsaran sequence at ~12 Ma [Homke *et al.*, 2004]. Considering the above cosine model and tilting

			Sinusoidal Fold model				Shortening using area conservation (m)	Shortening rate (mm/yr) including internal deformtion	Shortening rate (mm/yr) with adjacent syncline model
	Marker Tilt (%)	Age (kyr)	Present amplitude (m)	Amplitude change since terrace formation (m)	Length shortening (m)	Shortening rate (mm/yr)			
Site A	8 ± 0.5	120 ± 5	1420	330	320 ± 20	2.7 ± 0.15	750	6.3	3.3
Site B	$2.9^{+0.2}_{-0.4}$	40 ± 5	1420	120	124^{+8}_{-16}	$3.1^{+0.4}_{-0.5}$	270	6.8	3.9
Site C	$4.0^{+0.2}_{-0.7}$	40 ± 5	1100	160	130^{+7}_{-19}	$3.2^{+0.4}_{-0.6}$	370	9.3	4.0

Table III-2. Shortening rate calculations according to the considered fold model

rates, such a sedimentation rate would imply the pivoting point to be ~9.5 km away from the anticlinal axis and not ~7 km, as observed from the 0 elevation of terrace A (note that we implicitly assume here that this terrace has formed during the MIS 5e and that sea level at that time was close to the present-day sea level). Consequently, much higher local sedimentation rates are required, a hypothesis that is compatible with active subsidence of the synclines flanking the Mand anticline.

The above values and estimates of shortening, as well as the preceding argument supporting syncline flexure, are clearly model dependent and no definitive conclusion about fold kinematics and total shortening can be reached without detailed seismic data that would image the upper structures in the frontal syncline. The representation of the fold by a cosine shape probably represents an oversimplification, and the flanking synclines could be much broader than the anticline, as suggested by the cross-section of Figure III-2. However, as in the cosine model, the associated flexure absorbs a reduced amount of shortening and will not significantly location of affect the shortening estimates. Finally, it should be noted that the above argument

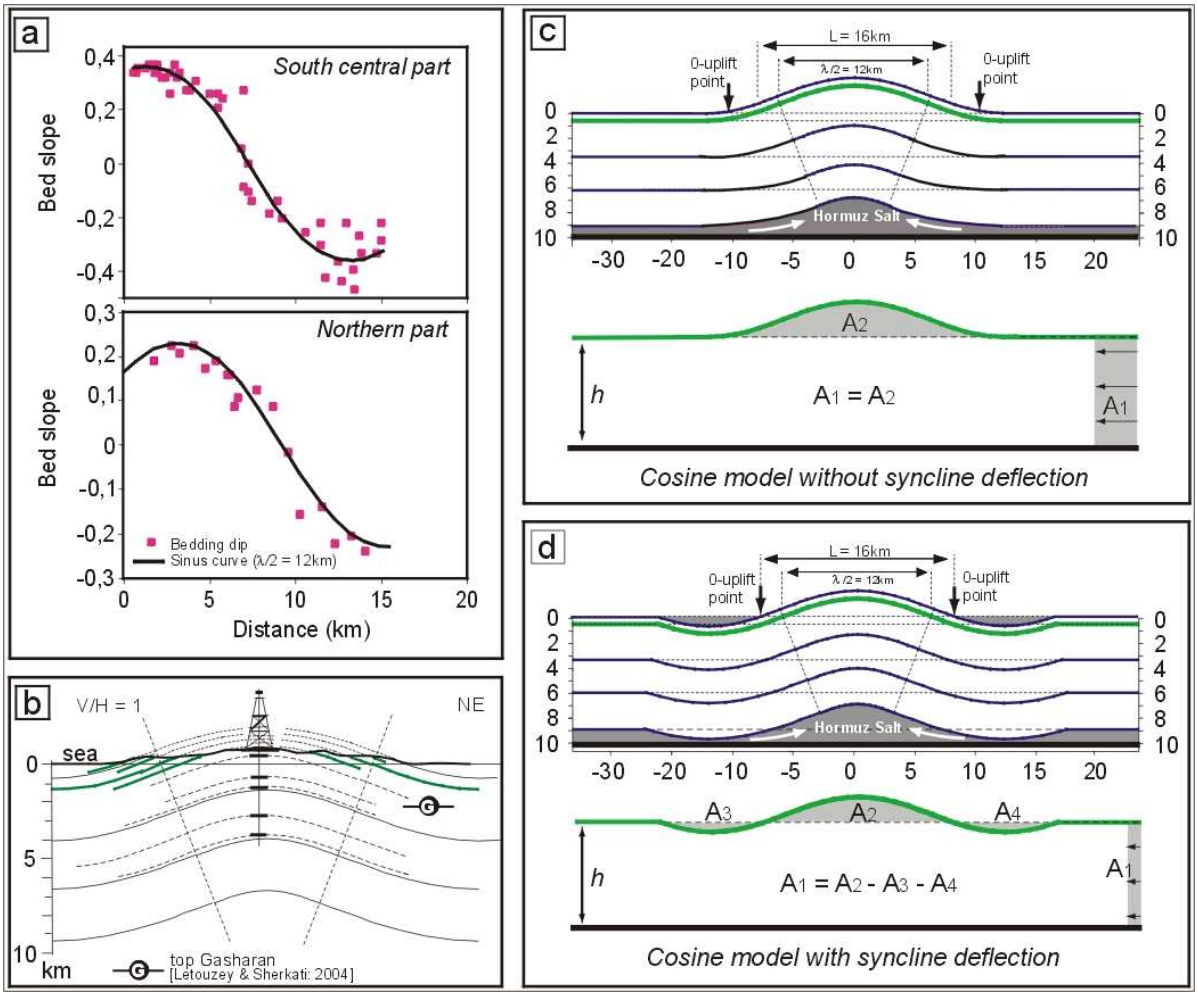

Figure III-10. Cosine model applied to upper folded units of the Mand anticline. (a) Bedding dips (from geologic maps and field survey) along the central and northern profiles (f2-f2' and f3-f3' in Figure III-3) follow a sinusoidal curve centred at the anticline axis. (b) Fold geometry approximated by a cosine model with a crest to through amplitude of ~3 km and a wavelength (λ) of 24 km. Models without (c) or including (d) flexure of the flanking synclines yield a distinct area conservation but also distinct locations of the no-uplift point between the anticlinal and synclinal axes.

about the the pivoting point depends on the inferred fold uplift rate, i.e. on terrace dating. If our ^{14}C ages are minimum ages and terraces are older than assumed here, the local uplift to regional subsidence ratio would consequently decrease, and the pivoting point would be located closer to the anticlinal axis.

5. DISCUSSION

Several recent morphotectonic studies have described and quantified different fold kinematics and associated deformation at the surface, as recorded by geomorphic markers [e.g., Lavé and

Avouac, 2000; Benedetti *et al.*, 2000; Thompson *et al.*, 2002; Ishiyama *et al.*, 2004; Gold *et al.*, 2006]. The present study on the Mand anticline is, however, to our knowledge one of the first to document the recent growth of a detachment fold. The progressive tilting of the coastal marine and fluvio-marine terraces along the Mand anticline highlights that this detachment fold primarily deforms by limb rotation, in contrast to many other fold models where deformation occurs by hinge migration in association with dominant fault motion at depth, like fault-bend folding or fault-propagation folding. Whereas these fold types are favoured by a homogeneous sedimentary sequence but with strong mechanical anisotropy permitting bedding slip, the Zagros sedimentary sequence is characterized by major mechanical stratification, with an upward sequence of basal ductile units, followed by competent units, and upper incompetent units. As proposed by Mitra [2002], such a setting favours the development of detachment folds like the Mand anticline. Although large uncertainties remain concerning its exact geometry at depth, as well as the original thickness of the basal Hormuz salt, the terrace data suggest that this ductile layer was sufficiently thick to permit ≥500 m flexure of the synclines flanking the Mand anticline and salt migration from the synclines towards the core of the anticline.

We are not able to provide strong evidence in favour of active flexure in the synclines, but several lines of evidence discard the alternative model characterised by dominant bed thickening. Firstly, clear evidence of thickening has not been observed; the anticlinal crest, in contrast, displays numerous extensional fractures. Secondly, the location of the no uplift points in profile indicates that either the anticline is narrower than imaged on seismic sections [Letouzey and Sherkati, 2004], or that the synclines are actively subsiding. Thirdly (but this argument is weaker) the shortening rates computed in sites A, B and C would present more dispersion in the case where bed thickening is accounted for and, in addition, the geological shortening rate in C would be higher than the total present-day shortening absorbed across the Zagros according to GPS data. In the absence of alternative models to describe fold detachment and solve their restoration paradox, the active synclinal flexure model represents our currently preferred model. Consequently, a total shortening of ~1 km, instead of 2.4 km as inferred from our initial fold construction (Figure III-4) that included bed thickening, and a shortening rate of 3-4 mm/yr are expected across the Mand anticline, which represents the regionally most frontal structure of the Zagros. If such a rate has persisted since fold inception, the Mand anticline would have begun to form only 300 kyr ago.

Despite the relatively rapid rates of deformation inferred for the Mand anticline, present-day seismicity associated with this structure is minimal, with only two M_w=5.2 earthquakes occurring below the Mand fold during the last 30 years (cf. Figures III-1 and 3). The Himalayan frontal fold-and-thrust belt is also characterized by the absence of recent seismicity, which has been attributed to the mechanical locking of the basal detachment [Lavé and Avouac, 2000] in between two major earthquakes. In the Zagros, in contrast, recent GPS results [Walpersdorf *et al.*, 2006], as well as the distributed seismicity that occurs mostly in the basement [Tatar *et al.*, 2004], indicate that the Mand anticline, like most of the Zagros sedimentary cover, deforms mostly aseismically. Focal mechanism solutions of the two M_w=5.2 events below the Mand fold present nodal planes that are sub-parallel to the surface structure of the fold (cf. Figure III-3). In the absence of reported centroid depths, we can infer three potential mechanisms: (1) an event occurring on a basement fault, i.e. below 10 km; such a fault could have controlled the initiation of the detachment fold; (2) an event produced on a propagating fault in the lower part of the sedimentary cover; the detachment fold could be evolving toward an asymmetric fault-propagation fold in the future, as observed in mature folds in the internal Zagros [McQuarrie, 2004]; (3) a seismic event associated to secondary faults that control thickening of the competent Palaeozoic to Mesozoic units in the core of the fold. The geologic cross-section below the Mand anticline does not require basement involvement, as opposed to the folds further north-east [Letouzey and Sherkati, 2004] and the two latter solutions could eventually be preferred. In any case, significant involvement of the basement seems precluded by the structural data that clearly indicate the symmetry of the fold, as well as by the seismic data [Letouzey and Sherkati, 2004].

Because of the symmetric shape of the fold, and because of the absence of an obvious strike slip fault that could partition oblique motion within the fold, we suggest that shortening is mostly perpendicular to the local fold axis. If so, this local shortening direction is oriented at 40° to 60° from the regional compression direction as indicated by seismicity [Gillard and Wyss, 1995]. As a consequence, shortening across the Mand anticline represents 35 to 50% of the strain in the Zagros in absolute value, but absorbs only ~20 to 35% of the 8mm/yr of the SSW-NNE convergence across the Zagros. On the other hand, the obliquity of the shortening directions in the sedimentary cover with respect to the basement, suggests that shortening and horizontal stress transfer in the sedimentary cover of the frontal Zagros are fully decoupled from the basement, most probably at the level of the Hormuz salt. This conclusion contradicts recent suggestions [e.g., Molinaro et al., 2005; Sherkati et al., 2005; Mouthereau et al., 2006]

that, in the Eastern Fars and northwest Zagros, deformation was initiated in the sedimentary cover, starting as early as Late Miocene at the northwest Zagros front [Homke *et al.*, 2004], and that more recent deformation has been dominated by thick-skinned tectonics and by the transfer of basement faulting upward to the sedimentary cover [Molinaro et al., 2005]. The rate and style of deformation of the Mand anticline suggest that such a tectonic model and chronology does not apply for the western Fars. The recent activity of the Mand anticline suggests, instead, that a forward-propagating deformation sequence in a thin-skinned tectonic regime is still an on-going process. This process does not preclude, however, simultaneous seismic, and possibly aseismic, deformation in the basement.

6. CONCLUSION

This study illustrates that combined structural and geomorphic investigations may concur to provide tight constraints on fold geometry and recent kinematics in the extensive and spectacular Zagros fold belt. Building balanced cross-sections of detachment folds requires solving a number of problems, in particular the length versus area restoration issue. Despite extensive structural and geophysical constraints, ambiguities on the fold solution for the Mand anticline still remain. The recent surface deformation, as recorded by dated fluvio-marine terraces on its western limb, helps to precise the fold kinematics and consequently the fold solution: first, progressive tilting of the geomorphic markers excludes deformation related to a fault with a kilometre-scale offset close to the surface; second, the location of the no-uplift point between the external hinge of the anticline and its axis indicates that flanking synclines could be affected by active subsidence. We therefore suspect that the Mand detachment fold is accompanied by the migration of Hormuz salt from below the synclinal flexures toward the core of the anticline. This preliminary conclusion suffers, however, from large uncertainties because of the controversial nature of the ^{14}C ages of marine terrace deposits in the Persian Gulf region [Page *et al.*, 1979; Fontugne *et al.*, 1997], and independent dating of the terraces would be welcome. Moreover, because of the limited extent of the deformed geomorphic markers, the fold solution is probably non unique. Additional geophysical data would add constraints to the fold model; detailed and high quality seismic data across the fold, the flanking synclines and, more importantly, in the Persian Gulf would permit to test our model by imaging the predicted absence of a major WSW-vergent fault close to the surface, the absence of important bed thickening, and the flexure of synclines below the regional level. They would also bring essential information on the existence of growth strata in the flanking synclines and

on the timing of fold inception. Additional work is also required (and has started) on several detachment structures at different stages of their development, in order to unravel the complete kinematic history of detachment folds in Zagros, and how they evolve at the surface from a subdued, wide and symmetrical anticline to a tight, faulted and asymmetric fold.

Notwithstanding these uncertainties, our geomorphic analysis unambiguously shows that the Mand anticline is a very active structure on the south-western-most front of the Zagros wedge. The Late Pleistocene shortening rate is inferred to be 3 to 4 mm/yr perpendicular to the anticline, which would absorb 35 to 50 % of the 8 mm/yr [Vernant *et. al.*, 2004] convergence across the entire Zagros. This result is consistent with a normal forward-propagating deformation sequence in a thin-skinned tectonic regime during at least the Late Pleistocene, with south-westward migration of the front of the wedge. Comparing the rate and direction of shortening across the Mand anticline, as well as recent GPS data [Walpersdorf *et al.*, 2006], with the distribution of seismicity [Talebian and Jackson, 2004; Tatar *et al.*, 2004], also suggests that the sedimentary cover of the frontal Zagros is fully decoupled from the basement, most probably at the level of the Hormuz salt. This conclusion has important implications for the modalities of stress transfer at the scale of the western Fars province in Zagros. It contradicts, in particular, recent models in which basement deformation currently controls the location of the deformation in the sedimentary cover through slip transfer along steep crustal faults.

CHAPTER IV

SYNCLINE CORES EXTRUSION ABOVE A VISCOUS LAYER EMBEDDED IN THE CRITICAL WEDGE OF THE CENTRAL ZAGROS FOLD BELT

CHAPITRE IV

EXTRUSION DE CŒURS DE SYNCLINAUX AU DESSUS D'UNE COUCHE VISQUEUSE DANS LE PRISME CRITIQUE DU ZAGROS

Résumé en français

L’évolution et la déformation d’un prisme sédimentaire au front d’une orogène dépendent en grande partie de la résistance à la traction du matériel à la base de ce prisme. Elle dépendent également de l’angle de friction interne du matériel consistant le prisme et de la présence éventuelle de niveaux de décollement intermédiaire ou d’unités ductiles au sein de la série sédimentaire. Nous analysons dans ce chapitre le déplacement vertical d'un marqueur géomorphologique pléistocène pour contraindre le modèle de déformation du prisme du Zagros central et évaluer le rôle d’une couche ductile intermédiaire dans ce prisme. Dans le secteur d'étude, c'est-à-dire le Fars occidental entre les failles de Kazerun et de Karebas, des niveaux à gypse, anhydrite, sel et marnes Néogènes, appelés formation de Gachsaran et d’épaisseur un kilomètre, ont partiellement découplé la déformation des unités superficielles Néogène-Quaternaires du reste des unités sous jacente de la pile sédimentaire. Cette formation Gachsaran a notamment permis la réactivation de structures synclinales préexistantes, via l'extrusion du coeur ou des bordures du synclinal, ce qui se traduit par plusieurs zones de soulèvement et de bombement du marqueur morphologique pléistocène, un niveau de conglomérats fluviatiles Bakthyari initialement subhorizontal. Le mouvement ascendant des unités superficielles s’accompagne probablement d’une déformation visqueuse dans le niveau d’évaporites Gachsaran. Afin de mieux documenter ce phénomène et le rôle de la géologie locale dans les modes de réactivation, un modèle numérique simple est envisagé : il s’agit d’une structure synclinale contenant une couche à rhéologie visqueuse (viscosité newtonienne) noyée dans un matériel à comportement élasto-plastique sensé représenter les unités sédimentaires ante-Gachsaran. Parce que l’angle d’ouverture du prisme sédimentaire du Zagros (angle de la topographie + angle du décollement basal) est très peu ouvert, c'est-à-dire inférieur à un, il est supposé dans le cadre de ce modèle que la contrainte principale compressive est subhorizontale. En réponse à ce régime régional compressif, la couche synclinale de faible viscosité va effectivement se déformer et produire le soulèvement du cœur et des bordures du synclinal. Après une première phase de soulèvement, un équilibre mécanique est atteint qui conduit à une topographie relativement stationnaire. Les valeurs choisies de la viscosité de cette couche et de son épaisseur vont avoir une influence directe sur la vitesse d’extrusion du matériel, tandis que le ratio des caractéristiques mécaniques aux valeurs de contraintes régionales va contrôler l’amplitude du soulèvement final. Enfin, suivant la forme du modèle choisi, la localisation de la déformation plastique sous jacente peut varier

et induire différents profils de soulèvement de surface : un modèle peu profond conduira au soulèvement en bloc du cœur du synclinal, tandis qu'un modèle plus profond induira un différentiel de soulèvement entre les bordures du synclinal et son cœur.

Dans le cas de la région du Fars occidental, ces modèles numériques suggèrent différentes conclusions. Les taux Pléistocènes de soulèvement des marqueurs géomorphologiques Bakthyari au-dessus des coeurs de synclinaux contraignent la viscosité moyenne et apparente du niveau Gachsaran à être inférieure à 2.10^{21} Pa.s. La variétés des profils de déformation de surface observés indique que le mode de réactivation des synclinaux dépend largement de la largeur du synclinal et du transfert de la déformation des unités basales vers la surface, c'est-à-dire du fait que cette déformation des unités basales peut structuralement s'effectuer à l'aplomb ou bien latéralement par rapport à la structure synclinal superficielle.

Syncline cores extrusion above a viscous layer embedded in the critical wedge of the central Zagros Fold belt *

Jérôme Lavé[1], Behnam Oveisi[1,2], Riad Hassani[3]

1. Laboratoire de Géodynamique des Chaînes Alpines, Université Joseph Fourier, BP 53, 38041 Grenoble Cedex, France
2. Geological Survey of Iran, Meraj St, Azadi Sq, Tehran, Iran
3. Laboratoire de Géodynamique des Chaînes Alpines, Université de Chambéry, 74000 Le Bourget du Lac, France

Abstract. In thin-skinned fold-and-thrust belts, the style of deformation is critically dependent on the resistance to sliding along basal detachment but also on the presence within the wedge of intermediate decollement levels or/and ductile units. Here, we analyse the vertical displacement of a Pleistocene geomorphic marker to constrain the spatial pattern of recent upper crustal deformation in the internal Southwest Central Zagros. There, Neogene gypsum and marls of the Gachsaran Formation have partially decoupled deformation within Neogene-Quaternary sediments from the underlying sedimentary units, and have permitted the re-activation of pre-existing synclinal structures, through upward extrusion of the syncline core. This upward movement is accommodated by viscous deformation within the upper evaporitic Gasharan level. Modelling the response of a syncline layer of low viscosity material embedded into a very shallow-sloping critical wedge, shows that syncline uplift occurs in response to the regional compressive stress regime, and reaches a steady topography, for which body forces equilibrate horizontal compression in the weakness zone. Observations as models indicate that the style of the syncline reactivation can, however, largely vary and depends among other factors on syncline deformation transfer from underlying units. The viscosity and thickness of the ductile Gachsaran layer influence the time required to achieve steady topography: Pleistocene uplift rates of the geomorphic markers above syncline cores constrain the apparent viscosity to be lower than 2.10^{21} Pa.s in Southwest Central Zagros.

1. INTRODUCTION

In orogens, folding and faulting are described from the microscale to the regional scale. They represent a common response of upper crustal rocks to deformation. The style of deformation is, however, usually not uniform in an orogen and can evolve both spatially and temporally. It also strongly depends on the rheology of the crust, on the presence or not of strong anisotropic patterns due to layering and/or to the existence of weaker units that permits décollement and detachment to propagate.

In sedimentary wedges and thin-skinned fold-and-thrust belts in particular, the style of deformation is critically dependent on the resistance to sliding along the basal detachment between the mass of deforming sediments and the underlying basement. The regional

* it's going to be submitted

topography in most foreland fold-thrust belts illustrates the balance between the frictional resistance above the basal décollement, and gravitational body force arising from the topography [Chapple, 1978; Davis et al., 1983]. Evaporites in particular can provide an extremely weak horizon within which a basal detachment can form and permit small shear traction to be supported. Due to such simple mechanical considerations, the fold-and-thrust belts that form atop a salt layer, such as the Appalachian Plateau, or the Jura Mountains, share several readily observable characteristics: a narrow cross-sectional taper, a shallow dipping mean topography, the absence of preferred vergence of folding or thrusting, and the presence of numerous widely but regularly spaced folds. However, when intermediate weak or ductile horizons exist within the detached sedimentary series, activation of shearing in these units may generate new decollement levels and promote shorter wavelength in fold deformation. Such process usually induces specific tectonic features like disharmonic deformation or duplexing that will be superimposed on the larger wavelength of the deformation field, and will perturb the regular fold spacing.

The central Zagros fold and thrust belt is a young and active orogenic wedge that results from the active continental collision between Arabia and Eurasia and that developed atop a major ductile detachment located in pre-Cambrian Hormuz evaporitic horizon. It presents similar characteristics as above examples, including a mean topographic slope lower than 0.5°, and an extensive succession of large-scale “whale-back” folds, considered as detachment folds developed above the 1-km-thick ductile Hormuz salt layer. Meanwhile, the ~10 km deformed stratigraphic pile of the Zagros is composed of an alternance of resistant units separated by weak and ductile layers that act as local or/and regional detachment levels. Several intermediate decollement levels have been documented within the Zagros Phanerozoic sedimentary sequence: the Triassic evaporates (Surmeh Fm), or the Eocene marl (Pabdeh Fm). In the Western Fars (central Zagros) and West of Kazerun fault in Izeh zone (inset in Figure IV-1b), the Neogene gypsum and marls of the Gachsaran Formation probably represents the major upper décollement level [Letouzey and Sherkati, 2004 ; Sherkati et al., 2006], and decouples the superficial Neogene-Quaternary sediments from lower units.

Although the general features of the geology and the structure of the Zagros belt are now well-understood, the distribution of active deformation across the belt, as well as the sequence activation within the wedge or the role of the different decollement levels on deformation style, are still poorly constrained. In critical taper wedge, deformation is considered to normally propagate toward the wedge front through activation of new frontal folds. But due to the balance between the frictional resistance above the basal décollement and the gravitational

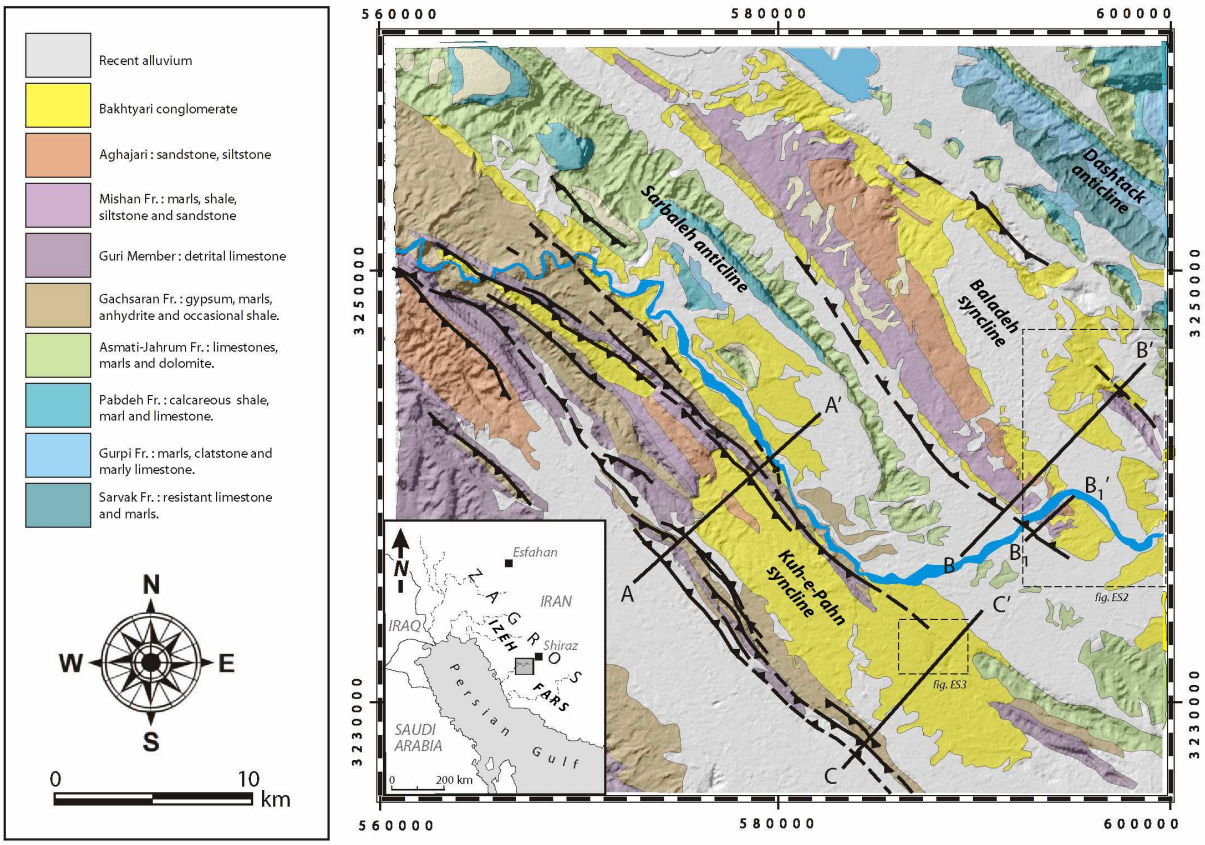

Figure IV-1: Geologic map superimposed on shaded Relief DEM of the study area, with cross sections AA' (Fig. 1b), BB', B_1B_1', CC' and DD' (Figure IV-2).

body force, any change in wedge geometry (by erosion or deep geodynamic processes) can modify the equilibrium geometry and promote the reactivation of internal structures. In western Fars province, the uplift of Mid Pleistocene surface evidence internal fold reactivation under the regional horizontal compressive stress prevalent in the orogenic wedge: in particular vertical escape or pop-upped synclinal cores, "detached" at the top of the Gachsaran Fm, in association with significant flexural flow and internal viscous-like deformation. Here, we first present the evidence of syncline reactivation and the role of syncline width and different structural situations on surface deformation. Then using a finite element numerical model, we try to mimic the observation and put constrains on the influence of syncline geometry, pressure boundary condition, rheology and thickness of detachment materials on the rate and pattern of the observed vertical deformation.

2. GEOLOGIC SETTING

The active deformation of the Zagros Mountains results from the collision (in an approx. N-S direction) between Arabia and Continental Eurasia at a rate of 25-30 mm/yr [De Mets *et al*. 1994; Sella *et al*. 2002]. The convergence started during Late Cretaceous times in the innermost Zagros and is still active. Recent GPS [Tatar *et al.*, 2002; Walpersdorf et al., 2006] indicate that present-day shortening rate reaches ~8mm/yr across the central Zagros, which would accommodate 40-50% of the total ~21 mm/yr convergence between Arabia and Eurasia (Vernant *et al.*, 2004). These GPS data, as seismicity [Berberian, 1995; Talebian and Jackson, 2004], or geomorphologic arguments [Oveisi et al., submitted] show that this shortening across the Zagros is rather concentrated in the Simply Folded Zone, which constitutes the foreland fold-and-thrust belt of the system, in particular on the two or three most frontal folds. Focal mechanisms (Harvard CMT solutions) of reported thrust earthquakes indicate a contraction direction between N0 and N45 in Central and Western Fars respectively, in rough agreement with the perpendicular to the trend of a majority of folds. Principal compressive stress in the central ZFTB is therefore suspected to be also oriented N-S to NE-SW.

The sedimentary rocks of the ~10 km-thick stratigraphic succession in Zagros present highly variable mechanical properties that strongly control deformation in the ZFTB. Lower Cambrian (Berberian, 1995) incompetent Hormuz series evaporites directly overlie the crystalline basement, forming a basal detachment level that plays an important role in guiding the deformation. According to cross sections based on seismic profiles [Sherkati et al., 2006], the basal decollement would deep at ~0.9° toward the SSW, and topographic slope would be lower than 0.5° [Mouthereau et al., 2006], suggesting a cross sectional taper angle of the order of -0.5° in the central Zagros, that most probably results from the very low basal traction in the Hormuz Salt horizon.

Above the Hormuz series, multiple decoupling levels have been described within the stratigraphy of the Central Zagros. In the North Western Fars Province, the Triassic evaporitic Dashtak Fm and the Miocene evaporitic Gachsaran Formation are considered as the main ductile décollements [Sherkati et al., 2006]. This formation has long been identified as a level of decollement and disharmony by previous workers (ColmanSadd, 1978; O'Brien, 1950). Disharmonic features as well as significant materiel transfer within the Gachsaran units are well imaged by recent interpretation of seismic profiles and surface geology, in particular in Izeh zone (inset in Fig. IV-1b), where Gachsaran weak formation separates two completely

different folded domains and favor development of non-isopach folding [Sherkati et al., 2006; Letouzey and Sherkati, 2004]. In the studied area, the Miocene Gachsaran formation is composed of marls, gypsum, anhydrite, thin limestone and locally salt (Fig. IV-2). Total thickness of the undeformed unit reach up to 1km, but the total thickness in evaporitic horizons is much lower, and, in the North-Western Fars province they are rather located in the upper part of the unit. Within this sedimentary package, thin limestone competent units can be highly folded but roughly isopachly, whereas thin marls, salt or gypsum levels absorb strongly disharmonic folding or can act as secondary decollement levels at meso-scale (1-10m) that promote multi-duplexing (Fig. IV-5), but appear at macro-scale like apparent continuous viscous deformation.

3. SURFACE DEFORMATION IN WESTERN INTERNAL FARS PROVINCE RECORDED BY BAKHTYARI FORMATION

3.1. Stratigraphic description

The Bakhtyari conglomerates (Bk Fm) represent the youngest lithostratigraphic unit of the Zagros sedimentary sequence. They usually lie in unconformity above underlying Agha Jari and Mishan formations and for that reason have been generally considered as an evidence of recent renewed tectonic activity in the Zagros [ref]. In the study area, the Bk Fm consists of polymictic and proximal coarse-grained conglomerate, locally cemented by pedogenic carbonate. In the western Fars province, South East of Kazerun (Fig. IV-1), the maximum thickness of these gravel units reach at least 60m. The Bk conglomerates are not well dated because they contain no diagnostic fossils. The unit is generally considered to be Late Pliocene [James & Wynd 1965] or younger because it overlies the fossiliferous Agha Jari Formation of Late Miocene-Pliocene age. The Bk Formation is, however, considered has diachronous across the Zagros fold belt [e.g. Hessami et al., 2001]. Cosmogenic dating of Bk surfaces and a paleomagnetic measurement [Oveisi et al., submitted] suggest that Bk conglomerates most probably deposited between 500 and 800 kyr in the study area.

Gravels in these deposits contain mostly fragments of Paleogene limestone and Neogene sandstone, but also clasts and pebbles of black dolomite, originated in the upstream part of the Dalaki watershed. This indicates that most of these sediments were deposited by a paleo-Dalaki river, whose course had probably a similar regional geometry as today, i.e. an E-W

draining direction. We also suppose that river gradient were as low as the present ones (~1%) and that any short wavelength or steep area in present Bk surfaces can be interpreted as resulting from tectonic deformations.

3.2. Deformation recorded by the Pleistocene Bakhtyari surfaces

Several indices of active or recent tectonics, expressed by deformation of Bk Fm, are observed in the western Fars province. Here, we will detail three typical examples of the different style of surface deformation that can be observed in that area.

3.2.1 Baladeh monocline uplift

The Baladeh monocline constitutes the south-western flank of a wide syncline, flanked by the Dashtak and Sarbaleh anticlines on the NE and SW respectively (Fig. IV-1, 2). It involves Agha Jari and Mishan formations and developed above a décollement level in the upper Gachsaran units (Fig. IV-2). The Bk Formations across the Baladeh monocline displays a broad fold with a moderately steeping (18°) back-limb, a flat 2-km-wide top, and a vertical or slightly overturned (70-80°) frontal limb. The uplift of the flat top-limb Bk conglomerates, relative to the present-day river, reaches 80 to 90 m (Fig. IV-2). Across this flat top-limb, a thin layer of Bk conglomerates lies in unconformity on top of the steeply dipping Neogene units, but the Bk thickness increase towards both frontal and back limbs. Progressive transition to growth strata on the backlimb (fig. IV-2) indicates in addition that the monocline folding was already active during Bk conglomerate deposition.

Based upon structural and geometrical arguments, the dip of strata in the monocline (~45-50 °NE) is suspected to be parallel to a more intense deformation zone at the Mishan / Gachsaran transition that probably flattens on a shallow décollement level further North East. Surface deformation mimics those produced by kink-like fold structure or fault propagation fold deformation above a flat-ramp system at depth. The development of the Baladeh monocline, in particular its abrupt frontal limb, suggests at depth faulting or possibly ductile flow but within a narrow low viscosity layer in the upper Gachsaran Fm (Fig IV-2). The role of the pre-existing syncline structure, i.e. the orientation of the SW limb of the syncline that present a 45°-dipping ductile or low friction decollement at ~90° from the regional compressive stress direction represents nearly optimal conditions for reactivation of the Baladeh monocline.

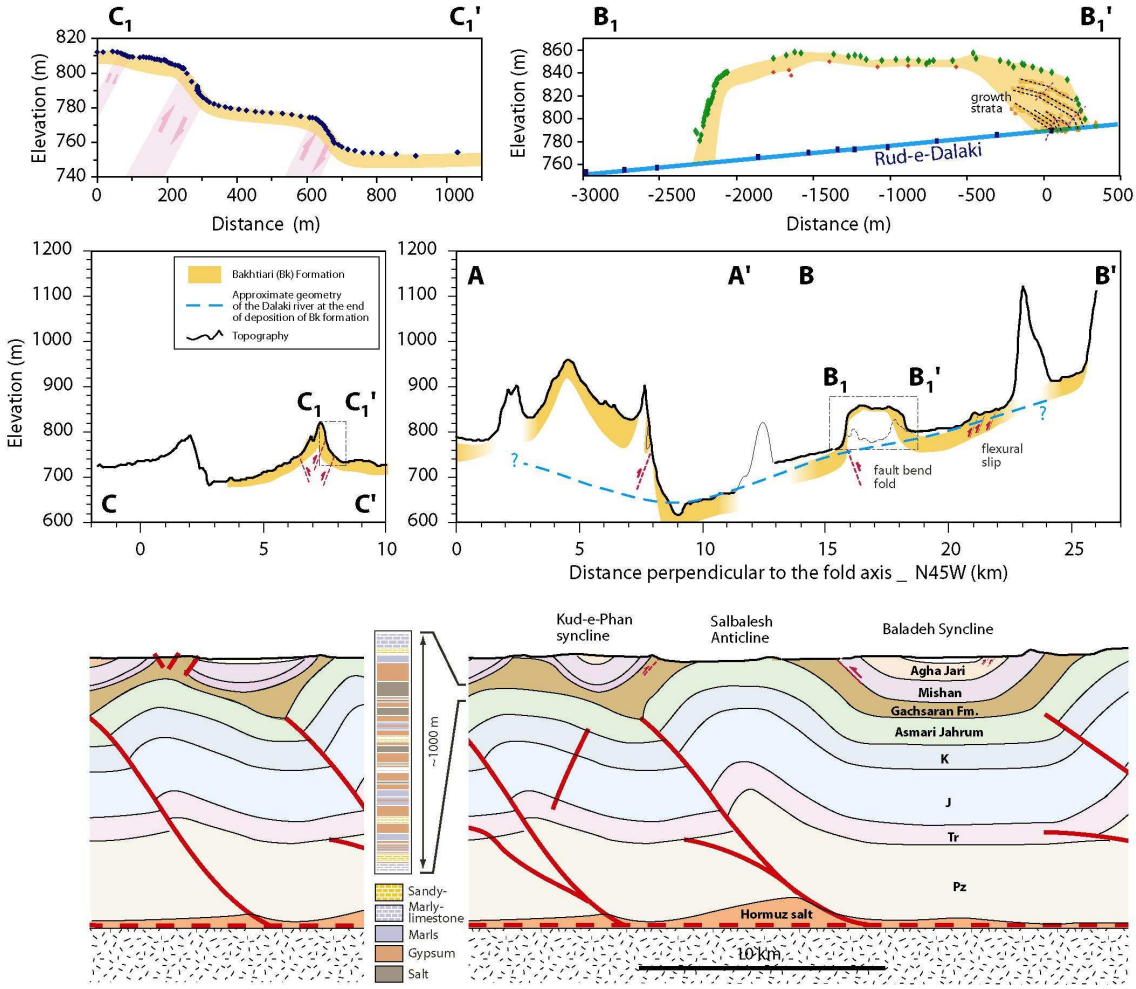

Fig. 2: Upper geologic cross sections adapted from Sherkati et al. [2006] (a and b) and associated profiles of Bakhtyari surfaces (c and d) across the Baladeh / Kuh e Pahn region. Assuming an initial subhorizontal geometry (dashed line on (c)) for the Bk formation provide a direct estimate of the amplitude of the deformation. (e) Close-up on the Baladeh monocline: topographic profile of the Bk surface indicates clear surface uplift. The flat (~2-km wide) top-limb suggests that the monocline developed by a mechanism of distributed upward movement, possibly fault bend folding. The back-limb is characterized by a growing strata, which shows that Baladeh monocline was already uplifted during Bk deposition. (f) Close-up on the southern part of the NE flank of the Kuh-e-Pahn syncline: topographic profile of the indurated Bk surface (in orange color) displays two large tectonic scarps associated to flexural flow in the upper Gachsaran sequence.

The North eastern flank of the syncline does not display, however, similar feature. There, the Bk fm does not correspond to alluvial deposits of the paleo-Dalaki river, but to deposits of small alluvial fans: it is therefore more difficult to reconstruct the deformation of the Bk surface. Nevertheless, an uplift profile as developed and locally abrupt as the profile observed across Baladeh monocline can be excluded. In contrast, an old Bk alluvial fan presents several fold parallel metric tectonic scarps that we interpret as evidence of flexural slip in Agha Jari in response to the general shortening of the syncline core (Fig. IV-6).

3.2.2. Kuh-e-Pahn North : syncline core extrusion

To the South-West of Baladeh monocline and in front of Sarbaleh anticline, another syncline structure, the Kuh-e-Pahn syncline, has been reactivated and produced uplift of the Bk surfaces (Figure IV-1 and 2). There, the surface of the Bk conglomerates display a 4-km-wide domal structure, with very steep and even locally vertical NE limb and more gentle (<35°) SW limb. The dome is however asymmetrical and its summit located close to the SW limb, in approximate concordance with the axis of a secondary anticline that affect the syncline SW limb. The transition between horizontal layering below the present Dalaki valley, just south of the Sarbaleh anticline, and the very steep NE limb of the reactivated syncline is quite abrupt and located in the upper Gachsaran units, just below the Guri formation.

In the South-Western part of the Kuh-e-Pahn syncline, the initial geometry of the Bk formation is less intuitive than across Baladeh monocline, because the extent of the Dalaki paleovalley can hardly be estimated. Supposing, however, that the Dalaki river and its tributaries were depositing sediment in a large and relatively flat basin with gradients comparable with the ~1% present Dalaki river gradient in this region, we estimate that the relative uplift of the Bk surface could reach up to 200m at the dome summit (Fig. IV-2), and more importantly that the present domal shape has mostly a tectonic origin.

3.2.3. Kuh-e-Pahn South: flexural flow

The width of the Kuh-e-Pahn syncline increases in its south eastern part. The shape of the deformed Bk surface radically changes also in that direction: the convex dome in the NW progressively flattens and loses elevation and then becomes a concave up shape in the South Eastern part. Uplift of the Bk Fm is restricted to the NE limb of the syncline and affects a width of 1-2 km mostly in the upper Gachsaran formation (Fig. IV-1, 2). Three large rectilinear tectonic scarps with >20m vertical offsets have permitted the step-like uplift of a narrow elongated plateau (Fig. IV-2 and Fig. IV-6). The restriction of the most intense uplift to the upper Gachsaran sequence, just below the Guri member, suggests in addition that syncline core uplift has been rather limited and replaced by lateral ductile flow and upward extrusion of the Gachsaran upper unit. The association of these scarps with evaporitic meter-thick levels (see Fig. IV-4) also suggests that this upward extrusion could be accommodated by flexural flow in the most ductile units within the upper Gachsaran sequence. Structural

section on the SW limb of the syncline indicates similarly a pop-up structure where Gachsaran units reach the surface: the absence of preserved Bk surface does not permit however to confirm that such upward extrusion result from recent Pleistocene deformation.

3.2.4. Gachsaran formation and syncline core deformation

In the three above cases, the evaporate-rich Gachsaran Formation appears to represent an important décollement level or ductile layer that controls the distribution of active Bk surface deformation in the study area. Pre-existing syncline structures, oriented at ~90° from the regional compression, are also a common controlling factor in the structural evolution of the surface deformation. In contrast, across the anticlinal structures like the Sarbaleh anticline, the Bk conglomerates have been buried by recent sedimentation. If the uplift of the Bk conglomerates above the syncline cores corresponds to the upward extrusion favoured by low friction or ductile detachment, then the anticlinal cores are logically expected to be immobile or extruded downward.

Despite above similarities, the Bk deformation profiles exhibit very distinct patterns between the three sites. The northern Kuh e Pahn syncline width is twice shorter than Baladeh syncline: interestingly the uplift has occurred on the whole width of the syncline and not only on the SW limb of the syncline like in Baladeh, suggesting that the syncline width might control the uplift pattern. On the other hand, the Gachsaran Fm displays large lateral variations of thickness due to the disharmonic folding during the main deformation phase of the western Fars, and possibly important lateral variations in evaporite amount. These variations could also produce different style of syncline response to compression: a South-Westward increase in evaporite amount could explain why deformation is very localized at the Mishan / Gachsaran transition below Baladeh monocline, whereas it appears as more distributed below the Kuh e Pahn syncline. Finally, the local stress conditions or the presence atop the Gachsaran of a >20m-thick oyster-rich competent limestone, the Guri formation, that presents a larger resistance to erosion and a mechanical contrast with adjacent formations, could also play significant roles in syncline reactivation.

4. NUMERICAL MODELLING OF SYNCLINE REACTIVATION

4.1. Model characteristics

In order to provide a first order quantification of the relative role of the rock rheology and syncline geometry on the Bk surface deformation across the central Zagros, we have designed a simple structural model, and performed 2D simulations using a Finite Element numerical model, ADELI [Hassani, 1997]. Geometrically, we consider a syncline structure embedded in a homogeneous material. The studied cross section, perpendicular to the fold axis, is 10 to 20 km long and 3 to 6 km deep (Fig. IV-3). The mechanical model contains three rheological units: a folded layer of Gachsaran evaporitic viscoelastic units (U2 in Fig. IV-3, ~1000-m), embedded in Oligocene and older elastoplastic units (U1) and overlain by Mishan and Aghajari sandstones and shales, also considered as an elastoplastic unit (U3) (Fig. IV-3).

In units 1 and 3, beyond the elastic domain, brittle rock deformation is reproduced using a Drucker-Prager criterium [e.g. Carter and Tsenn 1987 ; Leroy & Ortiz 1989] (Table 1). An apparent angle of internal friction of 15° in agreement with Byerlee's law for crustal rocks including hydrostatic pore pressure, and with observation from deep drill hole [Zoback and Healy, 1989; Brudy et al., 1997] has been considered, and maintained unchanged for the different experiments. Only the viscosity value of the viscoelastic law that reproduce U2 rheology has been varied. Salt and gypsum viscosities are usually considered as non Newtonian but at low stresses and in the presence of a very small amounts of water (0.05 per cent is sufficient) diffusional creep prevails and salt might behave as a Newtonian fluid [Weijermars *et al.*, 1993]. Due to the shallow and limited depth range of the studied deformation, the temperature influence on viscous rheology has been neglected. The Gachsaran evaporitic layers include gypsum and anhydrite and are mixed with marls and limestone: an apparent viscosity has to be considered and is expected to be higher than the viscosity of pure salt (~ 10^{17} Pa.s [ref]). The newtonien viscosity used for the unit U2 are therefore investigated in the range 10^{19} to 10^{22} Pa.s.

The model is loaded with gravitational body forces. Because of the presence of very low friction Hormuz salt at the base of the sedimentary wedge, the topographic slope and the wedge angles are lower than 1°. In that case, according to critical taper model [Dahlen, 1990] the principal stresses within the wedge can be approximately considered as horizontal and

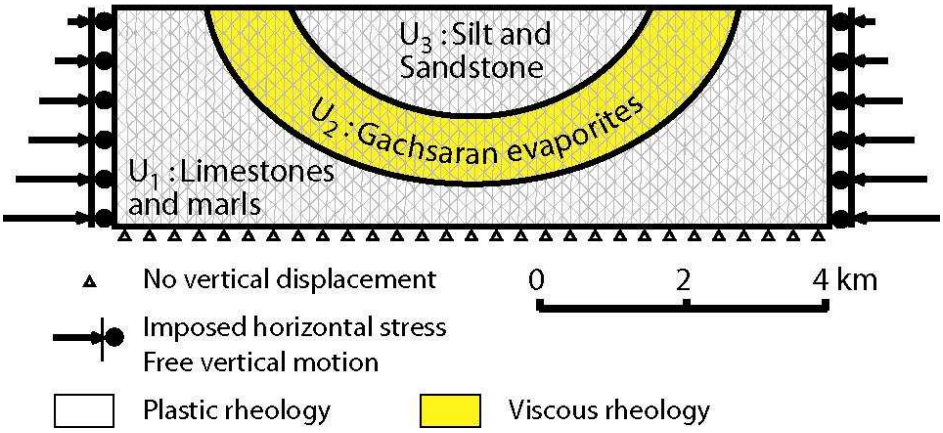

Fig. 3: Geometry and boundary conditions used for the modelling of a Kuh-e-Pahn-type syncline embedded into a very shallow-sloping critical wedge.

vertical. Such predicted orientations of the principal stress axes over a salt décollement are consistent with the commonly observed absence of preferred vergence of folding or thrusting within the Zagros thrust belt. In the simple case study of a Mohr-Coulomb criterium, principal stresses verifies $\sigma_V \approx \sigma_3 \approx \rho g z$, and $\sigma_H \approx \sigma_1 \approx 2C_0 \frac{\cos\phi^*}{\sin(1-\phi^*)} + (\frac{1+\sin\phi^*}{1-\sin\phi^*})\rho g z$, where g is the acceleration of gravity, and ρ is rock density, ϕ^* the apparent friction angle (accounting for hydrostatic pore pressure), $\bar{\sigma}_V$ and $\bar{\sigma}_H$ the vertical and horizontal effective stress. For a rock density of 2.8 and an apparent friction angle of 15°, this corresponds to a vertical gradient of ~47 MPa/km of the horizontal stress (i.e. a vertical gradient of ~20 MPa/km for the deviatoric stress (σ_H - σ_V)). Using a Drucker-Prager criterium provides also a linear increase of the deviatoric stress (σ_H - σ_V) with depth. We therefore account for stress regime by imposing on the vertical faces of the model box a constant gradient of horizontal stress in order to mimic the state of stress into a critical wedge characterized by a very shallow decollement angle and topographic angle (vertical velocities on these faces are left free). In our different experiments, deformation runs are pursued during up to 0.7 Myr, to ensure the surface geometry to reach some quasi-steady state.

4.2. Results and influence of the syncline geometry on surface deformation

Different model parameters have been varied to explore the syncline response to compressive stress and to provide preliminary explanation to the surface deformation recorded by Bk fm.

In a first set of experiments, we studied a small syncline enclosed in a 3-km-deep model box and varied the stress boundary conditions, the thickness and viscosity of the viscoelastic U2 layer. The syncline shape-like viscoelastic unit U2 acts as a weakness zone in our structural model. In response to the horizontal compression, the syncline existence favours the plastic deformation of the underlying U1, beneath the syncline axis, i.e. where the U1 material is the thinnest. This local thickening of U1 material combined to simple and pure shear within U2 leads to the uniform surface uplift above unit U3 (Fig. IV-4a). For a U2 viscosity of 10^{20} Pa.s, the surface reaches after 40 to 100 kyr a steady elevation, for which the gravitational forces due to the topographic increase equilibrate the horizontal compressive stress at the low viscosity layer boundaries. The viscosity value, within the range of the explored values, does not affect significantly the final plateau elevation, but determines, as U2 thickness, the relative uplift rate and the required time to reach a steady elevation (Fig. IV-4B). Because of the force equilibrium, the final plateau elevation is strongly dependent on the vertical gradient of the horizontal stress applied at the lateral boundaries, but its general shape does not significantly change. To reproduce final plateau uplift of 50 to 200m, the value of the applied vertical gradient of horizontal stress has to range between 50 and 55 MPa/km.

Parameter	Value
Relative density	2.7
Young's modulus	50 GPa
Poisson's ratio	0.25
Rheology of upper and lower units ($U_{1, 3}$)	
Cohesion	4 MPa
Apparent internal friction angle	15°
Rheology of Gachsaran units (U_2)	
Apparent Newtonian viscosity [variation range]	10^{20} Pa.s [10^{19} - 10^{22}]

Table 1: Rheologic parameters used in the mechanical models

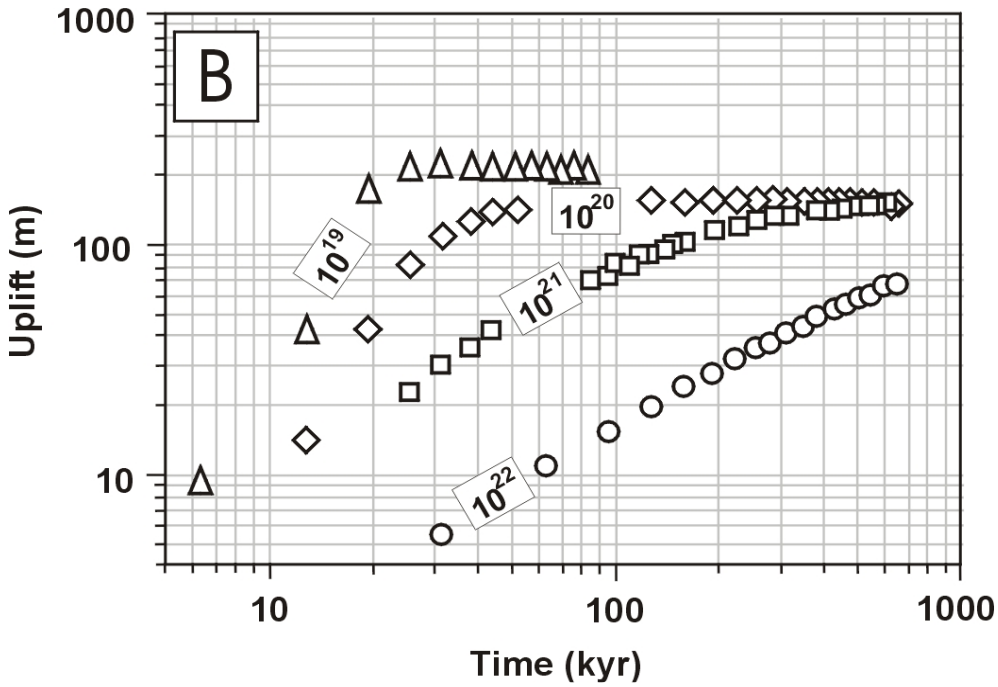
B
Uplift (m)
1000
100
10
10
100
1000
Time (kyr)
10^{19}
10^{20}
10^{21}
10^{22}

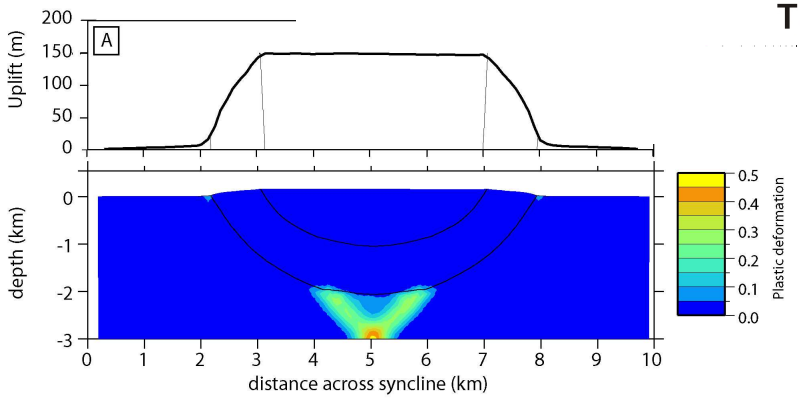
A
Uplift (m)
200
150
100
50
0
depth (km)
0
-1
-2
-3
0 1 2 3 4 5 6 7 8 9 10
distance across syncline (km)
Plastic deformation
0.5
0.4
0.3
0.2
0.1
0.0

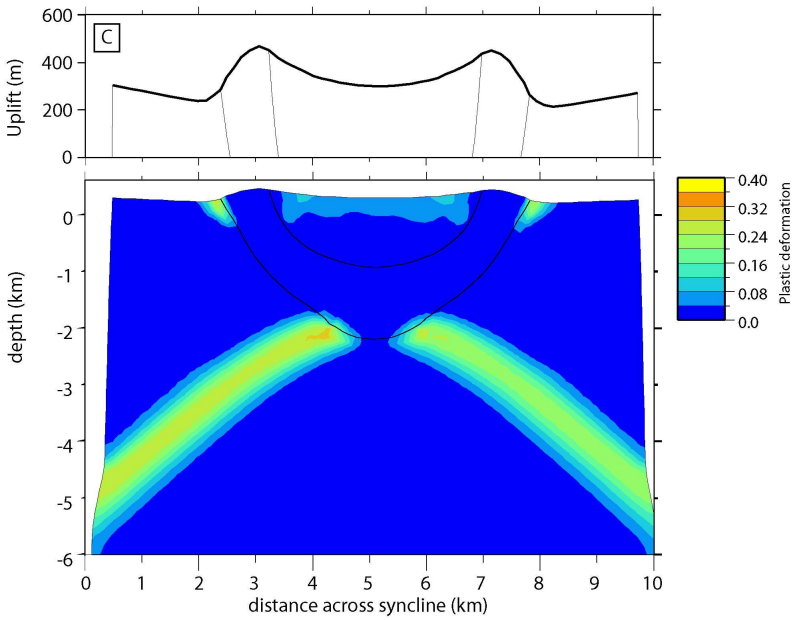
C
Uplift (m)
600
400
200
0
depth (km)
0
-1
-2
-3
-4
-5
-6
0 1 2 3 4 5 6 7 8 9 10
distance across syncline (km)
Plastic deformation
0.40
0.32
0.24
0.16
0.08
0.0

Fig. IV-4: Model results for two different syncline geometries. (a) Plastic deformation and final surface uplift for 3-km-deep model box (ν = 10^{20} Pa.s and vertical gradient of horizontal stress = 53 MPa/km). (b) Corresponding plateau uplift versus time for four different values of the Gasharan apparent Newtonian viscosity. (c) Plastic deformation and final surface uplift for 6-km-deep model box (ν = 10^{20} Pa.s and vertical gradient of horizontal stress = 53 MPa/km). In all cases, the syncline is first uplifted in response to the regional horizontal compressive stress, before reaching a steady topography, for which body forces equilibrate horizontal compression. Note that response time for viscosities of ν = 10^{19} and 10^{20} Pa.s are probably overestimated because of the numeric viscosity of the code and chosen time step. Response time to reach steady topography are expected to be ~2, ~20, ~200, ~2000 kan for respective values of viscosity ν = 10^{19}, 10^{20}, 10^{21} and 10^{22} .

In a second set of experiments we investigated the influence of the model box size and syncline width to depth ratio on the general shape of the surface uplift profile. Uniform uplift of the syncline core, as displayed on Figure IV-4a, is observed as long as two conjugate faults (or zones of localized plastic deformation) tangent to the syncline-like viscous layer can reach the bottom of the box before intersecting: in other words, as long as $\frac{h}{R} \leq \frac{1-\cos\theta}{\cos\theta}$, with h the vertical distance between the base of the viscous layer and the bottom of the model box, R the average radius of curvature of this viscous layer, and θ the preferred angle of "faulting" relative to horizontal (here for ϕ^* = 15°, $\theta = (90-\phi^*)/2 \approx 40°$). For larger values of this ratio, the surface deformation displays two areas of more intense uplift on both sides of the syncline, just atop the U2 units (Fig. IV-4C, see also Fig. IV-9 and Fig. IV-10). In addition, the two areas bordering the syncline are also uplifted, because shortening accommodation in the lower unit U1 is distributed on both sides of the syncline and not only restricted beneath the centre of the syncline. Whereas the uplift of the low viscosity syncline is a persistent feature in our experiments, geometric boundary conditions have a fundamental role in the expression of the deformation and uplift profile, because they control the way the lower unit U1 will plastically deform.

Several parameters, like potential density contrast between Gachsaran and Mishan formation, or mechanical anisotropy due to sediment layering Mishan Fm, have not been investigated but could have also significant influence on the uplift profile. Nevertheless, our reduced sets of experiments give some primary explanations to the syncline reactivation observed in Central Zagros.

5. DISCUSSION

The deformation of the syncline cores can be viewed at large scale as flexural flow in response to space reduction in syncline cores during tightening of the large detachment folds in the Zagros wedge. In the initial Zagros folding stages, the Neogene gypsum and marls of the Gachsaran Fm might have played an important role by decoupling thin-skinned deformation within Neogene-Quaternary sediments from lower portions of the wedge cover. But in the mature stage of the range, because of optimal orientation of the synclines limbs relative to regional compression, they mostly permit the upward extrusion of syncline core. The Gachsaran Fm represents in that sense a mechanical weakness zone that controls the distribution of active surface deformation in western Fars region, and internal tectonic reactivation. Pattern of surface deformation above syncline profiles exhibit, however, very distinct patterns from site to site, and numerical modelling confirm that uplift profile is particularly sensitive to model box geometry, i.e. to the way deformation and stress are transferred from the underlying units to the syncline.

Observations across Baladeh syncline suggest that deformation of the units embedding the syncline has to occur outside the syncline as displayed in Fig. IV-4c. Absence of uplift at the centre of the Baladeh syncline would also suggest an absence of thickening in units U1 and U2, and the necessity for the shortening, absorbed by the syncline, to be transferred at depth on a subhorizontal décollement within Gachsaran Fm and to be connected further North onto a steeper ramp below the Dashtak anticline. However, the difficulty to define the initial shape of the Bk Fm in an absolute vertical reference frame, makes also possible a scenario as displayed on Fig. IV-4c. The absence of kinematic information at depth prevents so far to fully document how deformation is accommodated below the synclines in the Paleozoic and Mesozoic series. The domal uplift of the NW Kuh e Pahn syncline and mostly the absence of uplift across the Sarbaleh anticline since Bk surface deposition suggest that syncline shortening is not transferred on a steep ramp below the Sarbaleh anticline, and could possibly be absorbed by diffuse plastic deformation within the sediment units just beneath the syncline, as depicted on Figure IV-4a. The relative uplift provided by Bk Fm prevents, however, as for Baladeh syncline to propose definitive conclusions. Nevertheless, the transition along Kuh e Pahn syncline from a convex surface in NW to a concave surface in SE could arise either from lateral variations of the transfer of the deformation in the underlying units, or from the South Eastward progressive increase in syncline width.

Assuming an age of 0.5-0.8 Ma for the end of the Bk deposits in the whole Baladeh/Kuh e Pahn region yields mean local uplift rates of 0.1 to 0.4 mm/yr. However, most of the uplift could have occurred soon after deposition of the Bk conglomerates and above rates might represent a minimum estimate of the instantaneous rates at those early times. Considering above minimum uplift rate, and a maximum thickness of the ductile layer of 1km, the apparent viscosity of the Gachsaran Fm has to be lower than 2.10^{21} Pa.s. Field observations suggest that deforming ductile zone is restricted in western Fars region to the upper Gachsaran and can localized on more evaporitic layers like in south Kuh e Pahn: this apparent viscosity for a homogeneous material is therefore an idealized view. This estimate, which could be further constrained by future more precise dating of the syndeformation Bk units, can be, however, particularly useful when modelling the mechanical behaviour of a geologic material made of a mix of evaporites and marls.

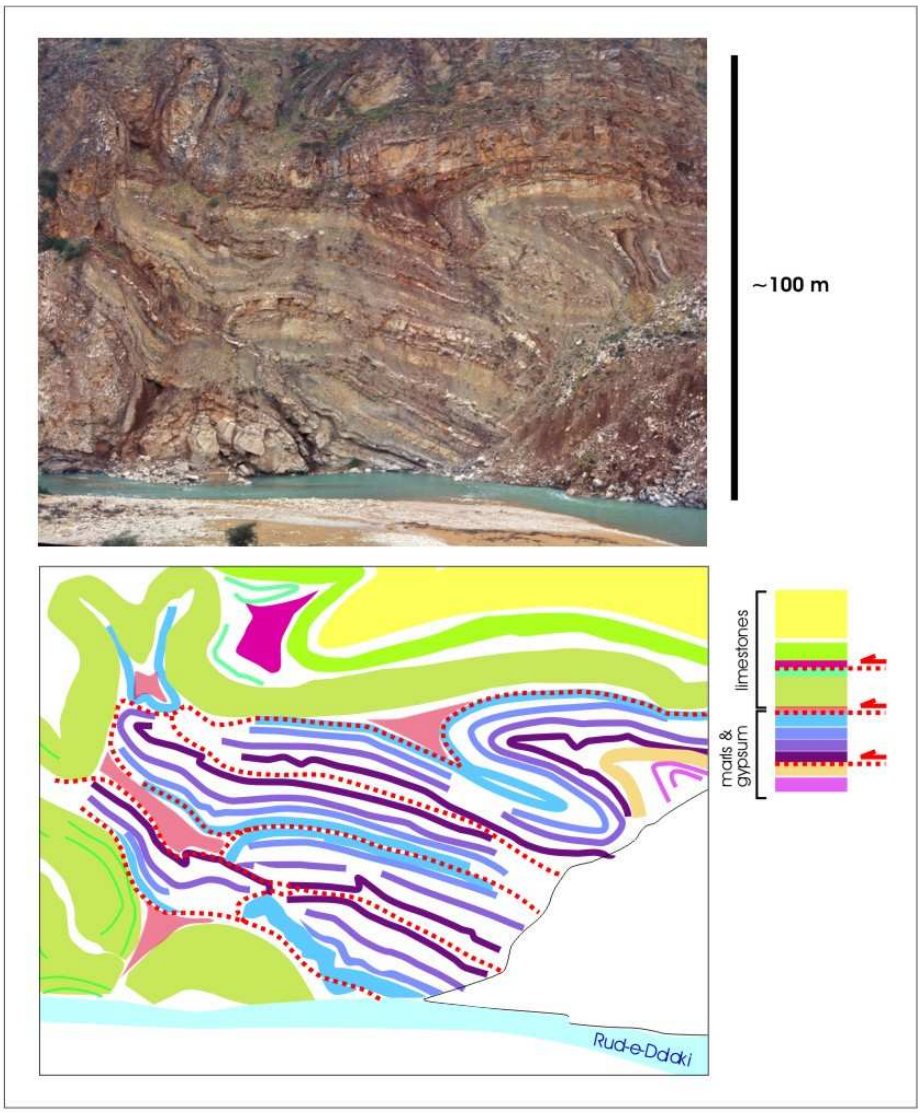

Figure IV-5: (upper) Photo of a high cliff along the left bank of the Rud e Dalaki on the North-West of the Kuh e Pahn syncline : incision of the Dalaki river has exhumed large thickness of deformed Gascharan formations. (lower) Interpretational scheme of the Gachsaran formation that exhibits intense folding and faulting.

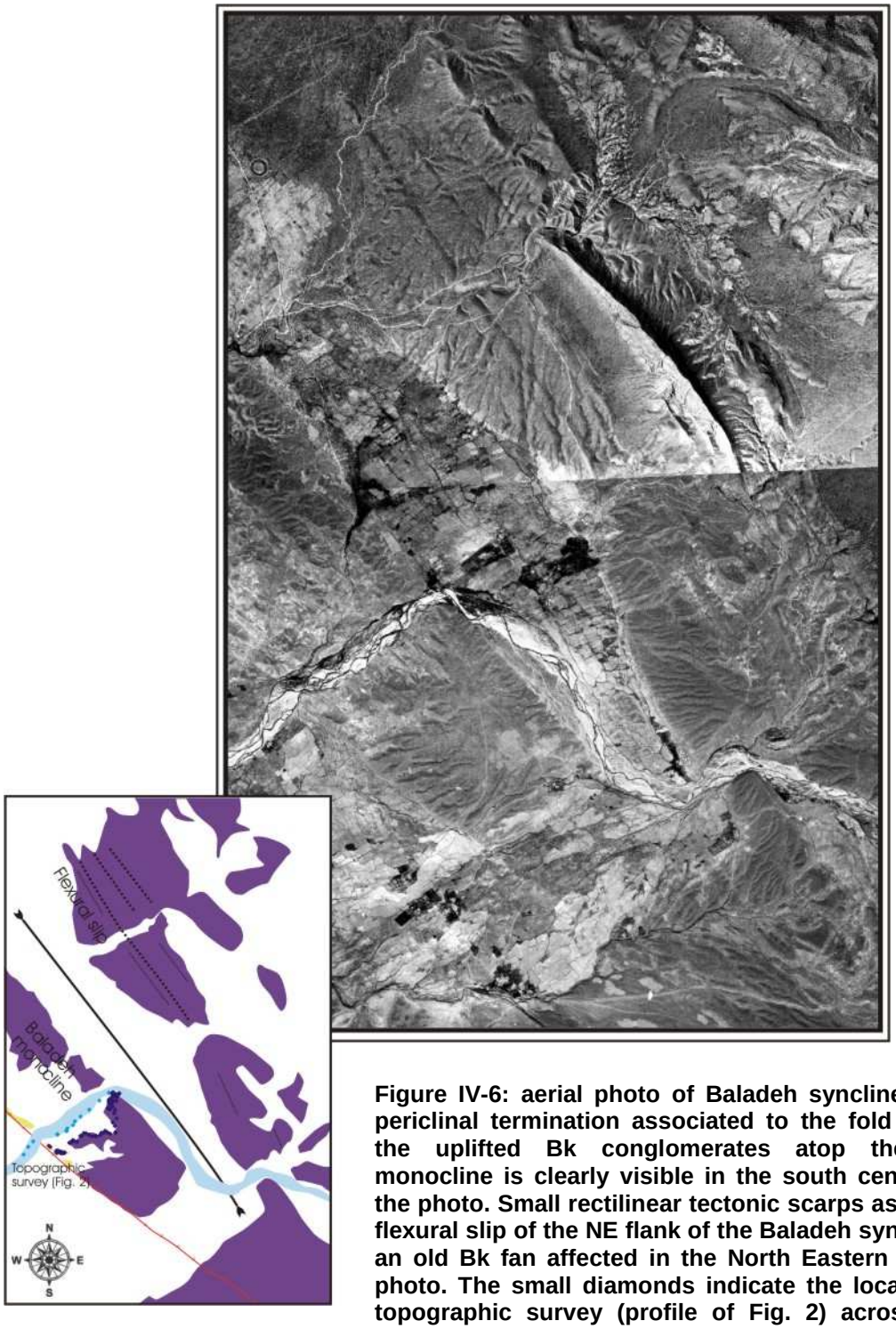

Figure IV-6: aerial photo of Baladeh syncline area. The periclinal termination associated to the fold formed by the uplifted Bk conglomerates atop the Baladeh monocline is clearly visible in the south central part of the photo. Small rectilinear tectonic scarps associated to flexural slip of the NE flank of the Baladeh syncline affect an old Bk fan affected in the North Eastern part of the photo. The small diamonds indicate the location of the topographic survey (profile of Fig. 2) across Baladeh monocline and along the Dalaki river.

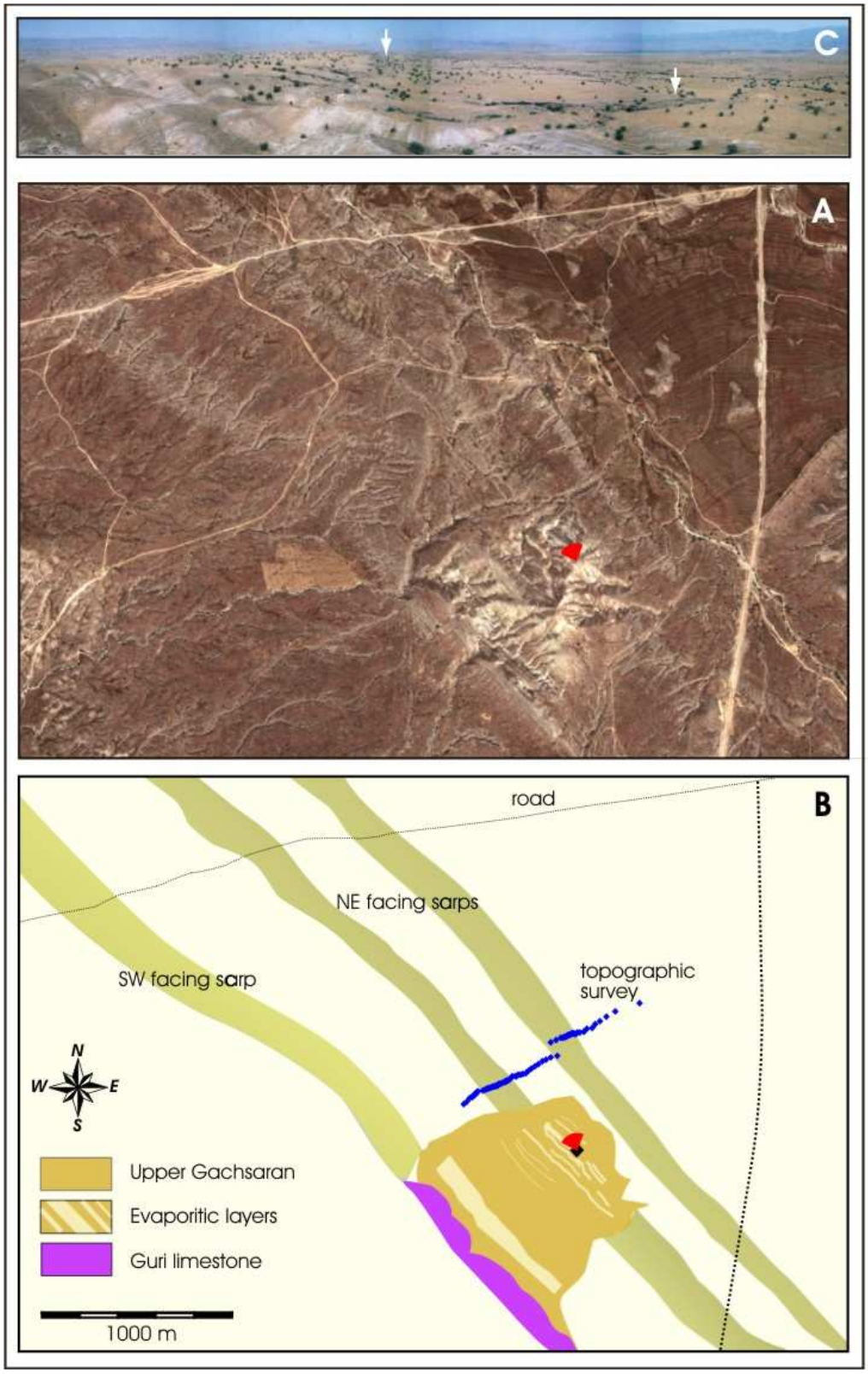

Figure IV-7: satellite image of the uplifted Bk surface across the southern part of the Kuh-e-Pahn syncline. Three large rectilinear tectonic scarps associated to flexural flow in the upper Gachsaran sequence and oriented N135 affect the Bk surface. The scarps seem to be located where evaporitic whitish layers are the thickest or numerous. The small diamonds indicate the location of the topographic survey across the two NE-facing scarps on the NE flank of the Kuh-e-Pahn syncline (profile of Fig. 2).

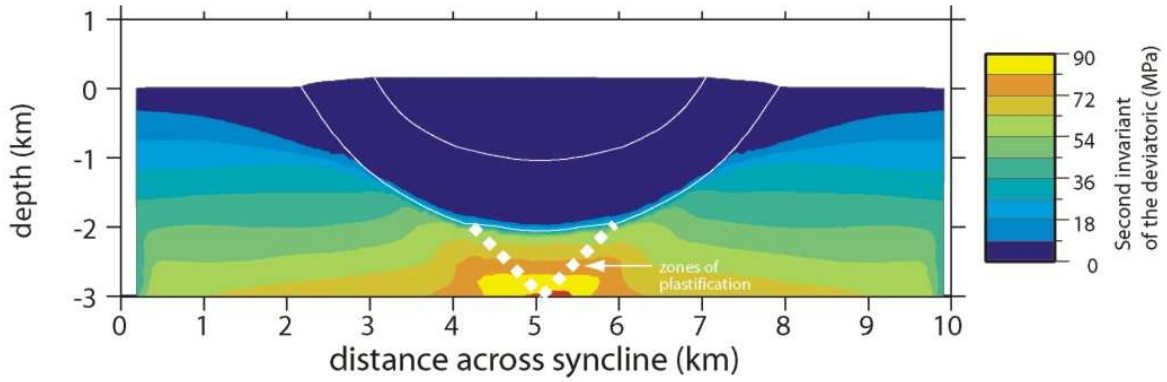

Figure IV-8: Second invariant of the deviatoric stress tensor, corresponding to the uplift profile and plastic deformation of Figure 4A, run with a vertical gradient of horizontal stress of 53 MPa/km and a viscosity ν = 10^{20} Pa.s.

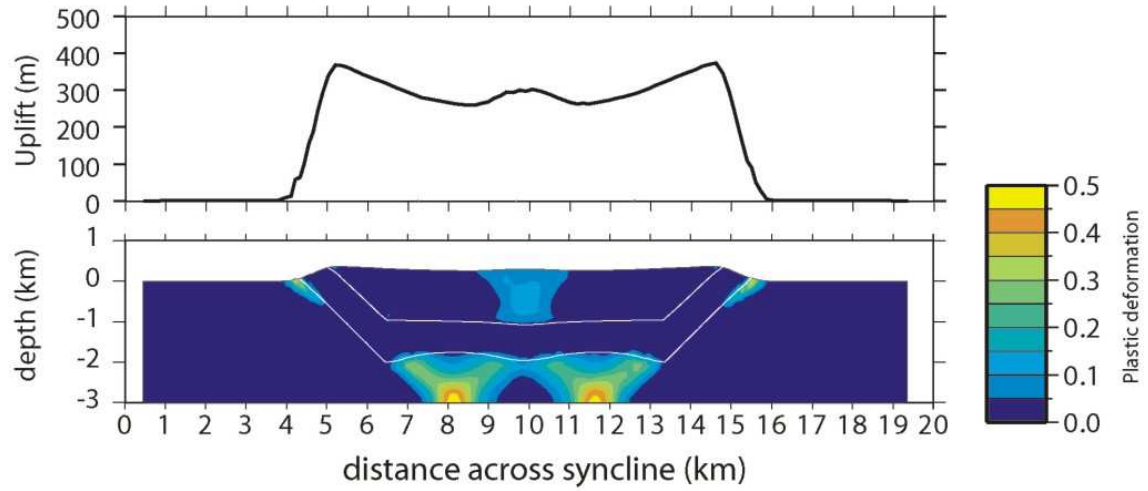

Figure IV-9: uplift profile and plastic deformation for a wide syncline after 56 kan (a vertical gradient of horizontal stress of 53 MPa/km and a viscosity ν = 10^{20} Pa.s have been applied)

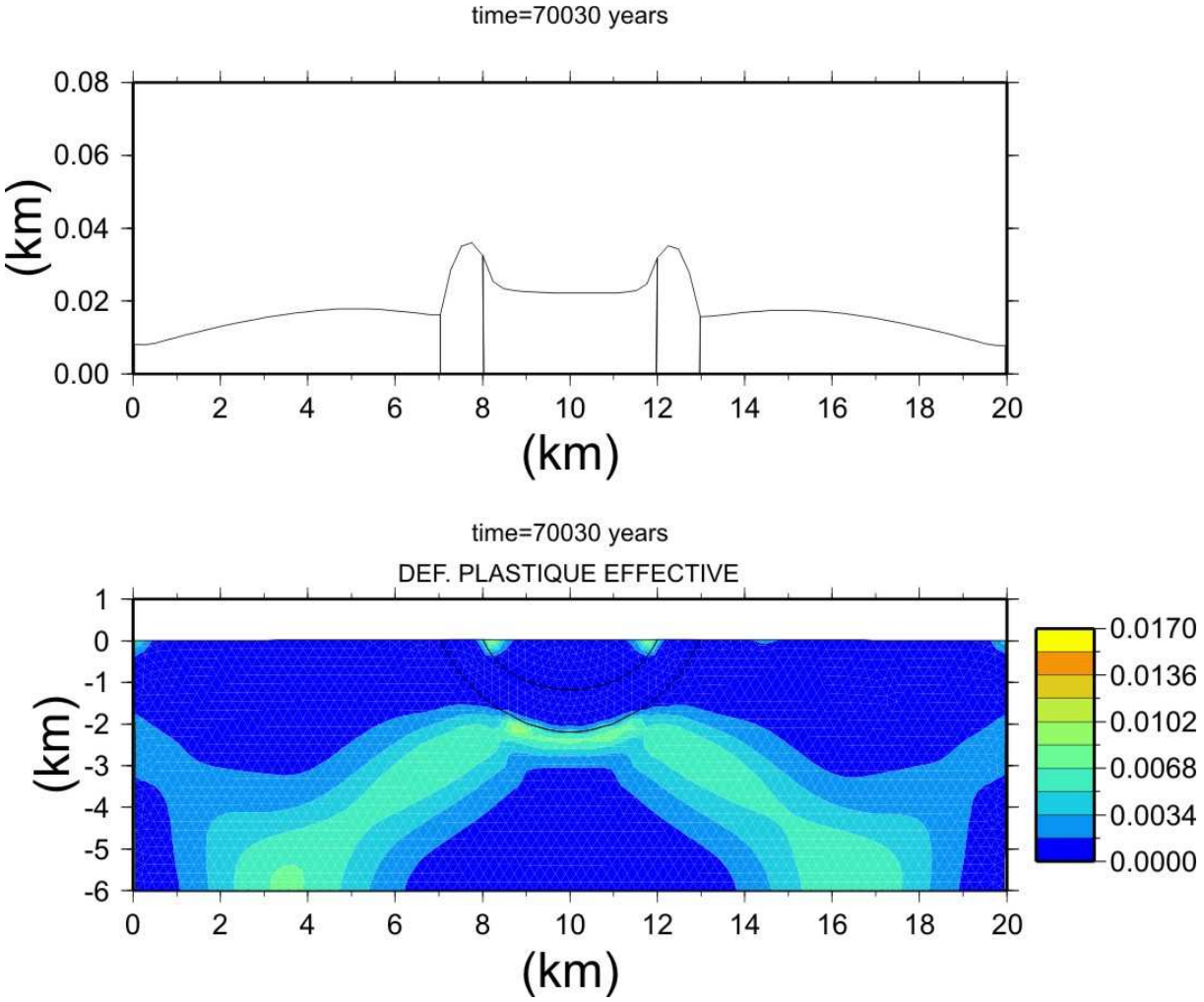

Figure IV-10 : uplift profile and plastic deformation after 70 kan for a narrow syncline, and for a 6-km-deep and 20-km-wide model box (a vertical gradient of horizontal stress of 53 MPa/km and a viscosity $\nu = 10^{20}$ Pa.s have been applied)

CHAPTER V

THICK- AND THIN-SKINNED DEFORMATION RATES IN THE ZAGROS SIMPLE FOLDED ZONE (IRAN) INDICATED BY DISPLACEMENT OF GEOMORPHIC SURFACES

CHAPITRE V

TAUX DE DÉFORMATION CRUSTALE ET SUPERFICIELLE DANS LA ZONE PLISSÉE DU ZAGROS (IRAN) A PARTIR DU DEPLACEMENT DE SURFACES GEOMORPHOLOGIQUES

Résumé en français

Dans ce chapitre, nous décrivons en détail la déformation active de la chaîne du Zagros comme observée à partir de la cartographie de terrasses fluviales le long de deux grandes rivières traversant la chaîne : les rivières de Dalaki et de Mand. En outre, nous résumons les résultats obtenus dans les chapitres 3 et 4 sur la déformation frontale et interne du prisme, respectivement, afin de proposer un modèle de déformation active du Zagros central. Nous discutons les conséquences sismotectoniques et géodynamiques de ce modèle.

Les terrasses fluviales permettent d'établir les vitesses d'incision des rivières, que nous supposons représenter en première approximation la quantité de soulèvement, même si cette hypothèse est discutée plus en détail dans le cas notamment de la partie amont de la Dalaki. En utilisant des modèles de pli fondés sur les données structurales existantes ou collectées sur le terrain, nous estimons le raccourcissement horizontal nécessaire pour générer les soulèvements observés au travers des différentes structures traversées par les rivières. L'obtention de taux de déformation dépend évidemment d'une datation bien contrainte des marqueurs. Nous avons mis en œuvre différentes méthodes de datation, notamment des datations de temps d'exposition des surfaces par isotopes cosmogéniques (^{10}Be et ^{36}Cl), des datations ^{14}C de matériel organique inclus dans les terrasses, et une datation paléomagnétique de la base des formations Bakhtyari. Bien que ces méthodes fournissent des résultats de qualité variable, nous avons pu proposer une série d'âges relativement cohérents. Cette démarche nous permet d'estimer les taux de raccourcissement absorbés par différentes structures dans le Zagros central à des échelles de temps de 10^4 à 10^6 ans.

Nous montrons notamment que le long de la rivière Dalaki, le pli de Gisakan, associé à la faille frontal principale (ou *Mountain Front Fault* = MFF), absorbe entre 1,3 et 3,4 mm/an de raccourcissement. La longueur d'onde de la déformation associée à ce pli suggère qu'elle pourrait impliquer le socle cristallin (sans pour autant fournir des preuves définitives). Par ailleurs, des observations de déplacements récents le long de failles à la surface, ainsi que l'occurrence de séismes peu profonds, indiquent que le MFF pourrait être activé sismiquement jusqu'à la surface. Ces taux de déformation s'ajoutent aux 3-4 mm/an de raccourcissement observé à travers l'anticlinal côtier du Mand, comme décrit dans le chapitre 3. En tenant compte de l'obliquité de ces structures par apport à la direction de raccourcissement régionale, entre 50 et 100% du raccourcissement actuel de 8 mm/an au travers du Zagros, et comme mesuré par GPS, est donc absorbé sur ces structures frontales. Plus à l'intérieur de ce transect, les seuls indices de déformation active que nous ayons rencontrées sont les surfaces de

Bakhtyari déformées que nous avons décrites et modélisées dans le chapitre 4. La déformation de ces surfaces correspond à des taux de raccourcissement de < 1 mm/an.

Le transect plus au sud-est, le long de la rivière Mand, montre un comportement un peu différent. Nous avons cartographié des terrasses marines entourant l'anticlinal côtier de Madar à partir d'imagerie satellitaire. Cet anticlinal peut être décrit comme un pli de propagation absorbant ~0,5 mm/an de raccourcissement. Des terrasses soulevées le long de la rivière Mand semblent liées à la branche Est du MFF, jusqu'à présent non cartographiée, qui absorberait 1,2 ± 0,5 mm/an de raccourcissement. Les terrasses les plus élevées se trouvent néanmoins plus à l'intérieur du prisme, là où la rivière traverse l'anticlinal de Halikan. Un soulèvement actif de cette structure est également souligné par une forte rupture de pente dans le profil en long de la rivière. Cette structure, qui se trouve structuralement entre deux failles de socle supposées actives, le MFF et la faille de Surmeh, se déforme de façon sûrement superficielle à des taux de 1 à 6 mm/an. Plus en amont de la rivière, notamment là où elle traverse la faille de Surmeh, la rivière est bordée par des terrasses de remplissage et nous n'avons pas trouvé de marqueurs de déformation active.

Nos résultats montrent que le raccourcissement du Zagros est concentré durant le tardi-Pléistocène dans la partie frontale de la chaîne, en conformité avec des données GPS récentes qui montre la même répartition de la déformation active. Trois ou quatre structures frontales semblent absorber pratiquement tout le raccourcissement actif à travers le Zagros, suggérant que la déformation s'est propagé vers l'avant-pays dans un régime tectonique superficiel pendant au moins le tardi-Pléistocène, avec migration vers le sud-ouest du front du prisme et une évolution prévisible de la structure et la cinématique des plis dans le temps. Une comparaison des taux et de la direction de raccourcissement à travers les différentes structures avec la distribution de la sismicité suggère que la couverture sédimentaire du Zagros frontal est découplée du socle, le plus probablement au niveau du sel de Hormuz. Ce niveau de détachement basal, en combinaison avec plusieurs niveaux de décollement intermédiaires, serait responsable de la déformation en grande partie asismique de la couverture sédimentaire du Zagros.

Thick- and thin-skinned deformation rates in the Zagros Simple Folded Zone (Iran) indicated by displacement of geomorphic surfaces *

Behnam Oveisi[1,2], Jérôme Lavé[1], Peter van der Beek[1], Julien Carcaillet[1], Lucilla Benedetti[3], Régis Braucher[3], Charles Aubourg[4]

1. Laboratoire de Géodynamique des Chaînes Alpines, Université Joseph Fourier, BP 53, 38041 Grenoble Cedex, France
2. Geological Survey of Iran, Meraj St, Azadi Sq, Tehran, Iran
3. Centre Européen de Recherche et d'Enseignement des Géosciences de l'Environnement, Université Aix-Marseille III, BP 80, 13545 Aix-En-Provence, France
4. Département des Sciences de la Terre, Université de Cergy Pontoise, 5 mail Gay Lussac, 95031 Cergy-Pontoise Cedex, France

Abstract. Although the geology and the structure of the Zagros fold-and-thrust belt (Iran) have been studied extensively, the distribution of active deformation and seismotectonic behavior across the belt remain poorly constrained. We have mapped deformed fluvial terraces along the Dalaki and Mand rivers in the central Zagros, as well as marine terraces along the Persian Gulf in order to unravel the spatial pattern of vertical displacements and to analyze active deformation and its implications for seismicity. Using appropriate fold models based on structural data allows to efficiently estimate horizontal shortening from tectonic uplift recorded by marine and fluvial terraces. Obtaining well-constrained rates of deformation depends on reliably dating deformed geomorphic markers; by combining different dating techniques and making sensible correlations to the regional climate and sea-level history, we propose an internally consistent set of ages, which allow the first geomorphic estimates of shortening rates absorbed by individual structures in the central Zagros. Our results show that shortening on Late Pleistocene timescales is concentrated in the frontal part of the belt, consistent with recent GPS data. Three or four frontal structures appear to absorb practically all of the active shortening across the Zagros, suggesting a normal forward-propagating deformation sequence in a thin-skinned tectonic regime during at least the Late Pleistocene, with south-westward migration of the front of the wedge and a predictable evolution of fold structure and kinematics. Comparing the rate and direction of shortening across across individual structures with the distribution of seismicity suggests that the sedimentary cover of the frontal Zagros is decoupled from the basement, most probably at the level of the Hormuz Salt. This weak basal detachment level, as well as several intermediate weak décollement levels, appear to be responsible for the overwhelmingly aseismic deformation of the Zagros sedimentary cover.

1. INTRODUCTION

The Zagros (Figure V-1) is a young and active orogenic belt where geomorphology and seismicity provide invaluable constraints on the style of deformation [e.g., Berberian, 1995; Talebian and Jackson, 2004]. Although the general features of the geology and the structure of the Zagros belt are now well-understood, detailed data on the distribution of active deformation

* To be submitted to : Geophysical Journal International

and seismotectonic behavior across the belt are still poorly constrained. For example, the spatial and temporal variations in deformation rate are mostly unknown. The style of wedge propagation has not been defined and neither is it clear what structures are currently active. The active deformation of the Zagros Mountains results from collision (in an approx. N-S direction) between Arabia and Continental Eurasia at a rate of 25-30 mm/yr [De Mets *et al*. 1994; Sella *et al*. 2002]. Convergence started during Late Cretaceous times in the innermost Zagros and is still active. According to seismicity [Berberian, 1995; Talebian and Jackson, 2004] and recent GPS [Tatar *et al.*, 2002; Walpersdorf *et al*., 2006] data, present-day convergence across the Zagros is concentrated in the Simply Folded Zone (SFZ), which constitutes the foreland fold-and-thrust belt of the system. From a recent GPS survey, Tatar *et al.* [2002] proposed a present-day shortening rate of 8-10 mm/yr for the Zagros, which would accommodate 40-50% of the total ~21 mm/yr convergence between Arabia and Eurasia [Vernant *et al.*, 2004]. Total shortening in the SFZ is estimated between ~50 and ~70 km [Blanc *et al*, 2003; McQuarrie, 2004; Sherkati *et al.*, 2006].

The stratigraphic succession of rock series with highly variable mechanical properties strongly controls deformation in the Zagros SFZ. Precambrian to Recent sedimentary cover rocks range in thickness from 5 to 15 km [Stocklin, 1968; Falcon, 1969; Colman-Sadd, 1978]. Lower Cambrian [Berberian, 1995] incompetent Hormuz series evaporites directly overlie the crystalline basement, forming a basal detachment level that plays an important role in guiding the deformation. Seismological data show that large earthquakes in the Zagros generally nucleate in the upper crust at depths of 8 to 15 km, i.e. in majority within the crystalline basement [Jackson and McKenzie, 1984; Ni and Barazangi, 1986; Baker *et al.*, 1993; Maggi *et al*., 2000; Talebian and Jackson, 2004]. A recent study of micro-earthquakes in the central Zagros [Tatar *et al*., 2003] suggests that much of the seismicity is restricted to the upper part of the basement between ~11 km (base of the sedimentary cover), and ~15 km (base of the seismogenic layer). Absence of seismogenic behavior in the sedimentary cover is supported by seismic moment summations [Masson *et al.*, 2005], which show that ~95% of the deformation is accommodated aseismically by creep on faults and folding, as suggested previously by Jackson *et al.* [1995]. Balanced cross-sections across the Zagros require involving several mid-crustal ramps with kilometer-scale steps in the basement [Molinaro *et al.*, 2004; Mouthereau *et al.*, 2006; Sherkati *et al.*, 2006], or alternatively to fill the voids with large amount of Hormuz salt [McQuarrie, 2004]. Geological observations are ambiguous on this point, although large

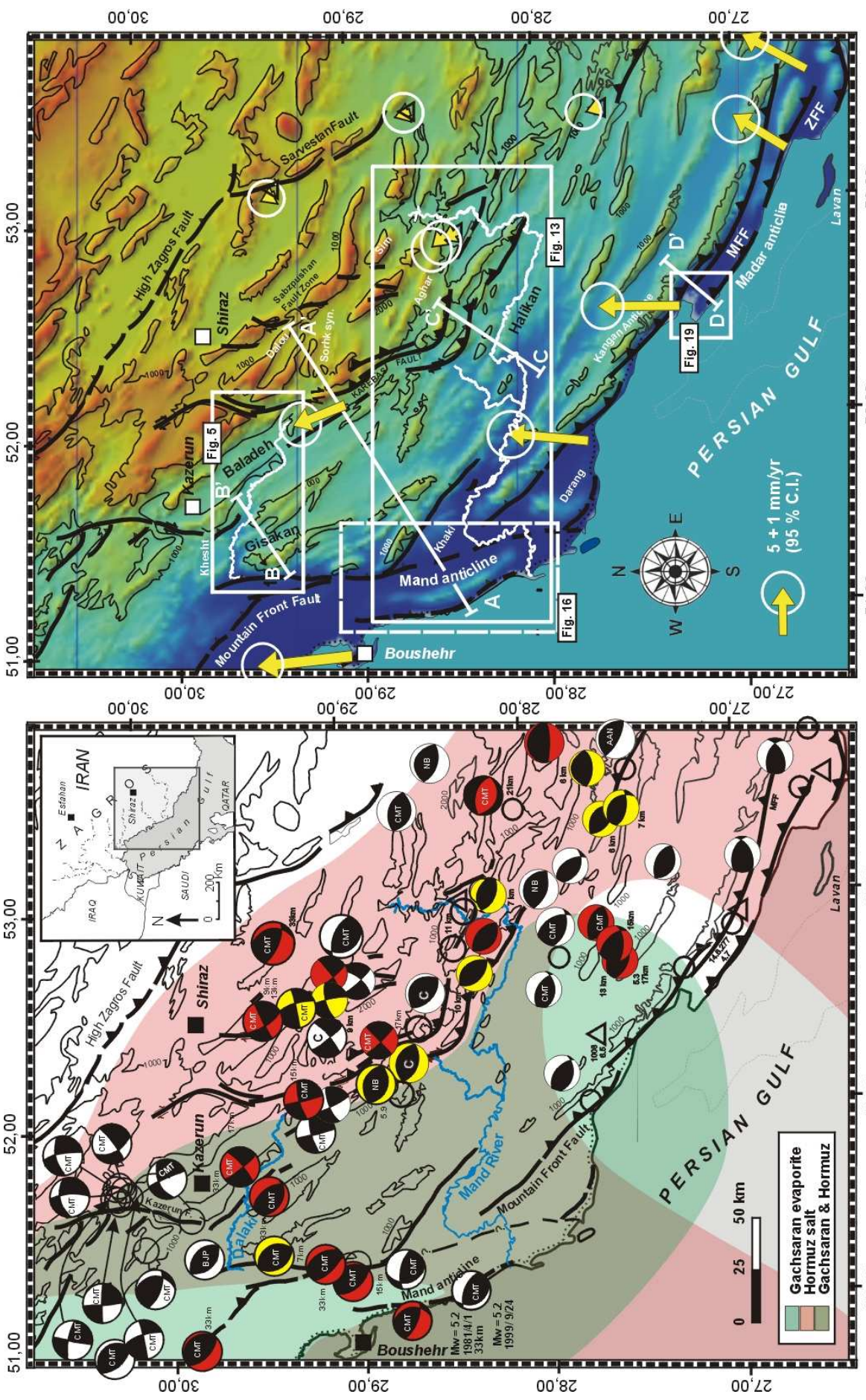
High Zagros Fault
Sarvestan Fault
Shiraz
Sabzpoushan Fault Zone
Sorkh syn.
Kazerun
Fig. 5
Baladeh
Gisakan
Khesht
Mountain Front Fault
Boushehr
Fig. 13
Halikan
Aghar
Syn.
Fig. 16
Mand anticline
Khaki
Darang
Fig. 19
MFF
Madar anticlia
ZFF
Lavan
PERSIAN GULF
5 +1 mm/yr
(95 % C.I.)
IRAN
IRAQ
KUWAIT
SAUDI
QATAR
Persian Gulf
Esfahan
Mand River
Dalaki
Kazerun F.
Gachsaran evaporite
Hormuz salt
Gachsaran & Hormuz
0 25 50 km
Mw = 5.2
1981/4/1
33km
Mw = 5.2
1999/9/24

Figure V-1: Seismotectonic (a) and topographic (b) maps of the central Zagros showing main faults, focal mechanism solutions and GPS results, as well as locations of subsequent figures. Fault plane solutions of large earthquakes are given with centroid depths (km) where well determined and are from different sources: C = Chandra [1984]; CMT = Harvard centroid-moment tensor solution; AAN = Nowroozi, 1972; BJP = Baker *et al*. [1993]; NB = Ni and Barazangi [1986]. Compressional quadrants are in red for events unequivocally located in the basement, in yellow for events in the sedimentary cover and in white for events without adequate depth control. Arrows in (b) indicate rate and direction of horizontal GPS vectors (mm/yr) in the central Iran-fixed reference frame for the period 1999-2003 [Vernant *et al.,* 2004; Walpersdorf *et al.*, 2006]. The fault map is modified from Berberian [1995]. Geographic extent of Gachsaran and Hormuz evaporitic facies in (a) are from Sherkati and Letouzey [2004]. Topographic contours with 1000-m interval. Regional cross-sections A-A', B-B' C-C' and D-D' are shown in Figures V-3, 11, 15 and 19, respectively.

topographic and structural steps have been interpreted as major flexures and faults in the basement [Berberian, 1995]. Regardless of the structural models presented, however, finite shortening in the basement is an order of magnitude lower than that affecting the sedimentary cover. One of the main issues in the Zagros is, therefore, to determine partitioning of the deformation and the coupling between basement and sedimentary cover, as well as the exact amount of shortening in the basement and the timing and activation sequence of mid-crustal ramps, if they exist.

In these conditions, studying the relative vertical displacement of geomorphic markers can help to unravel the present-day tectonic activity within the basement. More generally, such studies can help to unravel the spatial pattern of the vertical displacement field, in order to analyze active deformation and its implications for seismicity. In order to quantify recent tectonic deformation, we have mapped preserved fluvial terraces along the Rud e Dalaki and Rud e Mand rivers in the central part of the Zagros SFZ (western Fars province), as well as marine terraces along the Persian Gulf. In the following, we first detail the tectonic and physiographic setting of our study area. Then we present our approach to constrain uplift and shortening rates, and present the different geomorphic markers associated with actively deforming folds that we identified and mapped. Vertical deformation is discussed in terms of fold type, deformation style, fold evolution, and the partitioning of deformation between basement and sedimentary cover. Finally, inferred shortening rates are interpreted in terms of the spatial distribution of horizontal deformation in the central Zagros SFZ.

2. GEOLOGIC SETTING

2.1. Tectonics and stratigraphy of the Zagros SFZ

The Zagros Fold-Thrust Belt is bordered to the southwest by the Persian Gulf, which represents the present-day foredeep basin at the front of the orogen, and to the northeast by the Main Zagros Thrust (MZT), considered by many as the suture of the Neo-Tethys Ocean (Figure V-1). North of the MZT, the Sanandaj Sirjan Zone consists of strongly deformed and imbricated metamorphic and sedimentary rocks, and Andean-type volcanic rocks [Alavi, 1994]. The Zagros Fold-Thrust Belt can be laterally subdivided into three main regions of changing width, morphology and structural style, which are, from NW to SE: the Lurestan Arc, the Dezful Embayment and the Fars Arc. Our study area comprises the central part of the Zagros in the Fars region, where two main structural zones are classically distinguished on the basis of distinct topographies and outcropping units (Figure V-1): the High Zagros Belt (HZB) to the NE and the Zagros Simply Folded Zone (SFZ) to the SW. The High Zagros Fault separates these two structural domains. It is generally considered that deformation in the HZB initiated before deformation in the SFZ, according to a classical forward-propagating sequence scenario.

Sedimentation on the Arabian platform has led to deposition of a 5 - 15 km thick sedimentary sequence of passive margin to flexural basin series since pre-Cambrian times [Stocklin, 1968; Falcon, 1969; Colman-Sadd, 1978], interrupted by several sedimentary hiatuses [e.g., Alavi, 2004] (Figure V-2). Paleozoic to Early Miocene series are composed of mostly carbonates and clastic units with minor evaporitic levels overlying a thick basal evaporite (Hormuz Salt). The transition from oceanic subduction to continental collision is marked by obduction followed during Miocene times by continental collision, leading to incipient Zagros deformation. Concomitantly, the sediments accumulating in the flexural basin formed by the overloading of the Arabian plate by the rising Zagros display a progressive transition toward more continental facies from Oligo-Miocene shallow-marine limestones (Asmari Fm), to mid Miocene evaporites (Gachsaran Fm) and marls (Mishan Fm), Mio-Pliocene sandstones (Agha Jari/Lahbari Fms) and finally the Pliocene-Quaternary upper Bakhtyari conglomerates. The base of the Bakhtyari conglomerates correspond in many places to a major angular unconformity and for that reason has been associated with renewed erosion and tectonic

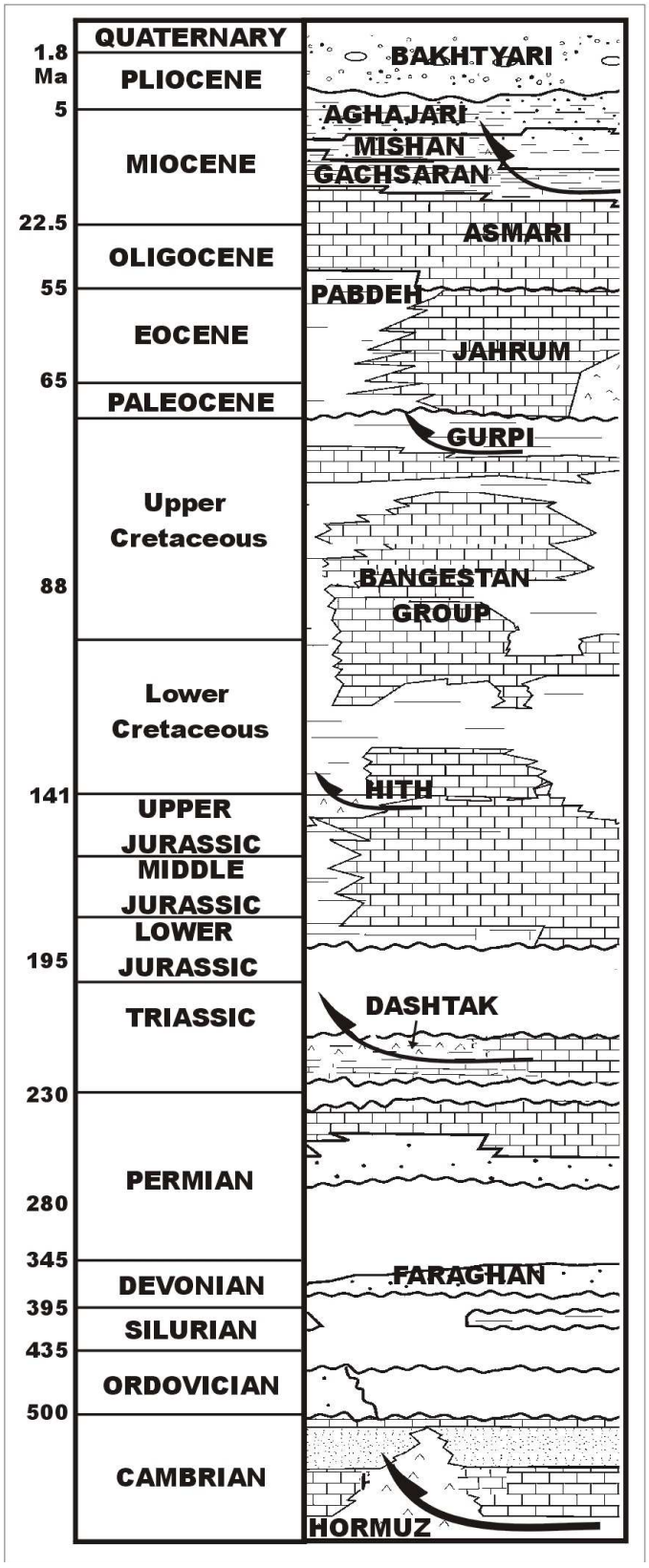

Figure 2: Stratigraphy of the Simply Folded Zone of the Zagros belt. Arrows indicate possible décollement levels within the sedimentary succession.

activity of the Zagros fold-and-thrust belt: this event is generally dated as Late Pliocene, but could be largely diachronous from NE to SW, and would accompany the propagation of the deformation front [Hessami *et al.*, 2001]. In addition, growth strata within the Agha Jari formation indicate deformation of the frontal folds in the Lurestan Arc as early as ~8 Myr ago [Homke *et al.*, 2004], seriously challenging the above simplified scenario of Late Pliocene forward propagation of the wedge.

During the Arabia-Eurasia collision, the Phanerozoic sedimentary pile accumulated on the Arabian margin has been detached from its Panafrican crystalline basement and folded. The deformation front advanced into the foreland, generating a fold-thrust belt of 200-250 km width. GPS data indicate active shortening across the Zagros in a roughly N-S direction. Present-day convergence rates increase from 5 ± 2 mm/yr in the northern Zagros to 7 ± 2 mm/yr and 9 ± 2 mm/yr in central and southeastern Zagros, respectively [Vernant *et al*., 2004; Walpersdorf *et al*., 2006].

The most striking manifestation of finite deformation in the SFZ is the extensive succession of large-scale folds with typical amplitude and wavelengths of ~4-5 km and ~15 km, respectively. Due to the presence of a major and thick décollement level in the Hormuz salt, as well as the general absence of clearly expressed faults at the surface, many of these folds are considered as detachment folds [e.g., Colman-Sadd, 1978; Sherkati *et al*. 2006]. However, numerous anticlines are bounded by faults with a clear surface expression, which have contributed to the deformation of the sedimentary cover of the SFZ in the Fars region. On the other hand, several major blind faults are inferred to be active beneath the sedimentary cover [e.g., Berberian, 1995]. Focal mechanisms indicate that both thrust and strike-slip faults are present in the basement and/or lowest part of the sedimentary cover of the SFZ. From W to E, active strike-slip faults are the Kazerun Fault, the Karebas fault, the Sabz-Pushan Fault and the Sarvestan Fault (Figure V-1). All of them are right lateral and they have been diversely interpreted as the result of either slip partitioning [Yamini-Fard *et al*., 2006], en echelon fault systems at the eastern end of the Main Recent Fault [Authemayou *et al.*, 2006], or oroclinal bending and more extensive wedge propagation in the Fars arc compared to the Dezful Embayment due to a thicker layer of incompetent Hormuz salt at the base of the sedimentary cover in the former [McQuarrie, 2004]. These faults, in particular the Kazerun and Karebas faults, are also the loci of important lateral variations in sedimentation facies and rates, as observed on isopach maps of the different sedimentary units from the Proterozoic-to-Recent sedimentary pile [Bahroudi and Talbot, 2003]. This suggests that these basement faults correspond to the reactivation of old crustal-scale features.

From NE to SW, the major thrust faults suspected to involve basement [Berberian, 1995] are the High Zagros (or Main Zagros) Thrust (HZT), the Surmeh Fault and the Mountain Front Fault (MFF). The extent of the studied geomorphic markers does not permit to estimate the tectonic activity of the HZT in the present study. However, according to the GPS data [Hessami *et al*., 2006; Walpersdorf *et al*., 2006], the absence of significant shortening in a region of at least 50 km on both sides of the HZT suggest minor or no active thrusting on the HZT. The moderate seismicity on the HZT, as compared to the SFZ further south, would suggest that the above conclusion is valid for the basement root of the HZT as well as for its more superficial expression.

The Surmeh Fault is classically interpreted as the SE termination of the Karebas Fault (Figure V-1) [e.g., Berberian, 1995], and thrusting on it would be intimately linked to strike slip motion on Karebas fault. Basement-involved thrusting on the Surmeh Fault would have permitted the exhumation in the core of the Surmeh anticline of the oldest sedimentary units (Paleozoic) of the Fars arc. Its eastern extension is poorly defined by topographic indices [e.g. Mouthereau *et al.*, 2006]. However, a general NW-SE trend of M_w=5.5-7.0 earthquakes with thrust focal mechanisms suggests that this fault could extend as far as 55°E, i.e. up to the easternmost Fars (Figure V-1a) [Berberian, 1995; Talebian and Jackson, 2004].

The Mountain Front Flexure [Falcon, 1961] or Mountain Front Fault [Berberian, 1995] (MFF) constitutes an important but unexposed structural element (termed blind master thrust by Berberian [1995]) that delimits Cretaceous-Paleogene outcrops in its hanging-wall throughout the SW SFZ. Strong topographic contrasts and abrupt structural terminations outline the regional trend of the MFF; however, this fault does not display a continuous structure at the surface, but rather a series of en-echelon structures involving several asymmetric folds. In its northern part, the MFF strikes roughly N-S, in marked contrast with the N45°W trend of fold axes and of the flexure further southeast (Figure V-1). East of the N-S trending fault segment, a zone of en-echelon faults branches parallel to the MFF trajectory. Whereas GPS vectors, which are oriented N-S and almost parallel to the trend of the oblique MFF segment [Vernant *et al.*, 2004; Walpersdorf *et al*., 2006], would suggest a strike slip component on the fault, the orientations of reported earthquake nodal planes (Harvard CMT solutions) indicate almost pure thrust motion and their trends of N25°-45°W are parallel to the regional orientation of the fault zone (cf. Figure V-5). Further SE, the MFF is drawn all along the main topographic front, since the Zagros Foredeep Fault (ZFF), associated with the most frontal folds, is clearly

discontinuous and probably only related to local deformation of the sedimentary cover [e.g., Berberian, 1995].

2.2. Regional structures and balanced cross sections

In order to estimate the finite deformation of the sedimentary cover, constrain the depth to basement, and provide a preliminary framework to interpret terrace deformation, we have constructed several balanced cross sections across the frontal part of the central Zagros (see locations on Figure V-1). In the Mand region, Sherkati *et al*. [2006] have recently proposed a detailed balanced cross-section based on both surface data and unpublished seismic reflection and well data provided by the National Iranian Oil Company (NIOC). Outcrop and borehole data provided them, in particular, a good thickness control on Permian to recent sedimentary units. Balanced cross-sections rely on the assumption that no material moves into, or out of, the plane of the section. In the study area, this assumption may not be valid, as there may be a significant regional component of oblique slip relative to structural orientations (e.g., Figure V-1). In constructing the section A-A' of Figure V-3, we have used the Sherkati *et al*. [2006] section for its south-western part. To complement it to the northeast, and to construct the other sections, we used surface structural data (our own detailed field data, as well as from geological maps published by the National Iranian Oil Company). In constructing the balanced cross-sections we followed the sinuous bed method, which supposes constant bed thickness for the competent layers during shortening [Dahlstrom, 1969]. In addition, we attempt to reach a solution that is laterally consistent with discontinuous north-eastern segments of Sherkati *et al.*'s [2006] sections. As discussed in the previous section, the progressive north-eastward increase in elevation of Paleozoic to Cenozoic units requires that large basement faults display vertical offsets of 1 to 2 km. However, the location of the basement faults as proposed by Sherkati *et al*. [2006] is not completely concordant with those proposed by Berberian [1995].

The balanced section of Figure V-3 indicates different fold wavelengths within the sedimentary cover. Whereas a majority of folds present a wavelength of ~15 km, some have clearly developed shorter wavelengths. Some wavelength reduction is expected for evolved detachment folds [Mitra, 2003], but such a process is generally insufficient to explain observed wavelengths of 3 to 6 km. We hypothesize that such short wavelengths result from different décollement depths at the level of distinct weak units within the sedimentary cover [see also

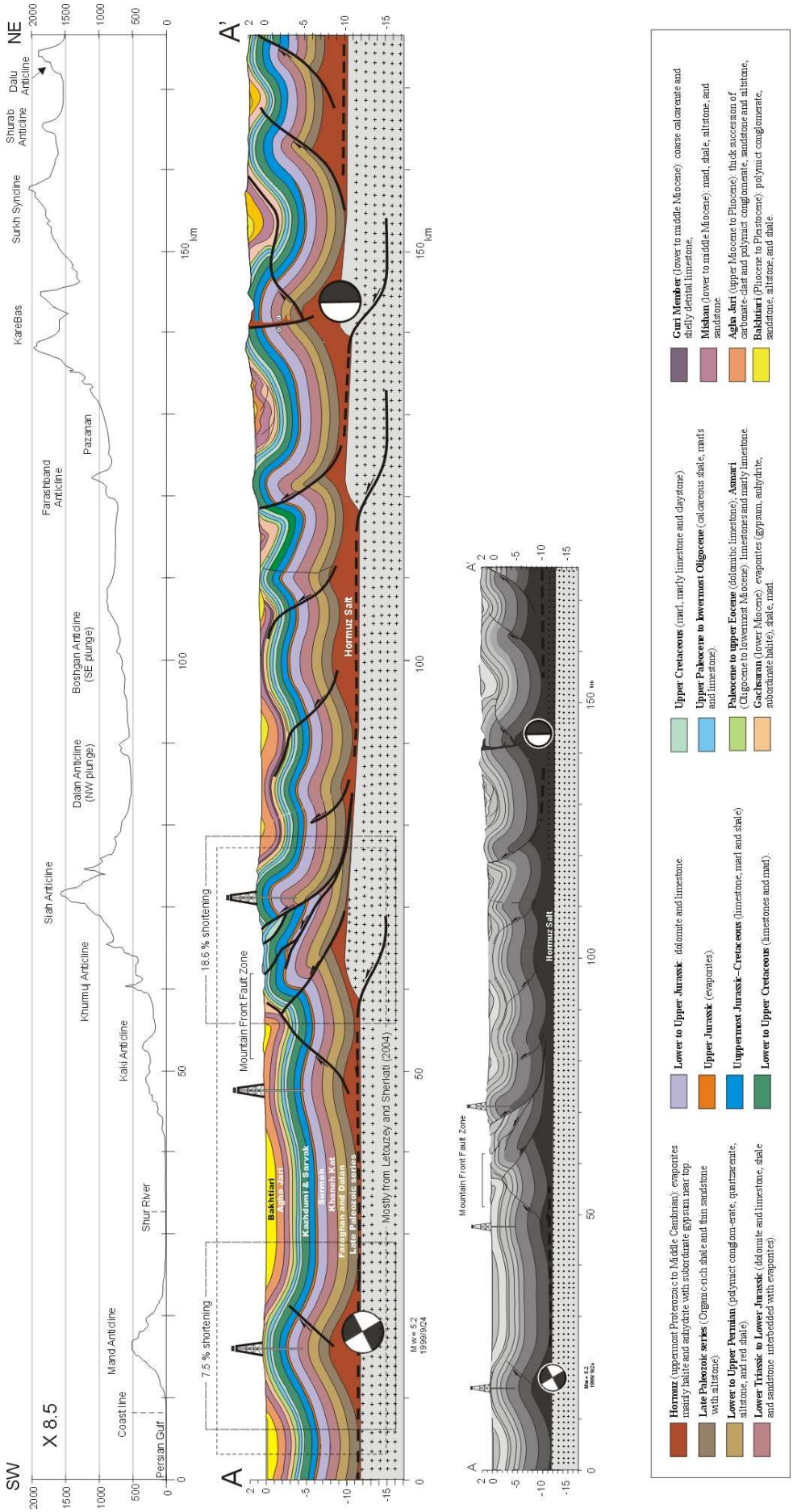
SW
NE
X 8.5
Persian Gulf
Coastline
Mand Anticline
Shur River
Kaki Anticline
Khumuj Anticline
Siah Anticline
Dalan Anticline (NW plunge)
Boshgan Anticline (SE plunge)
Pazanan
Farashband Anticline
Surkh Syncline
Shurab Anticline
Dalu Anticline
KareBas
A
A'
7.5 % shortening
18.6 % shortening
Mountain Front Fault Zone
Hormuz Salt
Bakhtiari
Agha Jari
Kazhdumi & Sarvak
Sachun
Khaneh Kat
Faraghan and Dalan
Late Paleozoic series
Mostly from Letouzey and Sherkati (2004)
Mw = 5.2
1999/9/24
km
Hormuz (uppermost Proterozoic to Middle Cambrian): evaporites mainly halite and anhydrite with subordinate gypsum near top.
Late Paleozoic series (Organic-rich shale and thin sandstone with siltstone).
Lower to Upper Permian (polymict conglomerate, quartzarenite, siltstone, and red shale).
Lower Triassic to Lower Jurassic (dolomite and limestone, shale and sandstone interbedded with evaporites).
Lower to Upper Jurassic: dolomite and limestone.
Upper Jurassic (evaporites).
Uppermost Jurassic–Cretaceous (limestone, marl and shale).
Lower to Upper Cretaceous (limestones and marl).
Upper Cretaceous (marl, marly limestone and claystone).
Upper Paleocene to lowermost Oligocene (calcareous shale, marls and limestone).
Paleocene to upper Eocene (dolomitic limestone). Asmari (Oligocene to lowermost Miocene) limestones and marly limestone.
Gachsaran (lower Miocene): evaporites (gypsum, anhydrite, subordinate halite), shale, marl.
Guri Member (lower to middle Miocene): coarse calcarenite and shelly detrital limestone.
Mishan (lower to middle Miocene): marl, shale, siltstone, and sandstone.
Agha Jari (upper Miocene to Pliocene): thick succession of carbonate-clast and polymict conglomerate, sandstone and siltstone.
Bakhtiari (Pliocene to Pleistocene): polymict conglomerate, sandstone, siltstone, and shale.

Figure V-3: Regional balanced cross-section A-A' across the Simple Folded Zone in the study area (see Fig. V-1 for location), modified from Sharkati *et al.* [2006], and including basement fault offsets. An alternative interpretation of the structural data (lower black and white section) requires a northward-thickening Hormuz salt layer to fill the void between the folded cover and the shallowly northward-dipping basement [McQuarrie, 2004].

discussion in Sherkati *et al.*, 2006]. The balanced section also indicates different degrees of fold asymmetry. In the NE and intermediate parts of the section, SW-vergent fault-cored folds present a steeper dipping forelimb than backlimb. The Gisakan anticline and its lateral continuation in the Siah anticline, for example, are asymmetric high-relief active structures that have been created by movement of thrust sheets over the MFF footwall ramp (Figure V-3). At the Zagros front (between the MFF and the ZFF), in contrast, the Mand and Kaki anticlines appear as distinctly symmetrical detachment folds (Figure V-3). Detachment folds usually develop when the sedimentary units are characterized by significant thickness and competency contrasts, with commonly a low viscosity basal layer overlain by thick competent units [Jamison, 1987; Mitra, 2003]. Along these anticlines, the near-symmetrical dip panels on each side of the folds do not show any structural vergence and no outcropping fore- or back-thrusts are associated with them. In contrast to the tightly folded anticlines associated with the MFF ramp, the Mand or Kaki anticlines are open folds (Figure V-3), with limbs dominated by gentle bedding dips between 10-27° and 5-11°, respectively. These two anticlines display the characteristic features of detachment folds and probably developed above the low-viscosity basal layer of Hormuz Salt, overlain by the thick competent Paleozoic to Cretaceous carbonate units. It is generally assumed that detachment folds evolve into tight lift-off folds, or into more asymmetric folds in association with fault propagation toward the surface [Mitra, 2003]. In the Zagros SFZ, the second evolution is by far the most common, and symmetric detachment folds with limbs steeper than 50° are uncommon.

For the entire section across the Western Fars SFZ, Sherkati *et al.* [2006] estimate 34 km of finite shortening, based on line-length restoration of the competent units. In the basement, finite shortening across the SFZ is estimated to be ~5-7 km, i.e. less than 25% of the shortening absorbed in the sedimentary cover. Several hypotheses have been developed to explain this difference. In the first scenario, deformation in the basement and cover are concomitant and the much larger deformation rates in the sedimentary cover are accommodated by a major decoupling level in the Hormuz Salt [e.g., McQuarrie, 2004]. In the second scenario, present deformation rates in the sedimentary cover are comparable to deformation rates in the

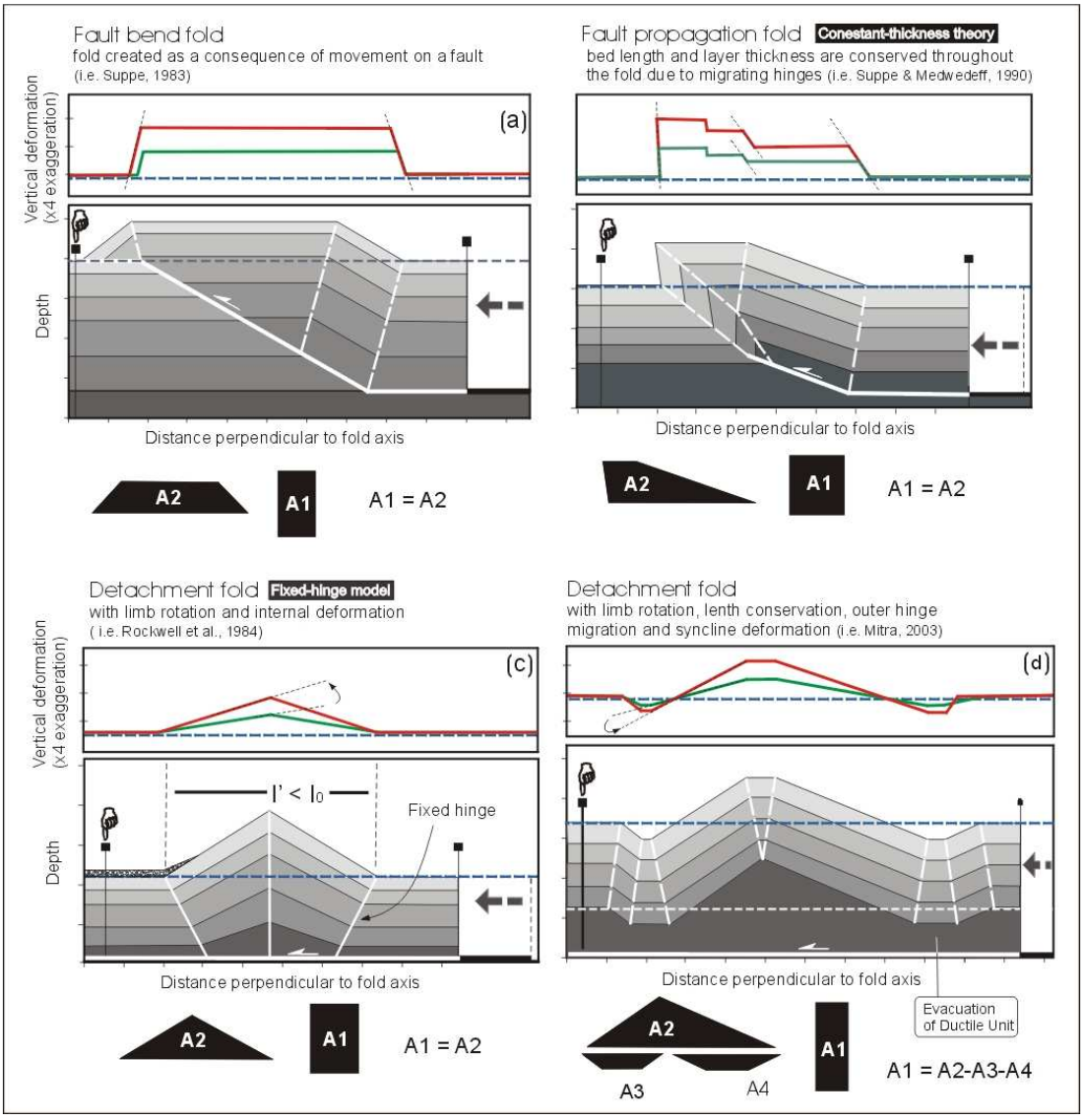

Figure V-4: Different fold models and associated incremental surface deformation: (a) fault-bend fold [Suppe, 1983], (b) fault-propagation fold [Suppe and Medwedeff, 1990], (c) detachment fold with limb rotation and internal deformation [Rockwell *et al.*, 1984], (d) detachment fold with limb rotation, length conservation, migration of outer hinges and syncline deformation [Mitra, 2002]. Fixed and migrating hinges are presented by solid and dashed white lines respectively.

basement, and as a consequence, basement deformation needs to have initiated very late in the orogen history [Molinaro *et al.*, 2005]. These two scenarios are expected to produce distinct deformation at the surface since dominant basement implication would produce large-wavelength vertical deformation profiles and maximum uplift would be located at the structurally identified steps in the basement.

3. DEFORMED GEOMORPHIC MARKERS, FOLD MODELS AND SHORTENING: methodology

3.1. Terrace mapping and dating

In our study area, two main rivers, the Rud e Dalaki and Rud e Mand, intersect several folds and structures, as well as hypothesized basement faults like the MFF or the Surmeh fault (Figure V-1). Numerous Quaternary terraces occur along both of these rivers. Fluvial terraces provide important records of river incision, rock uplift, and climatic perturbations [e.g. Merrits *et al.*, 1994; Pazzaglia and Brandon, 2001]. Remnants of fluvial terraces that are preserved along river reaches in active orogenic belts reflect the long-term incision history of a river and can be used as geomorphic markers to interpret active tectonics if it can be demonstrated that the river profile does not change through time [e.g., Lavé and Avouac, 2000]. Marine terraces can alternatively be used to unravel vertical deformation. In contrast to fluvial terraces, their initial elevation and geometry usually suffer less ambiguity and provide a more accurate tectonic signal. However, their restricted extension limits their use to the shorelines of coastal orogens. In our study area, marine terraces occur along the Mand and Madar anticlines on the Persian Gulf coast.

We mapped both fluvial and marine terraces using aerial photographs and Corona and SPOT satellite imagery. Terraces were classified based upon their spectral signature on SPOT imagery. The precise locations and elevations of the terraces were measured in the field using digital altimeter, theodolite or kinematic GPS and, where access was too difficult, with a laser distance meter from a GPS-referenced point. The terrace elevations were measured with an accuracy of a few centimeters for theodolite and GPS surveys, with an accuracy of 0.2–2 m for the laser distance meter (depending on the ranging distance, between 10 and 250 m), and with an accuracy of 3-4 m when using a digital altimeter. Where possible, we measured the elevation of the top of the terrace gravels or fill material, and also of the unconformity at the base of the terrace or strath level.

We determined the age of the surveyed geomorphic markers using different methods. Where possible, we collected organic-carbon rich material in the terraces. Along the Persian Gulf, it is easy to find shells, and locally corals, in marine terraces or mixed terraces to perform ^{14}C dating [e.g., Vita Finzi, 1979]. However, in most of the Zagros belt, organic material (i.e. shells, wood fragments or charcoal) is rare because of the arid environment and the rare occurrence of silty overbank deposits that typically host it. We only found and dated gastropods

from a terrace along the Dalaki River close to the MFF. In addition, many geomorphic markers are Middle to Late Pleistocene in age, that is, too old to be dated by the ^{14}C method.

Exposure ages determined from in-situ produced cosmogenic radionuclides (^{10}Be, ^{36}Cl) on pebbles and clasts from the terrace surface provide an alternative approach [e.g., Lal, 1991; Cerling and Craig, 1994; Gosse and Phillips, 2000]. Terrace exposure ages correspond to the time since terrace abandonment as fluvial incision resumed. Fluvial terraces in the central Zagros are characterized by a quasi-absence of fine sandy or silty deposits at the top of the alluvial cover, allowing, in principle, to reliably date terrace abandonment from clast samples. However, a crucial bias in dating alluvial surfaces with cosmogenic nuclides in clasts stems from inheritance acquired during erosion and fluvial transport [e.g., Anderson *et al*., 1996]. To circumvent this problem and to account for clast-specific exposure histories, we gathered 3-4 sandstone pebbles (10-20 cm in diameter) from each terrace surface, and also collected where possible samples from up to several meters deep profiles [e.g., Anderson *et al*., 1996; Brocard *et al*., 2003]. Unfortunately, many of the pebbles, even those originating from Agha Jari sandstones, turned out to be poor in quartz in the coarse sand fraction (> 200 μm). Moreover, due to the presence of uncommon mineral phases like strontianite or of crypto-crystalline quartz (agate, chert) in the sandstones, as well as to ^{10}B pollution, more than 50% of our samples produce inconsistent results. The final set of available results was insufficient to properly estimate the inheritance problem, and improvements in sampling and treatment strategies will be required in the future to deal with quartz-poor sandstones such as those encountered here.

In contrast to sandstones, limestone pebbles are abundant within all surveyed terraces. During one of our field seasons, we therefore collected limestone pebbles with the aim to date their exposure using the cosmogenic nuclide ^{36}Cl. In addition, limestone bedrock is particularly susceptible to preserve lateral fluvial erosion marks (e.g., potholes); we collected two samples (KAZ-9, KAZ-20) from fluvially sculpted Asmari limestone or limestone-rich and re-crystallized Bakhtyari formations. Finally, a sample was taken from an unexposed limestone boulder in a terrace deposit (KAZ-5) in order to estimate pre-depositional cosmogenic radionuclide inheritance.

The cosmogenic ^{10}Be samples were processed following standard procedures described by Brown *et al*. [1991]. Sample preparation was performed at CEREGE (B. Oveisi and R. Braucher) for a first set of samples and at the LGCA (B. Oveisi and J. Carcaillet) for a second

set. The ^{10}Be concentration was measured by accelerator mass spectrometry at the *Centre d'Etudes Atomiques*, Saclay, France. Production rates have been calculated using the scaling functions of Lal [1991] as modified by Dunai [2000] and a modern ^{10}Be production rate in quartz of 5.75 ± 0.24 atoms g^{-1} yr^{-1} at sea level and high latitude [Kubik *et al.*, 1998]. Topographic shielding has been measured in the field but was generally not significant except for the samples from fluvially-sculpted limestone. To account for the attenuation with depth of the production rates for subsurface samples collected in terraces, a depth-correction was applied assuming a density $\rho = 2.0 \pm 0.2$ g/cm^3 for the fluvial material. We considered contributions from neutrons, stopped muons and fast muons with relative contributions and attenuation lengths for each of these as determined by Braucher *et al*. [2003] for ^{10}Be-production.

In carbonate rocks, in-situ ^{36}Cl is produced primarily by interaction of neutrons and muons with Ca and Cl. Although production by thermal and epithermal neutrons from Cl is maximum at 20-50 cm depth, the total production rate can be described as an exponential decrease with depth with in-situ ^{36}Cl mostly accumulated at the surface [Gosse and Phillips, 2001], using a similar absorption mean free path as for cosmogenic ^{10}Be. Samples were grinded, leached and chlorine was chemically extracted by precipitation of silver chloride following the procedure described in Stone *et al.* [1996]. Sample preparation was performed at CEREGE by L. Benedetti; the ^{36}Cl and chloride concentration in the carbonate was determined for all samples by isotope dilution accelerator mass spectrometry at the Lawrence Livermore National Laboratory CAMS facility. Blanks were two orders of magnitude lower than the samples and replicates were within less than 5% similar. Major and trace elements were determined by ICP-OES at CEREGE. Surface exposure ages were calculated using ^{36}Cl production rates from calcium and chlorine of Stone *et al*. [1998] for all relevant pathways. Other published production rates [Gosse and Phillips, 2001 and references therein] are higher than the Stone *et al*. [1998] value and would lead to younger ages (by about 20%). These production rates were calibrated to our site latitude and altitude using Stone's [2000] coefficients. The exposure ages presented in Table 3 include analysis and processing errors, as well as the error on the Stone *et al.* [1998] production rate.

3.2. Terrace deformation and fold kinematics

Available geological and geophysical data usually constrain the present-day fold geometries in the study area, but do not always permit a clear determination of the fold evolution and

kinematics. Additional kinematic information can be gained, however, by mapping deformed geomorphic markers, in particular if several markers document different increments of deformation. As schematically presented in Figure V-4, different end-member fold models produce distinct surface deformation patterns. Fault-bend and fault-propagation folds will lead to uniform uplift above fault segments of constant dip. Geomorphic markers will record some short wavelength tilting where crossing axial surfaces; these dipping panels will be parallel, whatever the marker age (Figure V-4 a, b). The above models are based on the assumptions of plane strain, constant area, constant bed-length and parallel kink-style folding. The models provide specific relationships between fold and fault geometry. Some workers [e.g. Jamison, 1987] showed how the assumption of constant bed thickness and parallel folding can be relaxed to allow thinning or thickening of the frontal fold limb. Tri-shear models [e.g., Erslev, 1991] allow such deformation of the frontal limb. Consequently, whereas they present similar incremental deformation as constant-thickness fault-bend and fault-propagation folds along their back-limb, the latter models predict a progressive tilting of the frontal limb in association with significant bed thickening. The length of the tilted and thickened panel decreases, however, while the fault tip propagates toward the surface.

In contrast to the above fold models, detachment folds do not develop at the tip of a propagating ramp, but above the tip of a sub-horizontal detachment at depth. For detachment folds, limb rotation will produce progressive surface tilting, long and gently dipping panels and maximum uplift at the anticlinal crest (Figure V-4 c, d). Finally, adding synclinal flexure to the detachment model [Mitra, 2003] will be recorded at the surface by progressive tilting of markers, but also a transition from uplift to subsidence somewhere between the anticlinal and synclinal axes (Figure V-4d). These different fold solutions imply distinct amounts of finite fold shortening (see for instance, section 4.4.1. for an example from the coastal Mand anticline).

3.3. Fold deformation and absorbed shortening

The manner in which vertical deformation is translated to shortening across a given structure also depends on the length and quality of the deformation profile recorded by a passive geomorphic marker. A simple and robust way to deduce horizontal shortening from the uplift profile across a fold is to consider conservation of mass. As long as there is no major porosity change in the fold material and there is no material transfer across the considered plane, mass

conservation is equivalent to area conservation: $d = A/h$, where d is the mean horizontal displacement, A the area below the uplift profile recorded by a geomorphic marker, and h the sediment thickness above the detachment. This approach requires, however, a terrace tread or other marker that can be reconstructed across the entire growing fold. As an alternative, when the detachment depth is not known with certainty, a line length restoration technique can be applied to the geomorphic marker. However, this method can be biased by significant thinning or thickening of the layers at surface and of the deformed marker. In addition, for deformation associated to a fault, part of the marker in the footwall can be buried below the overriding hanging-wall and the present-day length of the deformed marker may be underestimated.

If treads are only partially preserved, the above methods cannot be applied to river terraces. Local measurements of incision can also be related to shortening by assuming fold kinematics, if river incision can be equated to tectonic uplift [Lavé and Avouac, 2000]. For mature folds, e.g., fault bend-folds with the ramp reaching the surface and internal deformation accommodated by flexural slip, local shortening d is related to the dip θ of the fault at depth (which is equal to the bedding dip on the back limb for a fault-bend fold): $d = U / \sin(\theta)$, with U the marker uplift. As a first approximation, this method can be used for any deformation associated to a fault ramp at depth. Alternatively, if a tilted panel crossing an axial surface is preserved without ambiguity, its length can be also used to unravel the shortening across the fold structure [Thompson *et al.*, 2002]. If the terraces are preserved only on the frontal limb of a fault-propagation or tri-shear fold, shortening can be deduced from local uplift through more complex analytical models, but solutions may be non-unique. Finally, for detachment folds, the upper layer geometry can be approximated by a simple geometric function like a triangle [Rockwell *et al.*, 1984] or a cosine [Oveisi *et al.*, in press], and the limb-tilting rate can be converted into a shortening rate assuming length and area conservation and wavelength reduction during shortening. For the cosine model, such a conversion will strongly depend on the location of the terrace along the fold limb.

4. INCISION AND DEFORMATION RECORDED BY QUATERNARY FLUVIAL AND MARINE TERRACES IN WESTERN FARS

4.1 Deformation of mid-Pleistocene Bakhtyari surfaces

4.1.1. Sedimentology and age of the Bakhtyari Formation

The Bakhtyari conglomerates represent the youngest lithostratigraphic unit of the Zagros sedimentary sequence. They fill the axial parts of most of the synclinal depression as a syn-orogenic molasse. In the study area, the Bakhtyari Formation consists of proximal, polymictic and coarse-grained conglomerates with subordinate cross-bedded sandstones. The conglomerates are locally cemented and strongly indurated by pedogenic calcrete carbonate. Within the region, the Bakhtyari Formation lies mostly unconformably on the underlying Agha Jari Formation or older formations (Mishan, Guri, Gachsaran and Asmari Formations).

Where we studied the deformation recorded by the Bakhtyari Formation in detail, the thickness of the unit reaches up to 60 m. Gravels in these deposits contain mostly fragments of Paleogene limestone and Neogene sandstone, but also clasts and pebbles of Mesozoic black dolomite. The latter lithology is only found in the upstream part of the Dalaki watershed; close to a diapir associated to the Karebas fault. This indicates that a paleo-Dalaki river, whose course probably had a similar regional geometry as today, i.e. an E-W draining direction, deposited most of these sediments.

The Bakhtyari conglomerates are not well dated because they contain no diagnostic fossils; the unit is generally considered to be Late Pliocene [James & Wynd 1965] or younger in age because it overlies the fossiliferous Agha Jari Formation of Late Miocene-Pliocene age. The Bakhtyari Formation is, however, considered as diachronous across the Zagros fold belt [James & Wynd 1965; Mina et al. 1967; Falcon 1974; Motiei 1993; Hessami et al., 2001]. In order to date the end of Bakhtyari deposition in the region southeast of Kazerun, several sandstone or limestone pebbles were sampled at the top of large Bakhtyari surfaces exposed along the Dalaki River (Figure V-5). The limestone pebbles, which measured ~20 to 30 cm in diameter and were located at the top of a wide and flat depression (Kuh e Pahn surface; Figure V-5, sample KAZ-7), display clear evidence for dissolution of several centimeters on their upper faces. The sandstone pebbles (several pebbles were crushed together to provide a sufficient amount of quartz) were sampled from an indurated calcrete at the flat top of an anticlinal form (Baladeh

surface; Figure V-5, sample KAZ-11) and also display significant erosion by dissolution as the initial round pebbles have been reduced to strongly oblate forms. Cosmogenic dating of such samples consequently provides only a minimum age for the end of Bakhtyari deposition in this area, as ages will be lowered by erosional loss. The two limestone pebbles on top of the Kuh e Pahn surface yield concordant apparent ^{36}Cl exposure ages of 640 ± 120 kyr (Table 2). In contrast, the sandstone pebbles give a younger ^{10}Be age of 325 ± 34 kyr (Table 1). Such a difference could, in principle, be ascribed to a different timing of the end of sedimentation between the Baladeh and Kuh e Pahn surfaces, but the similarity of their spectral response on Landsat images and of sediment thickness suggest that deposition of the Bakhtyari gravels in this large depositional basin ended roughly synchronously in the two areas. Given the above sample description and discussion on probable erosional losses, we suspect that the minimum age of Bakhtyari formation in that area is of the order of 600 kyr.

In order to better constrain the onset of Bakhtyari deposition, we also sampled an oriented block in a 30-cm-thick sandy/silty unit at the base of the Bakhtyari Formation in Baladeh for paleomagnetic analysis (Figure V-6e). We measured remanent magnetization of 6 cores with a spinner magnetometer JR6 (Agico ltd). Samples were stepwise demagnetized using an alternate magnetic field up to 100 mT and temperature up to 700°C. The main magnetization is carried by soft coercive minerals with maximum unblocking temperatures of ~600°C. Thermal demagnetization reveals a rather ill-defined component, consistent with the present-day magnetic dipole field (declination close to North, inclination of 55°). More importantly, this component indicates a normal polarity. In consequence, at least two potential scenarios can be considered: either rapid deposition of >50 m of sediments at the beginning of the Bruhnes normal chron, i.e. between 780 and ~600 kyr, or much slower sedimentation between the Gilsa/Jaramillo or Gauss normal chrons at ~1.7 and ~2.5 Myr, respectively, and ~600 kyr. An additional sample of calcareous conglomerate (KAZ-5) was taken within the Bk material at the level of a freshly cut cliff along the Rud-e Dalaki, in order to get a handle on pre-depositional erosion rates and potential inheritance. Its apparent exposure age is of the order of 3 kyr. Since we consider recent exposure negligible, the initial inherited age before Bakhtyari deposition must have been of the order of 13 kyr if deposition occurred 650 kyr ago, but would reach ≥100 kyr for deposition older than 1.5 Ma. Given that none of the pebbles sampled on different terraces in the region provide evidence for such strong inheritance, a deposition age ≥1.5 Myr seems less probable. In the absence of further constraints, we will therefore assume

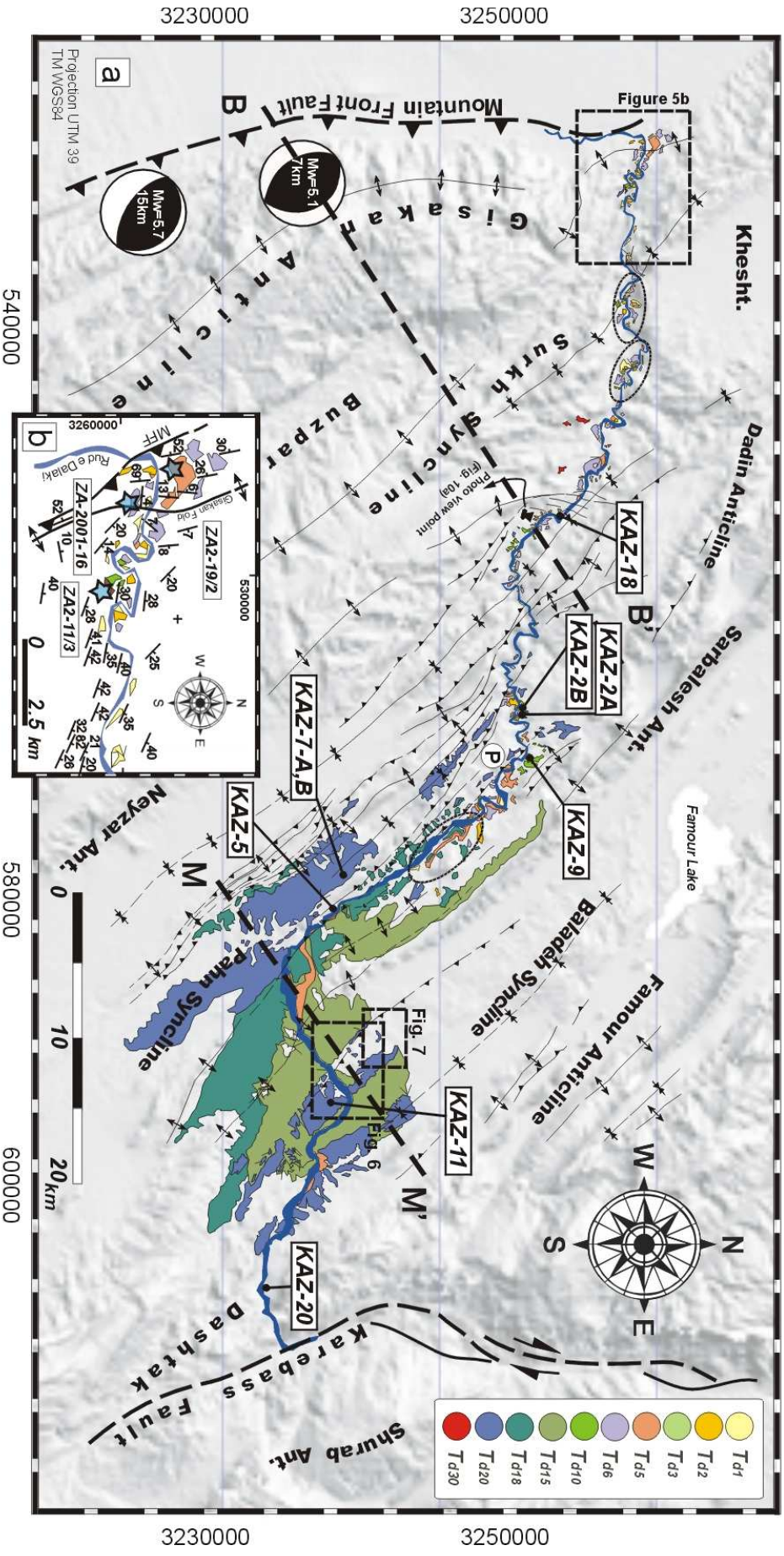

Figure V-5: (a) Geomorphological map of the fluvial terraces and Bakhtyari surface (T_{d20}) along the Dalaki valley, also showing sample locations. Locations of cross-sections B-B' and M-M' (Figures V-11 and 8, respectively) are indicated by dashed lines; P: upstream limit of significant incision as recorded by fluvial terraces (cf. Figure V-9). Inset (b) shows a detail of the valley where it crosses the MFF.

that the Bakhtyari conglomerates were deposited between 800 and ~600 kyr ago in the area SE of Kazerun.

4.1.2. Baladeh monocline

A case example of deformed Bakhtyari units can be observed across the Baladeh monocline in the northern part of our study area. The Baladeh monocline (Figures V-5, 6) involves Agha Jari and Mishan formations and constitutes the south-western flank of a wide syncline that has been reactivated above a décollement level in the Neogene gypsum and marls of the Gachsaran Formation. The Bakhtyari Formation displays a broad fold form across the Baladeh monocline, with steep frontal and back-limbs and a 2-km-wide flat top 80 m above the present-day river level, on which a thin layer of Bakhtyari uncomformably overlies a strath level beveled into the steeply dipping Neogene units (Figure V-6c). Growth strata on the back limb of the fold indicate active folding of the monocline during Bakhtyari conglomerate deposition. These growth strata preserve two axial surfaces with a cumulated dip change of 15° (Figure V-6d). Based upon structural and geometric arguments, the dip of strata in the back limb (~45-50° NE) should be parallel to a fault (zone) below the structure, which probably flattens on a shallow décollement level below the active Dalaki floodplain. The maximum vertical displacement of Bakhtyari conglomerates relative to the present-day river (~80 m) is encountered near the front of the structure (Figure V-6c). The flat ~2-km wide top of the Bakhtyari surface suggests continuous vertical displacement of the conglomerates, implying that the Baladeh monocline developed by a mechanism of distributed upward movement. The Bakhtyari layers are sub-vertical at the base of the front limb, or even slightly overturned (dipping up to 70-80° NE). Based upon the geometry of the monocline, we propose it developed as a kink-like fold structure that terminates laterally.

In order to constrain the horizontal shortening associated with the structure, we consider area conservation. From the bedding-dip variations within the Bakhtyari conglomerates, the décollement depth is estimated to reach 1.8 to 1.9 km. The thickness of the Bakhtyari unit preserved adjacent to the Baladeh monocline is at least 40 m. The kink-band geometry within surveyed growth strata on the back limb of the fold suggests a ratio of local fold growth to sedimentation rates [e.g., Suppe *et al.*, 1992] of ≤ 1 during deposition of the Bakhtyari units. Total uplift of the Baladeh structure since the onset of deposition of the basal Bakhtyari units is thus ~120 m, corresponding to ~150 m of shortening. Assuming an age of 0.5-0.8 Myr for the

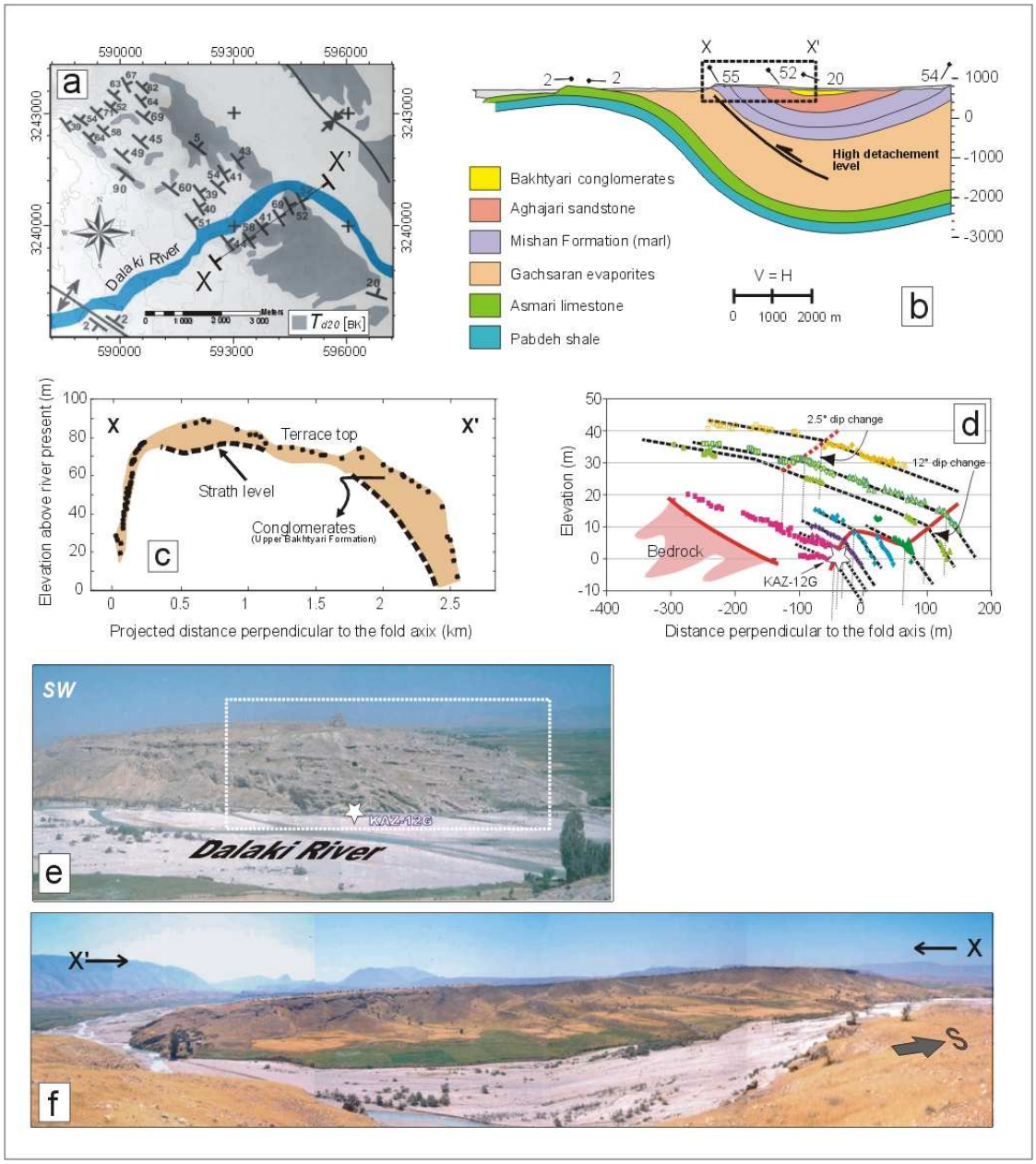

Figure V-6. (a) Geomorphological map and general topographic pattern of the Baladeh monocline (location on Fig. V-5); (b) Balanced cross-section; (c) Elevation of the T_{d20} terrace (Bakhtyari surface) projected onto profile X-X', perpendicular to the Baladeh monocline along the Dalaki River (location in a); (d) detail of growth strata in Bakhtyari conglomerate within back limb of the fold, mapped with a laser distance meter; note two clear axial planes. White circle correspond to the paleomagnetic sample site within a fine-grained unit; (e) Field photo of back limb of the fold along the right bank of the river, with location of growth strata mapped in (d); (f) Photo mosaic of the uplifted Bakhtyari surface along the left bank of the Dalaki River.

Bakhtyari Formation in the Baladeh / Kuh-e-Pahn region, as discussed previously, and roughly continuous deformation since, we estimate that the mean uplift (relative to surrounding areas) and shortening rates associated with the Baladeh monoclinal structure have been 0.15-0.24 mm/yr and 0.2-0.3 mm/yr respectively. Assuming deposition of the base of the Bakhtyari unit during the Brunhes period, the mean local sedimentation rate for the Bakhtyari formation was ≥0.15 mm/yr, and the shortening rate ≥0.2 mm/yr. In the absence of more precise dating of the Bakhtyari sedimentary units, it is not possible to determine if the shortening rate has been constant since inception of Bakhtyari deposition or if the structure was deforming faster 0.65 kyr ago than today.

North of the periclinal SE termination of the Baladeh monocline, a small river cuts through it, and has abandoned a well developed 20-m-thick fill terrace (Figure V-7). This Late Pleistocene terrace presents a 10-m-thick silty to sandy cover above a gravel deposit and a strath level a few meters above the modern river. This strath level cannot be followed but the surface of the alluvial cover is clearly folded, with an amplitude of 20-25 m. Unfortunately, insufficient organic material could be sampled for dating this level. Pedogenic arguments, like the absence of induration or recrystallisation, suggest, however, that this terrace tread is much younger than the nearby Bakthyari surface and that Baladeh monocline deformation has been an on-going process until recently.

4.1.3. General incision and deformation profile of the Bakhtyari surfaces

To the southwest of the Baladeh monocline, another syncline structure has been reactivated and has produced uplift of the Bakhtyari surfaces (Pahn syncline on Figure V-5). The initial geometry of the Bakhtyari Formation is less intuitive here than across Baladeh monocline: did the paleo-Dalaki drain the internal basin between the Neyzar and Dashtak anticlines (Figure V-5) or was deposition in the southern part of this basin controlled by northward draining tributaries? In any case, we suppose that the Dalaki River and its tributaries deposited sediments in a large and relatively flat basin with gradients comparable to the ~1% of the present-day Dalaki River in the Baladeh region. We thus estimate maximum uplift to range between 150 m and 250m in the Kuh e Pahn region (Figure V-8), decreasing to the southeast. Assuming a minimum age of 0.6 Ma for the end of Bakhtyari deposition in the whole Baladeh /

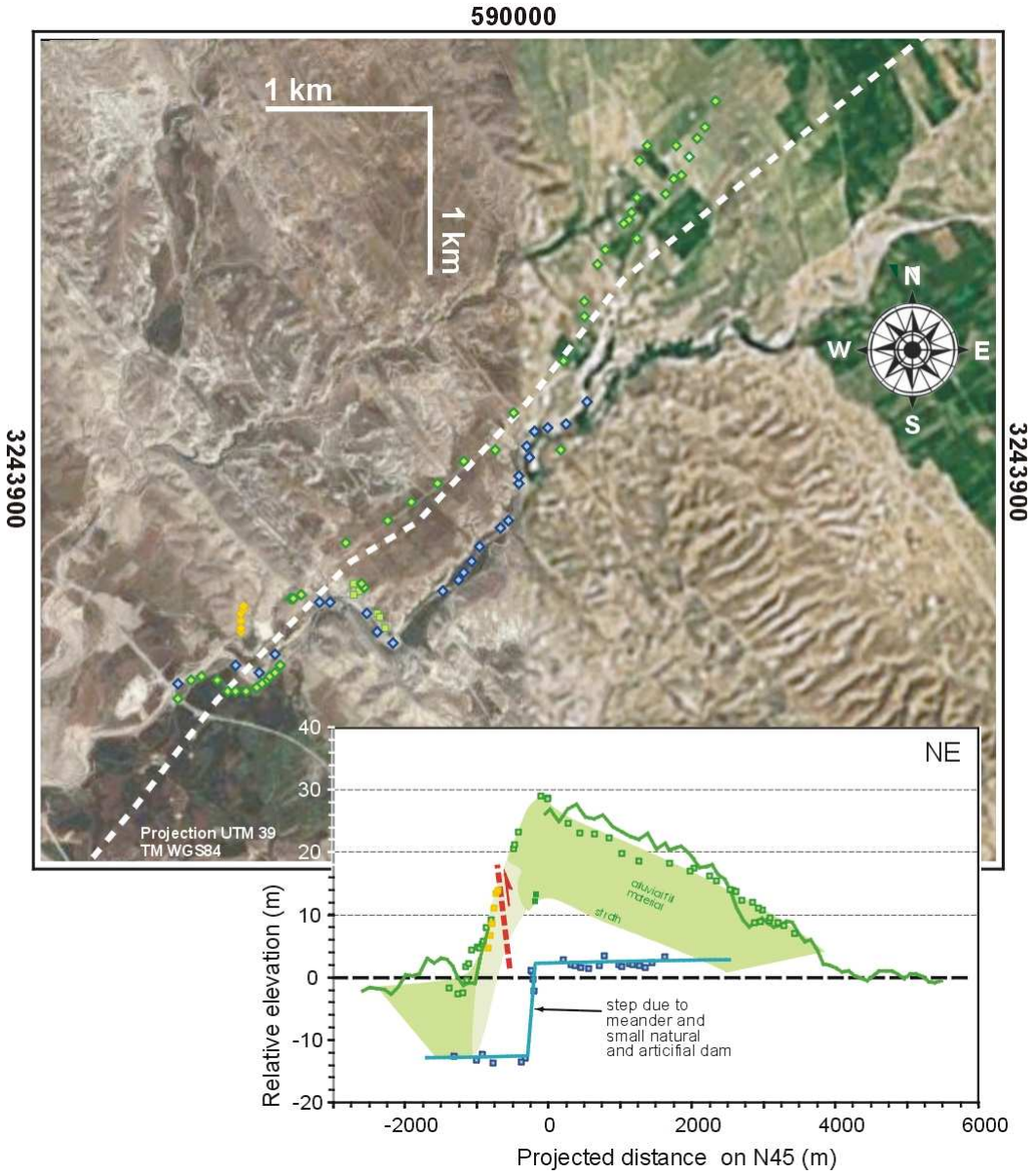

Figure V-7. (a) Satellite image of Baladeh monocline (see location on Fig. V-5) crossed by a small river that abandoned a large Late-Pleistocene fill terrace. This terrace (green squares) and present river (blue squares) were surveyed with a total station. (b) Profile of the elevation of the fill terrace and modern river relative to the initial surface of the terrace, assuming that the upper and lower parts of the terrace (on both sides of the monocline) have not been deformed. Note that this mean gradient is roughly equal to present river gradient. Continuous green line is topography.

Kuh e Phan internal basin yields a maximum local uplift rate of ~0.4 mm/yr. Assuming a shallow detachment level close to 2 km within the Gachsaran Formation, the shortening rate absorbed by the Kuh e Pahn structure is ≤1 mm/yr, and this rate decreases southeastward.

The NW extension of these Bakhtyari deposits crosses the Dalaki valley ≤100 m above the present channel in front of the Sarbalesh anticline. Consequently, the average Late Quaternary incision of the Dalaki River is limited to ≤0.2 mm/yr in that area. Thus, as observed in Baladeh or Kuh e Pahn, the synclinal structures are re-activated in uplift but the anticlines, in contrast, do not display uplift and are affected by active sedimentation. This observation implies that the Sarbaleh anticline, which has been interpreted as a "horsetail" termination of a segment of the Kazerun fault [e.g. Authemayou *et al.*, 2006] is currently inactive, implying either that this segment of the Kazerun fault is no longer active or that the Kazerun segment branches onto another structure. More generally, the entire Kuh-e-Neyzar / Dashtak region is affected by sedimentation; we thus consider that uplift is very limited in this region and that the different structures do not absorb major shortening. Active deformation takes place either further NE on more internal folds or SW on the most frontal structures.

The role of pre-existing structures (such as synclines) seems to be a controlling factor in the structural evolution of the Neogene to Quaternary cover, where the Gachsaran Formation is present as a detachment level and decouples deformation within Neogene-Quaternary sediments from lower portions of the rock column. Although it is not clear from available structural data how the shortening observed at the surface across the Baladeh and Kuh e Pahn synclines is transferred from the deeper part of the sedimentary pile toward the surface, we suggest that these synclines cores have been superficially reactivated over decoupling level(s) within the Gachsaran Formation (Figure V-6), and extruded upward during the late-stage evolution of an orogenic prism [Lavé *et al.*, in prep]. Thus, similar to the Izeh zone to the NW of our study area [Sherkati and Letouzey, 2004; Sherkati *et al.*, 2006], Neogene gypsum, salt and marls of the Gachsaran Formation appear to represent an important décollement level that controls the distribution of active surface deformation and the development of disharmonic short-wavelength folds in the study area.

4.2. Late Pleistocene fluvial terraces along the Dalaki River

4.2.1. Structural setting and general terrace description

Between its source, west of Shiraz, and its delta on the Persian Gulf, the Dalaki River (Rud e Dalaki) intersects several possibly active structures, including the MFF (e.g., Figures V-1 and 5). Along the Dalaki River, up to ten levels of Quaternary terraces can be distinguished that extend

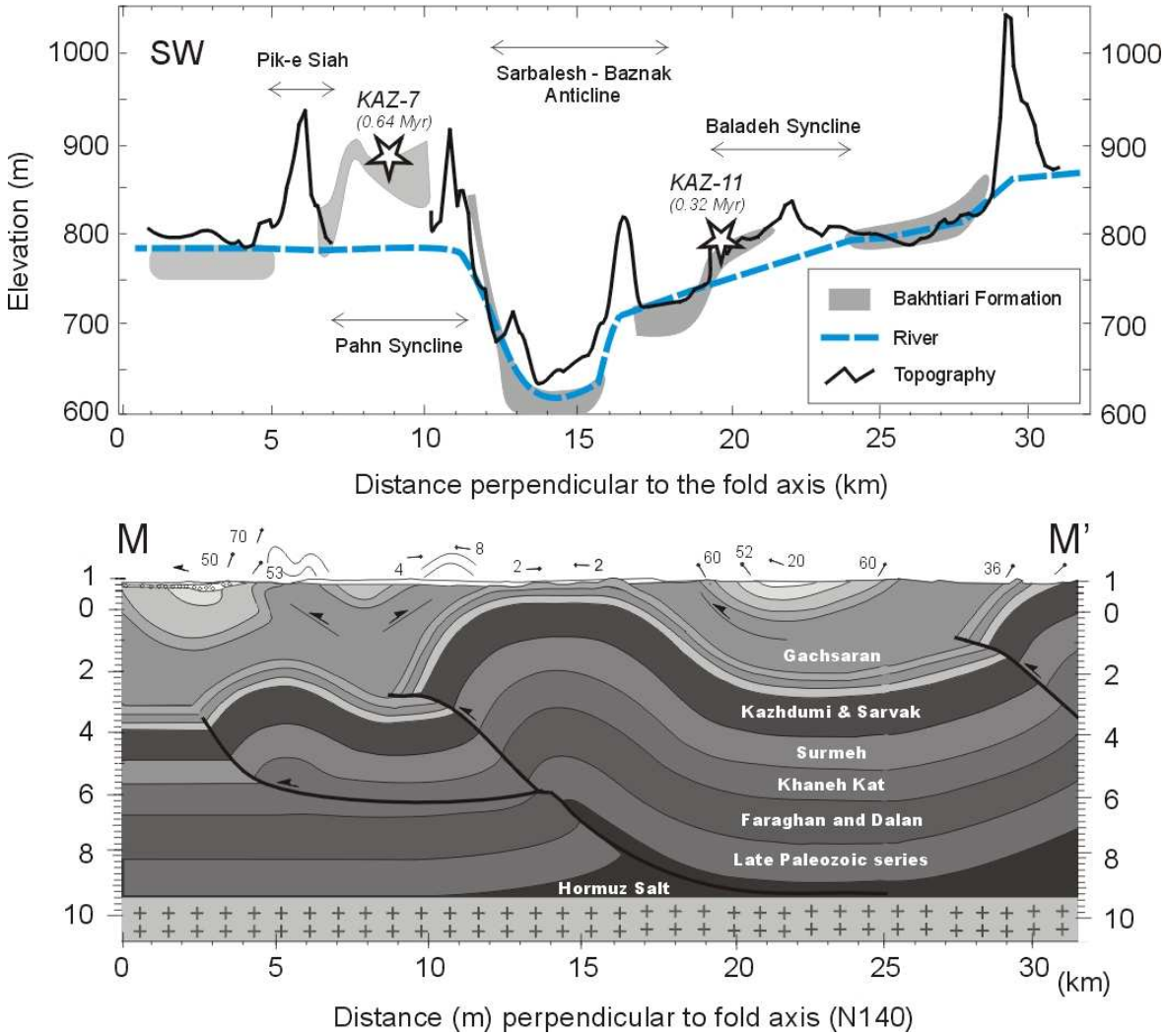

Figure V-8: Simplified topography, Dalaki River level and elevation of Bakhtyari Formation in the Baladeh / Kuh e Pahn Region, indicating active uplift of synclines with respect to anticlines. Lower panel shows balanced cross-section M-M' (location indicated in Fig. V-5).

~100 km upstream from the MFF (Figures V-5 and 9). Except for the uppermost and widespread Bakhtyari deposits, most of the levels are strath terraces with a relatively thin veneer of gravels. Here, we concentrate on four of the surveyed levels: T_{d2}, T_{d5}, T_{d6} and T_{d10}. The most elevated terrace level, T_{d10}, can reach up to ~160 m above the present river. The T_{d10} terrace consists of up to 20-m thick gravel, sand and clay deposits. Gravels in these deposits contain fragments of Paleogene limestone, Neogene sandstone and occasional dark cherts, derived from salt-plugs that occur in the Dalaki catchment further east. T_{d5} and T_{d6} terraces are encountered on both sides of the channel. The deposits of T_{d5} and T_{d6} terraces consist mainly of 3 to 5-m thick alluvial gravels and pebbles of Paleogene and Neogene sandy limestone and

limestone fragments. T_{d2} is the lowest preserved prominent level; this terrace is generally well exposed and is encountered on both sides of the river.

The relative elevation profile of these terraces above the present channel (Figure V-9) indicates significant incision up to a distance of 70 km upstream of the MFF along the river, which

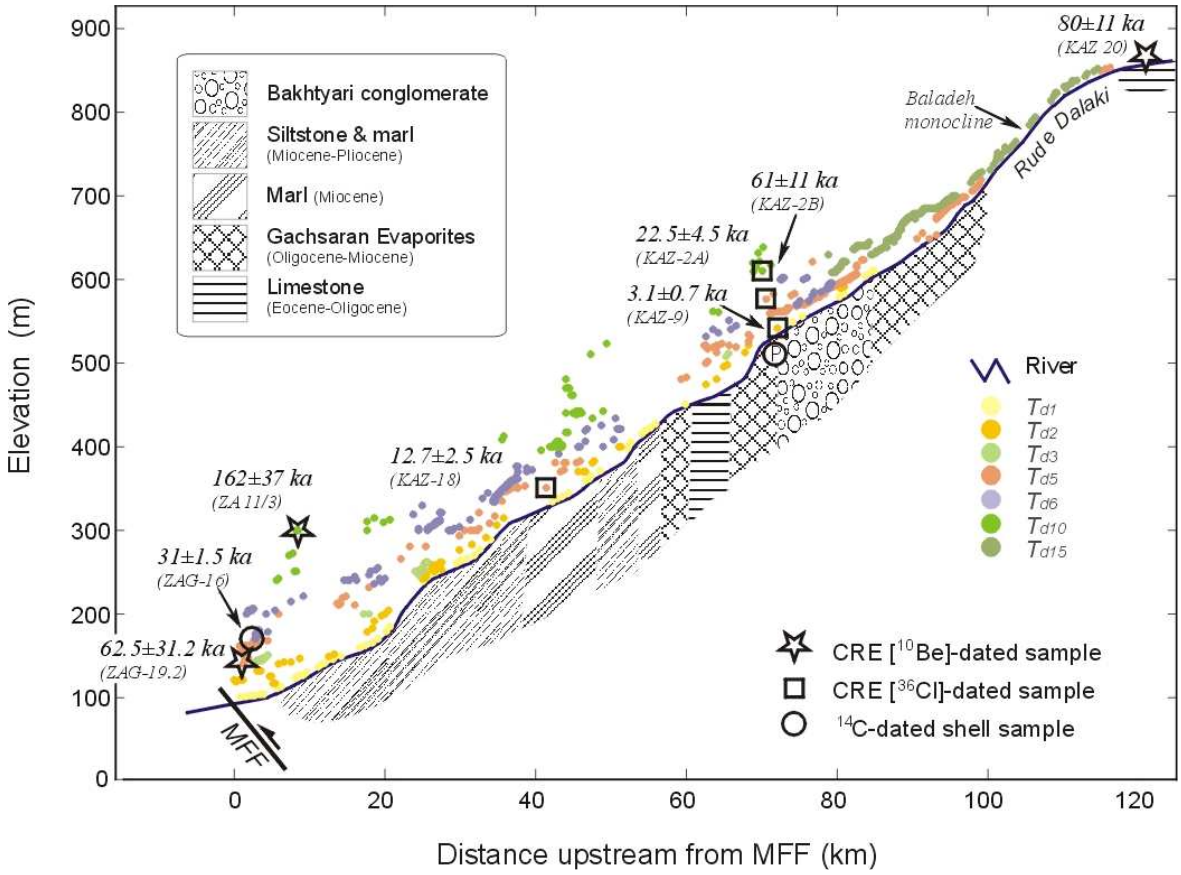

Figure V-9: Longitudinal profile of the Dalaki River and fluvial strath surfaces (terraces are projected onto the valley axis of the river). Upstream of the point P, the river drains parallel to the structures and the relative elevation of terraces drops to close to zero.

corresponds to a distance orthogonal to the fold strike of ~35 km, and increasing in amplitude toward the MFF. Further upstream, the river drains parallel to the structures and the relative elevation of the terraces drops to close to zero, indicating more subdued incision further east. The river is mostly characterized by a wide braided channel draining a large open valley in this region, and extensive Bakhtyari to recent deposits cover both synclines and anticlines.

Upstream of the Baladeh area, the Dalaki River drains a region affected by the Karebas fault (Figure V-5) and associated diapirism. Such a setting, in particular the presence of a salt diapir, makes this area inadequate to unravel regional uplift rates and fold activity from terrace

incision. Between this upstream area and the Baladeh region, the river crosses the Dashtak anticline, incising into Asmari limestones. There, a particularly well preserved lateral figure of fluvial abrasion occurs ~20 m above the present channel (Figure V-10b). A limestone sample (KAZ-20) was extracted from this potholed surface and dated by cosmogenic ^{36}Cl. The age of this surface, 80 ± 11 kyr (Table 2), constrains the Late Pleistocene incision rate to 0.25 ± 0.04 mm/yr across this anticline. This low rate confirms that tectonic activity in Baladeh region and just north of it is subdued.

4.2.2. Dalaki River terraces in the hangingwall of the MFF

West of the Baladeh-Kuh e Pahn region, the Dalaki River valley narrows and is entrenched several hundred meters into mostly Mishan and Agha Jari marls, silts and sandstones. Locally, where the river crosses more indurated layers of limestone or sandstone, it displays short and narrow gorges. At crossing the MFF, the Dalaki adopts a wider course, the fault marking a clear change in relief between a rugged topography in the hanging wall and a flat flood plain in the footwall (Figure V-12).

Where the Dalaki crosses it, the MFF is oriented ~N155°E, in marked contrast with the fold axes and the N125°E trend of the folds and faults further southeast (cf Figure V-1). This fault segment is associated with a complex fault-propagation fold, the Gisakan fold. The Gisakan fold is an active high relief structure that has been created by thrusting over the oblique footwall ramp of the MFF (Figure V-11). Movement along the MFF has brought Cretaceous limestone to the surface in the hangingwall, implying ~6000 m of vertical displacement (Figures V-3 and 11) in the sedimentary cover, whereas vertical offset in the basement is less than 2 km (Figure V-11). The balanced cross-section indicates that basement imbrication (i.e., thick-skinned deformation) is required to fill a large void between folded strata and the basement in the hangingwall. However, potential out-of-plane movements, uncertainties on the initial thickness of the basal Hormuz Salt or on the existence of a duplex make this solution (Figure V-11) poorly constrained.

A dip range of 36-42° is suggested for the MFF ramp at depth, based upon available geometrical and structural arguments. Reported earthquake nodal planes (Harvard CMT solutions) indicate almost pure thrust motion and their trends of N25°-45°W are parallel to the regional orientation of the fault zone (Figures V-1 and 5). These two earthquakes of 1990.12.16 (M_w=5.7) and 1994.03.29 (M_w=5.1) occurred at depths of 15 and 7 km, respectively

[Talebian and Jackson, 2004]. The M_w=5.1 seismic event would therefore be located above the basal detachment level, within the lower part of the Phanerozoic cover, and would reflect seismogenic deformation in the lower part of the sedimentary cover, at least close to the MFF. Its projection at the surface is located close to the topographic front of the Gisakan fold. The focal mechanism solution of the M_w=5.1 event presents a nodal plane dipping at 40° NE with a strike N334°, compatible with the orientation of the MFF and its structurally inferred dip.

Just upstream of the MFF, the Dalaki has abandoned numerous fluvial terraces that occur up to 160 m above the present-day channel. At the surface trace of the MFF, a 10 to 30-m high tectonic scarp bounds the lowermost T_{d1} and T_{d2} terraces, with locally verticalized alluvial terrace material. Along this scarp, we observed a surface rupture with >1 m of offset (Figure V-12b). Bachmanov *et al.* [2004] also describe surface ruptures in this area. The presence of surface ruptures indicates that seismic rupture can propagate along the MFF up to the surface and therefore that in certain conditions even the upper part of the Zagros sedimentary cover can be seismogenic in this area. This surface faulting, combined with the deformation pattern of the terraces that displays uniform tilting of the hanging wall of the MFF, demonstrates that Gisakan fold deformation is intimately associated to the MFF fault.

Further upstream, most of the fluvial terraces are unpaired but sufficiently continuous to allow unambiguous correlation up to ~5 km east of the MFF (Figures V-5b, 10). In this area immediately upstream of the MFF, terraces display parallel treads that suggest relatively

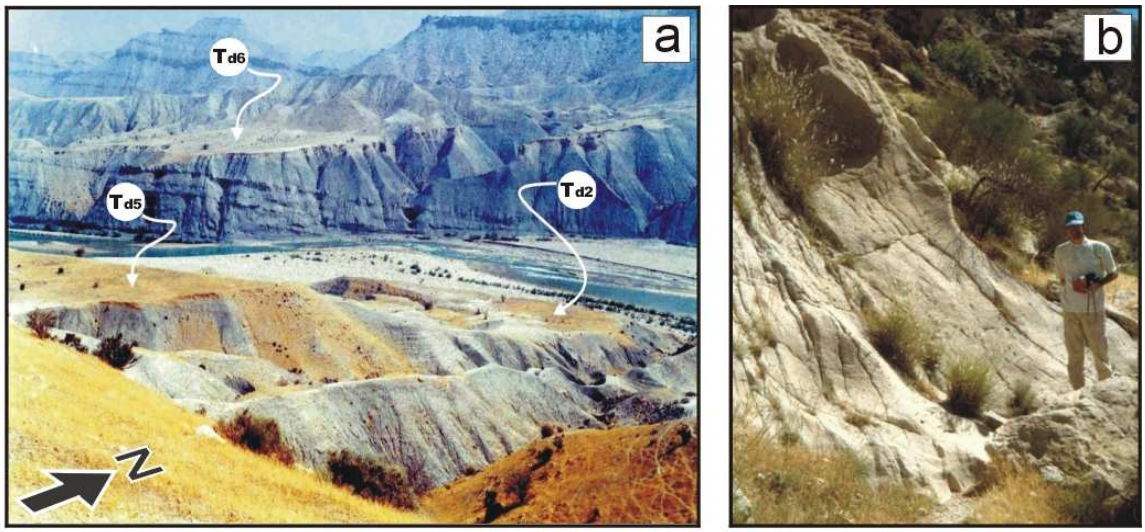

Figure V-10: (a) Northeastward view of three strath terraces along the Dalaki River, 45 km upstream from the MFF (location indicated by a white arrow on Fig. V-5). (b) Lateral fluvial abrasion figures sculpted in Asmari limestone along the right bank of the upper Dalaki River (KAZ-20 sampling site, cf. Fig. V-5 for location).

uniform uplift along the frontal hanging wall of the MFF. We have attempted to date three different terrace levels in this region. Small gastropods were found in silty material deposited on top of the fluvial gravels of terrace T_{d6} close to the MFF and one sample (ZA-2001-16) was ^{14}C dated by accelerator mass spectrometry at the Poznàn radiocarbon laboratory, (Poland). This sample yielded a raw ^{14}C age of 26940 ± 190 yr, which corresponds to a calibrated age of 31 ± 1.5 kyr BP using the NotCal04 calibration curve [*van der Plicht et al.*, 2004]. As the T_{d6} strath lies 70 m above the modern channel at the sampling site, the corresponding bedrock incision rate would be 2.3 ± 0.1 mm/yr. A depth profile was also sampled for cosmogenic dating on the prominent terrace T_{d5} on the right bank of the Dalaki River 55 m above the present-day river bed. Unfortunately, surface samples did not yield sufficient quartz material and two samples at depth were contaminated by boron and yielded unrealistic ages. Only one sample (ZAG-19/2), from a depth of 170 cm yielded an apparently reliable (if imprecise) apparent depth-corrected age of 63 ± 31 kyr (Table 1). If we consider that source-area erosion rates can be as low as 0.1 mm/yr (based on erosion of Bakhtyari surfaces in the Baladeh / Kuh e Pahn area; cf. section 4.1.1), the potential contribution of inherited ^{10}Be can be significant for this sample. The single ^{10}Be age thus only provides a maximum age for the terrace T_{d5}. The corresponding minimum incision rate is $0.9\ ^{+0.8}/_{-0.3}$ mm/yr, but could be much larger if an inherited component is taken into account. A sandstone pebble sampled on the highest terrace of the area, T_{d10}, however, yields a ^{10}Be age of 162 ± 37 kyr, implying a similar incision rate of 1.0 ± 0.2 mm/yr. In contrast to the previous estimate, this age is relatively insensitive to a potential heritage problem, as its ^{10}Be concentration is about 25 times higher. Given the above-mentioned problems on our first set of ^{10}Be samples, as well as a potential bias in the ^{14}C ages due to shell recrystallisation, it is not possible for the moment to ascertain whether the discrepancy of incision rates between T_{d6} and T_{d10} records a recent increase in incision rates, or whether it is only an artefact.

We thus estimate mean Late Pleistocene incision rates of the Dalaki River on the hangingwall of the MFF to range between 1 and 2.3 mm/yr. Taking into account a regional sedimentation rate downstream of the MFF of 0.2 mm/yr, by analogy with sedimentation rates at the frontal Zagros in Lurestan [Homke *et al.*, 2004], an average structural uplift rate [Lavé and Avouac, 2000] of 1.2 to 2.5 mm/yr is estimated for the MFF. The heritage of the early stage of the fold history, the presence of incompetent and deformable units in the sedimenteray cover, as well as the presence of secondary folds in the Gisakan structure prevent an accurate reconstruction of the fold and fault geometry at depth. However, from the cross section and available focal

mechanisms, we estimate the MFF ramp dip to be 39 ± 3°. Assuming rigid translation above this ramp, compatible with the uniform and parallel uplift of the different terraces close to the MFF, the structural uplift rate would correspond to a slip rate at depth on the ramp of 1.3 to 3.4 mm/yr.

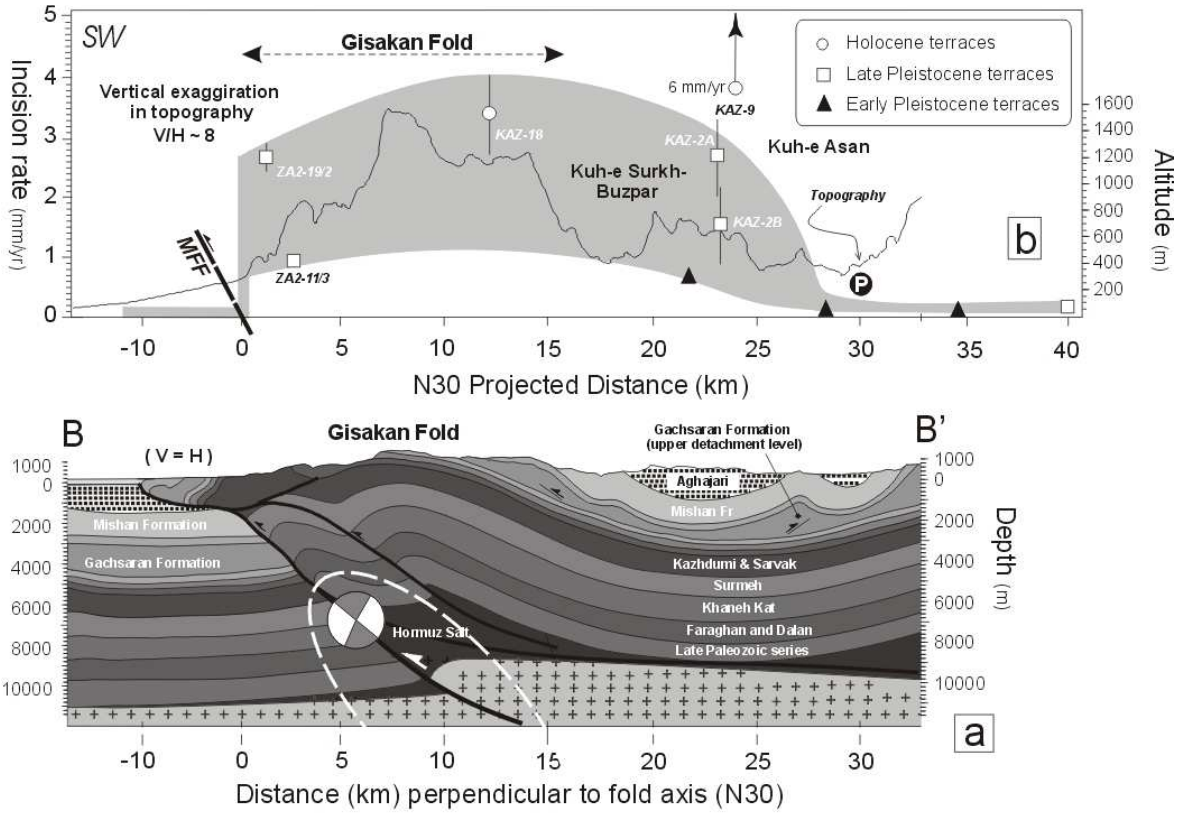

Figure V-11: (a) Balanced structural cross-section B-B' across the Gisakan Fold and MFF (location on Fig. V-5). Focal mechanism of 1994.3.20 M_w=5.1 event [Talebian and Jackson, 2004] is also plotted onto section. (b) Topography and inferred incision rates projected onto the cross-section. Note that region of high incision rates extends further from MFF than the frontal Gisakan fold.

4.2.3. Incision and fold model

To understand the transition from the downstream Gisakan section, where incision rates are >1 mm/yr, and an upstream section with low incision (rates ≤0.2 mm/yr) or sedimentation, the intermediate reach of the Dalaki River east of the Surkh syncline (Figure V-5) appears as a crucial area. The river is characterized by a single meandering channel along its entire downstream section, west of the Sarbalesh anticline. In several localities, abandoned meanders attest to the dynamic behavior of the meanders and to an evolving channel geometry (Figure V-5). Even though, in the long term, meander shortcuts are compensated by lateral migration of meanders, this observation suggests that the Dalaki River course is not a stable feature and that

the equivalence between incision and uplift is not always valid in detail [see discussion in Lavé and Avouac, 2000].

When we consider the river morphology, the transition between wide and entrenched valleys is located northeast of the Kuh e Pahn syncline where the river incises into a small patch of Asmari limestone (Point "P" indicated on Figure V-5). This transition in valley geometry coincides with a short and steep channel segment, which is clearly associated with the resistant limestone lithology in this reach.

On the other hand, the southern extension of the Bakthyari deposits, indicative of the transition to high long term incision rates, is located 10 km downstream of this knickpoint. In order to characterize the recent evolution of this area, we collected four samples from low and intermediate terrace levels for ^{36}Cl dating. As argued before, the Bakhtyari Formation suggests long-term (Pleistocene) incision rates ≤0.2 mm/yr in this reach. Two samples from a 60-m high fluvial terrace strath covered by 5 m of alluvium and correlated to the T_{d6} level (KAZ-2A and KAZ-2B; Figures V-5 and 9), provide (discordant) ^{36}Cl exposure ages of 22.5 ± 4.5 and 61 ± 11 kyr respectively, suggesting Late Pleistocene incision rates ranging between 1 and 3 mm/yr. A single sample (KAZ-18) from a terrace level ~40 m above the modern channel and correlated to the T_{d5} level, ~20 km downstream of the knickpoint (Figures V-5 and 9), yields a exposure age of 12.5 ± 2.5 kyr, implying Holocene incision rates of 3.2 ± 0.7 mm/yr in this area. Finally, a recent strath carved into cemented Bakhtyari units, ~20 m above the present-day channel, yielded an exposure age of 3.1 ± 0.7 kyr (sample KAZ-9), indicating Late Holocene incision rates as high as ~6 mm/yr.

These variable incision rates on different timescales illustrate the difficulties to interpret incision in terms of uplift, in particular for the most recent terrace levels. At least two scenarios can be envisioned: recent knickpoint retreat through the small gorge carved into the Bakhtyari Formation, or a recent increase in incision rates due to climatic fluctuations [e.g., Hanckock and Anderson, 2002]. In any case, the oldest geomorphic marker provides the most robust estimate for tectonic uplift when deriving it from incision values, because geomorphic or climatic fluctuations will be smoothed on the long term. As argued previously, the Bakhtyari Formation constrains the zone of high uplift to be further west than the Kuh-e-Pahn syncline, i.e. it affects an ~35 km-wide zone in the hanging wall of the MFF. Importantly, the zone of high incision rates is not restricted to the frontal Gisakan anticline but extends further northeast and encompasses its northeastern flank (Kuh e Buzpar) as well as the Surkh syncline (Figure

V-11). At least three different inferences can be drawn from this observation: the broad incision pattern may reflect a broad uplift pattern associated with thrust slip motion on the MFF rooting into the basement; the broad incision pattern may reflect broad uplift in association with the interference of two thin-skinned structures, the Gisakan and Neyzar anticlines; or the broad incision reflects uplift restricted to the Gisakan fold, as expected from thin-skinned tectonics, combined with recent incision upstream in response to climatic or geomorphic forcing. We will come back to this question in the discussion section.

4.3. Late Pleistocene fluvial terraces and river profile along the Mand River

4.3.1. Description of the fill and strath terraces along the Mand River

The Mand River (Rud e Mand) course is strongly affected by tectonics and fold structures. In its upper reach, the Mand follows a NW-SE course parallel to the major structures; it then adopts a sinuous roughly NS course between anticlinal noses in the Qir area (Figure V-13). The river cuts across anticlines both N and S of Qir, where it has carved narrow gorges into the resistant Asmari limestone units. Upon crossing the Surmeh fault, ~40 km south of Qir, the river starts draining ESE-WNW and follows a synclinal axis between the Shamshu and Halikan anticlines. The river long profile displays a major convex knickpoint about halfway along this

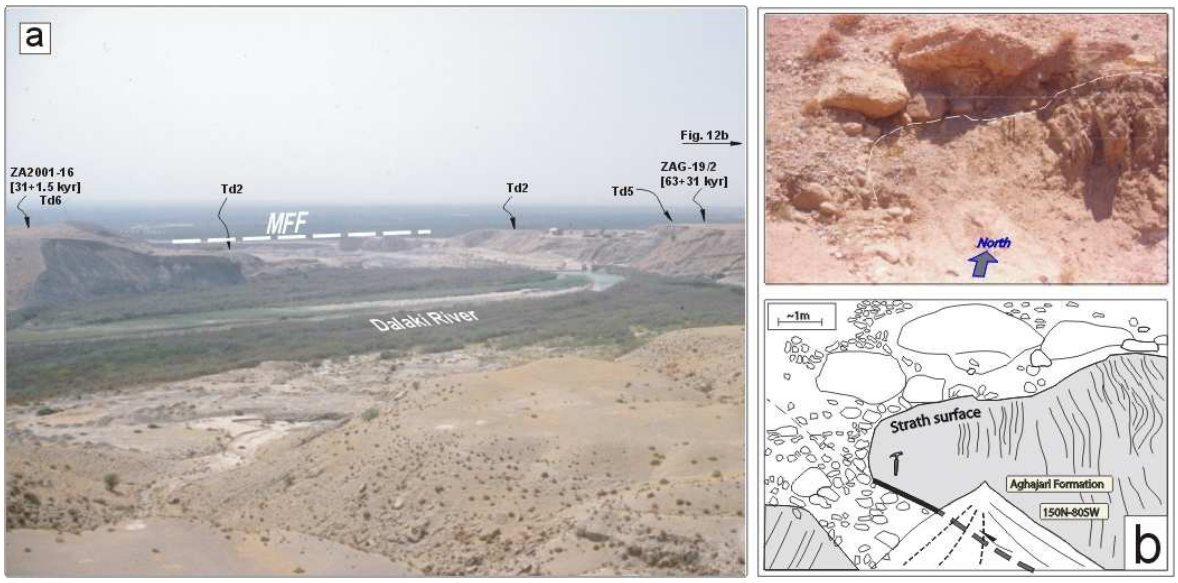

Figure V-12: a) View of Dalaki River where it crosses the MFF and frontal terrace system (see location on Fig. V-5); b) Field photo and interpretational line drawing of surface rupture associated with the MFF.

reach, where the river gradient steepens to about 4.3 m/km (K1 on Figures V-13 and 14). Around 25 km downstream of this knickpoint, the river cuts across the axial culmination of the Kuh e Halikan anticline; this area is characterized by the preservation of elevated strath terraces mostly in the core and fore-limb of the anticline (Figures V-14 and 15). Both the steepening of the river profile relative to adjacent areas and the high elevations of the fluvial terraces suggest that this area is experiencing more rapid bedrock uplift rates than regions upstream. Downstream of this reach the river turns westward again up to the MFF. This lower reach is again characterized by extensive fill terraces; some of these, in particular downstream of the confluence with the Shur River, preserve straths up to 40 m above the modern river bed, suggesting long-term incision. The Mand River exits its incised valley east of the Namak anticline (point K3 on Figure V-13) and drains a wide depositional plain before reaching the Persian Gulf, where it has built a large submarine fan. In its lowermost reach, the Mand River has been deflected northward and southward by the lateral propagation of the Kuh e Namak and Mand anticlines respectively.

Between the points K3 and K1, terrace remnants can be followed nearly continuously (Figures V-13 and 14). Five incised strath terraces (T_{m1}-T_{m5}), have been surveyed, ranging in elevation from 5 to 110 m above the modern river channel:

T_{m1} and T_{m2} are the youngest and most widely encountered terrace levels, which are characterized by prominent strath surfaces on both sides of the river. These terrace levels generally show >5 m of alluvial deposits, composed of gravels, cobbles and fine sand in a matrix of silty sand. T_{m1} and T_{m2} straths rise to up to ~20 and ~28 m above the present channel, respectively.

T_{m3} is a well-exposed strath level that is capped by ~10 m of gravels, cobbles and gritstone, the largest clasts reaching ~50 cm. A particulary large remnant of T_{m3}, measuring ~16 km^2, is encountered to the south of the Halikan anticline, where the river leaves the core of the fold, ~10 m above the present river (Figures V-13 and 14). In the core of the Halikan anticline, T_{m3} straths reach up to ~68 m above the stream channel, but their relative elevation drops toward the north, and the T_{m3} terrace almost merges with the modern floodplain at the knickpoint K1. The terrace level can be surveyed up to ~30 km upstream from the core of the Halikan anticline; further upstream, preserved terrace remnants are too discontinuous and sparse to permit confident correlations.

T_{m4} is the most extensively preserved and well exposed terrace level. In general, this level is capped by ~15 m of gravels with average clast diameter ~5-6 cm, cobbles and gritstone, the

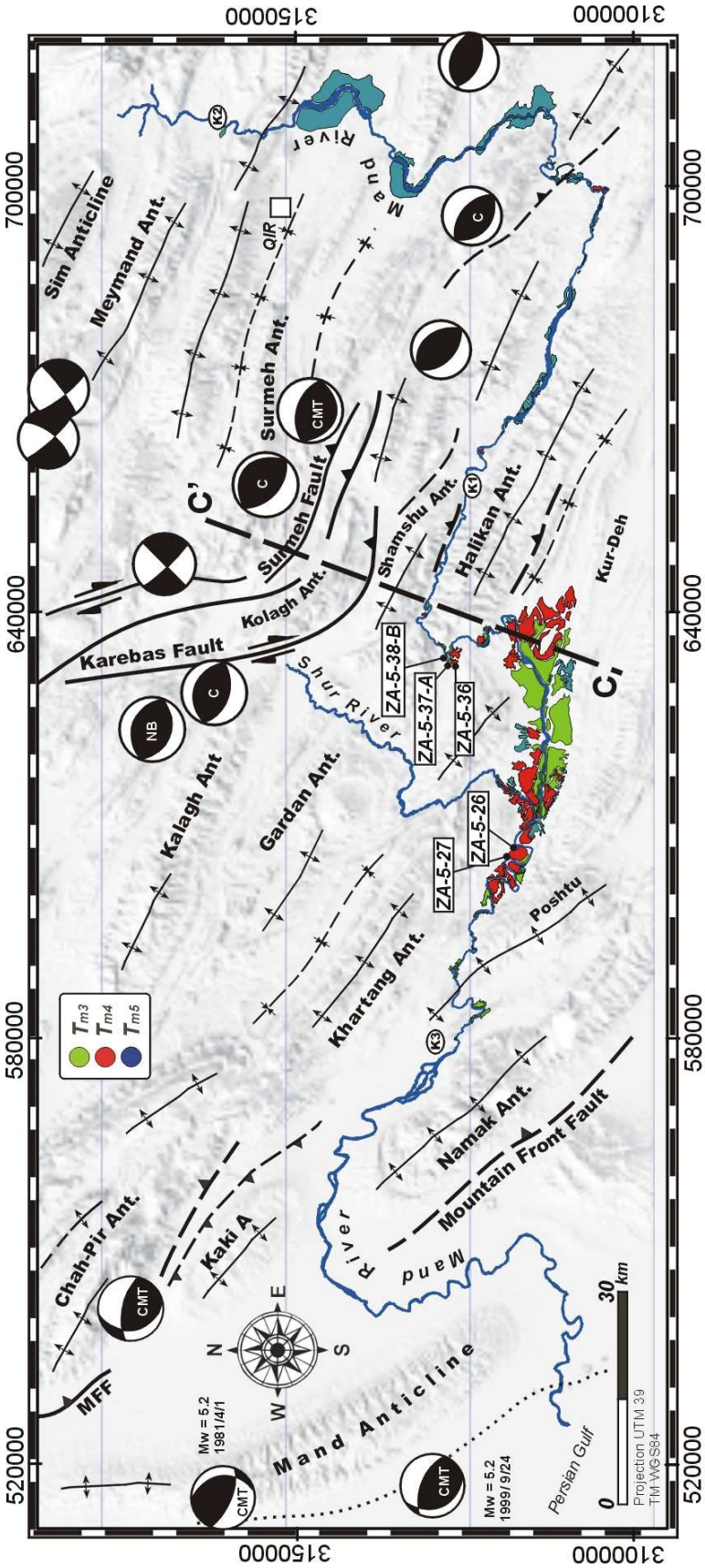

Fig. V-13. Geomorphological map of the fluvial terraces along the Mand valley, also showing sample locations and available focal mechanism solutions (coding of sources as for Figure V-1). Location of cross-section C-C' (Figure V-15) is indicated by dashed line; K1, K2 and K3 indicate locations of prominent knickpoints in the river long profile.

largest clasts reaching ~60 cm. Particulary wide (~4 km) and well-preserved remnants are observed between the front of the Halikan anticline and the major convex knickpoint K1 (Figure V-13). T_{m4} lies up to ~110 m above the present river channel at the core of the Halikan anticline.

Finally, T_{m5}, which is the highest of the terraces in the study area, exists as isolated remnants, with maximum widths of a few tens of meters along the east-west stretches of the Mand River. The thickness of the terrace deposits reaches up to 20 m, however it is occasionally difficult to constrain where no clear contact can be observed between the base of the terrace deposits and the top of the underlying unit. Downstream of the Halikan fold, the T_{m5} strath lies up to ~45 m above the present river level. A single but well-preserved T_{m5} remnant is encountered in the core of the fold, where its strath lies ~140 m above the modern channel.

Around Qir, the amplitude of bedrock incision appears limited; the Mand River has reincised mostly fill terrace material. The only exception is found where the river cuts the Eastern (eastward-plunging) part of the Meymand and Sim anticlines: river incision into the bedrock beneath fill terraces appears to increase upstream, suggesting 20-30 m of bedrock incision in this region, and corresponds to a second abrupt increase in river gradient (K2 on Figures V-13 and 14).

4.3.2. River and terrace profiles and basement fault activity

The terrace profiles suggest a major zone of incision and uplift across the Kuh e Halikan anticline, and possibly a secondary zone across the junction between the Kuh e Khartang and Poshtu anticlines, east of the MFF (Figures V-14 and 15). The modern long profile of the Mand River is consistent with such a pattern of recent deformation. Here, we use the stream gradient index [SI; Hack, 1973] as a rough proxy for unit stream power by accounting for discharge downstream increase. Although conceptually more advanced indices of stream power or shear stress have been developed [e.g., Kirby and Whipple, 2001; Lavé and Avouac, 2001], this first-order approach suffices for the qualitative analysis we perform here.

The SI value varies significantly along the Mand River (Figure V-15): it is low along the upper reaches of the river, between Qir and the major knickpoint K1, increases approximately fourfold across the northern limb of the Halikan fold, shows intermediate values further downstream with a slight increase across the junction between the Kuh e Khartang and Poshtu

anticlines, and finally a severe drop at point K3 where the river enters its wide depositional floodplain. An increase in SI value is expected to reflect an increasing degree of stream power expenditure to keep pace with larger uplift rate for a given lithology [e.g., Hack 1973]: high SI values provide in that sense a first-order indication of areas affected by high uplift rate, or alternatively resistant lithologies.

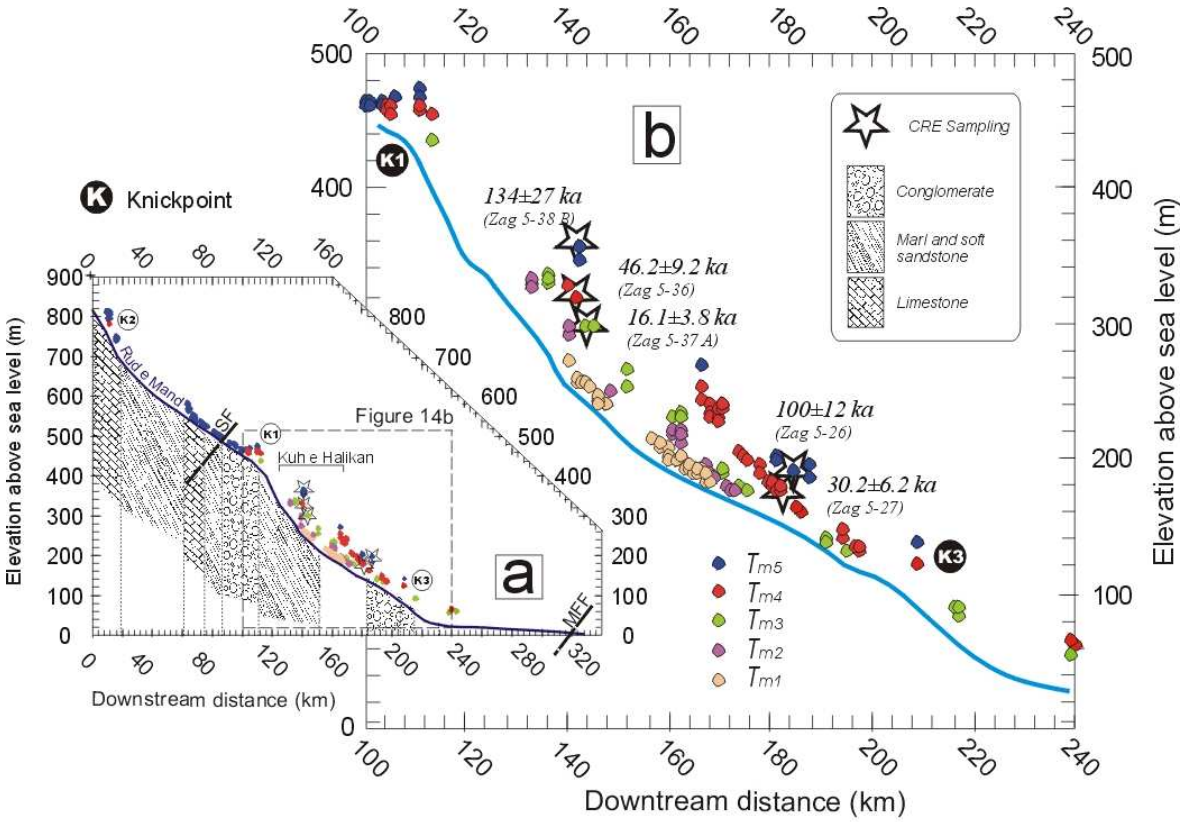

Figure V-14. (a) Longitudinal profile of the Mand River and fluvial strath surfaces (terraces are projected onto the valley axis of the river). Locations of presumed active faults and prominent knickpoints are indicated. (b) Detail of central reach of the Mand River, where it crosses the Halikan anticline (see text for discussion).

The concordant secondary peak observed in relative terrace elevation and SI value across the junction between the Kuh e Khartang and Poshtu anticlines could be related to the southeast-ward continuation of the MFF. In this area, the trace of the MFF is not clear, in particular it is unknown how the eastern branch, which reaches the surface east of Kaki anticline (Figures V-3 and 13), connects at depth with the western branch that continues southward in front of the Kuh e Namak anticline (Figure V-13). So far, no transfer fault or oblique ramp has been located between these two structures, and more importantly the geometry and continuity of the MFF trace within the basement remains undefined. There are no geomorphic indications for tectonic

activity on a basement fault located between the Namak and Kaki anticlines. Our terrace data and the long profile of the Mand River would be more consistent with the continuation of an active subsurface trace of the MFF further east, between the Khartang and Poshtu anticlines, but shortening rates would be relatively minor on this trace. Likewise, the absence of elevated strath terraces, as well as the continuous river gradient across the Surmeh fault trace (or the surface expression of this inferred blind thrust fault located at depth), suggest that this basement fault is currently inactive. In summary, terrace and river profiles suggest no salient activity of the mid-crustal Surmeh fault and a potential but limited uplift of the hanging wall of a mid-crustal MFF.

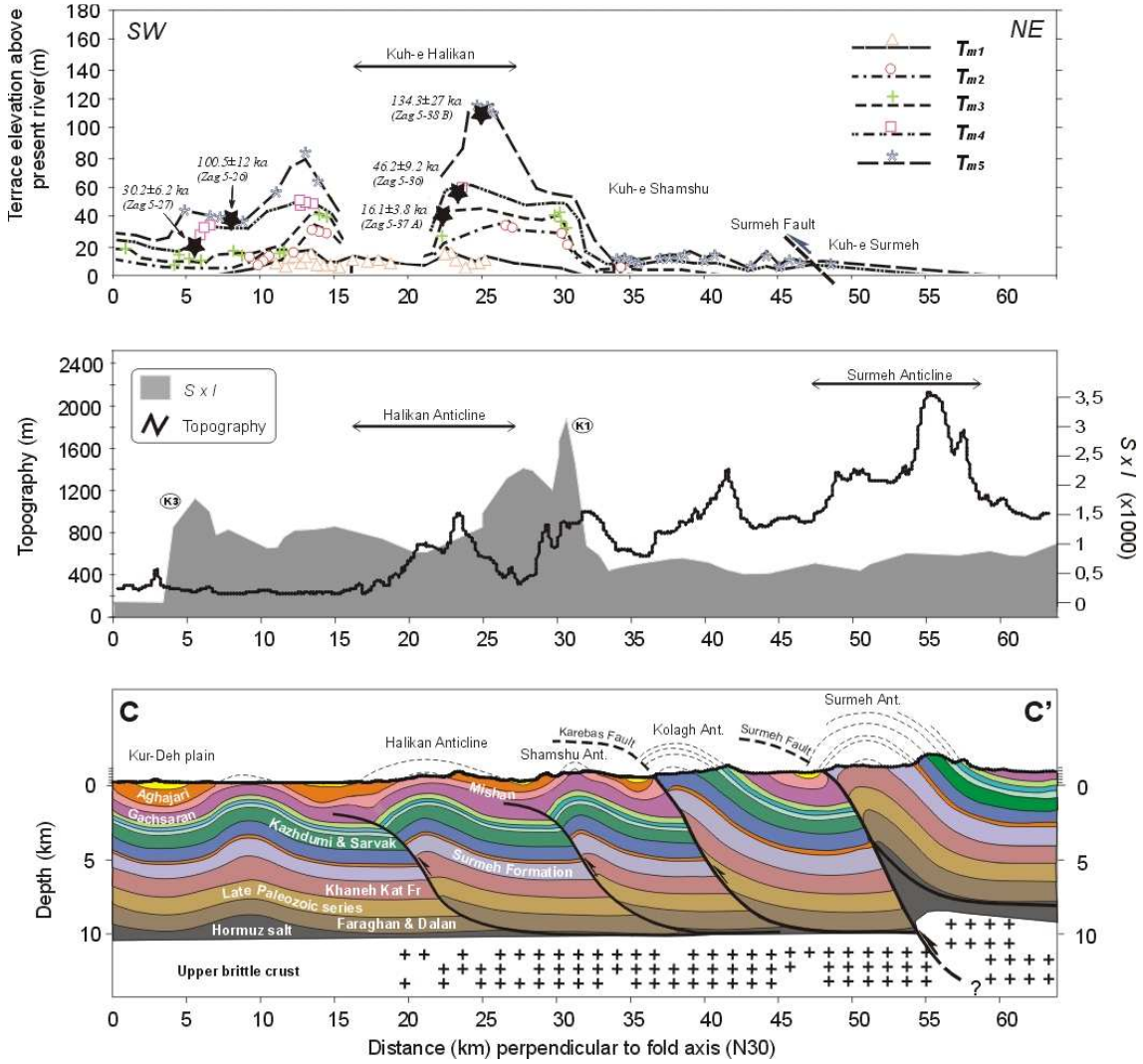

Figure V-15. (a) Relative elevation of the fluvial terraces along the Rud-e-Mand projected onto a N35Œ direction. (b) Projected profile of th e stream index. (c) Geologic section C-C' across the Kuh-e-Halikan anticline

In contrast, the terrace record and river profile across the Halikan anticline unambiguously indicate significant uplift and deformation of this structure, characterized by the highest channel gradient, stream index value and terraces elevation along the entire Mand River. The Halikan anticline is located between two major fault-related topographic steps associated with the Surmeh fault and the MFF (Figures V-13 and 15), and is a structure generally interpreted to result from thin-skinned folding of the sedimentary cover. Interestingly, this structure has developed a very limited topographic expression, despite its apparent high tectonic activity; this could indicate that the tectonic activity of this structure is recent, i.e. Late Pleistocene, or it could result from the poor resistance to erosion of the outcropping lithologies in this fold, i.e. unconsolidated Agha Jari and Mishan formations. If the Halikan anticline connects to a buried basal detachment in the mid-crust that feeds displacement into the thin-skinned system, such mid-crustal fault has to be sought further north than the Surmeh fault. Secondary knickpoints are observed along the upper Mand River at crossing the Meymand and Sim anticlines. However, as also observed along the Dalaki River, these are associated with narrow gorges carved into resistant Asmari limestone, and can be viewed as lithologic knickpoints rather than resulting from localized uplift.

4.3.3. Terrace dating and fluvial incision rates in the Kuh e Halikan region

To quantify the magnitude and spatial variation in incision of the Mand River across the Halikan fold and down to the MFF, sandstone pebbles were sampled at the surface of several elevated terraces for exposure age dating using cosmogenic ^{10}Be in quartz (Figures V-13 and 14). Three terrace levels in the core of the Halikan anticline provided usable ^{10}Be ages. The highest and oldest terrace unit preserved in the core of the fold (T_{m5}), consist of a ~20 m-thick strath terrace cut into the Mishan Formation, its tread lies 110 m above the active channel of the river (Figure V-14). A depth profile was sampled from this terrace, but only a single sample from 110 cm depth (ZA5-38 B) provided sufficient coarse quartz. Its depth-corrected exposure age is 134 ± 27 kyr (Table 1), but could be significantly younger if even modest inheritance is considered, suggesting an incision rate ≥ 0.8 mm/yr since terrace formation.

An intermediate terrace T_{m4}, which is composed of ~10 m-thick gravel and cobble deposit overlying a strath cut into the Mishan Formation and lies 76 m above the active stream channel, forms the most extensive unit in the Halikan Valley. A sample collected from the surface of this terrace (ZA5-36) yielded an exposure age of 46.2 ± 9.2 kyr and an estimated incision rate of 1.7 ± 0.3 mm/yr. The T_{m3} terrace level defines a narrow and elongate surface on the both

sides of the river across the core of the Halikan anticline. The level is composed of 10-20 m of gravels, cobbles and fine sand in a matrix of silty sand that rises up to 60 m above the present river. Based on a single exposure age of 16.1 ± 3.8 kyr (ZA5-37A), we estimate a vertical incision rate of 3.9 ± 0.9 mm/yr for the T_{m3} surface. Thus, this suite of samples also shows an apparent increase in incision rates for younger and lower terraces. Pebbles sampled from the lowermost T_{m2} level at the southwest flank of the fold are rich in ^{10}B, precluding calculation of meaningful exposure age. Thus, we estimate Late Pleistocene incision rates across the Halikan fold (which we equate to uplift rates on this active structure) to be $2.0^{+2.9}_{-1.2}$ mm/yr.

A second suite of terraces was sampled downstream of the confluence of the Mand and Shur rivers, where relative terrace elevations and the stream gradient suggest more subdued recent activity (cf. above section). Here, a flight of terraces with ~10 m thick alluvial fills is exposed in a series of inner meander bends. The highest level exposed here is correlated to T_{m5}; its tread lies 44 m above the active stream channel and its strath is 10 m lower. A set of surface clasts (sample ZA5-26) yields an exposure age of 100 ± 12 kyr, consistent within error with the age of 134 ± 27 kyr inferred for the correlated terrace level upstream. Because these are surface samples, they are less sensitive to inherited ^{10}Be than the depth sample taken from the correlated level upstream. This exposure age suggests a low long-term incision rate of 0.32 ± 0.04 mm/yr for this region. A lower terrace is correlated to T_{m4}; its strath lies 16 m above the stream channel and it yields an exposure age (from amalgamated surface clasts; sample ZA5-27) of 30.2 ± 6.2 kyr, suggesting an incision rate of 0.55 ± 0.11 mm/yr. Although this rate is slightly higher than that calculated above, the two consistently show that incision in this area is 2 – 10 times slower than across the Halikan anticline.

In order to translate incision / uplift rates into horizontal deformation rates, we interpret the structure of the Halikan anticline as representing a relatively immature and symmetric fault-propagation fold. The anticlinal axis of Halikan fold plunges westward and the topographic elevation of the anticlinal hinge decreases concomitantly from ~1500 to ~500 m, suggesting westward propagation of the fold (consistent with the westward deflection of the Mand River behind it). This suggests that development of the Halikan fold is not controlled by the Karebas-Surmeh fault system. The steep rise in terrace elevations along the forelimb of the Halikan fold suggests a NE-ward migrating hinge (e.g., Figure V-4b). Combining structural measurements to constrain the dips of the fore- and back-limbs of the anticline with the migrating hinge model for fault-propagation folding [e.g. Suppe and Medwedeff, 1990] predicts a ramp dip of 46 ± 4°

and fold core interlimb angle of ~63° for the Halikan fold. Using this ramp dip, a rigid translation model predicts that ~125 m, ~105 m and ~83 m of shortening has been absorbed since abandonment of the T_{m5}, T_{m4} and T_{m3} levels, respectively, indicating horizontal shortening across the structure at a rate of $2.8^{+3.9}_{-1.8}$ mm/yr since ~100 kyr.

We can make a rough estimate of shortening rates across the Khartang / Poshtu structure by supposing that shortening is controlled by slip along the MFF at depth in a similar manner as observed to the northwest in the Kaki and Siah anticlines (cf. Figure V-3). In this case, fluvial incision would indicate structural uplift at a rate of 0.7 ± 0.2 mm/yr, accounting for sedimentation rate in the foreland basin. Supposing a ramp dip on the MFF of 35 ± 5° (by analogy to that observed further northwest), shortening rates across this structure would amount to ~1.2 ± 054 mm/yr. Even though this is only a rough estimate, it is clear that a large part (≥70%) of surface shortening is absorbed on the inland Halikan fold rather than on the frontal MFF along the Mand transect, in stark contrast to the observed deformation field in the Dalaki River transect.

4.4. Deformation recorded by Late Pleistocene marine terraces along the Persian Gulf

4.4.1. Mand anticline

The Mand anticline represents the westernmost frontal structure of the Fars arc in front of the MFF. Its general orientation is NNW-SSE to N-S, in contrast with the NW-SE orientation of most folds in the Zagros belt, and it extends ~100-km along strike (Figure V-16). The topographically expressed width of the fold is relatively constant (~16 km), but its amplitude shows a gradient decreasing toward the northwest along the fold axis. In contrast to the tightly folded anticlines associated with the MFF ramp, the Mand anticline is an open and distinctly symmetrical fold (cf. Figure V-3). At the surface, the fold exhibits limbs dominated by gentle bedding dips between 10-27°. According to seismic and well data [Sherkati *et al.*, 2006] that provide a tight control on the thickness of sedimentary units involved in the fold, the flanks of the anticline are buried below 1-2 km of Plio-Pleistocene sediments of the Lahbari and Bakhtyari formations. The entire width of the anticline may therefore reach 20 to 25 km (e.g., Figures V-3 and 18). Seismic lines across the Mand anticline stop at the coast and the structure below the western limb of the anticline is mostly unconstrained, permitting several alternative balanced fold solutions [Oveisi *et al.*, in press]. At the surface, the Mand anticline displays the

characteristic features of a detachment fold that probably developed above the low viscosity basal layer of Hormuz salt, overlain by the thick and competent Paleozoic to Cretaceous carbonate units.

When constructing cross sections of Mand anticline, like for any detachment fold, a severe space incompatibility needs to be solved. Different fold solutions can be considered: folding at the tip of a propagating blind thrust [Sherkati *et al.*, 2006], detachment folding with increasing thickening of the internal layer, accommodated by secondary faulting, detachment folding flanked by synclinal flexures. These different fold solutions imply distinct amounts of finite shortening. Assuming a basal detachment between the sedimentary sequence and the crystalline crust at a depth of 11 km [e.g. Tatar *et al.*, 2003], modeling the Mand anticline as a fault-propagation fold or as a detachment fold with internal deformation predicts ~2.4 km of shortening across the central part of the Mand anticline. In contrast, for a detachment fold model accompanied by synclinal flexures, finite shortening would be limited to ~1 km, considering from the seismic data that local sedimentation has been ~1 km in excess of the regional subsidence [Oveisi *et al*., in press].

We have mapped tilted marine and fluvial terraces along the frontal limb of Mand anticline (Figures V-16 and 17). Terrace treads generally appear as a succession of 20 to 200 m-wide remnants of indurated beach deposits or conglomerates at the top of small steep hills within a badland eroded landscape. The correlation of these treads does not suffer any ambiguity in the barren coastal plain area. These terraces are described in detail by Oveisi *et al.* [in press].
The most extensive marine terraces are found along the southern part of the fold, and display impressive tilted tabular surfaces in the landscape. These terraces are constituted by 3-5 m of beach deposits, consisting of a partially to fully cemented sandy matrix with numerous shells (bivalves, oysters, clams…). Along the shore of the Persian Gulf, they occur 6-9 meters above the present-day sea level. Inland, their remnants are well exposed up to 1 km from the shoreline and at elevations up to 90 m above sea level. These marine terraces present remarkably linear profiles sloping at 9% to the SW (Figure V-17a). Generally, such marine terraces form in the tidal part of the shoreline, i.e. a few meters below average sea level, and with an angle of the order of 1% or less. Using such an initial geometry therefore provides a tilt perpendicular to the fold axis of the order of 8.0 ± 0.4% (~4.5°) since terrace formation. About 15 km north of this site, an almost continuous tread of fluvial (or fan) terrace remnants were surveyed up to 1.5 km inland from the shoreline. They also form well-preserved flat and

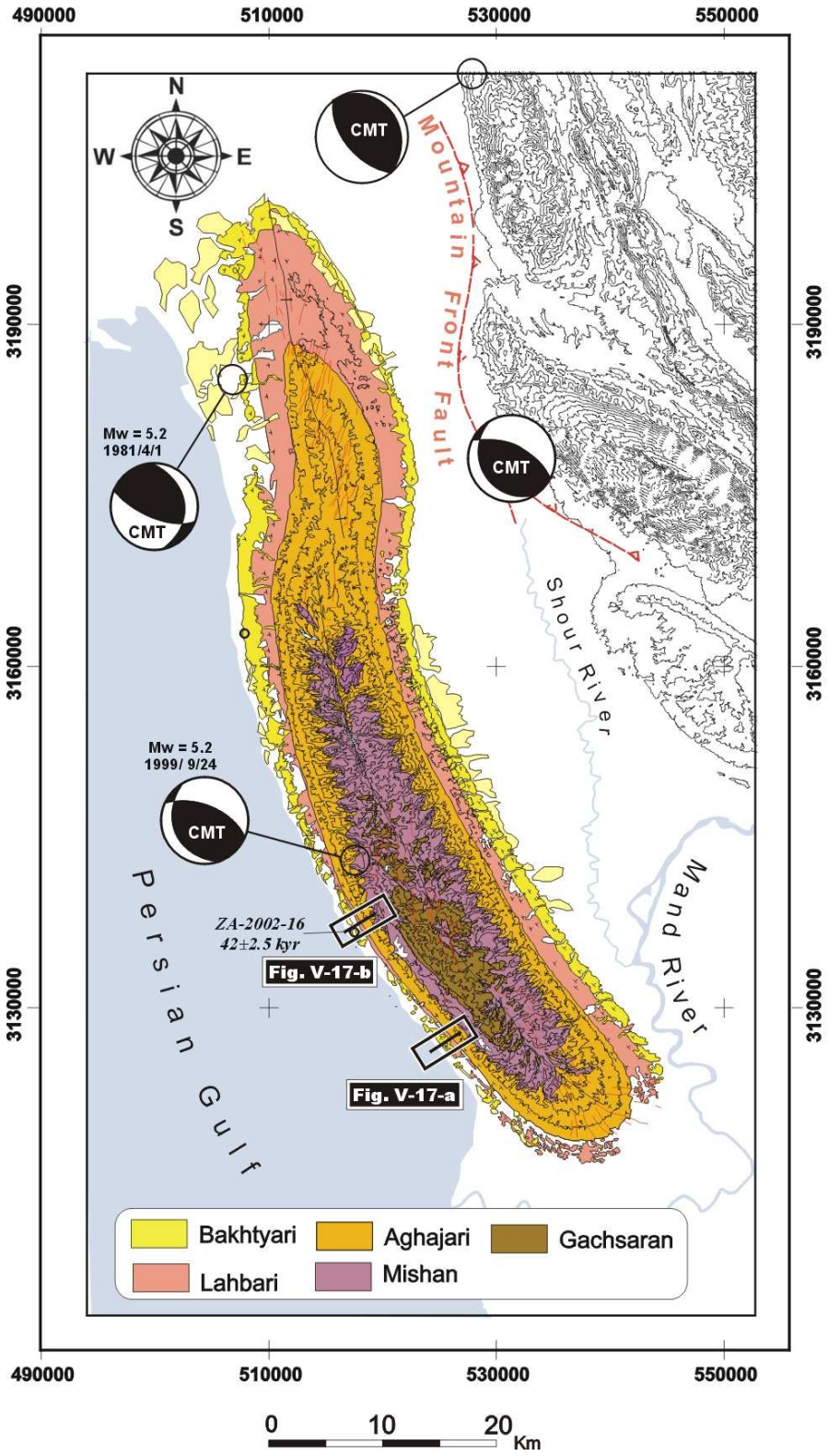

Figure V-16: Topographic and geologic map of the Mand anticline with elevation contour lines every 100 m. Focal mechanism solutions for large earthquakes from the Harvard CMT database are also indicated. Boxes show locations of surveyed terrace sites shown in Fig. V-17. Modified from Oveisi *et al*. [in press].

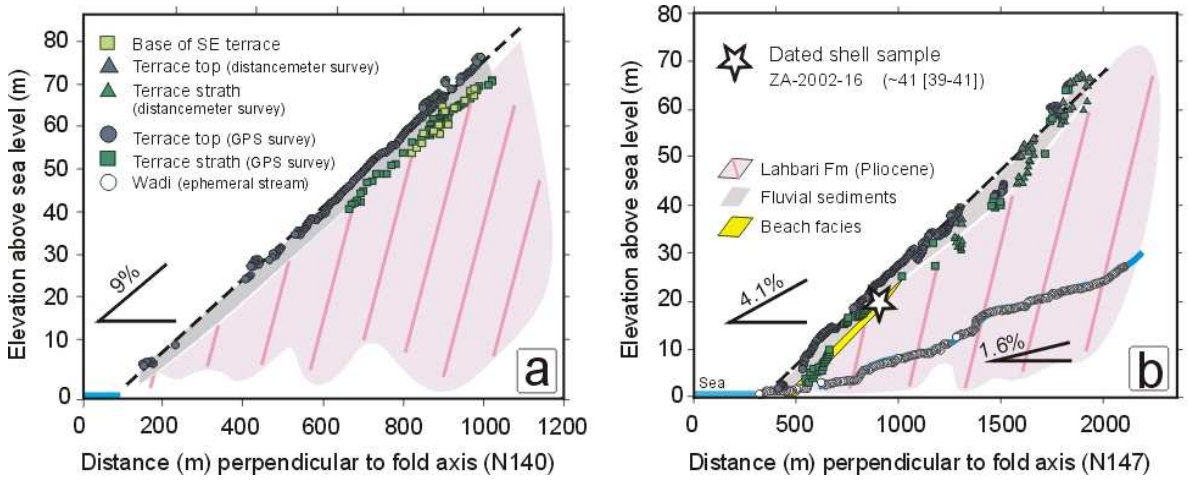

Figure V-17: Topographic profiles of the surveyed tilted terraces at the southern (a) and south-central (b) survey sites, along with present-day *wadi* profile for the latter, from kinematic GPS surveys. Slopes of best-fit straight lines through terrace and *wadi* data are indicated. Modified from Oveisi *et al*. [in press].

inclined surfaces, but here the strath is covered by 3 to 4 m of gravels, except close to the Persian Gulf coast, where the base of the terrace gravels is replaced by a 2 m-thick sandy beach facies, including a basal layer rich in marine shells. The terrace tread is nearly linear in profile, sloping at 4.1 % to the WSW (Figure V-17b). Assuming that the strath terrace has been carved by a ~1% sloping stream, similar to the one that currently drains the site, the terrace records a tilt perpendicular to the fold axis of ~2.9 ± 0.3 % (~1.7°).

Similar terrace are also developed further north along the frontal limb of the anticline [Oveisi *et al.*, in press]. The general pattern displayed by these marine or fluvio-marine terrace treads is remarkably consistent: whatever their nature, they all record a regional tilt perpendicular to the local fold axis, without any expression of faulting and other small-scale deformation features. These terrace levels clearly indicate persistent active folding of the Mand anticline. In addition, they record different degrees of tilting according to their ages and to the local fold maturity. The two sites detailed here are located in front of sections with similar structural development, and the difference in tilt should therefore be due to distinct formation ages; the southern terrace would be around three times older than the terraces further north.

Shells have been sampled from the beach deposits in the fluvio-marine terraces (Figure V-16), as well as from terraces further north. Three calcitic fragments of bivalves have been dated by Accelerator Mass Spectrometer (AMS) ^{14}C [Oveisi *et al.*, in press]. They all provide ^{14}C ages comprised between 28 and 37 kyr B.P., which correspond after a rough calibration [van der Plicht *et al.*, 2004] to ages ranging between 30 and 44 kyr B.P. Numerous ^{14}C ages in this range have been encountered around the Persian Gulf [e.g., Vita-Finzi, 1982; Haghipour and

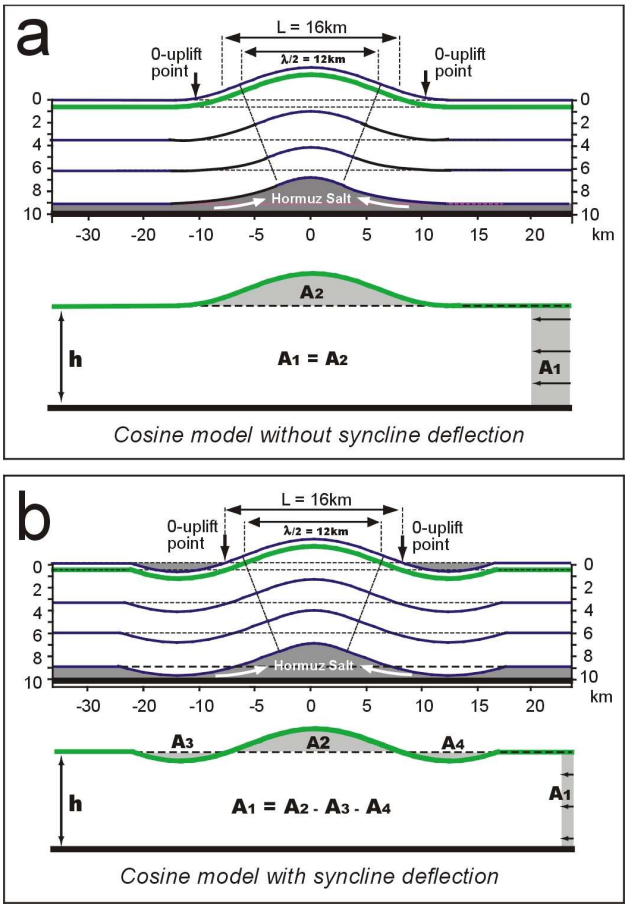

Figure V-18: Cosine model applied to upper folded units of the Mand anticline. (a) Fold geometry approximated by a cosine model with crest-to-through amplitude of ~3 km and wavelength of 24 km. Models without (a) or including (b) flexure of the flanking synclines yield a distinct area conservation but also distinct locations of the no-uplift point between the anticlinal and synclinal axes. Modified from Oveisi *et al*. [in press].

Fontugne, 1993; Uchupi *et al.*, 1999], but several studies [Page *et al.*, 1979; Fontugne *et al.*, 1997] have cast doubt on the validity of such ages because of potential partial recrystallisation of bivalve shells [a more detailed discussion of this problem is provided by Oveisi *et al.*, in press]. On the other hand, a sandstone pebble collected at the top of a fluvio-marine terrace (sample ZA2-14) provided an independent ^{10}Be exposure age of 171 ± 28 kyr (Table 1) inconsistent with ^{14}C dating. As already argued for Dalaki River terraces, however, not all results of our first ^{10}Be analyses series are consistent, so that it is difficult to trust this single age.

Marine deposits at the southernmost site are much more prominent than at other sites. For this reason, we expect them to correspond to a major and long-duration highstand associated with a major interglacial period. Marine terraces of Kish island, 300 km southeast, correlate for example with highstands of MIS 5e and 7a [Preusser *et al.*, 2003]. More generally, numerous U/Th ages of corals topping marine terraces around the Makran and Persian Gulf [Reyss *et al.*, 1998] indicate generally well developed and distributed terraces that formed during the penultimate interglacial (MIS 5e; 120-125 kyr). If the southernmost marine terrace along the Mand would also have formed at this time, they would record a tilting rate of 0.038 °/kyr. This value is comparable to tilting rates ranging between 0.035 and 0.054 °/kyr for the fluvio-marine terraces more to the North, adopting the calibrated ^{14}C ages as the formation age for these terraces.

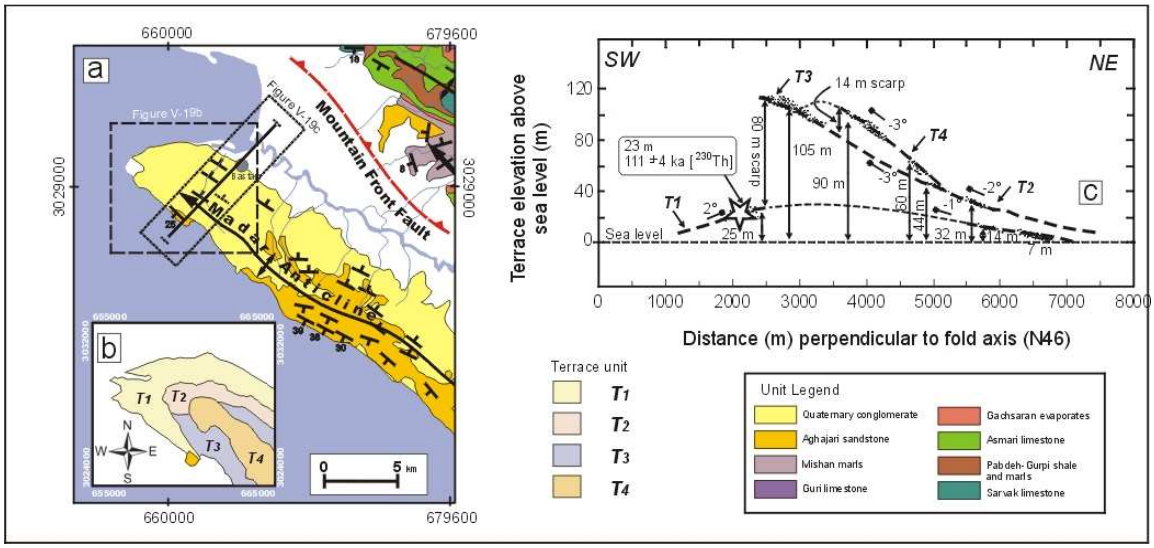

Figure V-19: (a) Geomorphic map of the marine terraces at the NW termination of Madar anticline. (b) Deformation profile of the late interglacial (MIS5) marine terrace and older terraces across the NW termination of Madar anticline.

The terrace deformation profiles in these two sites (Figure V-17) provide several first-order observations that can be used to unravel the fold kinematics. First, the observed wide-scale tilting precludes uplift above a shallow fault ramp, or geometric models like fault-bend or fault propagation folds (compare with Figure V-4). On the basis of the fold symmetry, terrace tilting, and increasing tilt with terrace age, it seems that only limb rotation associated with a detachment fold can account for the observed pattern of terrace deformation. If we consider a simple sinusoidal fold model, which approximately fits the bedding dips across the anticline along its whole length (Figure V-18), the observed bedding of 21° along the central and southern flank of the fold can be linked to a cosine of amplitude ~1.4 km and half wavelength of 12 km [Oveisi *et al.*, in press]. For such a geometry, the increasing tilt of the terraces with age can be simply related to the evolution of fold amplitude. Accordingly, tilting of 4.5° and 1.7°, as recorded by the terraces, would have been produced by shortening of the order of 320 m and 125 m respectively. As discussed in Section 3.2, one of the main problems with obtaining shortening estimates from detachment folds is related to the incompatibility between line-length versus area restoration. The two detachment fold cases lead to distinct values for the present shortening rate. If the restoration paradox is solved by bed thickening, the total shortening represents the sum of the shortening absorbed by limb rotation and the shortening absorbed by bed thickening. This latter component represents 54 % of the total shortening for limb angles of 21°. With such a model, the total shortening rate across the Mand anticline in its

south-central part could reach up to 6.5 mm/yr. If the restoration paradox is solved by synclinal flexure below a regional level, the additional flexure of the syncline increases the shortening absorbed by limb rotation by only 25%, and provides total shortening rates ranging between 3 and 4 mm/yr (Figure V-18).

From several lines of arguments, Oveisi *et al.* [in press] suggest that a detachment model including synclinal flexure agrees best with structural and terrace observations, but they recognize that no definite conclusions about fold kinematics and total shortening can be reached without detailed seismic data that would image the upper structures in the frontal syncline. The preferred model predicts ~1 km total shortening at a rate of 3-4 mm/yr across the frontal Mand anticline.

4.4.2. Madar anticline

The Madar fold represents the most frontal structure at the toe of the Zagros accretionary wedge south of Qir in the central Fars province (cf. Figure V-1). Although it is less developed both in width and amplitude than the Mand anticline further N, it displays clear evidence of recent tectonic activity and of superficial deformation. Extensive marine terraces have developed on the fold, recording deformation across the entire fold envelope (Figure V-19). The distinctly asymmetric structure appears to be actively propagating north-westward and has developed in front of the MFF and associated fault-cored Asaluyeh fold, with a probable partial transfer of the slip on this fault toward the Madar anticline in response to shortening across the MFF. The Madar fold exhibits up to 130 m of topographic relief in its northwestern part and extends for ~50 km along strike.

The limited width (6-7 km) of the Madar anticline, as compared to the Mand anticline (>16 km), suggests that the detachment is much shallower here than the depth of Hormuz salt. The relatively ductile Gasharan formation could present a potential detachment level. We thus consider the possibility that the Madar anticline is a fault-propagation fold in which the folding nucleated at a mechanical boundary within the upper portion of the Gachsaran Formation (~3 km depth).

Most of the WNW termination of the fold is covered by Bakhtyari units. Quickbird imagery with meter-scale resolution permits to identify and map several topographic steps associated with distinct risers that delineate a set of 4 marine terraces in this area (Figure V-19b and c). The upper terraces have been preserved northeast of the anticlinal axis and clearly display

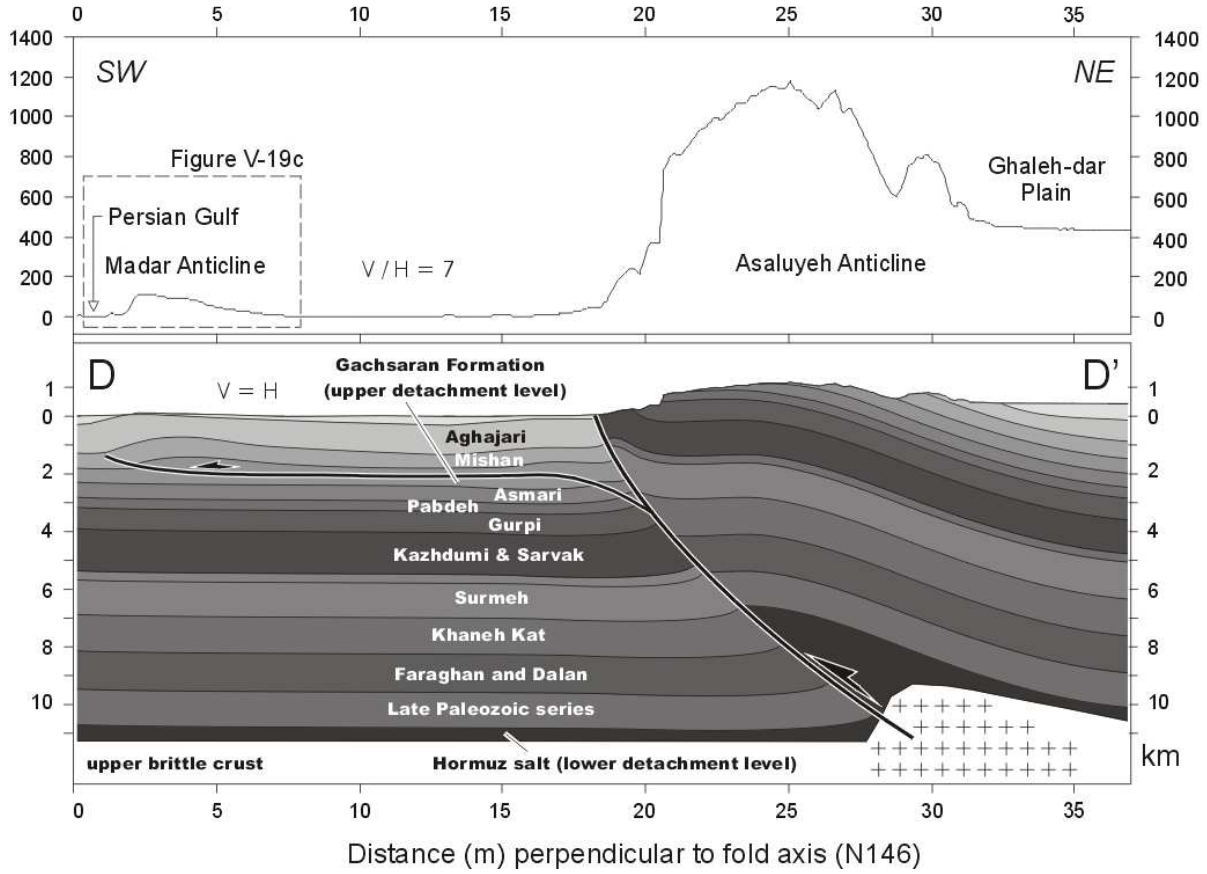

Figure V-20: Balanced structural and topographic cross-sections across the Kuh e Asaluyeh and Madar anticlines. Box outlines Madar anticline study area.

backtilting toward the northeast. Only the most recent terrace has been preserved on both fold limbs and displays a continuous asymmetrically folded structure (Figure V-19c). This most

recent and extensive marine terrace (T_1) has been dated by U/Th on aragonitic corals at 111 ± 4 kyr [Reyss *et al.*, 1998] and would have formed during the sea-level high stand of the last interstadial (MIS 5). Its deformation envelope can be reconstructed from the present-day topography (~90 m pixel size SRTM digital elevation model), and by assuming that the marine terrace was formed under a limited water depth, so that its initial geometry was nearly horizontal. Maximum uplift of the terrace reaches 30m close to the southern front of the fold.

In the absence of a complete structural data set, and in order to estimate shortening rate across the Madar fold without assuming specific fold kinematics or geometric fold models, we rely on classical methods based on area conservation. We hypothesize that, in contrast to the Mand anticline, for which the weak décollement zone presents a significant thickness that permits lateral syncline deflection, the interlayering of thin brittle and ductile units prevents significant

syncline deflection and that straightforward area conservation (as in Figure V-18a) can be applied. Assuming a detachment depth of 2 km, we therefore estimate the shortening across the Madar fold since T_1 formation to be 50 to 60 m. Consequently, the Madar structure absorbs a shortening rate of ~0.5 mm/yr, i.e. 6-8 times less than the Mand anticline further N. The fault-cored Asaluyeh fold probably absorbs a significant part of the frontal shortening, transferring the rest toward the superficial Madar structure.

5. DISCUSSION: spatial distribution of active shortening and seismotectonic implications

5.1. Thin versus thick-skinned tectonics

5.1.1 Surface deformation above inferred basement faults

It has long been recognized that the deposition and deformation of the Phanerozoic cover in the Zagros fold-and-thrust belt is strongly influenced by the reactivation of pre-existing faults in the basement [e.g., Bahroudi and Talbot, 2003]. However, the exact influence on present-day surface deformation of basement faults, whether reactivated or newly-formed, remain mostly unknown. Recent GPS results [Walpersdorf *et al.*, 2006] have so far not permitted to answer this question because they are not as yet sufficiently dense, and because horizontal motions do not provide the most constraining data. The presence of Hormuz Salt, which acts as a major decoupling level between the basement and the sedimentary cover, may strongly perturb the horizontal stress and strain transfer from the basement to the cover. In contrast, vertical displacement in the basement would be more directly transferred to the overlying sedimentary cover. Berberian [1995] or Mouthereau *et al.* [2006] implicitly make this hypothesis when they equate regional topographic and structural steps at the surface with underlying basement offsets on mid-crustal faults. In that sense, terrace uplift might appear as a primary source of information on the underlying mode of deformation, in particular across or above inferred basement faults.

The preserved records of the Dalaki fluvial terraces across the oblique NS ramp of the MFF and Gisakan fold are ambiguous with respect to basement involvement. A direct interpretation of the available terrace ages and incision rates in terms of uplift would suggest that the hanging wall of the MFF is affected by a broad (~35 km) zone of uplifting (Figure V-11). If such a broad uplift profile is related to a single structure at depth, geometric fold rules suggest rooting

of the MFF down to ~20 km and provide clear evidence for basement involvement. Two focal mechanism solutions (M_w=5.7 and 5.1 events, Harvard CMT solutions) have been reported below the Gisakan fold, with nodal planes dipping at 23°NE and 40°NE respectively and a strike of ~N333° (Figure V-5). For the M_w=5.7 event (>70% double-couple component), a reported centroid depth of 15 km confirms that the MFF indeed penetrates to mid-crustal depths. The depth of the second event, 7 km, is shallower and would require seismogenic behavior of the sedimentary cover, which would also explain observed surface features like tectonic scarps and surface ruptures along the trace of the MFF. Due to <70% double-couple component, the M_w=5.1 event depth is, however, poorly constrained and its location within the basement can not be excluded [cf. Talebian and Jackson, 2004].

The seismicity data would therefore confirm the rooting of the MFF into the basement. However, geologic arguments suggest that the basement activity and slip rate on the basal part of the MFF could be limited. The presence on the backlimb of the Gisakan fold of transported basins at relatively low elevations, that are partly filled with syn-tectonic Bakhtyari conglomerates (Figures V-5 and 11) show that a dominantly thin-skinned tectonic scenario cannot be ruled out. For example, the transported basins of the Kheshr syncline (~500 m elevation and ~10 km from the MFF; Figure V-5) limits the vertical offset on an inferred mid-crustal segment of the MFF to less than 400 m during the last 0.5-1 Ma, at a rate that must be lower than 0.9 mm/yr (taking into account footwall subsidence at 0.2 mm/yr). Our surface data suggest that both thick-skinned or basement involved deformation and thin-skinned structural styles could be simultaneously ongoing deformation processes in the Dalaki region. In absence of further terrace age constraints it is, however, difficult to propose to what proportion each mechanism contributes to surface deformation.

The activity of the MFF in the Mand region is more ambiguous because the surface expression of this inferred basement fault shows a major step-over in this area. If mid-crustal faults display a similar segmentation, with transfer through oblique ramps or transfer faults, river meandering in between the uplifted blocks across the transfer fault could obscure the activity of the MFF. It should be noted, however, that the uplift rate that affects the hanging wall of the northeast branch of the MFF (where we infer it to cross the Mand River) is 2 – 10 times lower than the uplift rate affecting the Halikan fold further northeast. In summary, even if the MFF has some basement expression, its present slip rate appears limited. In contrast, the interpretation of incision patterns along the upper Mand River presents less ambiguity. The absence of sharp breaks in vertical incision, generally subdued regional incision and the

Table V-1: ^{10}Be ages of sandstone pebbles sampled on terraces

Sample	Terrace	Alt. (m)	Lat. (°N)	Long. (°E)	depth (cm)	[^{10}Be] 10^5 at g^{-1}	P_{surf} (at g^{-1} yr^{-1})	mask corr.	Age (kyr)
KAZ-11	Bk-surf.	863	29.28	51.96	0	24.3 ± 2.7	8.04	1.00	325 ± 34
ZA2-14	MMT	27	28.35	51.18	0	6.60 ±1.11	4.01	1.00	171 ± 28
ZA2-11/3	T_{d10}	257	29.46	51.32	0	7.73 ± 1.81	4.96	1.00	162 ± 37
ZA2-19/2	T_{d5}	130	29.48	51.28	170	0.33 ± 0.16	4.47	0.99	62.5 ± 31.2
ZA5-26	T_{m5}	195	28.19	52.09	0	4.51 ± 0.54	4.60	1.00	100 ± 12
ZA5-27	T_{m4}	178	28.18	52.09	0	1.36 ± 0.28	4.54	1.00	30.2 ± 6.2
ZA5-36	T_{m4}	318	28.27	52.38	0	2.33 ± 0.46	5.10	0.99	46.2 ± 9.2
ZA5-37A	T_{m3}	300	28.27	52.38	0	0.81 ± 0.19	5.03	0.99	16.1 ± 3.8
ZA5-38B	T_{m5}	369	28.32	52.36	110	1.70 ± 0.35	5.32	0.99	134 ± 27

MMT: Mand marine terrace

Sample	Terrace	Alt. (m)	Lat. (°N)	Long. (°E)	Ca/ rock	[Cl] (ppm)	[^{36}Cl] 10^5 at g^{-1}	P_{surf} (at g^{-1} yr^{-1})	mask corr.	age (kyr)
KAZ-2A	T_{d6}	620	29.40	51.68	0.356	133.8	6.78 ± 0.17	31.2 ± 3.8	0.99	22.5 ± 4.5
KAZ-2B	T_{d6}	620	29.40	51.69	0.374	33.3	14.98 ± 0.31	26.5 ± 3.8	0.99	61 ± 11
KAZ-7A	Bk surf.	820	29.30	51.80	0.363	136.0	122.79 ± 2.60	36.5 ± 3.8	1.00	647 ± 128
KAZ-7B	Bk surf.	820	29.30	51.80	0.352	97.3	111.74 ± 1.71	33.4 ± 3.8	1.00	639 ± 113
KAZ-9	$T_{d1/2}$	550	29.40	51.73	0.366	101.3	0.71 ± 0.07	28.1 ± 3.8	0.83	3.1 ± 0.7
KAZ-18	T_{d5}	350	29.43	51.56	0.372	108.9	3.05 ± 0.07	24.6 ± 3.8	0.99	12.7 ± 2.5
KAZ-20	lateral incision mark	820	29.25	52.12	0.358	108.0	20.95 ± 0.44	34.4 ± 3.8	0.83	80 ± 11
KAZ-5	Un-exposed pebble	900$^{\#}$	29.30	51.80	0.216	333.9	1.61 ± 0.08	54 ± 4	1.00	13*

Table V-2: ^{36}Cl ages of limestone pebbles sampled on terraces

$^{\#}$Average elevation of the watershed draining to the Rud e Dalaki, upstream of the sampling point
*Apparent age at the moment of deposition (assuming an age of 650 kyr for this Bakthyari terrace)

continuity in the river gradient indicate no major uplift and tectonic activity across the hanging wall of the inferred Surmeh-Qir basement fault. Because the surface expression of the Surmeh-Qir fault is discontinuous, questions relative to its segmentation at the surface and at depth could also be addressed. However, seismicity along the Surmeh fault does not indicate any major step or discontinuity in the inferred basement fault, and the general subdued regional incision, as well as the absence of elevated strath terraces along the entire Mand River upstream the Halikan fold, preclude significant slip on basement fault(s) whatever their geometry.

5.1.2 Evidence for activity of shallow structures

Surface deformation of geomorphic markers clearly illustrates active thin-skinned tectonics in the central Zagros and that many active structures are shallowly rooted, in general above a weak detachment level, like the Hormuz or Gachsaran evaporites. The balanced cross-section across the active coastal Mand anticline, for example, does not require basement involvement, as opposed to folds associated with the MFF further north-east. Significant involvement of the basement seems precluded by the structural data that clearly indicate the symmetry of the fold, as well as by the seismic data [Sherkati *et al*., 2006]. Whereas a M_w=5.2 event located below the Mand fold at an approximate depth of 15 km (Harvard CMT solution, cf. Figures V-1 and 16) could have occurred on an underlying and unrecognized basement fault, structural data as well as tilted marine terraces are, in contrast, compatible with a detachment fold developing on top of the Hormuz thick salt layer and implying significant mobilization of evaporitic material. Likewise, the active Halikan fold is also suspected to have developed on this detachment level.
The differential incision recorded by fluvial terraces as well as the concave reach in the Mand River profile clearly indicate tectonic activity of this fold, which affects the sedimentary cover and grows over a ~45° ramp branching on a flat décollement at level of Hormuz salt. Such deformation must be fed from further northeast by slip on this décollement within a thin-skinned tectonic system. More generally, as has been recognized for a long time, the Hormuz detachment level plays a primary role in controlling the geometry and finite deformation of the Zagros (see cross-section of Figure V-3), but also in partitioning active deformation. Our surface data suggest, however, that stratigraphically higher décollement level also significantly affect folding styles, both in early and late stages of fold development. The Madar anticline that develops in front of the MFF appears to be activated by the horizontal transfer of convergence onto the Gachsaran level (Figure V-20). Reactivation of the Kuh e Pahn and Baladeh synclines is also strongly controlled by the existence of the incompetent Gachsaran level.

The above examples of active folds, whether they develop on the Hormuz or Gachsaran décollement levels, require the horizontal transfer of shortening on these levels on distances of at least 10 km, and up to 30 km for the Mand anticline. The major question is whether these horizontal décollements branch at depth onto the nearest mid-crustal ramps to the northeast, or whether the Hormuz décollement that feeds these fold runs sub-horizontally for ~200 km northeastward to finally branch onto a basement fault below the High Zagros. In any case, surface deformation does not appear to directly reflect significant mid-crustal deformation, if it exists, because intermediate weak levels distribute deformation within the sedimentary cover toward the foreland and influence the wavelength of folding. Shortening and horizontal stress transfer in the sedimentary cover of the frontal Zagros must thus be partly to fully decoupled from the basement at the level of Hormuz salt and secondary detachment levels. This conclusion contradicts recent suggestions [e.g., Molinaro *et al.*, 2005; Sherkati *et al.*, 2005; Mouthereau *et al.*, 2006] that, in the Eastern Fars and Northwest Zagros, deformation was initiated in the sedimentary cover, starting as early as Late Miocene at the Northwest Zagros front [Homke *et al.*, 2004], and that more recent deformation has been dominated by thick-skinned tectonics and by the transfer of basement faulting upward to the sedimentary cover [Molinaro *et al.*, 2005]. The rate and style of surface deformation suggest that such a tectonic model and chronology does not apply for the western Fars. There, forward-propagating deformation in a thin-skinned tectonic regime is still an on-going process; this does not preclude, however, simultaneous deformation within the basement, as evidenced by the preferential location of M_w>5 seismic events within the basement beneath large flexures such as the MFF or the Surmeh fault, or strike slip faults such as the Kazerun or Karebas faults.

5.2. Fold evolution: from detachment to fault-related folds

Observed large-scale folds within the Zagros study area can be adequately described by general geometric fold models (e.g., detachment, fault-bend, fault-propagation, etc), which have been commonly proposed as end-member kinematic models [e.g. Jamison, 1987; Fischer *et al.*, 1992; Mitra, 2003] and which are generally used to describe structural styles and the evolution of fault-related folds in fold-thrust belts and accretionary prisms. Fold geometries vary across strike, from the frontal zone toward the interior, throughout the central Zagros. In many cases, more complicated folds that have accumulated more strain are encountered close to the topographic steps. The kinematic evolution and structural style of the Zagros folds appear to be

strongly controlled by the mechanical stratigraphy and more specifically by the thickness, viscosity, and depth of incompetent rock units, as demonstrated by different examples from our study.

5.2.1. Detachment folding above Hormuz Salt

In the Zagros belt, the presence of a 1 km-thick layer of ductile Hormuz Salt favors the development of detachment folds, particularly in the early stages of fold evolution. The Mand anticline appears as a case example of a symmetric detachment fold. The progressive tilting of the marine and fluvio-marine terraces along the Persian Gulf coast highlights that detachment folds at the central Zagros front primarily deform by limb rotation, in contrast to fault-related-fold models (e.g., fault-bend or fault-propagation folding), where deformation occurs by hinge migration in association with dominant fault motion at depth [e.g., Jamison, 1987]. The Mand detachment fold is characterized by a relatively high wavelength/amplitude ratio (~8.3 in its central part), indicative of a rather immature fold [Mitra, 2003], and has developed over a viscous layer with a relatively low thickness/depth ratio (~0.08). Although large uncertainties remain concerning the exact geometry at depth as well as the original thickness of the basal Hormuz Salt layer, our fold reconstruction suggests that this ductile layer was sufficiently thick to permit $\geq$ 500 m flexure of the synclines flanking the Mand anticline associated with salt migration from the synclines towards the core of the anticline (eg., Figures V-3 and 18). Continued shortening by buckling over the ductile layer will, however, be limited by "grounding" of the overlying units when syncline deflection reaches the underlying basement. In that case, additional shortening can no longer be accommodated by limb-rotation and syncline-deflection but the kinematics will most probably change to hinge migration in association with a propagating fault.

5.2.2. Transition from detachment- to fault-propagation folding above the Gachsaran décollement

In marked contrast to the Mand anticline, the frontal Madar fold presents an asymmetric structure, despite having absorbed much less shortening. This active fault-related fold has a large wavelength/amplitude ratio of ~32.5 and manifests clear vergence to the southwest (Figures V-19 and 20). Asymmetric finite deformation of the structure is reflected in the fold kinematics, as shown by the recent folding recorded by extensive marine terraces. The absence

of a tectonic scarp or of a steep frontal limb in the most recent marine terrace suggests that a classic fault-propagation fold model does not adequately describe the Madar anticline. Tri-shear models [Erslev, 1991], in which folding develops incrementally in a triangular zone of distributed shear that expands ahead of the propagating fault tip, such that forelimb deformation is distributed within a wider and smoother region, seem more appropriate. The Madar anticline is inferred to develop over the Gachsaran detachment level at ~2 km depth; the development of a preferred vergence and asymmetry could result from the limited thickness of the ductile layer in the detachment level. Paleogeographic data [Alavi, 2004; Sherkati and Letouzey, 2004] suggest that the Madar fold has grown at the south-eastern border of the Gachsaran evaporite basin (Figure V-1a), where its thickness could be strongly reduced. A thin basal ductile layer would not permit a detachment fold to develop because of the difficulty to move large volumes of material toward the anticlinal core; a thin Gachsaran level would only act as an efficient décollement level on top of which fault-related folds can develop.

5.2.3. Fold evolution with increasing deformation

With increasing degrees of shortening, folds in the central Zagros may present different evolutionary styles. As discussed above, symmetric detachment folding can be blocked by limitations on synclinal flexure or on the amount of salt available for basal material migration. In many areas of the internal Zagros, mostly in between the main topographic steps, preservation of symmetric folds at the surface is evidenced by spectacular “whale back” anticlines of outcropping Asmari limestone. None of these folds present evidence for active deformation, suggesting that early shortening by detachment folding did not pursue further, and that shortening consequently was accommodated more frontally (i.e., further southwest-ward). Numerous other folds, in contrast, present a clear asymmetry with generally southwest-ward vergence (e.g., the Gisakan, Siah and Asaluyeh anticlines lining the MFF; Figures V-3, 11, 20); we speculate that such folds developed from early symmetric detachment in relation with fault propagation toward the surface in the core of the fold. Such an evolution appears to be associated or amplified by asymmetric boundary conditions: presence of an inferred northeast-dipping basement fault, fold development at the termination of a strike slip fault, or facies boundaries in the Hormuz or Gachsaran ductile units. In such settings, the folds evolve toward fault-propagation or fault bend folds and fault offset can reach the surface as observed north of the Dalaki River where it crosses the MFF (Figure V-12).

5.3 Seismotectonic model for the Zagros fold belt in the western Fars

The observed surface deformation patterns along the Dalaki and Mand rivers have several characteristics in common: they show in particular that the external belt of the Zagros SFZ is tectonically much more active than the internal part, as would be expected for a normal propagation sequence in a thin-skinned orogenic wedge. Along the Dalaki River, inferred deformation rates continuously increase toward the front, culminating on the MFF and the most frontal structure, the Mand anticline. In contrast, the Mand River transect further southeast displays a more irregular pattern: the most frontal structure, the Madar anticline does not absorb a significant part (< 10%) of the shortening accommodated by the Zagros; whereas the Halikan fold, which is the 3rd major structure inland of the MFF (Figure V-13), absorbs a major part of the regional shortening. The normal pattern of progressive activation of the most frontal folds varies therefore laterally and can affect at least the three most frontal anticlines.

Quantitatively, we can sum the shortening absorbed across the different active structures to determine the mean convergence across the Central Zagros SFZ during Late Pleistocene times. We will consider two N35°E transects, corresponding to a direction perpendicular to the mean fold axis in the central Zagros (except in the westernmost part), to the mean compression direction deduced from seismicity [Gillard and Wyss, 1995], and also to the orientation of the GPS vector in Bahrein (i.e., on the stable Arabian plate) relative to central Iran north of the MZT [Vernant *et al*., 2004; Walpersdorf *et al*., 2006]. We consider a northwestern transect across the Mand anticline and the Dalaki region and a southeastern one from north of the Madar anticline to Qir across the Mand River catchment (Figure V-21). Geomorphic studies have not been conducted at the exact location of the intersection of these transects with the active structures. As a first approximation, we will assume that we can use the shortening rates inferred for the same structure but at some distance of the transects, although we are conscious that deformation rates can vary laterally even along a single fold.

For the northwestern transect, we sum inferred shortening values across the Mand anticline, the Gisakan fold, and the Kuh e Pahn / Baladeh region. Because of the symmetric shape of the Mand anticline, and because of the absence of obvious strike-slip faults that could partition oblique motion within the fold, we suggest that shortening is close to perpendicular to the local fold axis. If so, this local shortening direction is oriented 20-30° from the regional compression

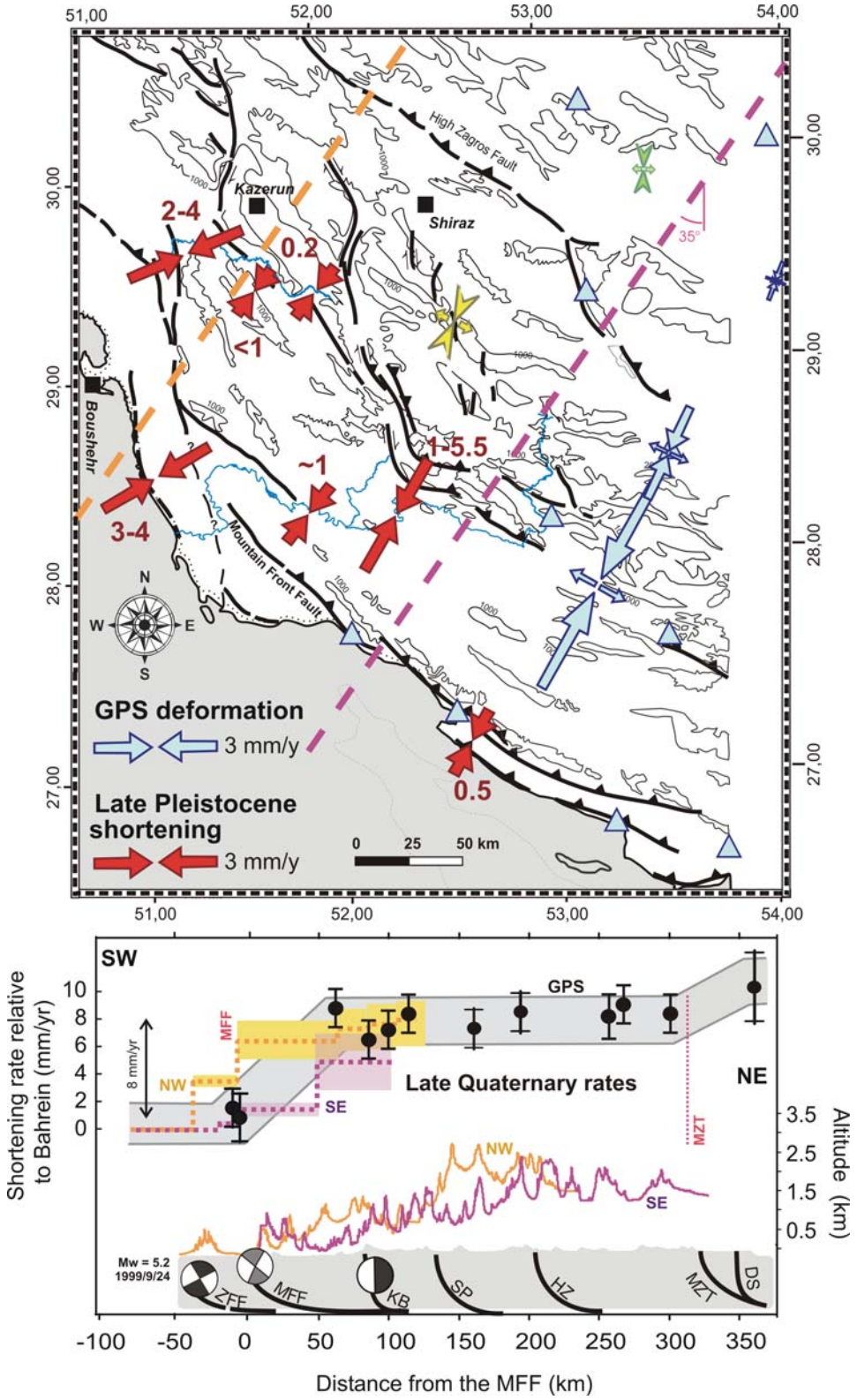
51,00
52,00
53,00
54,00
30,00
29,00
28,00
27,00
High Zagros Fault
Kazerun
Shiraz
Boushehr
Mountain Front Fault
35°
2-4
0.2
<1
~1
1-5.5
3-4
0.5
N
W
E
S
GPS deformation
3 mm/y
Late Pleistocene shortening
3 mm/y
0 25 50 km
SW
NE
GPS
Late Quaternary rates
MFF
NW
SE
MZT
8 mm/yr
Shortening rate relative to Bahrein (mm/yr)
Altitude (km)
Mw = 5.2
1999/9/24
ZFF
KB
SP
HZ
DS
-100 -50 0 50 100 150 200 250 300 350
Distance from the MFF (km)

Figure V-21: (a) Map of the central Zagros showing the inferred shortening rates across individual structures as deduced from surface deformation recorded by Late Pleistocene terraces (red arrows, annotated with inferred rate) compared to present-day shortening rates in three subregions of the central Zagros as determined by GPS [Walpersdorf et al., 2006]. Blue triangles are GPS stations used in the calculation of present-day deformation rates. Yellow and green arrows show paleostress directions reconstructed from fault striae analysis in the western Fars [Lacombe et al., 2006] and in the High Zagros [Navabpour et al., 2007], respectively. (b) Synthetic profiles of convergence rates (relative to stable Arabia) across the central Zagros according to GPS and geomorphic data, compared to topographic profiles along a northwestern (orange) and southeastern (purple) transect.

direction of N35°E in the southern part of the fold; the 3-4 mm/yr shortening rate across the fold (cf. Section 4.4.1.) thus represents 2.6 to 3.8 mm/yr of shortening orthogonal to the SFZ. As a consequence, shortening across the Mand anticline may absorb ~30 to 45 % of the present-day convergence across the Zagros [8 mm/yr; Walpersdorf *et al*., 2006]. The Gisakan fold is oriented ~N155°E, in good agreement with the nodal-plane orientations of two reported earthquakes (N332° and N334°) that occurred below it and indicate almost pure thrust motion [Talebian and Jackson, 2004]. There is no geomorphic evidence, from the drainage network or old alluvial fans, for a significant strike-slip component on the associated oblique segment of the MFF. Both observations strongly suggest that horizontal shortening is perpendicular to the Gisakan fold axis. From the uplifted and incised terraces along the fold, we infer that it absorbs a shortening rate of 1.3-3.4 mm/yr in a direction N65°E (cf. Section 4.2.2.), corresponding to ~1 to 3 mm/yr in the N35°E direction. Finally, both the Kuh e Pahn and Baladeh synclines are roughly perpendicular to the regional compression direction and these two structures contribute <1 mm/yr and 0.2-0.3 mm/yr, respectively, to Zagros shortening rates (cf. Sections 4.1.2. and 4.1.3.). The sum of these different contributions represents 4.5 to 8.1 mm/yr of shortening absorbed across the western Fars province by the three or four most frontal folds.

For the southeastern transect we sum inferred shortening values across the Madar, Asaluyeh, and Khartang / Poshtu anticlines, above the southwest and northeast branches of the MFF respectively, as well as across the Halikan anticline. All these structures are roughly perpendicular to the regional shortening direction N35°E and no obliquity correction is required. Before summing the different contributions it is, however, necessary to estimate shortening across the Asaluyeh anticline (cf. Figure V-20). From the data currently available to us, we cannot determine whether shortening across the Madar anticline equals the slip rate on a deep-

seated MFF ramp beneath Asaluyeh anticline that branches on the décollement feeding the Madar anticline, or if a significant part of the shortening across the Asaluyeh anticline is absorbed by folding or faulting up to the MFF trace at surface, with only a minor part transmitted to the frontal Madar fold. For a fault-bend fold (Figure V-4a) developing over a ~30° ramp, geometric rules [Suppe, 1983] impose that 70% of the shortening is transferred toward the front and 30% is absorbed by folding. The frontal Madar anticline is inferred to absorb ~0.5 mm/yr of shortening (cf. Section 4.4.2); we therefore suspect that the Asaluyeh anticline can absorb at least 0.2 mm/yr and possibly more if partitioned slip occurs on the upper segment of the MFF and reaches the surface. Shortening rates across the Khartang / Poshtu and Halikan anticlines were estimated at 1.2 ± 0.5 mm/yr and 3.1 $^{+4.1}/_{-2.2}$ mm/yr, respectively (cf. Section 4.3.3.). From the above considerations, the sum of the shortening contributions along the southeastern transect ranges between 2.3 and 10.1 mm/yr.

Despite large uncertainties, the above estimates predict consistent values for the shortening rates across the southern Fars province (Figure V-21). Moreover, these mean values for the Late Pleistocene period are similar within error to modern shortening rates of ~8 mm/yr, as deduced from GPS results [Tatar *et al*. 2002; Walpersdorf *et al.* 2006]. This similarity suggests that deformation rates in the Zagros have been constant during the past 50 to 100 kyr. More importantly, the correspondence between the GPS and geomorphic shortening profiles (Figure V-21b) confirms that the external part of the Zagros SFZ is tectonically much more active than the internal part, and that this part of the orogen is currently characterized by a normal propagation sequence. The shortening directions are also consistent with the present-day strain axes as inferred from the GPS surveys (Figure V-21a). Despite these similarities between present-day and geomorphic deformation, it is important to note, however, that the local shortening directions at the Zagros front are generally oblique (showing 30-45° clockwise rotation) relative to the GPS vectors. This requires that some dextral strain is developed within the Zagros fold belt in a direction N125°E; such deformation is compatible with the focal-mechanism solutions of numerous seismic strike-slip events that occur in the Central Zagros (Figure V-1) and with right-lateral movement on strike slip faults like the Kazerun or Karebas faults, or the Main Recent Fault (MRF) further north [e.g., Authemayou *et al*. 2006; Talebian & Jackson 2004].

The comparison of Late Pleistocene deformation with present-day seismicity yields several interesting insights on the seismotectonic behaviour of the Zagros SFZ. Despite the relatively rapid rates of deformation inferred for the most frontal folds, present-day seismicity associated with these frontal structures is minimal (Figure V-1). In contrast, the seismicity level is generally higher further north but corresponds to an area where shortening rates at the surface are an order of magnitude lower. The Himalayan fold-and-thrust belt is similarly characterized by the absence of recent seismicity close to its frontal part and by more intense (elastic) strain and seismic activity 80 km further north in the more internal part of the orogen [Pandey et al. 1995]. There, seismic quiescence of the front has been attributed to mechanical locking of the frontal part of the basal detachment in between two major earthquakes, while microseismicity accumulates in the more internal and deeper part of this detachment at the locking transition [Lavé & Avouac 2001]. In the Zagros, however, seismicity is more widely distributed than in the central Himalaya [e.g., Tatar *et al.* 2003] and, more importantly, the recent GPS results [Walpersdorf *et al.* 2006] show that the interseismic deformation profile does not indicate localized elastic strain above the area characterized by the most intense seismic activity. These observations suggest that there is no major locked detachment beneath the Zagros and that shortening is transferred toward the frontal folds and faults that deform mostly aseismically. The presence of a weak detachment level associated with the basal Hormuz Salt as well as several intermediate weak décollement levels could explain this remarkable absence of significant seismicity during deformation of the Zagros sedimentary cover.

Based on combined geodetic results and seismic moment summations, Masson *et al.* [2005] show a large deficit of seismic deformation, with 95% of the deformation in the Zagros occurring aseismically. We therefore propose that the Zagros is currently behaving primarily as a thin-skinned fold-and-thrust belt. Seismic and aseismic deformation within the basement cannot be excluded but probably absorb less than 25% of the shortening observed in the deformed sedimentary cover. In addition, the Hormuz Salt permits strong decoupling in terms of horizontal stress transfer between potential basement deformation and fold activation in the sedimentary cover. Such a model leads to a fundamental question: can the remaining >75% of crustal shortening that is not absorbed in the central Zagros basement be transferred beneath the High

Zagros through the main Hormuz detachment and contribute to underthrusting of Arabian middle crust below the High Zagros? And if so, why does this process occur fundamentally in an aseismic manner? To answer these questions, as well as to address the partitioning of shortening between folding and strike-slip fault deformation, further studies are required, in particular to obtain more precise temporal and spatial constraints on uplift and slip rates at depth via more detailed and precise geomorphic surface dating.

6. Conclusions

Geological and geophysical data constrain the present-day fold geometries in the central Zagros, but generally do not permit a clear determination of fold evolution and kinematics. This study illustrates how additional kinematic information can be gained from the incremental deformation recorded at the surface by deformed geomorphic markers, in particular if this information can be documented for different time steps. Using appropriate fold models based on structural data allows to efficiently estimate horizontal shortening from tectonic uplift recorded by marine and fluvial terraces. Obtaining well-constrained rates of deformation depends on reliably dating deformed geomorphic markers, which, as often, has constituted the most challenging aspect of this study. However, by combining different dating techniques and making sensible correlations to the regional climate and sea-level history, we have been able to propose an internally consistent set of ages, which allow the first geomorphic estimates of shortening rates absorbed by individual structures in the central Zagros to be made.

Our results show that shortening on Late Pleistocene timescales is concentrated in the frontal part of the belt, consistent with recent GPS data [Walpersdorf *et al.* 2006]. Three or four frontal structures appear to absorb practically all of the active shortening across the Zagros. In the northwest of our study area, the coastal Mand anticline and the Gisakan fold, associated with the MFF, together take up at least 70% and possibly all of the shortening between the stable Arabian and Iranian platforms. To the southeast, the situation is slightly more complex; with thin-skinned deformation concentrated on the Halikan fold located inboard of the MFF and only ~10 % of the shortening taken up on the most frontal structures.

For the active coastal anticlines, structural data as well as seismic sections preclude significant basement involvement. These evolve as open detachment or fault-propagation folds above the basal (Hormuz Salt) or intermediate (Gachsaran evaporates) décollement levels. Crustal-scale shortening is fed into these structures either from the MFF of from the most internal parts of the Zagros. Active folds associated with the MFF, in contrast, do suggest basement involvement and fault rupture up to the surface. Inboard of the MFF, minor (Baladeh and Kuh e Pahn synclines) to significant (Halikan anticline) amounts of shortening are absorbed by clearly thin-skinned structures, whereas the surface expressions of major basement faults (e.g., the Surmeh Fault) do not provide geomorphic evidence for recent activity.

The above pattern is consistent with a normal forward-propagating deformation sequence in a thin-skinned tectonic regime during at least the Late Pleistocene, with south-westward migration of the front of the wedge and a predictable evolution of fold structure and kinematics: folds initiate as detachment or fault-propagation folds, depending on the depth and thickness of the driving décollement level, and evolve into more or less complex fault-bend folds as material transfer within the detachment layer becomes inhibited. Such a scenario implies that most of the spectacular “whale-back” anticlines that characterize the Zagros are relict features from early stages of development. Later reactivation on the internal structures appears to be limited to superficial upward extrusion of synclinal cores over high-level decoupling levels.

Our geomorphic and structural analysis suggests that if the style of deformation through the Zagros accretionary prism has evolved through time, the forward transfer of motion into a thin-skinned system should be contemporaneous with or postdate thick-skinned tectonics involving major basement faults. Comparing the rate and direction of shortening across individual structures, as well as recent GPS data [Walpersdorf *et al.* 2006], with the distribution of seismicity [Talebian & Jackson 2004; Tatar *et al.* 2003] suggests that the sedimentary cover of the frontal Zagros is decoupled from the basement, most probably at the level of the Hormuz Salt. This weak basal detachment level, together with several intermediate weak décollement levels, appears to be responsible for the overwhelmingly aseismic deformation of the Zagros sedimentary cover.

CHAPTER VI

CHAPITRE VI

CONCLUSION GENERALE

CONCLUSION GENERALE

Dans cette thèse, nous avons combiné des études géomorphologiques et structurales afin de contraindre la géométrie et la cinématique récente des plis de la chaîne du Zagros central. L'utilisation de modèles de plis appropriés, basés sur des observations structurales, permet d'estimer le raccourcissement horizontal absorbé par les structures à partir du soulèvement tectonique enregistré par des marqueurs morphologiques tels les terrasses marines ou fluviales. La quantification des taux de raccourcissement nécessite de pouvoir dater de façon fiable ces marqueurs ; ces datations ont constitué un défi important au cours de ce travail.

Nos observations structurales, en comparant les plis les plus récemment formés le long du front de la chaîne avec des plis plus matures à l'intérieur, nous ont permis d'établir un schéma d'évolution cinématique des plis du Zagros. En général, les plis se forment comme des plis de décollement symétriques et ouverts (comme le pli du Mand décrit dans le Chapitre 3) et évoluent vers des plis plus asymétriques associés à la propagation vers la surface d'une faille de rampe (comme le pli de Gisakan ; Chapitre 5). Cette évolution peut être arrêtée à différents stades ; un grand nombre des plis à l'intérieur de la chaîne ont fossilisé le stade symétrique initial. Des plis ayant atteint un stade plus évolué sont généralement associés à des conditions aux limites asymétriques comme la présence d'une faille de socle, le développement du pli à la terminaison d'une grande faille décrochante, ou la présence de variations de faciès dans les unités ductiles contrôlant l'évolution des plis (évaporites d'Hormuz ou de Gachsaran). Des plis intérieurs peuvent aussi être réactivés par l'extrusion des cœurs synclinaux au-dessus d'une surface de décollement superficielle comme le niveau de Gachsaran, comme démontré par la structure de Baladeh (Chapitres 4 et 5). L'évolution précoce des plis de décollement, qui se développent au dessus d'une couche ductile d'épaisseur significative comme peut l'être le niveau d'évaporites d'Hormuz, semble par ailleurs être associée à la migration de matériel de ce niveau ductile basal depuis les synclinaux vers les cœurs d'anticlinaux (Chapitre 3). Ainsi, le style structural et l'évolution cinématique des plis du Zagros semble fortement contrôlé par la stratigraphie mécanique, et plus spécifiquement par l'épaisseur, la viscosité et la profondeur des couches incompétentes, à tous les stades de leur évolution.

Nous avons estimé la convergence à travers le Zagros central durant le tardi-Pléistocène en sommant le raccourcissement absorbé par les différentes structures actives que nous avons étudiées (Figure VI-1). Nous trouvons un taux de convergence à cette échelle de temps qui se rapproche aux erreurs près du taux de raccourcissement actuel de ~8 mm/a, déduit des données GPS [Tatar *et al*., 2002; Walpersdorf *et al.*, 2006]. Cette similitude suggère que ces taux ont été

constants durant les derniers 50 à 150 ka. La distribution de la déformation déduite de nos études morpho-structurales est également comparable à celle observée dans les données GPS et indique qu'une zone externe du Zagros, de ~100 km de large, absorbe la quasi-totalité de la convergence entre l'Arabie et l'Iran central (Figure VI-1). En particulier, les deux structures frontales que nous avons étudiées dans le nord-ouest de notre région d'étude (les plis de Mand et de Gisakan) absorbent chacun environ 3-4 mm/an de raccourcissement perpendiculaire à la chaîne, c'est à dire 35 à 50% du raccourcissement total (Chapitres 3 et 5). Plus au sud-est, la situation est un peu plus complexe, et c'est un pli plus interne (le pli de Halikhan) qui absorbe la plus grande partie de la convergence à travers la chaîne (Chapitre 5). Néanmoins, nos résultats peuvent être interprétés comme étant cohérents avec une histoire de propagation frontale de la déformation à travers la chaîne, devant un « *backstop* » passif constitué par le Haut Zagros. Un résultat important de notre travail est que les failles à l'intérieur du Zagros, qui ont été interprétées précédemment comme des failles de socle majeures [e.g., faille de Surmeh ; Berberian, 1995], semblent présenter une activité mineure à l'échelle de temps tardi-Pléistocène (Chapitre 5).

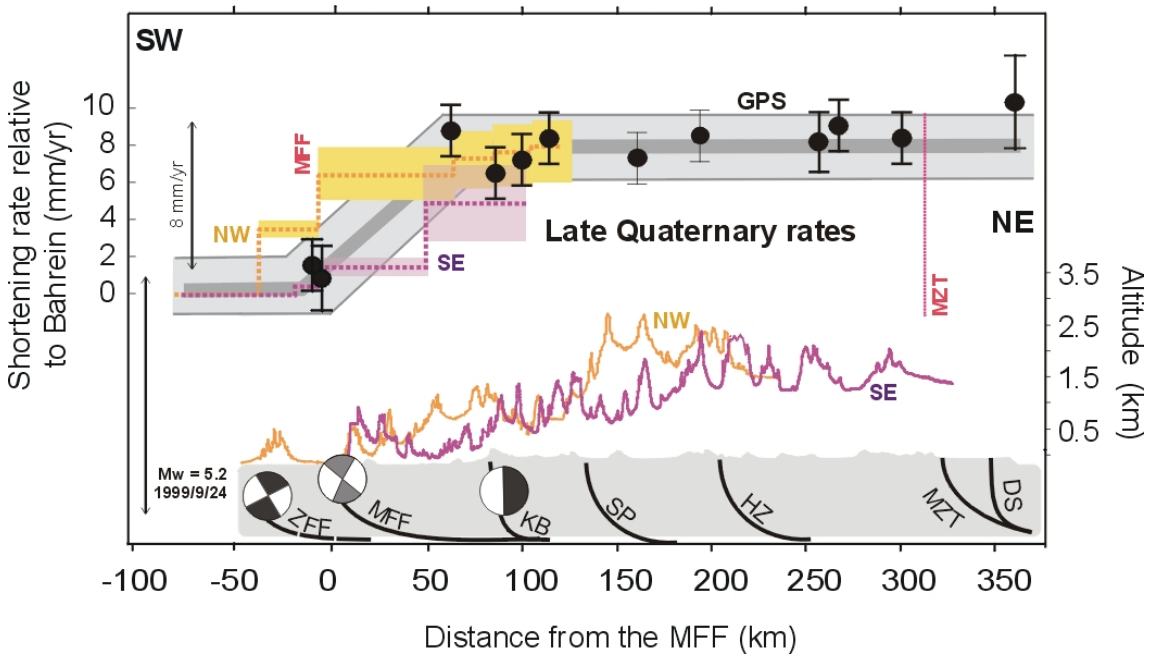

Figure VI-1 : Comparaison des taux de raccourcissement à l'échelle de temps tardi-Pléistocène le long de deux profils à travers le Zagros central (profil nord-ouest en orange, profil sud-est en violet), avec les taux de raccourcissement actuels observés par GPS [Walpersdorf *et al.*, 2006]. Les profils en bas montrent la topographie le long des deux profils ainsi que les failles majeures et les solutions focales de quelques séismes instrumentaux importants [Talebian & Jackson, 2004]. Voir le Chapitre 5 pour une discussion complète.

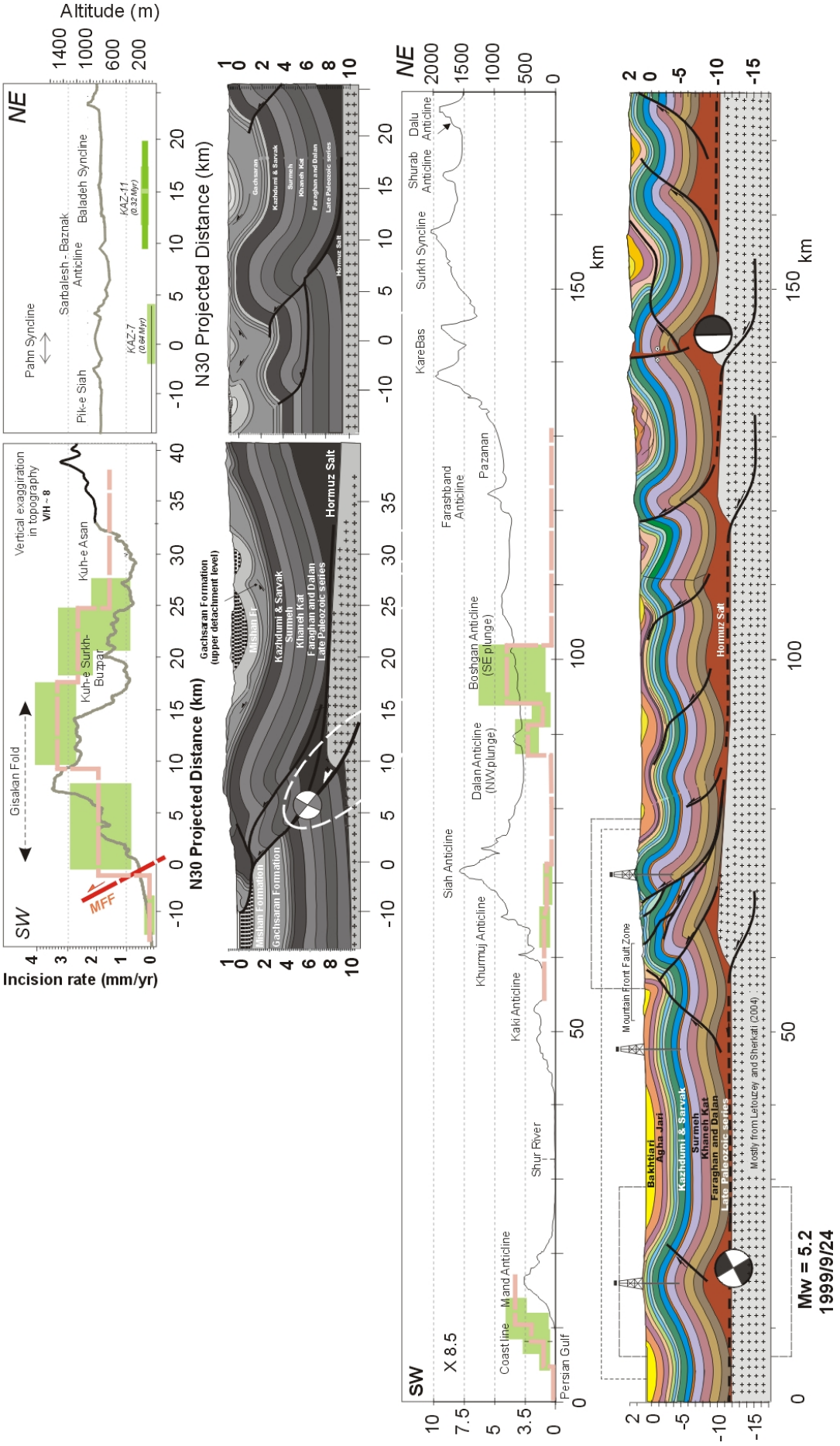

Figure VI-2. coupes structurales équilibrées, profils topographiques et variation des vitesses d'incision et de soulèvement le long des deux profils étudiées (en haut : le long de la rivière Dalaki ; en bas : le long de la rivière Mand). Notez le manque de corrélation entre structures profondes impliquant le socle et déformation de surface (sauf au niveau du pli de Gisakan frontal dans le profil de la Dalaki).

Même si les taux de déformation actuels sont très cohérents avec ceux observés à une échelle de temps intermédiaire, il est important de considérer le fait que les directions de raccourcissement local au front du Zagros sont généralement obliques par rapport aux vecteurs de mouvement GPS (montrant une rotation horaire de 30-45°). Cette disparité implique l'existence d'une composante de déformation décrochante dextre à travers le Zagros dans une direction N125°E ; une telle déformation est cohérente avec les solutions focales de nombreux séismes décrochants enregistrés dans le Zagros central, ainsi qu'avec le mouvement dextre le long de failles décrochantes comme celles de Kazerun ou de Karebas, et le long du *Main Recent Fault* (MRF) plus au Nord [e.g., Authemayou *et al*., 2006; Talebian & Jackson, 2004].

La comparaison de la localisation, des taux, et des directions de raccourcissement à travers le Zagros frontal (Figures VI-1 et VI-2), avec les données GPS récentes [Walpersdorf *et al.*, 2006], ou avec la distribution de la sismicité à travers la chaîne [Talebian & Jackson, 2004; Tatar *et al.*, 2004], suggère que la couverture sédimentaire est majoritairement découplée du socle dans la partie frontale du Zagros. Il ne semble donc pas y avoir de transfert local de contraintes entre un éventuel raccourcissement du socle et la couverture, et les plis de couverture se forment au-dessus d'un niveau de décollement important formé par le Sel d'Hormuz (ainsi que des niveaux plus superficiels comme le Gachsaran). Cette conclusion est en contradiction avec les suggestions récentes [e.g., Molinaro *et al.*, 2005; Sherkati *et al.*, 2005; Mouthereau *et al.*, 2006] que la déformation de la couverture du Zagros reflète passivement la déformation dans le socle par le transfert du raccourcissement le long de failles de socle vers la surface.

Nous proposons donc que la chaîne du Zagros (au moins dans sa partie centrale) se comporte principalement comme une chaîne de plissement superficielle (*thin-skinned fold and thrust belt*). Nous n'excluons pas une composante de déformation sismique ou asismique dans le socle mais celui-ci n'absorbe probablement pas plus que 25% du raccourcissement observé dans la couverture sédimentaire. Notre modèle de déformation découplée entre socle et couverture pose de ce fait la question fondamentale de l'accommodation du ≥75% de raccourcissement crustal non absorbé dans le Zagros central : est-ce que ce raccourcissement est transféré vers le Haut Zagros par le décollement d'Hormuz pour y être absorbé par sous-placage de la croûte moyenne arabe ? Si c'est le cas, pourquoi ce processus a-t-il lieu fondamentalement de façon asismique ? Des études supplémentaires seront nécessaires pour répondre à cette question, ainsi qu'à celle du partitionnement du raccourcissement entre plissement et failles décrochantes. Ces études devraient notamment viser l'obtention de données plus contraignantes sur les variations spatio-temporelles des taux de soulèvement et de glissement le long des failles, en mettant en œuvre des datations de surfaces plus détaillées et plus précises.

References

Alavi, M. (1994), Tectonics of the Zagros orogenic belt of Iran: new data and interpretations, *Tectonophysics, 229*, 211-238.

Al-Amri, A. M., Gharib, A. A (2000). Lithospheric seismic structure of the eastern region of the Arabian Peninsula, *Journal of Geodynamics*, vol. 29, 125-139.

Alavi, M., 1991, Tectonic map of the Middle East: Tehran, Geological Survey of Iran, scale 1:5,000,000.

Alavi, M. (2004), Regional stratigraphy of the Zagros fold-thrust belt of Iran and its proforeland evolution, *Am. J. Sci., 304*, 1-20.

Allen, M. B., J. Jackson, and R. Walker (2004), Late Cenozoic re-organization of the Arabia-Eurasia collision and the comparison of short-term and longterm deformation rates, Tectonics, 23, TC2008, doi:10.1029/2003TC001530.

Anderson, R. S., J. L. Repka, and G. S. Dick (1996), Explicit treatment of inheritance in dating depositional surfaces using in situ ^{10}Be and ^{26}Al, *Geology, 24*, 47-51.

Authemayou, C., O. Bellier, D. Chardon, Z. Malekzade, and M. Abbassi (2005), Role of the Kazerun fault system in active deformation of the Zagros foldand-thrust belt (Iran), *C. R. Geosci*., 337, 539 – 545.

Authemayou, C., D. Chardon, O. Bellier, Z. Malekzadeh, E. Shabanian, and M. R. Abbassi (2006), Late Cenozoic partitioning of oblique plate convergence in the Zagros fold-and-thrust belt (Iran), *Tectonics, 25*, TC3002, doi:10.1029/2005TC001860.

Bachmanov , D. M. , V. G. Trifonov , Kh. T. Hessami , A. I. Kozhurin , T. P. Ivanova , E. A. Rogozhin , M. C. Hademi, and F. H. Jamali (2004) Active faults in the Zagros and central Iran, *Tectonophysics, 380*, 221-241.

Badley, M.E., Price, J.D., Rambech Dahl, C. & Agdestein, T. 1988. The structural evolution of the northern Viking Graben and its bearing upon extensional modes of basin formation. *Journal of the Geological Society, London* 145, 455-472.

Badley, M.E. and Ranhech hhl, c, (1989), Discusion on the structural evolution of the Nortern Viking Graben and its bearing on extentional modes of basin formation: J. Geol. soc. London 146. 1038-1040.

Bagnold, R.A., 1977, Bed-load transport by natural rivers: *Water Resources Research*, v. 13, p. 303–312.

Bahroudi, A., and C. J. Talbot (2003), The configuration of the basement beneath the Zagros Basin, *J. Petrol. Geol., 26*, 257-282.

Bahroudi, A. & Koyi, H.A. (2003), Effect of spatial distribution of Hormuz salt on deformation style in the Zagros fold and thrust belt: an analogue modelling approach. Journal of the Geological Society, London, 160, 719-733.

Baker, C., J. Jackson, and K. Priestley (1993), Earthquakes on the Kazerun Line in the Zagros Mountains of Iran: Strike slip faulting within a fold and thrust belt, *Geophys. J. Int.*, *115*, 41-61.

Beaumont, C., P. Fullsack, and J. Hamilton (1992), Erosional control of active compressional orogens, in *Thrust Tectonics*, edited by K. R. McClay, pp. 1-18, Chapman & Hall, London.

Benedetti, L., Tapponnier, P., and King, G. (2000) Growth folding and active thrusting in the Montello region, Veneto, northern Italy. *Journal of Geophysical Research, 105,* 739–766.

Berberian, M, (1976), Scismotectonic map of Iran. in Contribution to the seismotectonics of Iran. Pt. II. - Iran Geol. Surv. Rept 39, Tehran.

Berberian, M. & Tchalenko, J., 1976. Earthquake of southern Zagros (Iran) : Bushehr region, in Contribution to the Seismotectonics of Iran, Part II, ed. Berberian, M., Geol. Surv. Iran Rept, 39, 346-358.

Berberian, M. (1977). Seismotectonic map of Iran, Geol. Min. Sur. of Iran.

Berberian, M., (1983), The southern Caspian: a compressional depression floored by a trapped, modified oceanic crust, Canad. J. Earth Sci., 20, 163–183.

Berberian, M., Qorashi, M., Jackson, J.A., Priestley, K. and Wallace, T., (1992). The Rudbar-Tarom earthquake of June 20, 1990 in NW Iran: preliminary field and seismotectonic observations, and its tectonic significance. Bull. Seismol. Soc. Am., 82(4): 1726-1755.

Berberian, M. (1995) Master blind thrust faults hidden under the Zagros folds: active basement tectonics and surface morphotectonics, *Tectonophysics*, *241*,193-224.

Berberian, M., and King, G.C.P., 1981, Towards a paleogeography and tectonic evolution of Iran: Canadian Journal of Earth Sciences, v. 18, p. 210–265.

Berberian, M., (1994), Natural Hazards and the First Earthquake Catalogue of Iran. International Institute of Earthquake Engineering and Seismology (IIEES), Vol 1, p620.

Beydoun, Z.R., Clarke, M.W.H., and Stoneley, R., 1992, Petroleum in Zagros Basin: A late Tertiary foreland basin overprinted onto the outer edge of a vast hydrocarbon-rich Paleozoic-Mesozoic passive-margin shelf, *in* Macqueen, R.W., and Leckie, D.A., eds., Foreland basins and fold belts: Tulsa, Oklahoma, American Association of Petroleum Geologists, p. 309–339.

Stocklin, J., 1968, Structural history and tectonics of Iran: A review: American

Bird P., Toksoz N. M. & Sleep N. H. 1975. Thermal and mechanical models of continentcontinent convergent zones. *Journal of Geophysics Research* 80: 4405-4416.

Bijwaard, H. and W. Spakman. Tomographic evidence for a narrow whole mantle plume below Iceland. *Earth Planet. Sci. Lett.*, **166**, 121-126, 1999.

Bijwaard, H., W. Spakman, E.R. Engdahl. Closing the gap between regional and global travel time tomography. *J. Geophys. Res.*, **103** (B12), 30,055 - 30,078, 1998.

Blanc, E. J.-P., M. B. Allen, S. Inger, and H. Hassani (2003), Structural styles in the Zagros simple folded zone, Iran, *Journal of the Geological Society, London, 160*, 401 – 412.

Bloom, A.L. 1991. *Geomorphology: A systematic analysis of late Cenozoic landforms*. Englewood Cliffs: Pretice-Hall, Inc.

Braucher, R., E. T. Brown, D. L. Bourlès, and F. Colin (2003), In situ produced ^{10}Be measurements at great depths: implications for production rates by fast muons, *Earth Planet. Sci. Lett., 211*, 251-258.

Brocard, G. Y., P. A. van der Beek, D. L. Bourlès, L. L. Siame, and J.-L. Mugnier (2003), Long-term fluvial incision rates and postglacial river relaxation time in the French Western Alps from ^{10}Be dating of alluvial terraces with assessment of inheritance, soil development and wind ablation effects, *Earth Planet. Sci. Lett., 209*, 197-214.

Brocard, G.Y., and P.A. van der Beek, Influence of incision rate, rock strength and bedload supply on bedrock river gradients and valley-flat widths: Field-based evidence and calibrations from western Alpine rivers (SE France), in: *Tectonics, Climate and Landscape Evolution, Geol. Soc. Am. Spec. Publ.* (S.D. Willett, N. Hovius, M.T. Brandon and D. Fisher, eds.), 398, 101-126, 2006.

Brown E.T., J.M. Edmond, G.M. Raisbeck, F. Yiou, M.D. Kurz, and E.J. Brook (1991), Examination of surface exposure ages of moraines in Arena Valley, Antarctica, using in situ produced ^{10}Be and ^{26}Al, *Geochim. Cosmochim. Acta, 55*, 2269-2283.

Brudy, M., Zoback, M.D., Fuchs, K., Rummel, F., and Baumgärtner, J., 1997, Estimation of the complete stress tensor to 8 km depth in the KTB scientific drill holes: Implications for crustal strength: Journal of Geophysical Research, v. 102, p. 18,453–18,475.

Burbank, D. W. & Anderson, R. S. 2000. Tectonic Geomorphology. 274 pp. Oxford: Blackwell Science.

Burnett, A.W., and Schumm, S.A., 1983, Alluvial-river response to neotectonic deformation in Louisiana and Mississippi: Science, v. 222, p. 49-50.

Carter, N. L., and M. Tsenn (1987), Flow properties of continental lithosphere, *Tectonophysics, 136*, 27-63.

Cerling, T. E., and H. Craig (1994), Geomorphology and in-situ cosmogenic isotopes, *Ann. Rev. Earth Planet. Sci., 22*, 273-317.

Cerling, T. E. and H. Craig, (1994), Cosmogenic production rates of ^{3}He from 39 to 46 °N latitude, western USA and France. Geochimica et Cosmochimica Acta 58: 249-255.

Cerling, T. E. and H. Craig, 1997, Geomorphology and in-situ cosmogenic isotopes, in (W. Dietrich and G. Sposito, eds) *Hydrologic Processes from Catchment to Continental Scales*. Annual Reviews, Menlo Park, California. (Reprint of : Cerling, T. E. and H. Craig, 1994, Geomorphology and in-situ cosmogenic isotopes. Annual Review of Earth and Planetary Sciences 22: 273-317.

Chappell, John. 1974. Geology of coral terraces, Huon Peninsula, New Guinea: a study of Quaternary tectonic movements and sea level changes. Geological Society of America Bulletin 85: 553-70.

Chapple,W.M.,1978, Mechanics of thin-skinned fold-and-thrust belts. Geol. Soc. Am. Bull., vol 89, p. 1189-1198.

Chappell, J. (2002) Sea level changes forced ice breakouts in the Last Glacial cycle: new results from coral terraces, *Quaternary Science Reviews, 21*, 1229–1240.

Chandra, U (1984) Focal mechanism solutions for earthquakes in Iran, *Physics of the Earth and Planetary Interiors, 34*, 9-16.

Cockburn HAP, Summerfield MA. 2004. Geomorphological applications of cosmogenic isotope analysis. *Progress in Physical Geography* **28**: 1- 42.

Colman-Sadd, S.P. (1978) Fold development in Zagros simply folded belt, southwest Iran, *American Association of Petroleum Geologists Bulletin, 62*, 984–1003.

Cotton, J. T., and H. A. Koyi (2000), Modeling of thrust fronts above ductile and frictional detachments: Application to structures in the Salt Range and Potwar Plateau, Pakistan, *Geol. Soc. Am. Bull., 112*, 351-363.

Dahlen, F. A., J. Suppe, and D. Davis (1984), Mechanics of fold-and-thrust belts and accretionary wedges: cohesive Coulomb theory, *J. Geophys. Res., 89*, 10087-10101.

Dahlen, F. A. (1990), Critical taper model of fold-and-thrust belts and accretionary wedges, *Ann. Rev. Earth Planet. Sci., 18*, 55-99.

Dahlstrom, C.D.A. (1969) Balanced cross sections. *Canadian Journal of Earth Sciences, 6*, 743–757.

Dahlstrom, C.D.A. (1990) Geometric constraints derived from the law of conservation of volume and applied to evolutionary models of detachment folding. *American Association of Petroleum Geologists Bulletin, 74*, 336–344.

Dahlstrom, C. D. A. (1969), Balanced cross sections, *Can. J. Earth Sci., 6*, 743-757.

Davis, D., J. Suppe, and F. A. Dahlen (1983), Mechanics of fold-and-thrust belts and accretionary wedges, *J. Geophys. Res., 88*, 1153-1172.

DeMets, C., R. G. Gordon, D. F. Argus, and S. Stein (1994) Effects of recent revisions to the geomagnetic time scale on estimates of current plate motions, *Geophysical Research Letters, 21*, 2191 – 2194.

De Sitter, L.U. (1964) *Structural Geology* (2nd edition), McGraw-Hill, New York, 551 pp.

Dehghani, G.A., and Makris, J., 1984, The gravity field and crustal structure of Iran: Neue Jahrbuch fur Geologische and Palaontische Abhandlungen, v. 168, p. 215-229.

Dehghani, G.A., Makris, J., 1983. The gravity field and crustal structure of Iran. In: Madelat, V. (Ed.), Geodynamic Project (Geotraverse) in Iran, Final Report. Geological Survey of Iran, Report No. 51, pp. 51–68.

Dunai, T.J., and Wijbrans, J.R., 2000. Long-term cosmogenic 3He production rates (152 ka-1.35 Ma) from 40Ar/39Ar dated basalt flows at 29°N latitude, Earth and Planetary Science Letters 176, pp. 147-156

Dunai, T. J. (2000), Scaling factors for production rates of in situ produced cosmogenic nuclides: a critical reevaluation, *Earth Planet. Sci. Lett., 176*, 157-169.

Dunne, J., Elmore, D. and Muzikar, P., 1999, Scaling factors for the rates of production of cosmogenic nuclides for geometric shielding and attenuation at depth of sloped surfaces: Geomorphology, v. 27, p. 3-11.

Edgell, H. S., 1996. Salt tectonics in the Persian Gulf basin. In: Alsop, G.L, Blundell, D.L., Davison, I. (Eds.), Salt tectonics. *Spec. Publ. Geol. Soc. London*, 100, 129-151.

Engdahl, E. R., R. D. van der Hilst, and R. P. Buland, Global teleseismic earthquake relocation with improved travel times and procedures for depth determination, *Bull. Seism. Soc. Am., 88*, 722-743, 1998

Epard, J.-L., Groshong, R.H. (1993) Excess area and depth to detachment, *American Association of Petroleum Geologists Bulletin, 77*, 1291-1302.

Epard, J.-L., Groshong, R.H. (1995) Kinematic model of detachment folding including limb rotation, fixed hinges, and layer-parallel strain, *Tectonophysics, 247*, 85-103.

Erslev, E.A. (1991) Trishear fault-propagation folding: *Geology, 19*, 617-620.

Erslev, E.A., Mayborn, K.R., 1997. Multiple geometries and modes of fault propagation folding in the Canadian thrust belt. Journal of Structural Geology 19, 321–335.

Falcon, N. L. (1969), Problems of the relationship between surface structure and deep displacements illustrated by the Zagros Range, in *Time and Place in Orogeny*, edited by A.M. Spencer, *Geol. Soc. London Spec. Publ., 4*, 9-22.

Falcon, N.L. 1967. The geology of the north-east margin of the Arabian basement shield. Advancement of Science, 24, 1-12.

Falcon, N. L. (1961), Major earth-flexing in the Zagros Mountains of southwest Iran: *Q. J. Geol. Soc. London, 117*, 367-376.

Falcon, N.L. 1974. Southern Iran: Zagros Mountains. In: SPENCER, A. (ed.) Mesozoic-Cenozoic Orogenic Belts. Geological Society, London, Special Publications, 4, 199-211.

Fairbanks, R.G., 1989, A 17,000-year glacio-eustatic sea level record--influence of glacial melting rates on the Younger Dryas event and deep-sea circulation, Nature, v. 342, p. 637-642.

Farhoudi, G. (1978) A comparison of Zagros Mountains geology to Island Arcs, *Journal of Geology, 86*, 323–334.

Fischer, M. P., N. B. Woodward, and M. M. Mitchell (1992), The kinematics of break-thrust folds, *J. Struct. Geol., 14*, 451-460.

Fifield, L.K., 1999, Accelerator mass spectrometry and its applications: Reports on Progress in Physics, v. 62, p. 1223–1274.

Fontugne, M., J.L. Reyss, C. Hatte, P.A. Pirazzoli, and A. Haghipour (1997), Global sea level changes as indicated by ^{14}C and $^{230}Th/^{234}U$ dating of marine terraces in the Persian Gulf and along the Makran Coast (Iran). In: *Earth Processes in Global Change—Climate of the Past. Proceedings of the Lanzarote-Fuerteventura UNESCO-IUGS Meeting*, 1–6 June 1995, Universidad de Gran Canaria, Las Palmas, pp. 81–88, 1997.

Ford, M. (2004), Depositional wedge tops: interaction between low basal friction external orogenic wedges and flexural foreland basins, *Basin Res., 16*, 361-375.

Gansser, A., 1992. The enigma of the Persian salt dome inclusions. Ecolgae geol. Helv. 85 (3), 825–846.

Gillard, D., and M. Wyss (1995), Comparison of strain and stress tensor orientation: application to Iran and southern California, *J. Geophys. Res., 100*, 22197-22213.

Gold, R. D., E. Cowgill, X.-F. Wang and X.-H. Chen (2006) Application of trishear fault-propagation folding to active reverse faults: examples from the Dalong Fault, Gansu Province, NW China, *Journal of Structural Geology, 28*, 200-219.

Goodwin, et al., 2003, New Departures in Structural Geology and Tectonics, National Science Foundation (GEO/EAR) http://pangea.stanford.edu/~dpollard/NSF/main.html].

Gosse, J. C., and F. M. Phillips (2001), Terrestrial in situ cosmogenic nuclides: theory and application, *Quat. Sci. Rev., 20*, 1475-1560.

Hack, J. T. (1973), Stream-profile analysis and stream-gradient index, *J. Res. U.S. Geol. Surv., 1*, 421-429.

Hancock, G. S., and R. S. Anderson (2002), Numerical modeling of fluvial strath-terrace formation in response to oscillating climate, *Geol. Soc. Am. Bull., 114*, 1131-1142.

Haghipour, A., and Fontugne, M. (1993) Quaternary uplift of Qeshm Island (Iran). *Comptes Rendus de l'Académie des Sciences, Paris, 317*, 419–424.

Hassani, R., D. Jongmans and J. Chery (1997). Study of plate deformation and stress in subduction processes using two-dimensional numerical models. Journal of Geophysical Research, 102, B8, 17951-17965.

Hatzfeld, D., Tatar, M., Priestley, K. & Ghafory-Ashtyany, M., 2003. Seismological constraints on the crustal structure beneath the Zagros mountain belt (Iran), *Geophys. J. Int.*, **155,** 403–410.

Haynes, S.J. & McQuillan, H. 1974. Evaluation of the Zagros suture zone, Southern Iran. Geological Society of American Bulletin, 85, 739-744.

Heidbreder, E., Pinkau, K., Reppin, C., Schöenfelder, V., 1971. Measurement of the distribution in energy and angle of highenergy neutrons in the lower atmosphere. Journal of Geophysical Research 76, 2905–2916.

Hessami, K., Koyi, H.A., Talbot, C.J., Tabasi, H., and Shabanian, E. (2001) Progressive unconformities within an evolving foreland fold–thrust belt, Zagros Mountains, *Journal of the Geological Society, London, 158*, 969-981.

Hessami, K., F. Nilforoushan, and C. J. Talbot (2006), Active deformation within the Zagros Mountains deduced from GPS measurements, *J. Geol. Soc. London, 163*, 143-148.

Homke, S., J. Vergés, M. Garcés, H. Emami, and R. Karpuz (2004), Magnetostratigraphy of Miocene–Pliocene Zagros foreland deposits in the front of the Push-e Kush Arc (Lurestan Province, Iran), *Earth Planet. Sci. Lett., 225*, 397-410.

Huber, H., 1977, Geological cross sections, north-central Iran: Tehran, National Iranian Oil Company, scale 1:500 000.

Ishiyama T., K. Mueller, M. Togo, A. Okada, K. Takemura (2004) Geomorphology, kinematic history, and earthquake behavior of the active Kuwana wedge thrust anticline, central Japan, *Journal of Geophysical Research, 109*, B12408, doi: 10.1029/2003JB002547.

Jackson, J.A. (1980), Reactivation of basement faults and crustal shortening in orogenic belts. Nature, bf 283, 343-346.

Jackson, J.A. (1980), Errors in focal depth determination and the depth of seismicity in Iran and Turkey. Geophysical Journal of the Royal Astronomical Society, 61, 285-301.

Jackson, J. A., and T. Fitch (1981) Basement faulting and the focal depths of the larger earthquakes in the Zagros mountains (Iran), *Geophysical Journal of the Royal Astronomical Society, 64*, 561 – 586.

Jackson, J. A., Fitch, T. J. and McKenzie, D. P. (1981) Active thrusting and the evolution of the Zagros fold belt, in: McClay, K. R. and Price, N. J. (eds.), *Thrust and Nappe Tectonics, Geological Society (London) Special Publication, 9,* 371-379.

Jackson, J.A. and McKenzie, D. (1984) Active tectonics of the Alpine-Himalayan Belt between western Turkey and Pakistan, *Geophysical Journal of the Royal Astronomical Society,* 77**,** 185–264.

Jackson, J.A. (1992), Partitioning of strike-slip and convergent motion between Eurasia and Arabia in eastern Turkey and the Caucasus. Journal of Geophysical Research, 97, 12,471-12,479.

Jackson, J., Haines, J., & Holt, W. (1995) The accommodation of Arabia-Eurasia plate convergence in Iran, *Journal of Geophysical Research, 100,* 15,205-15219.

Jackson, J, A.J. Haines, and W.E. Holt (1995), Accommodation of Arabia-Eurasia plate convergence in Iran, *J. Geophys. Res., 100,* 15,205-15,219.

Jamison, W. R. (1987) Geometric analysis of fold development in overthrust terranes, *J. Struct. Geol., 9,* 207 – 219.

James, G.A. & Wynd, J.G. 1965. Stratigraphic nomenclature of Iranian oil consortium agreement area. The American Association of Petroleum Geologists Bulletin, 49, 2182-2245.

Kassler P (1973) The structural and geomorphic evolution of the Persian Gulf. In: Purser B (ed) The Persian Gulf. Springer, Berlin Heidelberg New York: 11–32

Kirby, E., Whipple, K., 2001. Quantifying differential rock-uplift rates via stream profile analysis. Geology 29 (5), 415–418

Kubik, P. W., S. Ivy-Ochs, J. Masarik, M. Frank, and C. Schlüchter (1998), ^{10}Be and ^{26}Al production rates deduced from an instantaneous event within the dendro-calibration curve, the landslide of Köfels, Ötz Valley, Austria, *Earth Planet. Sci. Lett., 161,* 231-241.

Koyi, H., Experimental modeling of role of gravity and lateral shortening in Zagros mountain belt, AAPG Bulletin, 72, 1381-1394, 1988.

Koop, W.J. & Stoneley, R. 1982. Subsidence history of the Middle East Zagros basin, Permian to Recent. Philosophical Transactions of the Royal Society of London, 305, 149-168.

Kurz, M.D. and Brook, E.J. 1994. Surface Exposure Dating with Cosmogenic Nuclides. *In* Dating in Exposed and Surface Contexts. *Edited by* C. Beck. University of New Mexico Press. Albuquerque. pp. 139-159.

Lacombe O., Mouthereau F., Kargar S. et Meyer B., 2006, Late Cenozoic and modern stress field in the western Fars (Iran) : implications for the tectonic and kinematic evolution of Central Zagros. Tectonics, 25, TC1003, doi:10.1029/2005TC001831.

Lal D. (1988) Theoretically expected variations in the terrestrial cosmic-ray production rates of isotopes. *In Solar-Terrestrial Relationship and the Earth Environment in the Last Millennia*, 216-231.

Lal, D. (1991), Cosmic ray labeling of erosion surfaces: in situ nuclide production rates and erosion models, *Earth Planet. Sci. Lett., 104*, 424-439.

Lambeck, K. (1996) Shoreline reconstructions for the Persian Gulf since the last glacial maximum, *Earth and Planetary Science Letters, 142*, 43-57.

Lambeck, K., and Chappell, J. (2001) Sea level change through the last glacial cycle, *Science, 292*, 679-686.

Laubscher, H., 1986. The eastern Jura: relations between thin-skinned and basement tectonics, local and regional. Geol. Rdsch., 75, 535–553.

Lavé, J., Avouac, J.P. (2000) Active folding of fluvial terraces across the Siwaliks Hills, Himalayas of central Nepal. *Journal of Geophysical Research, 105,* 5735–5770.

Lavé, J., and J. P. Avouac (2001), Fluvial incision and tectonic uplift across the Himalayas of central Nepal, *J. Geophys. Res., 106*, 25561-25593.

Lees, G. M. and Falcon, N. L. (1952). The geographical history of the Mesopotamian Plains. *Geographical Journal*, 118, 24-39.

Letouzey, J., Colletta, B., Vially, R. & Chermette, J.C. (1995), Evolution of salt related structures in compressional setting. In Jackson, M.P.A., Roberts, D.G., and Snelson, S., eds., *Salt Tectonics: Global Perspective. American Association of Petroleum Geologists Memoir*, *65*, 41-60.

Letouzey J. and S.Sherkati (2004), Salt Movement, Tectonic Events, and Structural Style in the Central Zagros Fold and Thrust Belt (Iran), *24th Annual GCSSEPM Foundation Bob F. Perkins Research Conference, Salt-Sediments interactions and Hydrocarbon Prospectivity, Concepts, Applications and Case Studies for the 21st Century*: Houston, Texas, Society of Economic Paleontologists and Mineralogists.

Maggi, A., J.A. Jackson, D. McKenzie, and K. Priestley, (2000a), Earthquake focal depths, effective elastic thickness, and the strength of the continental lithosphere, *Geology*, *28*, 495-498.

Maggi, A., J. Jackson, K. Priestley, and C. Baker (2000b) A re-assessment of focal depth distributions in southern Iran, the Tien Shan and northern India: Do earthquakes really occur in the continental mantle? *Geophysical Journal International*, *143*, 629 – 661.

Masarik J., Reedy R. C., Terrestrial cosmogenic-nuclide production systematics calculated from numerical simulations, Earth and Planetary Science Letters 136 (1995) 381-395.

Masarik J., Wieler R., (2003), Production rates of cosmogenic nuclides in boulders, Earth and Planetary Science Letters 216 201-208.

Masson, F., J. Chéry, D. Hatzfeld, J. Martinod, P. Vernant, F. Tavakoli and M. Ghafory-Ashtiani (2005) Seismic versus aseismic deformation in Iran inferred from earthquakes and geodetic data, *Geophysical Journal International, 160*, 217-226.

McClusky, S., S. Balassanian, A. Barka, and a. others, Global Positioning System constraints on plate kinematics and dynamics in the Eastern Mediterranean and Caucasus, *J. Geophys. Res.*, *105*, 5695-5719, 2000.

McQuarrie, N. (2004) Crustal-scale geometry of the Zagros fold-thrust belt, Iran, *Journal of Structural Geology, 26*, 519–535.

Merritts D., K. Vincent, and E. Wohl (1994), Long river profiles, tectonism, and eustasy: A guide to interpreting fluvial terraces, *J. Geophys. Res., 99*, 14,031-14,050.

Mitra, S. (2002) Structural models of faulted detachment folds, *American Association of Petroleum Geologists Bulletin, 86*, 1673-1694.

Mitra, S. (2003) A unified kinematic model for the evolution of detachment folds, *Journal of Structural Geology, 25*, 1659-1673.

Molinaro, M., P. Leturmy, J.-C. Guezou, D. Frizon de Lamotte, and S. A. Eshraghi (2005), The structure and kinematics of the southeastern Zagros fold-thrust belt, Iran: From thin-skinned to thick-skinned tectonics, *Tectonics, 24*, TC3007, doi:10.1029/2004TC001633.

Molinaro M., Zeyen H., Laurencin X., (2004). Lithospheric structure underneath the south-eastern Zagros Mountains, Iran : recent slab break-off? *Terra Nova, 17*, 1-6.

Moores, E.M. and Twiss, R.J. 1995. *Tectonics*. W.H. Freman and Company, New York, 415 p.,

Mouthereau F., Lacombe O. and Meyer B., 2006, The Zagros folded belt (Fars, Iran) : constraints from topography and critical wedge modelling. *Geophys. J. Int., 165*(1), 336-356.

National Iranian Oil Company (1976), Geological Map of Iran, 1,100.000 series, Sheet 20860 W (Mand South).

National Iranian Oil Company (1977), Geological Map of Iran, 1,100.000 series, Sheet 20855 W (Mand North).

Ni, J. and Barazangi, M. (1986) Seismotectonics of the Zagros continental collision zone and a comparison with the Himalayas, *Journal of Geophysical Research, 91*, 8205-8218.

Nilforoushan, F., F. Masson, P. Vernant, C. Vigny, and a. others, GPS network monitors the Arabia-Eurasia collision deformation in Iran, *Journal of Geodesy, 77*, 411-422, 2003.

Niedermann, S., Graf, T., Kim, J.S., Kohl, C.P., Marti, K., and Nishiizumi, K., 1994, Cosmic-ray-produced 21Ne in terrestrial quartz: the neon inventory of Sierra Nevada quartz separartes: Earth Planet. Sci. Lett., v. 125, p. 341-355.

Niedermann, S., 2000, The 21Ne production rate in quarz revisited: Earth Planet. Sci. Lett., v. 183, p. 361-364.

Nowroozi A. (1971) Seismotectonics of the Persian plateau, Eastern Turkey, Caucasus and Hindu Kush regions, Bull. Seism. Soc. Am., vol.61, pp.317-342.

Nowroozi, A. (1972), Focal mechanism of earthquakes in Iran, Turkey, West Pakistan and Afghanistan and plate tectonics of the Middle East, *Bull. Seism. Soc. Am., 62*, 823-850.

Oberlander, T. M. (1965) The Zagros Streams. Syracuse University Geographical Series, No. 1.

O'Brien, C. A. E., 1957. Salt diapirism in South Persia. Geologie en Mijnbouw, 19, 337-376.

Ortiz, M., Y. Leroy , A. Needleman, 1987, A finite element method for localized failure analysis, Computer Methods in Applied Mechanics and Engineering, v.61 n.2, p.189-214,

Ouchi, S. (1985) Response of alluvial rivers to slow active tectonic movement. Geol. Soc. Am. Bull., 96, 504–515. of the Neogene West Natuna Basin, Indonesia.

Oveisi, B., J. Lavé, and P. van der Beek (2007), Rates and processes of active folding evidenced by Pleistocene terraces at the central Zagros front (Iran), in *Thrust Belts and Foreland Basins, "Frontiers in Earth Sciences" Series*, edited by O. Lacombe *et al.*, Springer-Verlag, New York, pp. 265-285.

Paul, H.J., Gillis, K.M., Coggon, R.M., and Teagle, D.A.H., 2006. ODP Site 1224: a missing link in the investigation of seafloor weathering. *Geochem., Geophys., Geosyst.*, 7(2).

Pazzaglia F.J., and M.T. Brandon (2001), A fluvial record of long-term steady-state uplift and erosion across the Cascadia forearc high, western Washington State, *Am. J. Sci., 301*, 385-431.

Pazzaglia, F.J., Gardner, T.W. and Merritts, D.J., 1998. Bedrock fluvial incision and longitudinal profile development over geologic time scales determined by fluvial terraces. In: K.J. Tinkler and E.E. Wohl (Editors), Rivers over Rock: Fluvial Processes in Bedrock Channels. Geophysical Monograph. AGU Geophysical Monograph 107, pp. 207-235.

Paysanos, M.E. & Walter, W.R. 2002. Crustal and upper mantle structure on North Africa, Europe, and the Middle East from inversion of surface waves, Geophys. J. Int., 149, 463-481.

Poblet, J. & McClay, K. (1996), Geometry and kinematics of single-layer detachment folds, *American Association of Petroleum Geologists Bulletin, 80*, 1085-1109.

Poblet, J., McClay, K., Storti, F., Muñoz, J.A. (1997) Geometries of syntectonic sediments associated with single-layer detachment folds, *Journal of Structural Geology, 19*, 369–381.

Preusser, F., Radtke, U., Fontugne, M., Haghipour, A., Hilgers, A., Kasper, H.U., Nazari, H., Pirazzoli, P.A. (2003) ESR dating of raised coral reefs from Kish Island, Persian Gulf. *Quaternary Science Reviews, 22*, 1317-1322.

Ramezani, J. and Tucker, R.D., 2003, The Saghand region, central Iran: U-Pb geochronology, petrogenesis and implications for Gondwana tectonics. *American Journal of Science* 303, 622-665.

Reyss, J.L., Pirazzoli, P.A., Haghipour, A., Hatte, C., Fontugne, M. (1998), Quaternary marine terraces and tectonic uplift rates on the south coast of Iran. In: Stewart, I.S., Vita-Finzi, C. (Eds.), *Coastal Tectonics. Geological Society* (*London) Special Publication, 146*, 225–237.

Regard V., O. Bellier, J.-C. Thomas, M.R. Abbassi, J. Mercier, E. Shabanian, Kh. Feghhi, Sh. Soleymani, 2004. The accommodation of Arabia-Asia convergence in the Zagros-Makran transfer zone, SE Iran: a transition between collision and subduction through a young deforming system. Tectonics, 23, TC4007, doi :10.1029/2003TC001599.

Ricou, L.E., 1971. Le croissant ophiolitique péri-arabe, une ceinture de nappes mise en place au Crétacé supérieur. Rev. Géogr. Phys. Géol. Dyn., XIII: 327-349.

Ricou, L.E., 1975. Position anté-tectonique des ophiolites et radiolarites du croissant ophiolitique péri-arabe à la lumière des corrélations avec les Taurides et les Hellènides. Teheran Symp. on Geodynamics, sept. 1975.

Rockwell, T. K., E. A. Keller, M. N. Clark, and D. L. Johnson (1984), Chronology and rates of faulting of Ventura River terraces, California, *Geol. Soc. Am. Bull., 95*, 1466-1474.

Sattarzadeh, Y., Cosgrove, J.W. & Vita-Finzi, C. 2000. The interplay of faulting and folding during the evolution of the Zagros. In: Cosgrove, J.W. & Ameen, M.S. (eds) Forced Folds and Fractures. Geological Society, London, Special Publications, 169, 187-196.

Sella, G.F., Dixon, T.H. and Mao, A. (2002), REVEL: a model for recent plate velocities from space geodesy, *Journal of Geophysical Research, 107*, 2081, doi:10.1029/2000JB000033.

Sengör AMC, Kidd WSF (1979) Post-collisional tectonics of the Turkish-Iranian plateau and a comparison with Tibet. Tectonophysics 55:361–376.

Sepehr, M. & Cosgrove, J.W., 2004. Structural framework of the Zagros fold-thrust belt, Iran. *Marine and Petroleum Geology***,** 21**,** 829-843.

Scott, W. Richard. 1992 [1981]. *Organizations: Rational, Natural, and Open Systems.* New York: Prentice Hall.

Seibold, E. and Vollbrecht, K., 1969. Die bodengestalt des Persischen Golfs. Meteor Forschungsergeb., Reihe C, 2: 29-56.

Sherkati. S., and Letouzey, J. (2004) Variation of structural style and basin evolution in the central Zagros (Izeh zone and Dezful Embayment), Iran. *Marine and Petroleum Geology, 21*, 535-554.

Sherkati, S., Molinaro, M., Frizon de Lamotte, D. and Letouzey, J., (2005) Detachment folding in the Central and Eastern Zagros fold belt (Iran). *Journal of structural Geology, 27*, 1680-1696.

Sherkati. S., J. Letouzey, and D. Frizon de Lamotte (2006), The Central Zagros fold-thrust belt (Iran): New insights from seismic data, field observation and sandbox modelling, *Tectonics*, *25*, doi:10.1029/2004TC001766.

Snyder, D.B.and M.Barazangi, 1986, Deep crustal structure and flexure of the Arabian plate beneath the Zagros collisional mountain belt as inferred from gravity observations: Tectonics, v. 5, p. 361-373.

Stocklin, J. (1968), Structural history and tectonics of Iran: A review, *American Association of Petroleum Geologists Bulletin, 52*, 1229-1258.

Stocklin, J. (1968), Structural history and tectonics of Iran: A review, *AAPG Bull.*, *52*, 1229–1258.

Stone, J. O., G. L. Allan, L. K. Fifield, and R. G. Cresswell (1996), Cosmogenic chlorine-36 from calcium spallation, *Geochim. Cosmochim. Acta*, *60*, 679-692.

Stone, J. O., J. M. Evans, L. K. Fifield, G. L. Allan, and R. G. Cresswell (1998), Cosmogenic chlorine-36 production in calcite by muons, *Geochim. Cosmochim. Acta*, *62*, 433-454.

Stone J.O. (2000), Air pressure and cosmogenic isotope production, *J. Geophys. Res.*, *105*, 23753-23759.

Stoneley, R. 1981. The geology of the Kuh-e Dalneshin area of southern Iran, and its bearing on the evolution of southern Tethys. Journal of the Geological Society (of London), **138**: 509–526.

Suppe, J. (1983), Geometry and kinematics of fault-bend folding, *Am. J. Sci., 283*, 684-721.

Suppe, J., and D. A. Medwedeff (1990), Geometry and kinematics of fault-propagation folding, *Eclog. geol. Helv., 83*, 409-454.

Suppe, J., G. T. Chou, and S. C. Hook (1992), Rates of folding and faulting determined from growth strata, in *Thrust Tectonics*, edited by K. R. McClay, pp. 105-121, Chapman & Hall, London.

Snyder, D.B. & Barazangi, M., 1986. Deep crustal structure and flexure of the Arabian Plate beneath the Zagros collisional mountain belt as inferred from gravity observations, *Tectonics*, 5, 361–373.

Talbot, C.J., and Alavi, M. (1996), The past of a future syntaxis across the Zagros, In: *Salt Tectonics* (Ed. By G.I. Alsop, D.J. Blundell & I.Davison), *Geological Society (London) Special Publication, 100*, 89-109.

Talebian, M, & Jackson, J. (2004), A reappraisal of earthquake focal mechanisms and active shortening in the Zagros mountains of Iran. *Geophysical Journal International, 156*, 506-526.

Talebian M, Jackson J (2002) Offset on the Main Recent Fault of NW Iran and implications for the late Cenozoic tectonics of the Arabia–Eurasia collision zone. Geophys J Int 150:422–439.

Tatar, M., Hatzfeld D., Martinod J., Walpersdorf A., Ghafori-Ashtiany M., and Chery J. (2002), The present-day deformation of the central Zagros from GPS measurements: *Geophysical Research Letters, 29*, 1927, doi: 10.1029/2002GL015427.

Tatar, M., Hatzfeld D., and Ghafory-Ashtiany M. (2004) Tectonics of the Central Zagros (Iran) deduced from microearthquake seismicity. *Geophysical Journal International, 156*, 255-266.

Tchalenko, J. S., and J. Braud, 1974. Seismicity and structure of the Zagros (Iran)—the main recent fault between 33 and 35_N, Phil. Trans. Roy. Soc. London, 277, 1 – 25.

Thompson, W. G., and S. L. Goldstein (2006), A radiometric calibration of the SPECMAP timescale, *Quat. Sci. Rev., 25*, 3207-3215.

Thompson, S., Weldon, R., Rubin, C., Abdrakhmatov, K., Molnar, P., Berger, G. (2002), Late Quaternary slip rates across the central Tien Shan, Kyrgyzstan, central Asia. *Journal of Geophysical Research, 107*, 2203, doi:10.1029/2001JB000596.

Trowell, C.G., 1995. Lithospheric stretching, subsidence and magmatism in Oman and the Middle East, PhD thesis, University of Cambridge.

Uchupi, E., S.A. Swift, and D.A. Ross (1999), Late Quaternary stratigraphy, Paleoclimate and neotectonism of the Persian Gulf region, *Mar. Geol., 160*, 1–23.

Van der Plicht, J., Beck, J.W., Bard, E., Baillie, M.G.L., Blackwell, P.G., Buck, C.E., Friedrich, M., Guilderson, T.P., Hughen, K.A., Kromer, B., McCormac, F.G., Bronk Ramsey, C., Reimer, P.J., Reimer, R.W., Remmele, S., Richards, D.A., Southon, J.R., Stuiver, M., and Weyhenmeyer, C.E. (2004) NOTCAL04 comparison-calibration ^{14}C records 26-50 cal kyr BP. *Radiocarbon, 46*, 1225-1238.

Vernant, P., F. Nilforoushan, D. Hatzfeld, M.R. Abbassi, C. Vigny, F. Masson, H. Nankali, J. Martinod, A. Ashtiani, R. Bayer, F. Tavakoli, J. Chéry, (2004) Present day crustal deformation and plate kinematics in the Middle East constrained by GPS measurements in Iran and northern Oman, *Geophysical Journal International*, *157*, 381-398.

Vita-Finzi, C. (1979), Rates of Holocene folding in the coastal Zagros near Bandar Abbas, Iran, *Nature, 278*, 632-634.

Vita-Finzi, C. (1982), Recent coastal deformation near the Strait of Hormuz, *Proc. R. Acad. Sci. A. Math. Phys. Sci., 382*, 441-457.

Walpersdorf, A., D. Hatzfeld, H. Nankali, F. Tavakoli, F. Nilforoushan, M. Tatar, P. Vernant, J. Chéry, and F. Masson (2006), Difference in the GPS deformation pattern of North and Central Zagros (Iran), *Geophys. J. Int., 167*, 1077–1088, doi:10.1111/j.1365-246X.2006.03147.

Wallace, W.K. and Hanks, C.L. (1990), Structural provinces of the northeastern Alaska Brooks Range, Arctic National Wildlife Refuge, Alaska : American Association of Petroleum Geologists Bulletin, v. 74, p. 1100-1118.

Weijermars, R., Jackson, M.P.A., Vendeville, B.C., 1993. Scaling of salt tectonics. Tectonophysics 217, 143–174.

Whipple, K. X. and Tucker, G. E. (1999), Dynamics of stream-power river incision model : Implications for height limits of mountain ranges,land-scape response timescales, and research needs, J. Geophys. Res., 104, 17,661-17,674.

Willett et. al. (2003), New Departures in Structural Geology and Tectonics, National Science Foundation (GEO/EAR) http://pangea.stanford.edu/~dpollard/NSF/main.html].

Whipple, K. X., and B. J. Meade (2006), Orogen response to changes in climatic and tectonic forcing, *Earth Planet. Sci. Lett., 243*, 218-228.

Yamini-Fard, F., D. Hatzfeld, M. Tatar, and M. Mokhtari (2006), Microearthquake seismicity at the intersection between the Kazerun fault and the Main Recent Fault (Zagros, Iran), *Geophys. J. Int., 166*, 186-196, doi:10.1111/j.1365-246X.2006.02891.x.

Yonkee, W.A., and Mitra, G., (1993). Comparison of basement deformation styles in the Rocky Mountain Foreland and Sevier Orogenic Belt. In Schmidt, C., Chase, R., and Erslev, E., (eds), *Basement Behavior in Rocky Mountain Foreland Structure*. Geological Society of America, Special Papers 280, 197-228.